Development of thallium as a tracer of igneous process in contrasting tectonic settings

Elizabeth Katharine

Alex Brett

A thesis submitted for the degree of
Doctor of Philosophy

Department of Earth Science and Engineering
Imperial College London

Statement of originality

I declare that this thesis is my own work, carried out under the supervision of Julie Prytulak and Mark Rehkämper. Any content that is not original to this thesis is appropriately referenced throughout. Where I have received assistance from, or collaborated with, others, this is noted and acknowledged. No portion of this work has been submitted for any other degree or qualification at any other university or institute of learning.

Copyright declaration

The copyright of this thesis rests with the author. Unless otherwise indicated, its contents are licensed under a Creative Commons Attribution-NonCommercial-ShareAlike 4.0 International Licence (CC BY NC-SA).

Under this licence, you may copy and redistribute the material in any medium or format. You may also create and distribute modified versions of the work. This is on the condition that: you credit the author, do not use it for commercial purposes and share any derivative works under the same licence.

When reusing or sharing this work, ensure you make the licence terms clear to others by naming the licence and linking to the licence text. Where a work has been adapted, you should indicate that the work has been changed and describe those changes.

Please seek permission from the copyright holder for uses of this work that are not included in this licence or permitted under UK Copyright Law.

London, 5th September 2021
Alex Brett
(they/them/their)

Abstract

Some volcanoes erupt relatively undifferentiated melts, which can be used to investigate the otherwise inaccessible mantle. Tectonic setting influences which portions of the mantle are sampled by volcanic activity. At mid-ocean ridges, passive upwelling causes decompression melting of the upper mantle. In subduction settings, arc lavas provide chemical evidence for the incorporation of slab materials and fluids from the downgoing plate. The geochemistry of ocean island basalts (OIB) indicate that at least some of this surface material is recycled into the deep mantle and then re-sampled. However, identifying geochemical signatures that can be linked to a specific type of subduction input is often challenging.

This thesis investigates the potential of thallium stable isotope and elemental systematics to further constrain recycling of surface materials through the mantle via subduction. Thallium (Tl) is a heavy (mass $\sim$204), volatile, highly incompatible trace metal, which is both depleted and isotopically homogeneous in mid-ocean ridge basalts (MORB). In contrast, much higher concentrations of isotopically diverse Tl are found in potential subduction inputs, meaning that addition of exotic Tl to the mantle should be readily identifiable.

I provide new analyses of global OIB and the first analyses of thallium stable isotopes in samples from a continental arc volcano, alongside trace element compilations for MORB, OIB, and arcs. The accuracy and precision of these datasets are supported by characterisation and evaluation of igneous reference materials. I show that the mantle is likely to be even more depleted in Tl than previously recognised, and that recycling of Tl into the deep mantle and OIB source regions is likely limited. Variations in the Tl isotopic composition of OIB reflect some combination of heterogeneous residual slab Tl and shallow-level assimilation during magma ascent. Instead, the majority of subducted Tl is reprocessed through subduction-related volcanism, eventually accumulating in the continental crust.

Plain language summary

When a tectonic plate subducts, its crust and sediment layers are mixed back into the mantle by convective stirring. This stirring is not perfect, so the mantle is chemically variable. The differences in chemistry of the mantle can be detected in lavas erupted at the Earth's surface. Lavas from different plate tectonic settings are made by melting different regions of the mantle: mid-ocean ridge basalts are made from the upper mantle; "hotspot" intraplate volcanoes include magmas made by melting the deep mantle; and arc magmas, formed above subduction zones, are made up of a mixture of melts and fluids from the subducting slab, the overlying tectonic plate, and the mantle in between the two.

Eight elements (Fe, O, Si, Mg, S, Ni, Ca, Al) make up 98.8% of the Earth. The other 1.2% is made of 'trace elements'. We can use the trace elements in rocks to work out how they formed. On average, thallium makes up about 2 parts per billion (20 millionths of 1%) of the Earth. I measured thallium concentrations in lavas from intraplate and arc volcanoes, and compiled published data for samples from mid-ocean ridges, intraplate volcanoes, and arcs. I found out that only trace amounts of thallium get mixed into the deep mantle, and overall the mantle contains very little thallium at all. This means it is difficult to use thallium to follow how surface materials get mixed back into the deep mantle. Instead, most thallium stays near the surface, and gets gradually concentrated in continental crust at subduction zones.

Acknowledgements

First, of course, Dr Julie Prytulak, whose remarkable patience has given me the opportunity to learn all sorts of things (only some of them related to geochemistry). Alongside Julie, I am endlessly grateful to Dr Katharina Kressig, Mr Barry Coles, Professor Mark Rehkämper, and everyone else in the MAGIC group during my lengthy sojourn there. Elsewhere, Sarah Humbert is the best subject librarian I could wish for.

Most of my work was done using free/open-source software, starting with my operating system, Debian. I used Python in a variety of ways, including plotting graphs with Veusz. Additional image manipulation was performed with Inkscape and GIMP. I used LibreOffice as an office suite, and LaTeX with free fonts DejaVu, JuniusX and Pazo Math. Workrave mitigated my determined efforts to aggravate my RSI into a flare-up (or several).

This thesis would never have been written without the support of my therapists, Dr Igi Moon and Dr David Leigh-Smith; my GPs, Dr Mark Daniels and Dr Faisal Qureshi; and the various teams at University College Hospital who've looked after me, particularly the Hypermobility Clinic.

More teachers: Ruth McIntyre, who for many years taught me the piano and, less formally, a host of other skills; and Dr Katharine Hutchinson, who let me sit at the back of the classroom during GCSE Geography and dumped A-level textbooks on me in (I presume) the hope that reading about the Coriolis effect for the first time might shut me up for five minutes. (I cannot at this juncture remember whether it worked – it seems very plausible that I was excited enough about it that the entire scheme backfired...)

I wouldn't be writing these words without support from a great many other people, whose names this margin is too small (and my memory too leaky) to contain, much – but by no means all – of it via Dreamwidth. Two, however, I cannot fail to mention: Dr Deepthi Gopal, who has variously entertained and encouraged me for over a decade now, and for whom words do not suffice; and Adam Dinwoodie, who has been unwaveringly gracious about late nights and early mornings and weekends devoted to the mass spec, and, at the last, reading through this entire document with pencil in hand. The fault for any remaining typographical errors and formatting infelicities is entirely mine.

Finally: my mother, Dr Katharina Brett, who nudged me onto this path with a formal introduction to the Gaisbergferner in the late summer of 2008. For all of the obvious things too, of course, and most especially for demonstrating how to reconsider and to say "I was wrong".

This work would not exist without all of them (all of you). Thank you.

Contents

1 Introduction **1**
1.1 Overview . . . 1
1.2 Mantle heterogeneity . . . 3
1.3 Mechanisms of stable isotope fractionation . . . 5
1.4 Thallium as a potential tracer of recycled surface materials . . . 8
1.5 Aims . . . 9

2 Methodology and reference materials **11**
2.1 Reagents . . . 11
2.2 Trace element analysis by ICP-QQQ . . . 12
2.2.1 Sample digestion . . . 12
2.2.2 ICP-QQQ measurement . . . 13
2.3 Analysis by MC-ICP-MS . . . 16
2.3.1 Sample preparation . . . 16
2.3.2 Sample digestion . . . 16
2.3.3 Chromatographic separation . . . 17
2.3.4 MC-ICP-MS isotope ratio measurements . . . 18
2.3.5 MC-ICP-MS Tl concentration estimates . . . 20
2.4 Characterising reference materials for use with Tl . . . 21
2.4.1 Determination of Tl concentrations . . . 22
2.4.2 Determination of Tl isotope ratios . . . 27
2.5 Summary . . . 31

3 Thallium systematics in MORB and OIB **32**
3.1 Introduction . . . 32
3.1.1 Thallium: a potential tracer for recycled materials . . . 33
3.1.2 Sample selection and aims . . . 34
3.2 Results . . . 36
3.2.1 Trace element concentrations . . . 36
3.2.2 Thallium isotope ratios . . . 37
3.3 Discussion . . . 40
3.3.1 Thallium elemental systematics . . . 40
3.3.2 Modelling Tl variations in MORB and OIB . . . 46
3.3.3 Thallium isotopic composition of OIB . . . 52

3.4 Conclusions . . . 56

4 Thallium transfer from slab to wedge: elemental evidence from arc lavas 58

4.1 Introduction . . . 58
4.2 Methods . . . 62
4.3 Results . . . 67
4.3.1 Chalcophile and siderophile elements . . . 67
4.3.2 Lithophile elements (LILE, HFSE and REE) . . . 69
4.4 Discussion . . . 70
4.4.1 Which phase(s) host Tl in the subducting slab? . . . 70
4.4.2 How is Tl transferred from slab to mantle? . . . 75
4.4.3 Thallium accumulation in the continental crust . . . 79
4.5 Summary . . . 83

5 Thallium isotope insight into processes operating in thick continental crust 84

5.1 Introduction . . . 84
5.1.1 Thallium isotope studies in arcs . . . 84
5.1.2 A role for kinetic isotope fractionation? . . . 88
5.1.3 Aims and study location . . . 90
5.2 Methods . . . 94
5.2.1 Sample selection . . . 94
5.2.2 Processing and analysis . . . 95
5.3 Results . . . 95
5.4 Discussion . . . 96
5.4.1 Isotopic composition of Popocatépetl lavas . . . 96
5.4.2 Elemental and isotopic composition of Popocatépetl pumices . . . 108
5.4.3 Thallium isotope variations in pumices . . . 111
5.5 Conclusions . . . 112

6 Outlook 114

6.1 Context . . . 114
6.2 Findings . . . 115
6.3 Future work . . . 117
6.3.1 ‘Invariant’ trace element ratios . . . 117
6.3.2 Vapour distillation of heavy metal isotopes within thick crust . . . 118

Bibliography 121

A List of publications 153

B Supporting data 155

List of Tables

1.1 Proposed mantle components 4

2.1 Anion exchange separation of Tl 17
2.2 Literature reports of ε^{205}Tl for igneous reference materials 22
2.3 Reference materials for which new data are reported 22
2.4 Thallium concentration data for reference materials 24
2.5 Thallium isotope ratios determined for reference materials 27

3.1 OIB localities with published Tl data 35
3.2 Key geochemical data for OIB samples 35
3.3 Elemental co-variation in MORB and OIB 40
3.4 Mineralogical parameters used in melting models 45
3.5 Geochemical parameters used in melting models 45
3.6 Elemental concentrations used in melting models 45
3.7 Mixing parameters for St Helena lavas 56

4.1 The core arc lava dataset 62
4.2 Effective ionic radii of LILE and Tl 69

5.1 Statistical assessment of Tl isotope variation in arc lavas 86
5.2 Isotope results for Popocatépetl samples 97
5.3 Concentration estimates for Popocatépetl leachates and residues 97
5.4 Assessing the calibration of Tl concentration data for DSDP Site 487 99
5.5 Geochemical and petrographic data for Chipiquixtle samples 100
5.6 Geochemical data for Popocatépetl xenoliths 104
5.7 Comparing Tl concentrations of lavas and pumices 109

List of Figures

1.1 Distribution of Tl between terrestrial reservoirs . . . 2
1.2 Distribution of lavas in radiogenic isotope space . . . 4

2.1 ε^{205}Tl determined for the Aldrich Tl solution solution . . . 21
2.2 Comparison of synthetic and geological calibrator materials . . . 23
2.3 Comparison of MC-ICP-MS and ICP-QQQ for determination of Tl concentration . . . 25
2.4 MC-ICP-MS determations of ε^{205}Tl and Tl concentration for reference materials . . . 26
2.5 Variation of Tl with K_2O in reference materials . . . 28
2.6 Influence of digested sample mass on 2sd of ε^{205}Tl determinations . . . 30

3.1 ε^{205}Tl versus Tl concentration for OIB samples . . . 37
3.2 ε^{205}Tl versus MgO (wt%) for OIB samples . . . 38
3.3 Primitive Mantle-normalised trace element plots . . . 41
3.4 Depleted Mantle-normalised trace element plots . . . 41
3.5 Variation of Tl anomaly with Tl abundance . . . 42
3.6 Variation of Tl and Ce/Tl against MgO . . . 43
3.7 Co-varation of Tl and Ce/Tl . . . 44
3.8 Varation of Tl and X/Tl . . . 44
3.9 $D^{Ce}_{cpx/melt}$ values versus CaO in clinopyroxene . . . 47
3.10 MORB melting models . . . 48
3.11 OIB melting models . . . 50
3.12 Process identification plot for Tl/Ce against 1/Tl . . . 51
3.13 Lack of co-variation between ε^{205}Tl and Sr-Nd-Hf-Pb radiogenic isotopes . . . 53
3.14 Evidence for AOC contribution to HIMU-type OIB? . . . 54
3.15 ε^{205}Tl against Tl/Tl* . . . 55
3.16 Mixing models for St Helena lavas . . . 56

4.1 Schematic of plate tectonic processes relevant to the Tl cycle . . . 59
4.2 Variation of Tl concentration with depth in altered oceanic crust . . . 60
4.3 Thallium concentrations in subducting sediments . . . 61
4.4 Variations of Ce/Tl with Tl in arc lavas and OIB . . . 65
4.5 Correlations between Tl and other elemental concentrations . . . 66
4.6 Variations of chalcophile elements and Tl . . . 68
4.7 Variations of lithophile elements and Tl . . . 70
4.8 Phengite retention of Tl in the slab . . . 75

4.9 Reanalysis of Noll et al. (1996) samples . . . 77
4.10 Assessing fluid mobility using arc lavas . . . 78
4.11 Normalised incompatible trace element plots for arc lavas . . . 80
4.12 Comparison of arc lavas and continental crust . . . 81
4.13 Variation of thallium anomaly with crustal thickness . . . 82

5.1 Schematic of plate tectonic processes relevant to the Tl cycle . . . 85
5.2 Map: global subduction zones . . . 86
5.3 Literature Tl isotope data for arc lavas . . . 87
5.4 Literature Tl isotope data for subducting sediments . . . 88
5.5 Map: Trans-Mexican Volcanic Belt . . . 90
5.6 Map: geology of the Popocatépetl Volcanic Complex . . . 91
5.7 Total alkali-silica plots for TMVB and Popocatépetl samples . . . 92
5.8 Incompatible trace element plots for Popocatépetl samples . . . 93
5.9 Tl isotope determinations for reference materials . . . 96
5.10 Thallium isotope ratio data for Popocatépetl samples . . . 98
5.11 The ‘Chipiquixtle trend’ . . . 101
5.12 Thallium concentrations for all Popocatépetl samples . . . 102
5.13 Modelling the Chipiquixtle trend with degassing . . . 103
5.14 BSE images of the skarn xenolith POP-97sk . . . 106
5.15 Modelling the Chipiquixtle trend with mixing . . . 107
5.16 Variation of Tl concentration with indices of differentiation . . . 109

6.1 Modelling ‘invariant’ MORB Ce/Tl systematics . . . 118
6.2 Vapour distillation of heavy metal isotopes . . . 119

Chapter 1

Introduction

1.1 Overview

Unexpectedly large stable isotope variations of thallium (Tl) in terrestrial settings were first reported in 1999. Since this initial discovery, the isotopic composition of thallium has been explored in both extraterrestrial and a variety of Earth materials, from magmas to seawater, and – increasingly – in soils, to assess anthropogenic pollution. This thesis focusses on applying the Tl isotopic system to tracing chemical heterogeneities in magmas generated in the three major melting regimes on Earth: mid-ocean ridge basalts (MORB), ocean island basalts (OIB), and arc lavas. The utility of thallium as a 'passive' tracer in magmatic processes lies in the combination of resolvable isotope fractionation in potential magmatic 'additives' and the simple fact that these exotic inputs often have orders of magnitude higher concentrations of thallium than the ambient mantle from which the majority of the mass of magma is derived. For example, altered oceanic crust (AOC) and pelagic sediments exhibit Tl concentrations up to ∼1 µg/g of potentially isotopically distinct Tl compared to the upper mantle, which has low concentrations of ∼0.3 ng/g of isotopically homogeneous Tl (Fig. 1.1). Slab components such as sediments and altered crust are recycled into the mantle via subduction zones, and are often invoked to explain the geochemical heterogeneity of the mantle as sampled by OIB. In principle, the concentration and isotopic contrasts in Tl systematics have the potential to unambiguously identify even minor contributions of AOC or sediment to the sources of intraplate OIB. I present three major data compilations and three new datasets comprising both elemental and isotope analyses of thallium for reference materials, oceanic basalts, and arc lavas, which I use to investigate cycling of Tl through the silicate Earth.

First, I report Tl isotope analyses and new trace element determinations for 16 internationally-available reference materials, alongside assessment of a compilation of previously-published values for those same materials. To support future investigations, I provide recommended values for Tl isotope ratios and concentrations for the fifteen materials that are homogeneous for Tl (Chapter 2).

I then explore Tl processing in natural igneous settings, from the creation of oceanic crust at mid-ocean ridges to its destruction during subduction. A compiled and filtered dataset of ∼900 analyses of Tl in MORB reveals useful systematics in trace element ratios such as Ce/Tl. Using

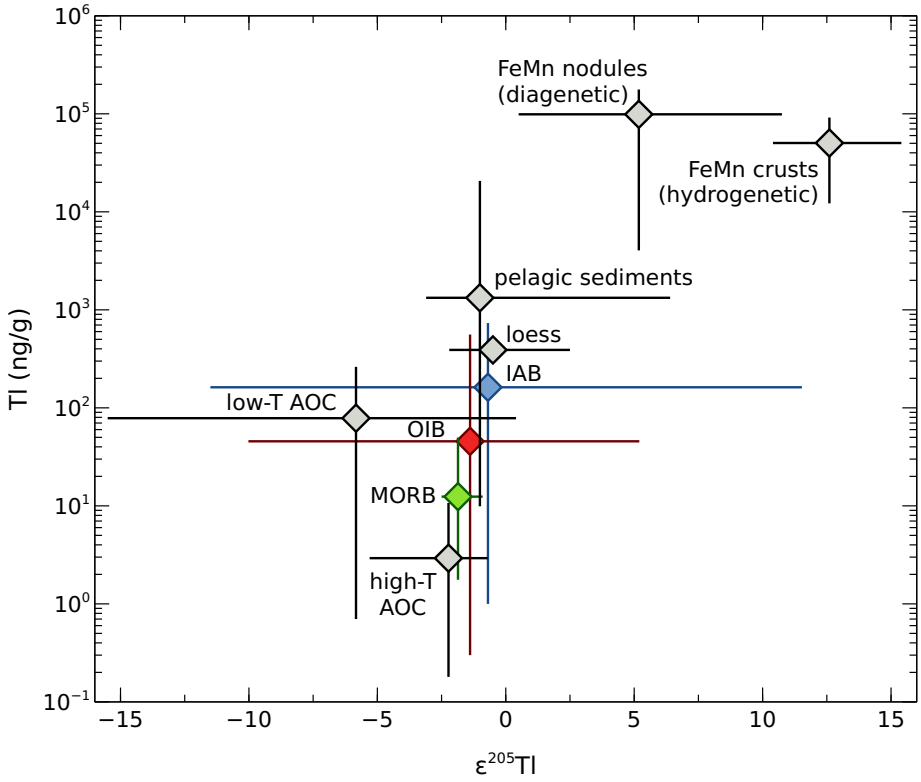


Figure 1.1: Thallium concentrations and isotopic composition ranges reported in the literature for potential subduction inputs (grey symbols; AOC = Altered Oceanic Crust) and igneous products (coloured symbols; MORB = Mid-Ocean Ridge Basalt, OIB = Ocean Island Basalt, IAB = Island Arc Basalt). Loess is considered a proxy for the composition of average continental crust. Bars indicate documented ranges. Data sources for inputs: Blusztajn et al. (2018), Chauvel et al. (2012), Coggon et al. (2014), Cox et al. (2019), Jenner and O'Neill (2012a), Kawabata et al. (2011), Mangler et al. (2019), Nielsen et al. (2005, 2006b,c, 2007), Nielsen and Rehkämper (2011), Nielsen et al. (2014, 2016, 2017a), Prytulak et al. (2013, 2017), Rehkämper et al. (2002), Shu et al. (2017), Yang et al. (2018).

simple melting models, I show that (i) the mantle source of MORB is more depleted in Tl than previously recognised, and (ii) during MORB melting, Tl elemental behaviour is dominated by incompatibility (Chapter 3).

For OIB, new trace element and isotope analyses of 48 samples representing the full range of observed radiogenic isotopic heterogeneity are presented. Although significant variations in Tl isotopic compositions are found in OIB samples, the variations are not systematic with any other geochemical indicators of sediment or AOC contribution to the lavas' sources. Instead, elemental systematics provide the key to understanding this finding: again, simple melting models seeking to reproduce the distinctive Ce/Tl variations in OIB require both highly incompatible Tl behaviour and variable but very low Tl abundances in lava sources. To achieve such low Tl concentrations in OIB sources, Tl must be efficiently stripped from the downgoing slab during subduction instead of being returned to the deep mantle. The observed variations in OIB Tl isotope ratios are best explained through some combination of (i) the contribution of residual, isotopically heterogeneous subducted Tl to OIB source regions, and/or (ii) assimilation of Tl at shallow depths during magma ascent (Chapter 3).

Instead of being recycled into the mantle, Tl is reprocessed through subduction-related arc volcanism. Using a database compiled and filtered from literature Tl concentrations in arc lavas, I find indications that Tl is cumulatively concentrated in continental crust through both magmatic and non-magmatic transfer from the subducting slab (Chapter 4). I selected the arc volcano

Popocatépetl (México) for detailed Tl isotope analysis, providing the first Tl isotopic data for an arc volcano which lies on thick continental crust. I investigated both effusive and explosive materials (i.e. both lavas and pumices) to investigate potential kinetic isotope fractionation. Popocatépetl samples exhibit remarkably uniform Tl isotope ratios that are indistinguishable from those inferred for the upper mantle, with little difference between explosive and effusive eruptions (Chapter 5). The lack of variation at Popocatépetl may be due to either a lack of distinct inputs, or homogenisation of potentially distinct slab components during extensive crustal processing. Such crustal processing and lack of Tl isotopic variation is in clear contrast to oceanic settings, where variations in the Tl isotope ratio of offboard subducting sediment are often reflected in erupted lavas. More study of continental arcs is necessary to determine whether Tl isotopic homogenisation is commonplace, or if Popocatépetl is an exception.

I conclude that the majority of the Earth's Tl is locked into a shallow cycle in (near-)surface environments. Rivers provide input of continental Tl to the marine environment, which is then scavenged by pelagic sediments and deposited in the upper oceanic crust via low-temperature hydrothermal alteration. High-temperature hydrothermal circulation strips Tl from the lower crust, and returns it to the marine environment. During subduction, Tl is efficiently removed from the downgoing slab and is gradually concentrated in continental crust, which then erodes to deliver Tl back to the oceans. Residual Tl recycled into the mantle resurfaces via intraplate volcanism, and will ultimately also be transferred to the continental crust.

1.2 Mantle heterogeneity

The Earth's mantle exhibits significant heterogeneity, revealed through the chemical composition of mantle-derived lavas. Approximately 80% by volume of magma emplaced annually is produced at mid-ocean ridges, where passive upwelling results in ∼10% melting (e.g. Crisp 1984). In contrast, oceanic intraplate magmatism, which generally occurs away from plate boundaries, accounts for ∼5% by volume of annual magma emplacement, resulting from ∼1-4% fractional melts (e.g. Crisp 1984). Compared to mid-ocean ridge basalts, ocean island basalts exhibit considerable geochemical heterogeneity, perhaps best expressed by the well-known global ranges in radiogenic isotopic composition of Sr, Nd, Hf and Pb (e.g. Sun 1980, White and Hofmann 1982, White 1985, Hofmann 1997).

OIB are generally considered to be the surface expression of hot upwelling mantle 'plumes', which may contain material sourced from depths down to the core-mantle boundary (e.g. Morgan 1971, Richards et al. 1989, Duncan and Richards 1991). The chemical composition of OIB has been explained through recycling of surface components into the deeper mantle via subduction (e.g. White and Hofmann 1982, Hofmann 1997, Stracke et al. 2005, Weaver 1991, White 1985, 2015, Zindler and Hart 1986). Surface materials form via a wide variety of processes that cause distinct elemental and isotope fractionation, which may be traced from the surface through subduction to ultimately be expressed in OIB. A classification system in terms of Sr-Nd-Hf-Pb isotope ratios has been developed for OIB, based around the concept of 'mantle components' (e.g. Allègre and Turcotte 1985, White 1985, Zindler and Hart 1986) that mix to form the observed array of

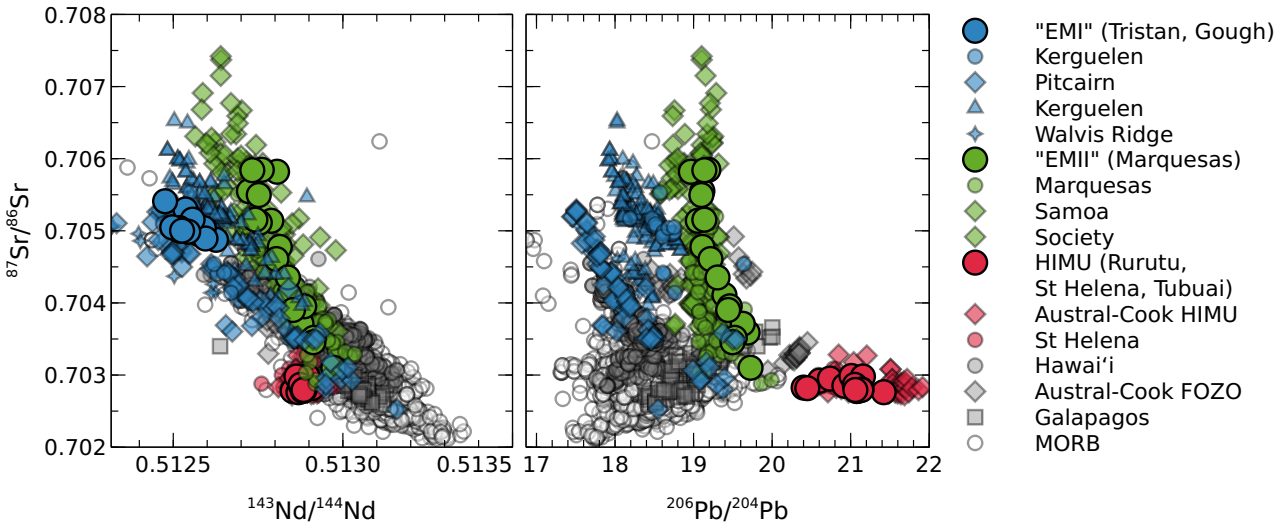


Figure 1.2: Data for radiogenic isotopes in oceanic basalts, highlighting the variations between mantle components. Large symbols: samples for which I report new analyses (Chapter 3). Data from the compilation of Stracke et al. (2003), except large symbols (see Appendix B3.v).

Table 1.1: The 'mantle zoo': a summary of proposed mantle components.

Component	Characteristics
Bulk Silicate Earth (BSE)	Composed of those elements that do not enter the core or atmosphere, theoretically represented in their 'primordial' abundances (Zindler and Hart 1986).
Depleted Mantle (DM)	Unique-to-MORB 'depleted' isotope characteristics: high $^{143}Nd/^{144}Nd$, low $^{87}Sr/^{86}Sr$ and $^{206}Pb/^{204}Pb$; possibly restricted to the uppermost mantle (Zindler and Hart 1986). Also called *Depleted MORB Mantle (DMM)*.
Enriched Mantle (EM)	Characterised by low $^{208}Pb/^{204}Pb$ for a given $^{206}Pb/^{204}Pb$. Historically, low $^{87}Sr/^{86}Sr$ is referred to as 'EMI' and high $^{87}Sr/^{86}Sr$ as 'EMII'. Chauvel et al. (1992) ascribed this difference to the incoroporation of old (>1.5 Ga) pelagic and terrigenous sediments, respectively, but more recent trace element data compilations do not support this subdivision (Willbold and Stracke 2006).
Focus Zone (FOZO) Common (C) Prevalent Mantle (PREMA)	FOZO (also called 'Common'; Hanan and Graham 1996) was proposed by Hart et al. (1992), who argue that DM is rarely a parent to observed mixing arrays between mantle components. Named for the convergence/'focal area' defined by observed arrays within a compositional tetrahedron whose vertices are D(M)M, EMI, EMII, and HIMU. Considered a widespread/common component entrained by mantle plumes. It is suggested to have high ^{3}He; a similar component is designated Primitive He-Enriched Mantle (PHEM) by Farley et al. (1992). PREMA is characterised by $^{143}Nd/^{144}Nd$ around 0.5130 and $^{87}Sr/^{86}Sr$ around 0.7033 (Zindler and Hart 1986). Some authors (e.g. Homrighausen et al. 2018) consider FOZO and PREMA interchangeable terms; others (e.g. Stracke 2012) prefer PREMA.
High μ (HIMU)	Characterised by high μ (= $^{238}U/^{204}Pb$) and unradiogenic Sr. Zindler and Hart (1986) suggest isolation of AOC at 1.5–2.0 Ga as the source, while Chauvel et al. (1992) suggest a three-stage process involving subduction of AOC, storage of the subducted slab within the mantle for ∼2 Ga, and upwelling and melting of slab material together with entrained peridotite.

compositions (Fig. 1.2). An overview of proposed mantle components, termed the 'mantle zoo' by Stracke et al. (2005), is provided in Table 1.1.

However, it is unclear whether mantle components are the result of processes such as sediment recycling, or instead represent physical reservoirs in the mantle that can be directly sampled. For example, geophysical imaging has identified 'large low-velocity shear provinces' in the lowermost mantle. Some researchers argue that these regions consist of compositionally distinct thermochemical piles, with mantle plumes preferentially initiating along their edges (for reviews and discussion see e.g. Jellinek and Manga 2004, Burke et al. 2008, Davies et al. 2012, 2015).

The constraints on the nature and origin of these 'components' provided by radiogenic isotopes can be ambiguous. Radiogenic isotope ratios are dependent on the initial mantle concentrations of parent and daughter isotopes, the partitioning of parent and daughter between melt and minerals, the number of parent-daughter fractionations that have occurred, and the time elapsed between parent-daughter fractionation events. The inherent difficulty of placing unique constraints on all of these factors means that arriving at a single unambiguous interpretation of radiogenic isotope data is challenging. Within this classification framework, additional constraints can be established through identifying correlations between radiogenic isotope systems (used to define mantle components) and non-radiogenic geochemical tracers, e.g. elemental ratios and stable isotope systematics. Such independent constraints help to reduce the number of routes via which it is possible to generate the chemical signatures of a given lava.

The combination of time-dependent radiogenic isotopic composition and time-independent variables can be used to explore the origin of lavas from any tectonic setting. For instance, arc lavas also display significant radiogenic isotopic heterogeneity. In many cases it has been possible to link the chemical composition of arc lavas with that of sediments subducting directly outboard of the active arc. Perhaps the most compelling demonstration of this connection is the presence in some arc lavas of significant ^{10}Be, which is only produced via cosmogenic spallation in the atmosphere (Brown et al. 1982, Tera et al. 1986). Further, the short half-life of ^{10}Be ($\sim$1.5 Ma) provides tight constraints on the timescale over which sediment must be subducted, incorporated into a mantle wedge melt, and then erupted.

In this thesis, I combine the compilation and filtering of existing datasets with new analyses of well-characterised samples. New data for the thallium isotopic compositions of carefully selected OIB (Chapter 3) and lavas from a continental arc (Chapter 5), in conjunction with elemental thallium abundances, are used to evaluate existing interpretations of chemical heterogeneity in the mantle, and to assess the utility of Tl and Tl stable isotopes as a tracer of mantle recycling.

1.3 Mechanisms of stable isotope fractionation

Stable isotopic compositions are a well-established component of the geochemical toolbox. By 1954, stable isotope fractionations had been reported for hydrogen, boron, oxygen, silicon, sulphur and germanium (see Allenby 1954 and references therein). Continuing improvements in analytic capability have enabled the resolution of small fractionations of stable isotopes in elements spanning the periodic table. The first issue of *Reviews in Mineralogy and Geochemistry* devoted to stable isotopic compositions in 'non-traditional' stable isotope systems was published

in 2004 (Johnson et al. 2004), featuring work on the elements lithium, magnesium, chlorine, calcium, chromium, iron, copper, zinc, selenium and molybdenum. A second issue of *Reviews in Mineralogy and Geochemistry* was published in 2017 (Teng et al. 2017), summarising more recent stable isotopic work for these systems as well as stable isotopes of the elements silicon, nickle, geranium, mercury and uranium, in addition to a chapter devoted to thallium isotopes (Nielsen et al. 2017b). Broadly, stable isotope fractionation can arise from either mass-dependent or mass-independent processes.

Mass-dependent equilibrium isotope fractionation

Theoretical calculations performed by Urey (1947) and Bigeleisen and Mayer (1947) predicted the magnitude, direction and temperature relationships of equilibrium fractionation of light stable isotopes using a simplified thermodynamic model.

The classical thought experiment models a simple diatomic molecule as an harmonic oscillator. Qualitatively, at short interatomic separations r the bond energy E is extremely high, corresponding to atomic repulsion. For large r the atoms no longer interact, and E is independent of r. At intermediate distances, an energy well is present, corresponding to bond formation. However, within the well available energy states are quantized rather than continuous. They are described by the equation

$$E = \frac{hv(n+1)}{2}$$

where n is a positive integer describing the atomic energy level (the principal quantum number), h is Planck's constant, and v is the vibrational frequency. In the ground state ($n = 0$), bond energy E is always greater than 0, but for any given element is lower for bonds involving heavier isotopes than bonds involving lighter isotopes. This is because the vibrational frequency v depends on the mass of the atoms involved according to

$$v = \frac{1}{2\pi}\sqrt{\frac{k_f}{\mu}}$$

For a diatomic molecule with atoms of mass m_1 and m_2, the reduced mass $\mu = \frac{m_1 m_2}{m_1+m_2}$. The force constant of the bond, k_f, is controlled only by electronic interactions between atoms in the harmonic approximation. The mass-dependence is obvious in the expanded equation for the energy levels of a simple harmonic oscillator, which is

$$E = \frac{h(n+1)}{4\pi}\sqrt{\frac{k_f(m_1+m_2)}{m_1 m_2}}$$

In more complex systems, such as a magma containing both crystals and exsolved volatiles, it is possible to predict which phase will concentrate heavier isotope(s) of interest at equilibrium. This requires considering the equilibrium constant in terms of vibrational partition functions (Q) for each species:

$$Q = \sum_n g_n^{-E_n/k_B T}$$

where E_n is the n^{th} energy level, g_n describes the probability that molecules will occupy the n^{th} energy level, k_B is Boltzmann's constant, and t is the temperature in Kelvin.

The temperature dependence of this expression is of great importance in natural systems. As T increases, the partition function for each species approaches one, and so the difference between partition functions decreases. As a result, the magnitude of isotope fractionation under equilibrium conditions increases as (i) T decreases, and (ii) the relative mass difference between the isotopes of interest increases.

Mass-dependent kinetic isotope fractionation

Under equilibrium conditions both forward and reverse reactions proceed at the same rate, favouring a final system state with the lowest overall energy. However, where kinetic effects dominate – for example, in open systems where products are removed as they form – it is (broadly) the lowest-energy *reactions* that determine the isotopic composition of the products. For example, in the case where the reactants must pass through a high-energy transition state, the lighter isotope preferentially accumulates in the product. This is because isotopically lighter compounds have a higher ground-state energy, such that less energy input is required in order to reach the transition state than for isotopically heavier reactants (for more detailed discussion see e.g. Bigeleisen 1949, Schauble 2004).

Again, both temperature and mass affect the extent of enrichment. At higher temperatures, a greater proportion of reactants exist in excited energy states, reducing the effect of differences in ground-state energies. As with equilibrium fractionation, lower temperatures and greater differences in relative mass promote the development of larger isotope fractionations. Kinetic fractionation in geological applications is commonly associated with either diffusion or volatility. For example, it has been shown that ^{6}Li and ^{7}Li diffuse at different rates in pyroxene, resulting in marked isotopic heterogeneity on the crystal scale (e.g. Jeffcoate et al. 2007). Similar effects are seen for Fe and Mg isotopic diffusion, documented both within olivine grains and between (or along thermal gradients across) synthetic melts (e.g. reviews of Teng 2017, Dauphas et al. 2017). The evaporation of an element can also cause kinetic fractionation, and the more volatile the element, the more likely it is that resolvable fractionations will develop. Thallium is a markedly volatile element, and the effect of volcanic degassing has been explored by Baker et al. (2009) and Nielsen et al. (2021). In Chapter 5, pumices produced by explosive eruptions of Popocatépetl volcano (México) are analysed to investigate the potential effects of kinetically-induced isotope fractionation.

Mass-independent isotope fractionation: nuclear volume effect

In general, the contribution of mass-independent processes to the development of stable isotope fractionations is negligible compared to the effects of mass-dependent processes. Mass-independent processes that create identifiable isotope fractionations in nature include photochemical reactions (e.g. oxygen isotopic compositions measured for refractory inclusions in the Allende meteorite; Clayton et al. 1973, Clayton 2002, Lyons and Young 2005), spin-forbidden reac-

tions (e.g. the formation of ozone; Thiemens and Heidenreich III 1983, Mauersberger 1987, Gao and Marcus 2001), and nuclear volume effects.

The importance of the nuclear field shift effect (NFSE) in causing stable isotope fractionation of very heavy elements has been well-recognised for a quarter of a century (e.g. Bigeleisen 1996a,b). Qualitatively, when the nucleus is so large that it can no longer be approximated as a point charge, isotopes with larger nuclear volumes (typically the more neutron-rich isotopes) will preferentially enter more oxidised phases with lower electron density at the nucleus. Consequently, the magnitude of NSFE-driven fractionations decreases as atomic mass decreases. As with other forms of stable isotope fractionation, the NFSE is temperature-dependent, with the magnitude of fractionations decreasing as temperature increases. Schauble (2007) performed calculations to estimate the equilibrium stable isotope fractionation of Hg and Tl including the effects of the nuclear volume term, accounting for observed fractionations of stable Tl and Hg of up to 3‰ at room temperature. While subsequent work suggests that the anomalous fractionation of Hg is instead due to mass-independent kinetic processes (Blum and Bergquist 2007, Berquist and Blum 2009), the NFSE has been proposed as a contributing factor to stable isotope fractionations observed for a wide range of elements with masses >100 a.m.u. (e.g. Moynier et al. 2013, Dauphas and Schauble 2016), with recent calculations suggesting that these effects might also be detectable for Pb stable isotopes (Yang and Liu 2015). The large range of stable Tl isotope fractionation in terrestrial surface materials (approximately -15 to +15) is, at present, best explained by the NFSE.

1.4 Thallium as a potential tracer of recycled surface materials

First isolated in 1861 (Crookes 1862, Lamy 1862), thallium is one of the highest atomic mass naturally-occurring elements. A volatile, highly incompatible trace metal, Tl has two oxidation states in addition to the neutral charge state. Univalent thallium (Tl^{+}) has a large ionic radius (1.49 Å), comparable to that of the alkali metals potassium, rubidium and caesium, and can therefore substitute for these elements in mineral crystal structures (Shaw 1952, Shannon and Prewitt 1969, Shannon 1976). Trivalent thallium (Tl^{3+}) can also exist on Earth under highly oxidising conditions (Batley and Florence 1975, Vink 1993), such as in the structure of the ferromanganese (Fe–Mn) mineral hexagonal birnessite (Peacock and Moon 2012, Nielsen et al. 2013).

Thallium has two stable isotopes with mass numbers 203 (29.5%) and 205 (70.5%). Because the relative difference in mass between thallium's two stable isotopes is less than 1%, it was historically assumed that there would be little mass-dependent thallium isotope fractionation in nature. Resolvable Tl isotopic differences were therefore thought to arise solely due to decay of the relatively short-lived radioisotope ^{205}Pb to ^{205}Tl, with a half-life of ∼15 Ma. Initial investigations (Anders and Stevens 1960, Ostic et al. 1969, Huey and Kohman 1972, Chen and Wasserburg 1987, 1994) thus aimed to provide constraints on the delivery and distribution of ^{205}Pb during the early stages of solar system formation by tracking differences in Tl isotope ratios, but were unable to resolve variations for a large number of extraterrestrial and some selected terrestrial

materials. This was for the most part due to the uncertainties (>2‰, 2sd) associated with TIMS measurement of Tl (see Summary in Nielsen et al. 2017b).

The development of multicollector ICP-MS (MC-ICP-MS) allowed for higher-precision Tl isotope ratio measurements, with precisions >3–4 times better than those achieved by the best TIMS protocols then reported (0.1–0.2‰, 2sd; Arden 1983). Using these new measurement principles, Rehkämper and Halliday (1999) analysed a number of terrestrial samples to define the baseline terrestrial Tl isotopic composition for the purpose of comparison with extraterrestrial materials, again assuming that variations in extraterrestrial materials would reflect early ^{205}Pb decay. They unexpectedly discovered large variations in Tl isotope ratios for terrestrial materials, reported relative to the Tl reference material NIST SRM 997 (defined as 0) using ε-notation:

$$\varepsilon^{205}\mathrm{Tl} = \frac{\left(\frac{^{205}\mathrm{Tl}}{^{203}\mathrm{Tl}}\right)_{\mathrm{measured}} - \left(\frac{^{205}\mathrm{Tl}}{^{203}\mathrm{Tl}}\right)_{\mathrm{standard}}}{\left(\frac{^{205}\mathrm{Tl}}{^{203}\mathrm{Tl}}\right)_{\mathrm{standard}}} \times 10^4$$

The natural range of Tl stable isotope variations documented on Earth is approximately 30 $\varepsilon^{205}\mathrm{Tl}_{\mathrm{SRM997}}$ units ('εunits'; see review in Nielsen et al. 2017b). With the exception of volcanic fumaroles and some meteorites (Nielsen et al. 2006b, Baker et al. 2009, 2010b), these variations are best explained by the NFSE (§ 1.3). As of 2018, there were more than thirty studies utilising Tl isotope ratio variations to investigate the natural environment. The utility and versatility of the system lie in the large isotope ratio differences and relatively high concentrations (of the order of µg/g) associated with low-temperature environments, in contrast with very low concentrations and negligible isotope ratio differences in mantle-derived lavas (see review of Nielsen et al. 2017b, Prytulak et al. 2017; Fig. 1.1).

Historically used primarily as a poison, applications of Tl now include investigations of extraterrestrial materials (Nielsen et al. 2006a, Andreasen et al. 2009, 2012, Baker et al. 2010b, Palk et al. 2011); riverine and marine fluxes (Rehkämper et al. 2002, Nielsen et al. 2004, 2005, 2006c, Rehkämper and Nielsen 2004, Owens et al. 2017); anthropogenic mobilisation of Tl (Nriagu 1998, Xiao et al. 2003, 2004, Peter and Viraraghavan 2005, Kersten et al. 2014, Vaněk et al. 2018); ore exploration (Ikramuddin et al. 1983, Baker et al. 2010a, Hettmann et al. 2014b,a, Fitzpayne et al. 2018); and tracing contributions to the source regions of igneous materials (Nielsen et al. 2006b, 2014, 2015, 2016, Prytulak et al. 2013, 2017, Shu et al. 2017, Blusztajn et al. 2018).

1.5 Aims

Thallium isotopic and elemental systematics have great potential as a tracer of sediment and altered oceanic crust as they are recycled through subduction and igneous processes, in addition to applications in ore exploration and environmental monitoring. This thesis investigates how Tl is distributed and cycled through the solid Earth alongside accompanying Tl stable isotope fractionations. Published work is listed in Appendix A.

In Chapter 2, I provide assessment of, and analyses and recommended values for, a variety of internationally-available igneous reference materials, to support acquisition of robust Tl isotope and elemental data for this and other research.

In Chapter 3, I use simple melting models to estimate the concentrations of Tl in MORB and OIB source regions. I present new Tl isotope and trace element data for 48 OIB samples spanning the range of known mantle geochemical variation. This dataset allows me to explore whether Tl isotope systematics can be used to trace recycling of sediment and altered oceanic crust from the surface into OIB source regions.

In Chapter 4, I compile trace element data, including Tl, for subduction-related lavas from around the world. I seek to constrain both the proportion of Tl that is removed from the downgoing slab during subduction processing, and the mechanisms by which Tl is transferred.

In Chapter 5, I use Tl elemental and isotopic systematics at Popocatépetl volcano, México, to investigate the processing of Tl in igneous systems within thick, mature continental crust. I also evaluate potential kinetic isotope fractionation by examining both effusive and explosive materials.

Chapter 2

Methodology and reference materials

Much of this chapter has been published, following peer review, as:

> A. Brett, J. Prytulak, S. J. Hammond. and M. Rehkämper. (2018) Thallium mass fraction and stable isotope ratios of sixteen geological reference materials. *Geostandards and Geoanalytical Research* **42:**339-360. doi:10.1111/ggr.12215

This chapter may be used for non-commercial purposes in accordance with Wiley Terms and Conditions for Use of Self-Archived Versions.

The analytical procedures used in this thesis are presented in this chapter, alongside data obtained for reference materials, including some data first published in Prytulak et al. (2017) and Brett et al. (2021). AB performed digestions, chemistry, and dilutions for reference material samples with guidance from JP, with contributions from M. Mangler, B. Mitchell-Bunce, S. Munson and F. Wei to digestions for trace element analysis. AB carried out Tl isotope analyses with guidance from JP and Barry Coles. SJH (Open University) performed trace element analyses. NIST SRM 607 was provided by B. Charlier. Brett et al. (2018) was primarily written by AB, with details of ICP-QQQ techniques contributed by SJH.

Three new datasets are presented in this thesis, consisting of trace element and Tl isotope analyses for reference materials (§ 2.4, Brett et al. 2018) and 48 OIB samples (Chapter 3, Brett et al. 2021), and Tl isotope analyses for 23 samples from Popocatépetl volcano, México (Chapter 5). All samples were processed using the same techniques, detailed in the first sections of this chapter. Results obtained for analyses of reference materials are then described. All data obtained over the course of this thesis are given in Appendix B.

2.1 Reagents

All sample digestions and chemical separations were carried out in the MAGIC Laboratories, Imperial College London. Purified water from a Milli-Q® (Merck, Darmstadt, Germany) system (resistivity 18.2 MΩ.cm) was used throughout. HNO_3 (concentrated, ∼14 M) and HCl (6 M) were

purified once by sub-boiling distillation in quartz or PTFE stills, whilst ultrapure HF (47–51% ≈ 24 M) was either purchased from SCP Scientific or prepared in the laboratory from reagent-grade acid by a single distillation step in a PTFE still. Saturated bromine water was prepared by the equilibration of high-purity bromine with purified water in a 125 ml PTFE bottle. Dilute HNO_3 and HCl containing 1–3 vol% saturated bromine water were prepared by adding the appropriate volume of bromine water to the acid immediately before use. A solution of 5–6 wt% SO_2 in 0.1 M HCl ("0.1 M HCl–5% SO_2") was used for the reductive elution of Tl from anion-exchange resin. This solution was prepared in a 250 ml PTFE bottle containing 100–200 ml 0.1 M HCl, through which was bubbled gaseous SO_2 from a small pressurised cylinder containing liquefied SO_2 (purchased from Sigma-Aldrich, Taufkirchen, Germany). The solution was reweighed at regular intervals until the required amount of SO_2 had dissolved in the acid. After preparation, the reagent was stored for a maximum of 1 week for reuse then discarded, as SO_2 oxidises to form sulphate. Finally, a 0.1 M HNO_3–0.1 vol% H_2SO_4 solution used for sample dilution and subsequent mass spectrometric measurement was made up using distilled-grade concentrated H_2SO_4 (96 vol%).

2.2 Trace element analysis by ICP-MS/MS ('ICP-QQQ' or 'triple quad')

2.2.1 Sample digestion

Tabletop digestions

Between approximately 50 and 100 mg of each sample was weighed accurately into PFA vials, to which a 3:1 mixture of HF (24 M):HNO_3 (14 M) was added. The solutions were treated ultrasonically for 20 minutes after initial addition of the acids, then placed on a hot plate at 160 °C for at least 24 hours. Sample solutions were further treated ultrasonically for 20 minutes twice during the initial digestion. Solutions were then evaporated to near dryness, redissolved in 2 ml of HCl (6 M) and refluxed at 120 °C for at least 24 hours. The solutions were next evaporated to complete dryness at 120 °C, redissolved in 1 ml of HNO_3 (14 M) and then evaporated at 180 °C. The last step was repeated a minimum of three times, or until the colour of the residue changed from white to brown, which indicates that fluorides formed from the initial HF digestion have been destroyed. Samples were then transported to the Open University as HNO_3 (14 M) solutions and transferred into acid-cleaned PP bottles, where an appropriate amount of purified H_2O was added to each to achieve a 1000-fold dilution of the original sample mass in an HNO_3 matrix (0.14 M).

Bomb digestions

Refractory phases such as zircon that may not be completely digested using hot plate dissolution alone. Although thallium is not expected to reside in phases such as zircon, we investigated the potential role of refractory phases on Tl concentration and isotope ratio by performing additional bomb digestions of selected samples. To this end, approximately 50 mg of powder was accurately weighed into PFA hexagonal bomb vials (Savillex®), to which was added ∼0.2 ml HNO_3 (14 M)

and 1.5 ml HF (24 M). The prepared bombs were sealed tightly and placed in an oven at 150 °C for five days. Subsequent sample processing was identical to that for hot plate digestions of silicate materials.

2.2.2 ICP-QQQ measurement

Trace element concentration determinations including thallium were undertaken at the Open University, UK, with an Agilent 8800 ICP-QQQ-MS inductively coupled plasma-mass spectrometer. Sample solutions were aspirated using a quartz microflow nebuliser with an uptake rate of 0.5 ml min^{-1}. Machine sensitivity was on the order of 1–5 $\times$ 10^7 cps per µg ml^{-1}, depending on the element. The Agilent 8800 has a collision/reaction cell (Octopole Reaction System, ORS), which separates two quadrupoles. The first quadrupole was used as a mass filter to ensure that only specific masses entered the ORS; reactions could therefore be targeted to remove on-mass interferences. The second quadrupole could be used in either mass shift or on-mass mode, depending on whether the analyte or interference reacts with the gas. We employed two collision/reaction gas configurations to undertake measurements: (i) no gas in the collision cell, and (ii) O_2 gas in the cell. Thallium was determined in the 'no gas' mode, with oxide levels (measured as CeO^+/Ce^+) kept below 1% and double-charged species (Ce^{2+}/Ce^+) at 1.6%. All other elements were similarly measured except for most rare Earth elements (La, Pr, Ce, Nd, Sm, Gd, Ho, Tb, Dy, Er, Yb, Lu), which were reacted with O_2 gas for a mass shift measurement.

Selection of calibrators

Calibrator materials were run at the beginning of each measurement session. Additionally, an internal solution standard consisting of Be, Rh, In, Tm, Re and Bi was added online to all standard and unknown solutions to monitor and correct instrumental drift. Drift was further monitored every five unknown measurements with a measurement block consisting of BIR-1 (a separate digestion to that used in the initial calibration block), HNO_3 (0.3 M), and a repeated unknown sample.

The USGS reference materials (RMs) BIR-1, BHVO-2 and AGV-1 were chosen as calibrators for trace element determination of Tl in particular. In addition, RMs W-2 and DNC-1 are used for calibration: for most trace elements (not including Tl), these are well-characterised materials. BIR-1, BHVO-2 and AGV-1 were selected because they are commonly used for analysis of other isotopic systems (that is, they are well characterised), and span three orders of magnitude of Tl concentration. Only AGV-1 has a USGS listed Tl concentration (0.34 µg/g, recommended value; no uncertainty given). All three RMs have preferred GeoReM (Jochum et al. 2005) Tl concentration values, per Jochum et al. (2016): BIR-1, 2.1 ± 0.7 ng/g (n = 13); BHVO-2, 22.4 ± 1.5 ng/g (n = 28); AGV-1, 337 ± 31 ng/g (n = 10) (95% confidence intervals). Specifically, we used Tl concentrations of: BIR-1, 1.6 ng/g (n = 12); BHVO-2, 22 ng/g (n = 32); and AGV-1, 349 ng/g (n = 13), determined using our own compilation of reported concentration data (Appendix B2.i). All values are within error of the GeoReM recommended values.

We note that both AGV-1 and BHVO-2 exhibit heterogeneity seen in Pb isotope ratio and concentration results, which have been provisionally attributed to contamination during processing

using steel mortar and pestle (Weis et al. 2006). It has long been suggested that the similarity between properties of Tl and Pb might result in similar behaviours in some geochemical contexts (Lamy 1862), but as Tl has historically not been routinely analysed, it is not clear whether Tl systematics in these RMs correlate with Pb heterogeneity. We therefore used our compilation of reported Tl concentrations in these RMs (Appendix B2.i) to identify and characterise potential Tl heterogeneity in our calibrators.

We found no identifiable heterogeneity for AGV-1 (n = 13, RSD = 15%). Reported BIR-1 Tl concentration results have a notably high RSD (34%); however, this material has a very low Tl concentration and is therefore analytically challenging. Consequently, determining whether the high uncertainty reflects powder inhomogeneity or analytical error is not straightforward, and BIR-1 remains the best-characterised candidate for a low concentration Tl calibrator. For BHVO-2, there is some variation in reported Tl concentration between studies: of the 36 reported measurement results (mean concentration value of 28 ng/g; RSD = 58%), a small minority (n = 4) have a mean of 65 ng/g (RSD = 7%). The remaining measurement results give a mean of 22 ng/g (RSD = 20%). For comparison, BHVO-1 has a reported Tl concentration of 46 ng/g (RSD = 19%, n = 25). The four anomalous reports of Tl concentration in BHVO-2 (Bouman et al. 2004, Deegan et al. 2012, Deng et al. 2013, Søager et al. 2015) are suggestive of either confusion between the two generations of the BHVO RM, or of possible contamination.

For many trace elements, BHVO-1 and BHVO-2 have USGS listed concentration values that are within error of one another. Elements for which this is not true, where determined, can be used to positively identify instances of confusion between the two generations. For the majority of these elements (notably Sc, Cr, Cu, Zn, Y, Zr and Hf as well as Tl), the concentrations reported by Bouman et al. (2004) as BHVO-2 are consistent with listed values for BHVO-1 and disagree with listed values for BHVO-2; the reported Tl concentration is 59 ng/g. Only USGS listed BHVO-2 values are quoted as reference concentrations for trace element determinations, and these do not include a Tl concentration; however, the same paper employs BHVO-1 as a Li isotope RM, suggesting a source of possible confusion. Similar is true for the trace element concentrations reported by Deng et al. (2013), and in this case, it appears that the quoted reference Tl concentration is not for BHVO-2, but instead that given for BHVO-1 by Govindaraju (1994). Deng et al. (2013) report a Tl concentration of 66 ng/g for BHVO-2.

For the two remaining anomalous reports of Tl concentration, the trace element pattern is less suggestive of confusion between generations of this reference material. Trace element concentrations reported by Deegan et al. (2012) are on average 10% higher than USGS listed values (2–20% higher), with the exception of Ta, which is in agreement with the listed value. Two Tl concentrations are reported for BHVO-2, of 60 and 80 ng/g. Søager et al. (2015) used reference values provided by the Hamburg laboratory that performed sample analysis (pers. comm., 2017) and report a Tl concentration for BHVO-2 of 63 ng/g. These Tl concentrations are anomalously high for BHVO-2, but are consistent with the listed and compiled values for BHVO-1; however, there is no compelling indication that in these cases confusion between the two generations of powder occurred. These results appear to be best explained by some combination of analytical uncertainty and powder contamination.

The available data therefore suggest that if BHVO-2 suffers from inhomogeneity with respect to Tl concentrations, it is not a widespread or common problem. Furthermore, there are very few generally available igneous RMs with low Tl concentrations. BIR-1, with a Tl concentration an order of magnitude lower than BHVO-2, is employed as a calibrator in this study, but as noted presents analytical challenges. The Geological Society of Japan provides three basalt RMs, but all have higher Tl concentrations than BHVO-2: JB-2 has the lowest Tl concentration, reported as 34 ± 3.6 ng/g (Jochum et al. 2016). As such, BHVO-2 is the best widely available, well-characterised choice for a low-Tl calibration material.

Trace element concentrations were generally determined with the chosen geological calibrating RMs (AGV-1, BHVO-2, BIR-1). However, partially separated mineral RMs have unusual and, in some cases, extreme trace element concentrations. For example, a Tl concentration of 16 µg/g was reported for the biotite reference material Mica-Fe (Baranov et al. 2002, Dampare et al. 2008, Parks et al. 2014), well outside the Tl concentration range of the calibrators. Linear extrapolation of the calibration curve is a potential source of error for the reported concentrations of such high-Tl samples. Two approaches that are potentially suited to address this concern are (i) isotope dilution ICP-MS (ID-ICP-MS), and (ii) the use of synthetic calibrating reference solutions with known, high Tl concentrations. The ID-ICP-MS technique was not deemed appropriate, due to the lengthy preparation times required and the possible powder heterogeneity of at least some samples. In other words, obtaining highly accurate trace element concentration data for a single dissolution of a potentially heterogeneous material is of limited utility. In contrast, the use of synthetic calibrating standards requires significantly less preparation time. However, it is known that the sample matrix can affect the ionisation potential of elements during analysis and, consequently, concentration measurement results (e.g. Brown and Milton 2005). To the best of our knowledge, it has not previously been established whether using synthetic calibrators result in any systematic effect on measured Tl concentrations. Therefore, for one measurement session, a pure internal trace element reference solution (made from single element plasma grade standards from Alfa Aesar) was employed as a synthetic calibrating reference solution to assess whether this procedure produced Tl concentration data that differed significantly from those obtained with geological calibrators.

Reproducibility

Typical precisions reported for Tl in the literature are on the order of 5–15% RSD, compared with <5% RSD for commonly determined trace elements. Precision is normally deemed excellent if RSDs are <3%, or good if 3–7%. For the majority of analyses over the course of this project, RSDs <7% were achieved.

2.3 Analysis by MC-ICP-MS

2.3.1 Sample preparation

Between 25 and 350 mg of pre-powdered sample was accurately weighed into PFA vials (Savillex®). Target masses were chosen based on either known or estimated concentration of Tl in the sample, with very approximate preliminary estimates of concentration based on the widespread co-variation of Tl with K_2O.

Thallium can be concentrated in secondary clays and ferromanganese coatings. Therefore, for some powders leaching experiments were performed to assess possible effects of secondary, low-temperature alteration processes on Tl isotopic composition. The leaching protocol followed the cold acid leaching of Weis and Frey (1991). Approximately 10 ml 6 M HCl was added to 100–300 mg of a sample powder, and the suspension was ultrasonicated for 30 minutes. After settling for at least 30 minutes, the leachate was drawn off, and a further ∼10 ml 6 M HCl was added to samples, which were then ultrasonicated again for 20–30 minutes. This process was repeated until the leachate ran clear (a minimum of 3 cycles), and was then repeated a further 2 times with purified water in place of HCl. In some cases leachate was discarded, but for most samples leachates were combined in a separate PFA vial. Leached powders and leachates were then evaporated, digested, separated and measured in the same manner as unleached powders.

2.3.2 Sample digestion

Tabletop digestion of silicates

The majority of digestions were performed on a tabletop hot plate (quoted temperatures are the hot plate temperature setting, unless otherwise specified) at 140 °C for 1–3 days, in an initial mixture of 3 ml HF (24 M) and ∼0.3–0.5 ml HNO_3 (14 M). Samples were then evaporated to near (rather than total) dryness, to minimise formation of insoluble fluorides (Croudace 1980, Yokoyama et al. 1999); taken up in ∼1 ml of HNO_3 (14 M); and evaporated to dryness at 180 °C at least three times, to destroy any fluorides formed and to evaporate SiF_4.

Tabletop digestion of non-silicates

Sulphide samples (Meggen pyrite and the massive magmatic sulphide OREAS 14P, reported in Kersten et al. 2014 and Brett et al. 2018, respectively) were digested on a hot plate at 130 °C for a minimum of 12 hours in ∼5 ml HNO_3 (3 M), following the protocol of Nielsen et al. (2011). Samples were then evaporated to near dryness at 155 °C and redissolved in 12 ml HCl (1 M). The solution was then centrifuged, and detrital residue was discarded.

Bomb digestions

Selected samples underwent bomb digestion, following the protocol described in § 2.2.1.

Table 2.1: Anion exchange separation of Tl (adapated from Nielsen et al. 2004)

		Volume (ml)	
Step	Eluent	Stage I	Stage II
Load resin	AG® 1-X8 (200–400 mesh) in 0.1 M HCl	1	0.15
Condition	0.1 M HCl–5 wt% SO_2	1 + 10	0.1 + 1.5
Condition	0.1 M HCl	1 + 10	0.1 + 1.5
Condition	0.1 M HCl–1 vol% Br_2	1 + 3 + 1	0.1 + 0.3 + 0.3 + 0.3
Load sample	1 HCl–3 vol% Br_2		
Elution (matrix)	0.5 M HNO_3–3 vol% Br_2	1 + 1 + 1 + 5 + 10	0.1 + 0.1 + 0.1 + 1.5
Elution (matrix)	2 M HNO_3–3 vol% Br_2	1 + 1 + 1 + 4 + 10	0.1 + 1.5
Elution (matrix)	0.1 M HCl–1 vol% Br_2	1 + 1 + 1 + 4 + 10	0.1 + 1.5
Thallium elution	0.1 M HCl–5 wt% SO_2	1 + 1 + 1 + 3 + 9 + 1	0.1 + 1.5

2.3.3 Chromatographic separation

In preparation for chromatographic separation, samples were redissolved and evaporated once from 4 ml HCl (6 M) at 120 °C; redissolved in 2 ml HCl (6 M) and refluxed at 120 °C for a minimum of 12 hours; and finally made up to a 12 ml HCl (1 M) solution subsequently used to load into the first separation column. The final loading solution of 12 ml HCl (1 M) for column chromatography was refluxed at 140 °C for a minimum of 12 hours. Sample solutions were cooled, and 400 µl of saturated Br_2 water was added, then left for a minimum of 3 hours to ensure complete oxidation of thallium to its Tl^{3+} state.

Separation of the Tl fraction from sample matrices largely follows the two-stage ion-exchange procedure devised by Rehkämper and Halliday (1999) and refined by Nielsen et al. (2004), as described in Table 2.1. The separation technique utilises the two oxidation states of thallium. Oxidised Tl^{3+} adsorbs much more strongly to anion resins than Tl^{+} under a variety of conditions, with a general decrease in distribution coefficients with increasing HCl concentration (Kraus et al. 1954). Experimental work by Horne (1958) established that at a temperature of 25 °C the distribution coefficient of Tl^{3+} on Dowex®1-X8 from aqueous HCl solutions (10^{-3} to 2 M) has values of $D \geq 10^5$. Under identical conditions, the distribution coefficient for Tl^{+} is much smaller; the maximum value ($D = 10^3$) occurs for 1 M HCl and decreases rapidly with small variations in HCl concentration. Horne (1958) also observed that adsorption of Tl^{3+} onto Dowex®1-X8 from HBr media was too strong to be reliably measured. The ion-exchange procedure thus employs HCl (at concentrations $\leq$2 M) and HNO_3 admixed with 1–3 vol% saturated bromine water for sample loading and elution of major and trace elements, to ensure that all Tl remains strongly adsorbed to the resin as Tl^{3+} complexed with chloride and trace bromide present in the bromine solution.

Collection of the thallium fraction was accomplished using a solution of 0.1 M HCl–5% SO_2 (see § 2.1). This reduces Tl^{3+} to Tl^{+}, whereby the latter can be readily eluted from the column. Yields of >95% are routinely achieved (Nielsen et al. 2004, Rehkämper and Nielsen 2004), with no isotope fractionation of the separated Tl with respect to the original sample (Rehkämper et al. 2002, Nielsen et al. 2004).

For these experiments, AG®1-X8 (200–400 mesh) anion resin was used. The resin was cleaned prior to use in 4 M HNO_3 (3 times), 18 MΩ.cm water (3 times), quartz-distilled 6 M HCl (once) and again in 18 MΩ.cm water (3 times); finally, the resin was stored in quartz-distilled HCl (0.1 M). Between each stage of cleaning the resin was left to stand for 5 days with intermittent shaking. A fresh resin bed was prepared for each separation, and a two-stage process was used to (i) ensure

complete elution of other ions and particularly of Pb, and (ii) minimise the amount of sulphuric acid present prior to measurement.

Table 2.1 outlines the two-step chromatographic procedure. Briefly, the first stage of separation utilised quartz columns with an inner diameter of 6 mm, fitted with quartz wool plugs for support of the resin bed, which was filled with 1000 µl resin (wet volume). Once collected in acid-cleaned PFA vials, the Tl fraction was evaporated at 200 °C, which left <20 µl residual concentrated H_2SO_4, formed via oxidation of the SO_2 used during collection of Tl. The sample was then redissolved in a few drops (∼0.1 ml) of concentrated HCl (12 M) and evaporated again at 200 °C to reduce the amount of residual H_2SO_4. Subsequently, the Tl fraction was dissolved in 1.5 ml HCl (1 M) and refluxed for 12 hours at 140 °C. Once cooled, 60 µl of saturated Br_2 water was added to this solution. The sample was then left for a minimum of 3 hours to ensure complete oxidation of all Tl ions to the Tl^{3+} state.

The second stage of chromatographic separation was a scaled-down version of the first column, to provide a final 'clean-up' of matrix elements from the Tl fraction. Shrink-fit PFA columns fitted with polypropylene frits were filled with 150 µl of resin. Once collected, the Tl fraction was evaporated to near dryness on a hot plate set at 200 °C, leaving <10 µl residual concentrated H_2SO_4. The residue was taken up in a few drops (∼0.1–0.3 ml) HNO_3 (14 M) and evaporated to dryness at 200 °C 3 times, in order to remove as much of the remaining sulphuric acid and chloride ions as possible.

2.3.4 MC-ICP-MS isotope ratio measurements

The use of PFA beakers and the high evaporation temperature of H_2SO_4 means that it was not possible to remove all H_2SO_4 from the Tl fraction by evaporation. Nielsen et al. (2004) demonstrated that analytical artefacts of up to 1 ε unit can be generated if H_2SO_4 is present in samples but not in bracketing calibrators, and that the mass bias-corrected $^{205}Tl/^{203}Tl$ ratio is essentially independent of the concentration of H_2SO_4 up to 1 vol%. Therefore, all sample residues were dissolved in 1 ml of 0.1 M HNO_3–0.1 vol% concentrated H_2SO_4 for isotope analysis. Sample solutions were made up in 3 ml acid-cleaned PP autosampler vials. Reference solutions were prepared in dedicated PFA autosampler vials using the same batch of 0.1 M HNO_3–0.1 vol% concentrated H_2SO_4 to minimise matrix mismatch between samples and reference solutions. Dedicated PFA autosampler vials were also used for wash solutions.

Thallium has only two stable isotopes, precluding the possibility of isotopic spiking. Sample-calibrator bracketing was therefore employed by interspersing unknown samples between analyses of NIST SRM 997 (defined as $\varepsilon^{205}Tl_{SRM997} = 0$) at the same concentration and with the same acid matrix (i.e. a 'matching calibrator').

An external means of monitoring and correcting for mass bias must be employed when measuring an element with only two stable isotopes. For Tl isotope analyses, samples and standards were doped with NIST SRM 981 Pb. The certified $^{208}Pb/^{206}Pb$ isotope amount ratio is used to carry out online correction for mass discrimination of the measured $^{205}Tl^+/^{203}Tl^+$ ratio during the measurement. The Pb/Tl concentration ratio of samples and standards was between 3 and 4, and matched to within 15%, as variations in the Pb/Tl concentration ratio may cause real or apparent

changes in the mass bias response of Pb and Tl (Rehkämper and Mezger 2000). This methodology is analogous to the use of Tl doping when performing Pb isotope ratio measurements via MC-ICP-MS (e.g. Rehkämper and Mezger 2000, White et al. 2000).

Nu HR MC-ICP-MS

Most isotopic ratio measurements were carried out using a *Nu HR MC-ICP-MS* in low-resolution mode at the MAGIC Laboratories, Imperial College London. Sample introduction systems used over the course of this study included the *Aridus*, *Aridus II* and *Nu Instruments DSN* (Desolvation Nebuliser System), coupled with either PTFE or glass nebulisers, with measured uptake rates between 70 and 120 µl min^{-1}.

Typical instrument sensitivity was between 600 and 900 V per µg/g of Pb or Tl. The repeatability of bracketing NIST SRM 997 reference solutions degrades significantly with $^{205}Tl^{+}$ beam intensities below 1 V. Therefore, sample solutions were prepared with typical Tl concentrations of 2–5 ng/g and Pb concentrations between 15 and 20 ng/g.

Samples were run in a sequence using a CETAC autosampler. The ion beams at m/z 202 (Hg^{+}), 203 (Tl^{+}), 204 (Pb^{+} with possible Hg^{+} interference), 205 (Tl^{+}), 206 (Pb^{+}), 207 (Pb^{+}) and 208 (Pb^{+}) were monitored simultaneously with the Faraday collectors L2, L1, Ax, H1, H2, H3 and H4, all fitted with 10^{11} Ω resistors. Data collection was performed in three blocks of twenty cycles with 5 second integrations with the electrostatic energy analyser (ESA) deflected for a 15 second electronic baseline at the beginning of each block.

Nu Plasma II MC-ICP-MS

The limited availability of powder for some OIB samples, coupled with low Tl concentrations, required measurement of solutions with Tl concentrations of <1 ng/ml. Measurements of these low-concentration analytes on the *Nu HR MC-ICP-MS* are less precise than those of solutions with 2-5 ng/ml Tl. Measurements on a *Nu Plasma II MC-ICP-MS* during the later phase of the project have significantly increased sensitivity compared to the *Nu HR MC-ICP-MS*. For Tl, sensitivity on the *Nu Plasma II* was routinely well in excess of 1000 V/ppm at the same measurement conditions, and data collection was performed as a single block of sixty cycles. Otherwise, the method for isotope ratio determination on the *Nu Plasma II* was identical to that on the *Nu HR*.

Solution blanks

Due to the low concentration of Tl (typically tens of ng/g) in many rock samples, it is necessary that Tl concentrations of total procedural blanks are below the detection limit of the MC-ICP-MS. This equates to a maximum of 2 pg Tl. The total procedural Tl blank for each batch of samples was determined by dissolving the total procedural blank in 1 ml of analysis solution (0.1 M HNO_3–0.1 wt% H_2SO_4) and monitoring the intensity of the m/z 205 ion beam. In all cases, there was no deviation of the signal from the wash background, indicative of a maximum blank of <1 pg.

Residual Pb can produce significant errors in the measured $^{208}Pb/^{206}Pb$ isotope ratio used for correction of mass bias. Any Pb present in the sample solution prior to addition of NIST SRM 981,

whether residual from the sample matrix or introduced via contamination, thus has the potential to affect the precision and repeatability of $\varepsilon^{205}Tl_{SRM997}$ measurements. Therefore, to ensure accuracy of measured $\varepsilon^{205}Tl_{SRM997}$, residual Pb concentrations of below 0.01 ng/g were required for every sample solution and for the total procedural blank, as determined from the observed m/z 208 ion beam signal prior to NIST SRM 981 addition. Typical residual Pb concentrations were approximately equivalent to 1 pg/g.

Quality control and reference solutions

Machine performance was monitored by measurement of a Tl secondary standard solution obtained from Aldrich and first characterised by Rehkämper and Halliday (1999) ('Aldrich Tl solution'), which has subsequently been analysed repeatedly in at least seven laboratories worldwide (see compilation of Nielsen et al. 2017b). A minimum of three measurements of the Aldrich Tl solution were performed at the beginning and end of each measurement session, and periodically throughout – typically every four to six unknown sample measurements. Over the course of this study, >200 measurements of the Aldrich Tl solution yielded a mean $\varepsilon^{205}Tl_{SRM997}$ value of 0.78 ± 0.34 (2sd, n = 225) for analyses on the *Nu HR* (Fig. 2.1). Due to the large number of analyses, our intermediate precision (2sd) was calculated using the average $\varepsilon^{205}Tl_{SRM997}$ values obtained for the Aldrich Tl solution during each measurement session. For the *Nu Plasma II*, the mean value was 0.78 ± 0.80 (2sd, n = 28) (also shown in Fig. 2.1). These values are in excellent agreement with the most recent compilation of Nielsen et al. (2017b), in which the value is given as $\varepsilon^{205}Tl_{SRM997}$ = 0.79 ± 0.35 (2sd, n = 187).

A well-characterised USGS RM (typically BCR-2) was processed through the complete sample preparation procedure with every batch of samples prepared for MC-ICP-MS analysis. Thallium concentrations and $\varepsilon^{205}Tl_{SRM997}$ values were compared with in-house and interlaboratory long-term averages, to assess trueness and long-term precision.

2.3.5 MC-ICP-MS Tl concentration estimates

Estimates of thallium concentrations were acquired during MC-ICP-MS measurements of Tl isotope ratios by comparing ion beam intensities for reference solutions of known concentration and those for unknown samples, assuming chemical separation returns 100% thallium yields.

In detail, the Tl concentrations were estimated based on measurements of Pb/Tl concentration ratios using the known absolute mass of NIST SRM 981 Pb added to sample and reference solutions. However, these measurements are sensitive to small variations in sample dilution, which may occur during sample preparation due to (i) small variations between pipette tips and pipettes; (ii) differences in the volume consumed during initial concentration checks of the diluted sample (for standard-matching purposes); (iii) variations in how long a sample is left to stand in the autosampler before a measurement is made (i.e. how much evaporation occurs prior to measurement).

Overall, the trueness of such Tl concentration estimates has been improved from ∼25% (Rehkämper et al. 2002, Rehkämper and Nielsen 2004) to ∼5–10% (e.g. Prytulak et al. 2013, Shu et al. 2017) provided care is taken during sample handling. However, ICP-MS analysis with well-characterised

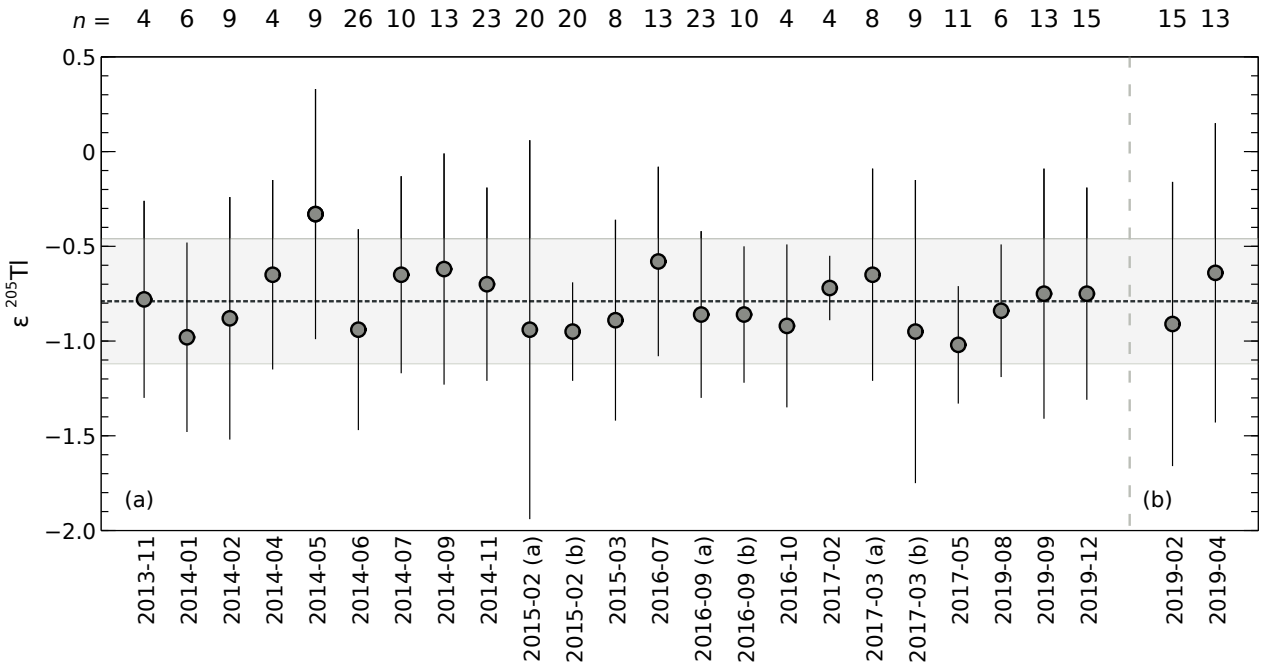


Figure 2.1: Tl isotope ratios (as $\varepsilon^{205}Tl_{SRM997}$) determined for the Aldrich Tl solution, relative to NIST SRM 997, using (a) the *Nu HR* (23 measurement sessions) and (b) the *Nu Plasma II* (2 measurement sessions). The number of measurements (*n*) made during each session is shown at the top of the figure, and the error bars indicate the precision (2sd) calculated from those measurements for each analytical session. The overall long-term intermediate precision of session averages (2sd) is shown as a grey band.

calibration materials and/or standard addition techniques returns the least biased and most precise Tl concentration data.

Some materials, such as the sulphide reference material 14P, cannot reasonably be analysed for trace elements on quadrupole or sector field ICP-MS instruments dedicated to silicate analyses due to memory effects associated with very high iron and sulphur concentrations. It is also difficult to calibrate and matrix-match this type of material. This is not, however, a concern when measuring a purified Tl fraction via MC-ICP-MS. Thallium concentrations of these materials are therefore reported based on the estimates made during MC-ICP-MS isotope ratio measurement, with correspondingly higher uncertainty.

2.4 Characterising reference materials for use with Tl

Despite the variety of applications of Tl isotope ratios, literature reports of thallium isotope ratios for geological reference materials have been restricted to three basalts, one andesite and one granite (Table 2.2), in addition to two ferromanganese sediments, one meteorite and one seawater sample. In response to the growing application of thallium isotopes in Earth systems, we provide the first measurements of Tl isotope ratios for the bulk rock reference materials COQ-1, GSP-2, ISH-G, MDO-G, STM-1 and UB-N, alongside determinations for previously analysed bulk rock reference materials AGV-2, BCR-2, BHVO-2 and G-2. Investigations of emerging stable isotope systems commonly reveal equilibrium intermineral isotope fractionations at high temperatures, as reviewed in Teng et al. (2017). We therefore also present the first determinations of Tl concentrations and isotope ratios for the mineral reference materials 14P, AL-I, AN-G, FK-N, NIST SRM 607, Mica-Fe and Mica-Mg, in an effort to establish an estimate of the possible magnitude

Table 2.2: Literature reports of MC-ICP-MS Tl isotope ratio data for igneous reference materials

Reference material	ε^{205}Tl	2sd	Dissolutions[a]	Measurements[b]	References
AGV-2	−1.9	0.5	1	1	Baker et al. (2009)
AGV-2	−3	0.6	8	15	Prytulak et al. (2013)
BCR-2	−2.5	0.4	4	19	Prytulak et al. (2013)
BIR-1	1.1	1.2	6	9	Nielsen et al. (2007)
BHVO-1	−3.5	0.5	10		Nielsen et al. (2015)
BHVO-1	−3.6	0.4		16	Shu et al. (2017)
BHVO-2	−2.1	0.5	2	2	Baker et al. (2009)
BHVO-2	−1.5	0.4	2	2	Prytulak et al. (2013)
BHVO-2	−1.5	0.3	10		Coggon et al. (2014)
G-2	1.3	0.7	1	1	Rehkämper and Halliday (1999)

[a] Number of independent digestions.
[b] Number of measurements.

Table 2.3: Reference materials for which new Tl isotope ratio data are reported.

RM	Supplier[a]	Lithology	Key reference	Reported Tl concentration	Reported ε^{205}Tl
14P	OREAS	massive magmatic sulphide			
AL-I	SARM-CRPG/CNRS	albite	Govindaraju (1984a)		
AN-G	SARM-CRPG/CNRS	anorthosite	Govindaraju (1980)		
BCR-2	USGS	basalt	Wilson (1997a)	x	x
BHVO-2	USGS	basalt	Wilson (1997b)	x	x
COQ-1	USGS	carbonatite			
FK-N	SARM-CRPG/CNRS	alkali feldspar	Govindaraju (1984b)		
G-2[b]	USGS	granite	Fairbairn et al. (1951)	x	x
GSP-2	USGS	granodiorite	Wilson (1998)	x	
ISH-G	SARM-CRPG/CNRS	trachyte	Gillot et al. (1992)	x	
MDO-G	SARM-CRPG/CNRS	trachyte	Gillot et al. (1992)		
Mica-Fe	SARM-CRPG/CNRS	biotite	Govindaraju (1979)	x	
Mica-Mg	SARM-CRPG/CNRS	phlogopite	Govindaraju (1979)		
SRM 607	NIST	alkali feldspar	Heinrich (1960)		
STM-1[b]	USGS	nepheline syenite	Snavely et al. (1976)	x	
UB-N	SARM-CRPG/CNRS	serpentinite	Govindaraju (1982)		

[a] OREAS, Ore Research & Exploration Assay Standards (Australia); SARM-CRPG/CNRS, Service d'Analyse des Roches et des Minéraux – Centre de Recherches Pétrographiques et Géochimiques/Centre National de la Recherche Scientifique (France); USGS, United States Geological Survey.
[b] No longer available for purchase.

of stable isotope ratio variation in phases potentially rich in Tl. These reference materials are intended to be used as matrix-matching RMs for future investigations rather than be interpreted in isolation as indicative of natural Earth processes.

A minimum of three separate digestions, separations and measurements were performed for each RM. With the exception of 14P, the reference materials were also analysed for high-precision trace element concentrations, including thallium. We focus on reference materials useful for high-temperature applications. Table 2.3 provides background information on each selected material.

2.4.1 Determination of Tl concentrations

Concentration measurements by ICP-QQQ

Thallium concentrations determined for RMs are presented in Table 2.4, whilst Appendix B2.ii gives full trace element results. RSDs for Tl concentration measurement results obtained for RMs using

ICP-QQQ with geological calibrating standards were calculated as follows. (i) Where the number of measurements $n > 4$, the RSD was calculated using the mean and standard deviation of those n analyses. (ii) Where $n = 1$, the reported RSD is based on the within-run standard deviation of the five ICP-QQQ mass scans that comprise each individual analysis. (iii) For $1 < n < 5$, RSDs calculated using method *(i)* were compared with the within-run standard deviation for each of the n analyses, and the worse of the two precisions is reported.

With the exception of three RMs (AL-I, AN-G and BIR-1), RSDs for Tl concentration measurement results obtained during this study using ICP-QQQ with geological calibrators were <7%, and all RSDs except that for BIR-1 were <10% (Appendix B2.ii). We note that RM AN-G has a low Tl concentration (10 ng/g, RSD = 8.1%), making precise measurements technically challenging. Similarly, BIR-1 has a very low Tl concentration (1 ng/g); even for this material, an RSD of 21% ($n = 18$) was achieved. Multiple dissolutions were analysed for trace element concentrations using ICP-QQQ for BCR-2 (multiple hot plate digestions), BHVO-2 (multiple hot plate digestions measured as unknowns, in addition to the calibrator solution) and GSP-2 (hot plate and bomb digestions). Notably, the hot plate versus bomb dissolution of GSP-2 showed no resolvable variation of Tl concentration with digestion method (RSD = 4.5%), suggesting, as expected, that Tl is not hosted in refractory phases present in this material (Appendix B2.ii).

Analyses employing synthetic calibration reference solutions produced measured Tl concentrations that were 10 ± 3% (1sd) lower than the same sample solutions measured relative to geological reference materials (Fig. 2.2) for all samples except AN-G. This suggests that the presence of a geological matrix alters the ionisation potential of Tl relative to synthetic trace element reference solutions. Indeed, the 10 ± 3% (1sd) offset in concentrations observed is apparent even for those materials that fall within the Tl concentration range of the geological calibrators employed. Therefore, despite the fact that using geological RMs is a more time-consuming process and that linear extrapolation must be employed with caution, we recommend using geological rather than synthetic calibrators to avoid under-reporting of Tl concentrations.

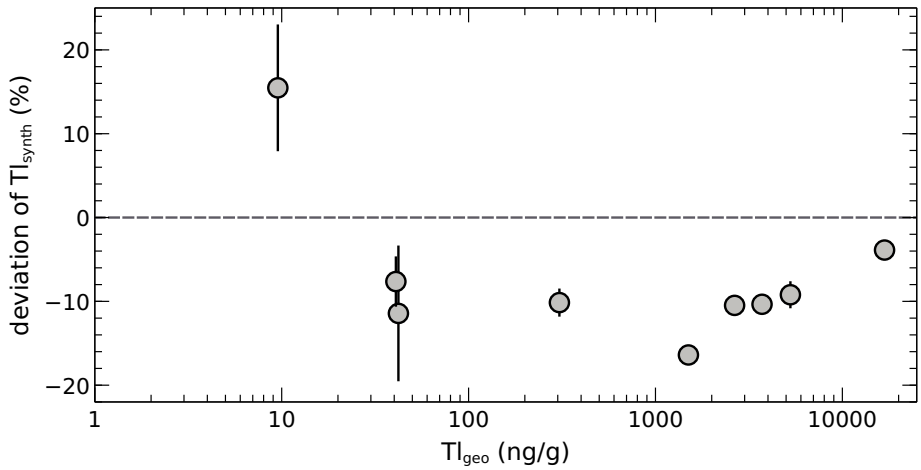


Figure 2.2: Comparison of Tl concentrations obtained when using geological versus synthetic calibrators (see text for details). Both sets of measurements were performed using the same ICP-QQQ instrument (Open University) and on the same solutions. Error bars are often smaller than symbols.

Table 2.4: New thallium concentration data and comparison with the literature data[a]

RM	Dissolutions[b]	Measurements[c] (*n*)	Tl (ng/g)	% RSD	References
Calibrators					
AGV-1			*349*	*14.9*	7, 8, 13, 17, 24, 25, 33, 34, 49, 50, 53, 55
			337	*4.7*	28 (GeoReM preferred value)
BHVO-2	2	6	23	4.9	This study[d]
			22	*20*	1, 2, 5, 6, 8–10, 16, 20, 21, 23, 25–27, 30, 31, 36–41, 43, 45, 48, 49, 51–53, 58
			22.4	*20*	28 (GeoReM preferred value)
BIR-1	3	15	1	21	This study[d]
			1.8	*41*	1, 8, 18, 25, 32, 35, 42, 46, 47, 53–56
			2.1	*34*	28 (GeoReM preferred value)
Measured reference materials					
14P	3	10	100	20	This study[e]
AL-I	1	2	42	8.3	This study
AN-G	1	1	10	8.0	This study
BCR-2	3	19	306	6.7	This study
			265	*13*	3, 10, 12, 14, 15, 19–22, 25, 26, 29, 36–38, 40, 41, 43, 45, 58
			267	*13*	28 (GeoReM preferred value)
COQ-1	1	7	96	3.9	This study
FK-N	1	1	3720	0.5	This study
G-2	1	1	942	6.6	This study
			888	3.1	18, 23, 25, 26, 28, 50, 57, 58
			884	3.0	28 (GeoReM preferred value)
GSP-2	2	4	1500	5.4	This study
			1290	*7.9*	26, 36, 58
ISH-G	1	1	788	0.7	This study
MDO-G	1	1	61	2.0	This study
Mica-Fe	1	1	16 800	0.4	This study
			16 000	n.g.	4, 11, 44
SRM 607	1	1	2650	1.1	This study
STM-1	1	1	258	1.4	This study
			220	*6.4*	17, 44
UB-N	1	2	41	4.3	This study
			49	*18.3*	8, 17, 46, 52, 56

[a] Concentration values quoted in italic text are compiled values. Concentration values quoted in plain text are measured values.
[b] No longer available for purchase.
[c] Number of measurements.
[d] These Tl concentration results were obtained for solutions of the calibrator reference materials that were run as unknowns.
[e] Concentration estimated using MC-ICP-MS.
References: [1] Babechuk et al. (2010), [2] Babechuk and Kamber (2011), [3] Baker et al. (2010a), [4] Baranov et al. (2002), [5] Barnes et al. (2014), [6] Brandl et al. (2012), [7] Bolge et al. (2006), [8] Chauvel et al. (2011), [9] Chauvel et al. (2012), [10] Condomines et al. (2015), [11] Dampare et al. (2008), [12] Deng et al. (2013), [13] Eggins et al. (1997), [14] Elmaleh et al. (2012), [15] Espanon et al. (2014), [16] Gale et al. (2011), [17] Garbe-Schönberg (1993), [18] Gaschnig et al. (2014), [19] Geldmacher et al. (2008), [20] Gibson et al. (2013), [21] Gómez-Tuena et al. (2011), [22] González-Álvarez and Kerrich (2011), [23] He et al. (2010), [24] Hettmann et al. (2014b), [25] Hu and Gao (2008), [26] Hu et al. (2013), [27] Jacques et al. (2013), [28] Jochum et al. (2016), [29] Kamber et al. (2005), [30] Kawabata et al. (2011), [31] Kirchenbaur et al. (2012), [32] Kodolányi et al. (2012), [33] Makishima and Nakamura (2006), [34] Makishima et al. (2011), [35] Martin et al. (2015), [36] Marx and Kamber (2010), [37] Marx et al. (2010), [38] McCoy-West et al. (2010), [39] Mohan et al. (2013), [40] Mori et al. (2007), [41] Mori et al. (2009), [42] Nielsen et al. (2007), [43] Park et al. (2012), [44] Parks et al. (2014), [45] Prytulak et al. (2013), [46] Robin-Popieul et al. (2012), [47] Søager et al. (2015), [48] Stromsoe et al. (2013), [49] Timm et al. (2009), [50] Uysal et al. (2011), [51] van der Straaten et al. (2008), [52] Wang et al. (2015), [53] Wehrmann et al. (2014), [54] Woodhead et al. (2011), [55] Worthington et al. (2006), [56] Yu et al. (2000), [57] Yu et al. (2001), [58] Zhang et al. (2012).

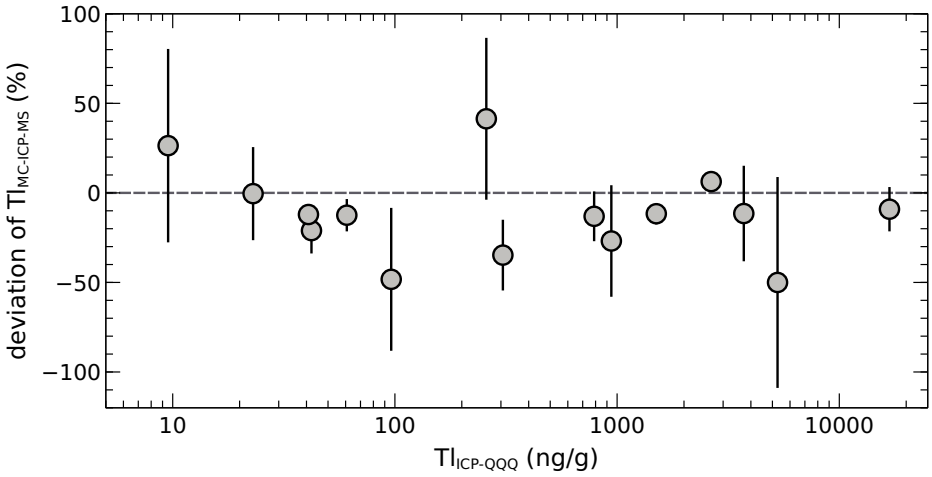


Figure 2.3: Comparison of Tl concentrations obtained during MC-ICP-MS isotope analysis and those determined by ICP-QQQ (using geological reference materials as calibrators). Some error bars are smaller than symbols.

Concentration measurements by MC-ICP-MS

Concentration measurements made during isotope ratio analysis via MC-ICP-MS were indistinguishable from ICP-QQQ results, but showed substantial variance (Fig. 2.3) with RSDs (calculated for each material as the RSD of the individual concentration measurement results) ranging from about 2% to 54%. For ten of the RMs measured, the RSD is <20%, whilst five have >30% RSDs of the mean. This suggests that concentration measurements made during MC-ICP-MS isotopic determinations may be suitable for assessing sample heterogeneity. Importantly, there was no resolvable variation of Tl concentration with digestion method: for materials analysed following both hot plate and bomb digestion, Tl concentration RSDs were <15% (see also Fig. 2.4). This strongly suggests that Tl is not hosted in refractory phases present in these RMs.

Comparison with literature concentration data

Jochum et al. (2016) provide GeoReM preferred values for the nineteen most frequently queried RMs, including AGV-2, BCR-2, BHVO-2 and G-2. Additional literature reports of Tl concentration exist for Mica-Fe, BCR-2, GSP-2, G-2, STM-1, and UB-N. These values are reported in Table 2.4 alongside the concentration results obtained over the course of this study. Only the concentrations determined for GSP-2 and STM-1 differ significantly from published values.

For AL-I, AN-G and Mica-Mg only proposed values are available, from the compilation of Govindaraju (1995). No Tl concentration estimates are available for COQ-1, trachytes ISH-G and MDO-G, or K-feldspars FK-N and NIST SRM 607. To the best of our knowledge, we provide the first reported values for these reference materials. Good agreement between the literature reports of Tl concentrations in these materials and our results, particularly for well-characterised RMs, provides reassurance that the BHVO-2 digestions used as calibrator did not exhibit anomalously high Tl concentrations. We are confident that the concentration data presented are robust.

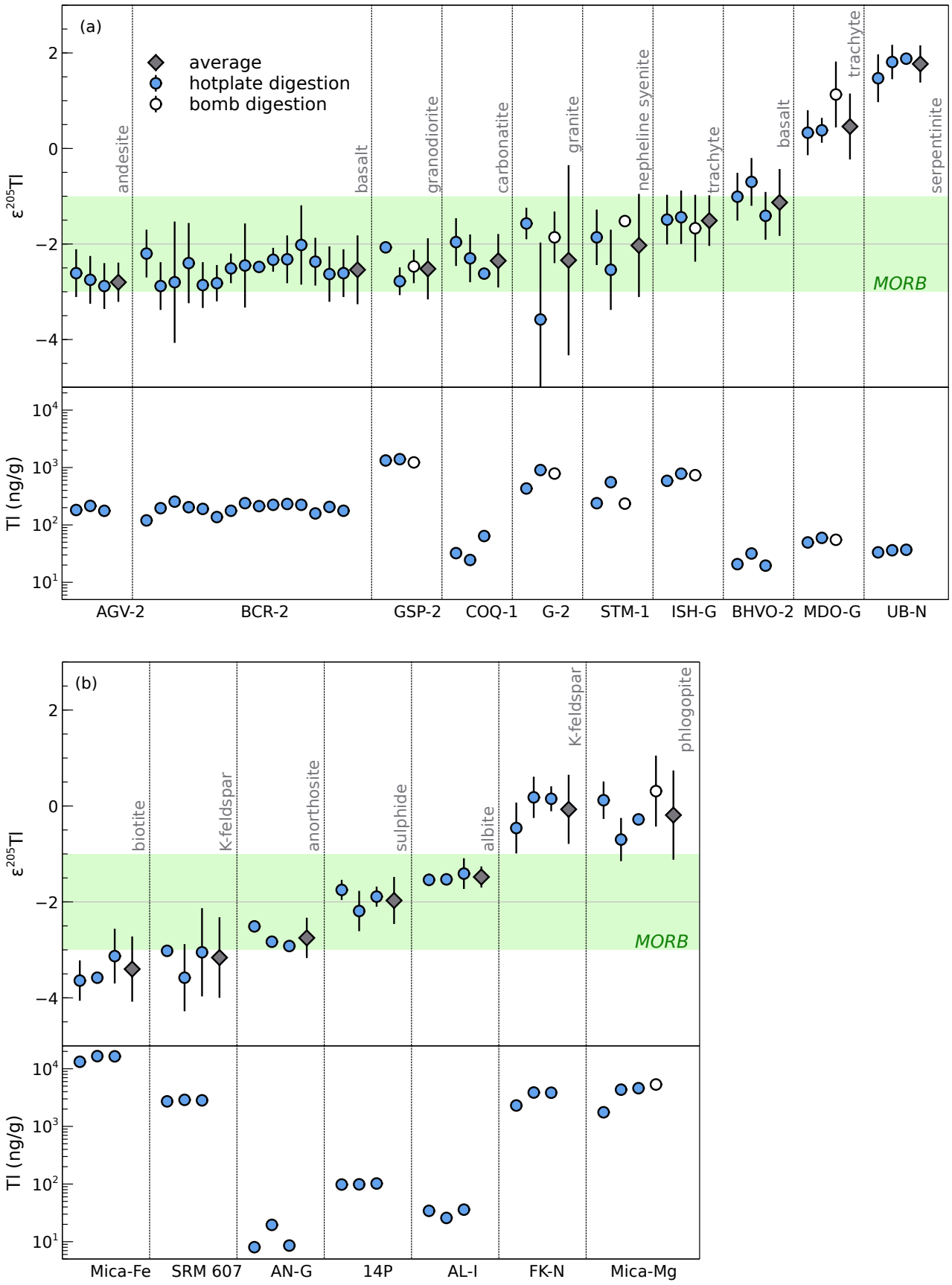


Figure 2.4: Tl isotope ratios (as $\varepsilon^{205}Tl_{SRM997}$; error bars: 2sd) and Tl concentrations (error bars indicate a conservative RSD of 20%) of RMs determined by MC-ICP-MS for (a) whole rock and (b) partially separated mineral reference materials. Shown are data for each individual digestion and the mean values for each RM. Thallium concentration data obtained via MC-ICP-MS simultaneously with isotope ratio measurement was used to aid qualitative assessment of material heterogeneity.

Table 2.5: Thallium isotope ratio measurement results obtained during this study

RM	Dissolutions[a]	Sessions[b]	Measurements[c]	ε^{205}Tl	2sd
14P	3	1	10	−2.0	0.5
AGV-2	3	2	5	−2.8	0.4
AL-I	3	3	5	−1.5	0.2
AN-G	3	3	3	−2.8	0.4
BCR-2	15	9	31	−2.5	0.7
BHVO-2	3	3	4	−1.1	0.7
COQ-1	3	2	5	−2.3	0.6
FK-N	3	4	11	−0.1	0.7
G-2	3 (1)	3	11	−2.3	2.0
GSP-2	3 (1)	2	9	−2.5	0.6
ISH-G	3 (1)	3	9	−1.5	0.5
MDO-G	3 (1)	3	7	0.5	0.7
Mica-Fe	3	4	11	−3.4	0.7
Mica-Mg	4 (1)	5	12	−0.2	0.9
SRM 607	3	2	9	−3.2	0.8
STM-1	3 (1)	2	10	−2.0	1.1
UB-N	3	3	5	1.8	0.4

[a] Total number of independent digestions; numerals in parentheses indicate the number of bomb digestions.
[b] Number of measurement sessions during which the RM was analysed.
[c] Number of separate analyses.

2.4.2 Determination of Tl isotope ratios

Data quality

Results for the Tl isotope ratio measurements are given in Table 2.5. As a minimum of three isotope ratio measurements were made for each RM, the reported intermediate precision (2sd) is based on at least three measurement results obtained following independent sample preparation. For comparison, the typical 'external' reproducibility for multiple digestions performed in multiple institutions of $\varepsilon^{205}Tl_{SRM997}$ for geological samples is ±0.5 ε units (see compilation in Nielsen et al. 2017b).

Literature reports of $\varepsilon^{205}Tl_{SRM997}$ exist for AGV-2, BCR-2, BHVO-2 and G-2 (Table 2.2). Of these, BCR-2 has the most widely reported $\varepsilon^{205}Tl_{SRM997}$, and can be considered isotopically homogeneous with respect to Tl isotope ratio. The values we obtain for BCR-2 and BHVO-2 are in excellent accord with Prytulak et al. (2013) and Coggon et al. (2014), and are indistinguishable from values obtained by Baker et al. (2009).

However, the value we obtained for G-2 is in disagreement with the single previously reported value (Rehkämper and Halliday 1999), in spite of large variance for both measurements. The low precisions and difference in isotope ratio measurement results most likely arise from (i) G-2 exhibiting powder heterogeneity in terms of Tl (see subsequent discussion), (ii) analysis of different bottles of G-2 and (iii) difficulties with the development of the techniques for isotopic determination of Tl.

We are therefore confident that the measurement procedure employed did not introduce any systematic bias, and that our $\varepsilon^{205}Tl_{SRM997}$ values and precisions for previously uncharacterised RMs provide a range where the true value is likely to be. Together with concentration measurements obtained via MC-ICP-MS on the same dissolution, these Tl isotope ratios are displayed in Figure 2.4, as mean values for each individual dissolution. There is no correlation of precision with

digestion batch or analytical sessions, implying that the better precisions (2sd = 0.4–0.6 ε units) are representative of the precision achievable with this analytic approach, whilst the higher measurement results with lower precision (up to 2 ε units) are unlikely to be a consequence of our laboratory techniques or poor measurement precision.

Evaluation of reference material heterogeneity

Despite the demonstrated ability of the analytical techniques to achieve excellent precision, the variances for some samples are surprisingly high, suggesting possible isotopic heterogeneity in the RM powders. Reference materials must be homogeneous in the element system of interest if they are to be used for method development, validation or interlaboratory comparisons (BIPM et al. 2012). Homogeneity is routinely tested for major elements and some trace elements during RM preparation, but heterogeneity for other elements and for isotope systems has been identified in a number of these materials (e.g. BHVO-2: Baker et al. 2004, Weis et al. 2006, Chauvel et al. 2011; SRM 607: Nebel and Mezger 2006). Furthermore, the statistical nature of observed heterogeneity can provide information on the dispersal of an enriched phase or phases through a material. For example, Chauvel et al. (2011) discuss the possibility that relatively large, rare Pb-rich microparticles are responsible for the distinctive bimodal distribution of Pb concentrations in BHVO-2. However, we are not aware of any general assessment of Tl heterogeneity in igneous RMs.

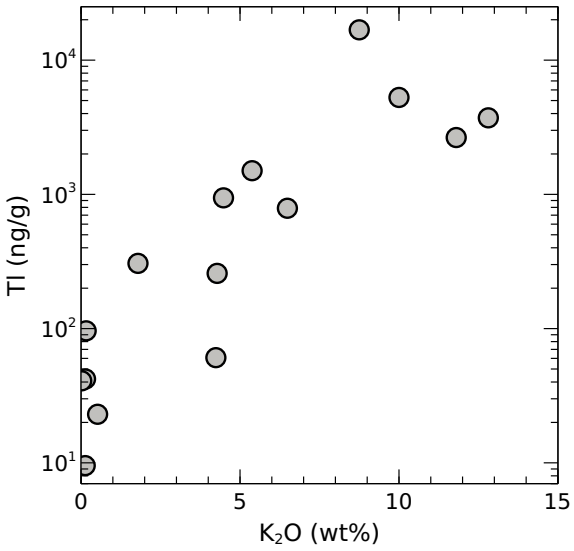


Figure 2.5: Variation of Tl concentration with K_2O concentration for all reference materials except sulphide 14P. Error bars are smaller than symbols. All K_2O data are as listed by the material's supplier. Thallium concentrations were determined by ICP-QQQ at the Open University.

As Tl^+ readily substitutes for K^+ in igneous minerals, it is expected that, if present, K-rich phases will dominate the Tl budget of a rock. Indeed, as shown in Figure 2.5 for silicate rocks, Tl concentration correlates with K_2O. Figure 2.4 presents mean $\varepsilon^{205}Tl_{SRM997}$ and concentration values obtained using MC-ICP-MS for each RM and for each individual dissolution, to aid qualitative assessment of any Tl heterogeneities. There are no resolvable differences in either Tl concentrations or isotope ratios between bomb and hot plate digestions for the RMs studied, providing

evidence that Tl is not hosted in refractory phases. Small variations in the proportions of K-rich phases in the powder portion sampled could, therefore, significantly affect both the concentration and isotope ratio of Tl.

Having performed a minimum of three digestions for isotope ratio measurement of each RM included in this study, we are able to assess whether these materials are heterogeneous for Tl. Examination of the data set (Fig. 2.4) reveals heterogeneity of concentration with weak or no isotope ratio heterogeneity for COQ-1, STM-1, AN-G and Mica-Mg, marked heterogeneity of both isotope ratio and concentration for G-2, and possible weak isotope ratio heterogeneity for BHVO-2. AN-G consists primarily of anorthosite (An_{80}–An_{85}), with hornblende (10–15 vol%), relict clinopyroxene and some secondary minerals (Govindaraju 1980). In this rock, hornblende is likely the major host of K and therefore of Tl; if the hornblende crystals have identical Tl isotope ratios to the rest of the bulk sample, it follows that Tl isotope ratios will be unaffected by modal proportion of hornblende in any individual dissolution, but the Tl concentration will be strongly dependent on the amount of hornblende incorporated into the digested portion. STM-1 contains multiple K-bearing phases including alkali feldspar, nepheline and biotite (Snavely et al. 1976), and features a bulk Tl concentration two orders of magnitude higher than AN-G. On the basis of three dissolutions, STM-1 appears to exhibit a bimodal distribution for Tl: two distinct concentration populations, with the higher concentration possibly weakly associated with an isotopically lighter $\varepsilon^{205}Tl_{SRM997}$ signature. This may reflect the existence of at least two distinct hosts of Tl, variably incorporated into the sample portion. In contrast, across four dissolutions Mica-Mg appears to display a range in both Tl concentration and $\varepsilon^{205}Tl_{SRM997}$, with no clear systematics; this is consistent with relatively small, frequent microparticles of several Tl-rich and isotopically distinct phases unevenly dispersed throughout the powdered RM.

G-2 appears to exhibit significant heterogeneities in Tl concentration and isotope ratio. As with STM-1, these heterogeneities appear to be weakly coupled. G-2 is a micaceous granite, known to contain microcline, biotite and muscovite (Fairbairn et al. 1951, Chayes and Suzuki 1963, Flanagan 1969). These K-rich phases are likely to be the major hosts of Tl in G-2; given the difficulty of ensuring even crushing and even distribution of sheet silicates, it is plausible that small variations in the amount of each phase sampled in any given digestion could account for the coupled heterogeneity seen here.

Petrographic information is not available for BHVO-2, but as a basalt, it is unlikely to contain significant amounts of K-rich phases. We do not observe any evidence for the significant Tl concentration variations reported in the literature (Appendix B2.i), but do see potential evidence of weak Tl isotope ratio heterogeneity.

Constraints on the scale of isotope ratio heterogeneities are provided by a comparison of dissolved mass versus the 2sd precision of the measurement result of $\varepsilon^{205}Tl_{SRM997}$ (Fig. 2.6). For samples with higher (known or predicted) Tl concentrations, smaller masses were digested to yield similar amounts of Tl for measurement. However, it is precisely the samples with high Tl contents and low digested mass that, in general, display the largest variance in the isotope ratio measurements. For most RMs included in this study, it appears that weighing out at minimum 100 mg of powder might mitigate the effects of small-scale heterogeneity and enable routinely achievable $\varepsilon^{205}Tl_{SRM997}$ measurements with 2sd precisions on the order of 0.5 ε units.

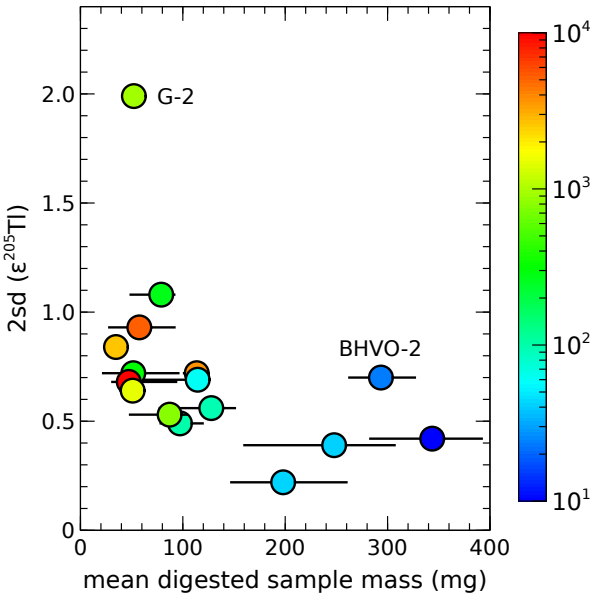


Figure 2.6: Assessment of relationship between mass of digested sample and isotope ratio variance (2sd). For the digested sample mass, the plotted point represents the mean mass weighted by the number of measurements made per dissolution; error bars represent the full range of masses digested for each sample. Points are coloured according to Tl concentration as determined by ICP-QQQ.

However, it is unlikely that dissolving larger initial masses would improve the precisions achievable for G-2 and BHVO-2. G-2, in particular, exhibits a high variance given initial dissolved masses, suggesting that the discrepancy with the one previous report (Rehkämper and Halliday 1999) arises in large part from powder heterogeneity. Rehkämper and Halliday (1999) are known to have made their analysis using a different vial of G-2, potentially indicating heterogeneity between vials. We therefore recommend against use of G-2 as a Tl reference material. For BHVO-2, the variance for $\varepsilon^{205}Tl_{SRM997}$ is less extreme and, unlike G-2, there is no strong evidence for heterogeneity in Tl concentration. We therefore recommend caution when employing BHVO-2 as a Tl isotope reference material, but as it is the only basaltic RM with a Tl concentration of ∼20 ng/g, we recognise that it is likely the most appropriate choice for studies involving low-Tl igneous samples. As BHVO-1 and BHVO-2 are distinctly different in terms of both concentration and isotope ratio values (Appendix B2.i and Table 2.2), care must be taken to ensure that these materials are not confused if using either as a reference material.

In the light of concerns regarding potential inhomogeneous contamination during the generation of RMs, we find no evidence that the overall reported range in $\varepsilon^{205}Tl_{SRM997}$ for the RMs analysed here (5.5 ε units, comparable to that of other natural igneous products: see Nielsen et al. 2017b) is due to contamination of the samples. In particular, there is no systematic variation of Tl isotopic composition with RM provider or date of preparation. Furthermore, the most isotopically distinct result (serpentinite UB-N: $\varepsilon^{205}Tl_{SRM997}$ = +1.8 ± 0.4 2sd) is consistent with the findings of Nielsen et al. (2015). To the best of our knowledge, these authors provide the only literature report of $\varepsilon^{205}Tl_{SRM997}$ in natural serpentinite samples, and these show similarly heavy Tl isotopic compositions, providing indirect validation of our isotopically heavy serpentinite RM.

2.5 Summary

Thallium concentration and isotope ratio measurements were performed for a comprehensive suite of sixteen geological reference materials, including both bulk rock and partially separated mineral powders. We provide the first reported Tl concentration and $\varepsilon^{205}Tl_{SRM997}$ measurements for geochemical reference materials 14P, Albite AL-I, Anorthosite AN-G, Carbonatite COQ-1, Potash Feldspar FK-N, Trachyte ISH-G, Trachyte MDO-G and Phlogopite Mica-Mg, and additionally provide the first reported $\varepsilon^{205}Tl_{SRM997}$ values for Biotite Mica-Fe and Serpentinite UB-N.

Of the sixteen reference materials included, all but G-2 are in principle appropriate for use as Tl isotopic reference materials, provided a sufficient mass of powder (minimum 100 mg) is digested. The $\varepsilon^{205}Tl_{SRM997}$ represented spans from -3.5 to +1.8, comparable to the range thus far reported in global igneous rocks (e.g. Nielsen et al. 2017b).

Chapter 3

Thallium systematics in MORB and OIB

Much of this work has been published, following peer review, as:

> E. K. A. Brett, J. Prytulak, M. Rehkämper, S. J. Hammond, C. Chauvel, A. Stracke and M. Willbold. (2021) Thallium elemental and isotopic systematics in oceanic island lavas. *Geochimica et Cosmochimica Acta* **301:**187–210. doi:10.1016/j.gca.2021.02.035

This chapter is licensed under a Creative Commons Attribution-Non Commercial-No Derivatives 4.0 International Licence (CC BY-NC-ND).
AB performed digestions and chemistry for all samples with guidance from JP and MR. AB carried out Tl isotope analyses with guidance from JP and Barry Coles. SJH performed dilutions and trace element analyses. Brett et al. (2021) was primarily written by AB.

3.1 Introduction

The majority of intraplate oceanic volcanism is the surface expression of deep-rooted thermo-chemical upwellings, or 'mantle plumes' (e.g. Morgan 1971, Hofmann and White 1982, Montelli et al. 2006). Ocean island basalts (OIB) thus provide a window into geochemical heterogeneity of the otherwise inaccessible deep mantle (e.g. White 2015). Zindler and Hart (1986) first proposed a classification scheme for oceanic basalts based on the observation that their radiogenic Sr-Nd-Pb isotope ratios vary systematically between a restricted number of isotopic signatures, termed mantle 'end-members' or 'components'. Decades of subsequent work has subdivided or refined the details and interpretations of the radiogenic Sr-Nd-Pb isotopic variability in oceanic basalts (e.g. Weaver 1991, Chauvel et al. 1992, Hofmann 1997, Workman and Hart 2005, Willbold and Stracke 2006). In general, the chemical variations observed in OIB can be reproduced via mixing of ambient mantle with other components, commonly identified with various recycled crustal lithologies (e.g. Hofmann and White 1982, Weaver 1991, Chauvel et al. 1992; see also § 1.2). Within this framework, it is suggested that the so-called HIMU (high $\mu = {}^{238}U/{}^{204}Pb$) signature may represent ancient subducted oceanic crust, isolated in some cases for >2.5 Ga, while enriched mantle (EM)-type signatures might represent incorporation of heterogeneous continental

components in the form of clastic sediments or continental crust eroded at destructive plate margins (e.g. Hofmann and White 1982, Zindler and Hart 1986, Chauvel et al. 1992, Hofmann 1997, Stracke et al. 2003, 2005, Willbold and Stracke 2006, 2010, Stracke 2012).

Inferring mantle source compositions from the radiogenic isotope ratios observed in basalts is challenging, because sampling of the different source components via partial melting depends on a number of factors, such as initial concentrations, melting behaviour, partition coefficients, extent of melt mixing, and time elapsed between parent-daughter fractionation events. As a consequence, it is often difficult to reach unambiguous interpretations of the origins and history of mantle sources.

Resolving such ambiguities about the nature and origin of mantle composition and evolution on the basis of radiogenic isotopic variation observed in OIB is necessary to constrain global geochemical cycles and the Earth's thermal evolution. Stable isotope systematics may provide useful independent constraints, as low-temperature surface environments have the potential to generate resolvable stable isotope fractionations, which might then be traced through subduction recycling into the mantle and subsequently sampled via OIB. Analytical advances have enabled the development and application of a variety of stable isotope systems to igneous rocks, motivated in part by the potential for such systems to act as a tracer of recycled materials. Many of these advances were recently reviewed in Teng et al. (2017), for stable isotope systems from Li to U. In general, larger isotope fractionations occur in surface environments than magmatic environments, and so a logical aim is to identify the incorporation of recycled surface material by determining whether magmatic rocks carry a stable isotopic signature that is distinguishable from the mantle.

3.1.1 Thallium: a potential tracer for recycled materials

Thallium is a highly incompatible element, conventionally grouped with the alkali elements due to the similar ionic radii of Tl^+ and the heavier alkali metals (e.g. Shaw 1952, Shannon 1976, Heinrichs et al. 1980). The relative abundance of the two stable isotopes, ^{205}Tl (∼70%) and ^{203}Tl (∼30%), is reported as $\varepsilon^{205}Tl$ relative to the NIST SRM 997 Tl isotope standard (Rehkämper and Halliday 1999):

$$\varepsilon^{205}\mathrm{Tl} = \frac{\left(\frac{^{205}\mathrm{Tl}}{^{203}\mathrm{Tl}}\right)_{\mathrm{measured}} - \left(\frac{^{205}\mathrm{Tl}}{^{203}\mathrm{Tl}}\right)_{\mathrm{standard}}}{\left(\frac{^{205}\mathrm{Tl}}{^{203}\mathrm{Tl}}\right)_{\mathrm{standard}}} \times 10^4$$

Thallium does not appear to undergo isotope fractionation during the high-temperature igneous processes of partial melting, metasomatism, and anhydrous fractional crystallisation. A systematic study of two co-genetic igneous suites spanning a range of SiO_2 contents from Iceland and the Mariana island arc found a restricted range in $\varepsilon^{205}Tl$ (Hekla: $\varepsilon^{205}Tl$ from -2.2 to -0.7; Anatahan: $\varepsilon^{205}Tl$ from -2.9 to 0.0), and indicates that no analytically resolvable Tl isotope fractionation occurs during anhydrous magmatic differentiation (Prytulak et al. 2017). Fitzpayne et al. (2020) analysed phlogopite mineral separates from highly metasomatised mantle xenoliths, again finding a strikingly restricted range in isotopic composition $\varepsilon^{205}Tl$ = -2.5 ± 1.3 (2sd, n = 25). This implies that the Tl isotopic composition of magmatic products should correspond to that of

their sources, allowing the use of Tl isotope ratios to disambiguate the history of even evolved igneous rocks.

Direct measurements of Tl isotope ratios in mantle peridotites are hindered by their low concentrations (e.g. primitive mantle <4 ng/g: McDonough and Sun 1995; 4.1 ng/g: Palme and O'Neill 2014). However, a harzburgite analysed by Nielsen et al. (2015) with ε^{205}Tl = -2.0 ± 0.8 (2sd) is indistinguishable from the Tl isotopic composition of mid-ocean ridge basalts (MORB; ε^{205}Tl = -2.0 ± 1.0 2sd; Nielsen et al. 2006b, 2017b), thus suggesting that Tl isotopes are not fractionated by partial melting processes.

Thallium elemental systematics in MORB are constrained by several large self-consistent (i.e. samples measured by the same protocols in the same laboratory) datasets collected in recent years that include well-calibrated high-precision Tl concentrations (Jenner and O'Neill 2012a, Nielsen et al. 2014, Yang et al. 2018). One further study (Kelley et al. 2013) also reports a large set of Tl concentrations in MORB, but unfortunately these measurements were calibrated using natural standards for which the Tl concentration was not, at the time, well-known. As such, this data set is not directly comparable and is therefore not considered.

Thallium concentrations are generally 100s to 10,000s of ng/g with large isotope fractionations at the Earth's surface. The continental crust is the main terrestrial host of Tl (∼500 ng/g, e.g. Rudnick and Gao 2003, Jenner 2017), with a Tl isotopic composition, inferred from loess, indistinguishable from MORB (Nielsen et al. 2005, 2006b). Relative to the mantle, modern altered upper oceanic crust (AOC) has elevated Tl concentrations (∼200 ng/g) and light Tl isotopic compositions (ε^{205}Tl ≈ -20 to -5; Nielsen et al. 2006c, 2017b), whereas FeMn sediments have very high Tl contents (>10,000 ng/g) and preferentially incorporate the heavier Tl isotope (ε^{205}Tl ≈ +5 to +15; review of Nielsen et al. 2017b). The Tl concentration contrast between the mantle and potential recycled components spans orders of magnitude, and is coupled with resolvable and opposite directions of isotope fractionation in surface materials relative to the mantle. These features theoretically render Tl isotopic compositions extremely sensitive to contributions of recycled surface materials to the mantle. Indeed, previous work investigating subduction settings has shown that Tl isotope ratios of arc lavas can be directly linked to the isotopic composition of materials subducting outboard of the associated trenches (Prytulak et al. 2013, Nielsen et al. 2015, 2016, 2017a, Shu et al. 2017, 2019). By the same reasoning, Tl isotopic compositions may co-vary with traditional radiogenic isotope ratios in ocean island basalts, used to define mantle components. If some EM-type signatures reflect incorporation of recycled sediments, then isotopically heavy Tl is predicted. Likewise, if the HIMU OIB signature develops via input of AOC, then HIMU lavas would be expected to exhibit isotopically light Tl.

3.1.2 Sample selection and aims

Previous Tl isotope studies of OIB have used the interpretive framework of isotopically heavy thallium indicating contribution of FeMn sediments and/or pelagic clays, and isotopically light thallium indicating contribution of AOC. Previous work has focussed on Hawai'i (Nielsen et al. 2006b), the Azores (Nielsen et al. 2007), Iceland (Nielsen et al. 2007, Prytulak et al. 2017), and St Helena (Blusztajn et al. 2018), documenting an overall range of ε^{205}Tl = -10 to +3.9 (see

Table 3.1: Summary of OIB localities with published Tl concentration and isotopic composition data.

	FOZO/PREMA		EMI		EM		HIMU		
Locality	Hawai'i	Iceland	Gough	Tristan	Marquesas†	Azores	St Helena	Rurutu	Tubuai
reported [Tl]	x	x			x	x	x		
reported ε^{205}Tl	x	x				x	x		
$^{87}Sr/^{86}Sr$	○	range	x	x	x	x	x	x	x
$^{143}Nd/^{144}Nd$	○	x	x	x	x	x	x	x	x
$^{176}Hf/^{177}Hf$		range	x	x	x		x		○
Pb isotopes	x	range			x	x	x	x	x
this study			x	x	x		x	x	x
key references	1*	2*,3	4,5	4,5	6	2	4,5,7	8	9

* picrites. † Note that Marquesas lavas exhibit variable composition covering a very wide range of radiogenic isotopic compositions. x = data exists; ○ = partial data; range = a range is known, but samples have not been individually analysed. [1] Nielsen et al. (2006b); [2] Nielsen et al. (2007); [3] Prytulak et al. (2017); [4] Willbold and Stracke (2006); [5] Willbold and Stracke (2010); [6] Chauvel et al. (2012); [7] Blusztajn et al. (2018); [8] Chauvel et al. (1997); [9] Chauvel et al. (1992).

Appendix B3.i for details). This large range is mostly due to variations in rocks from Hawai'i, ascribed to the addition of FeMn sediments, and St Helena, ascribed to the addition of AOC. Thus far, no published studies have examined EM-type lavas, or HIMU lavas from localities other than St Helena. Here, we investigate EM-type lavas and expand the number of HIMU localities, to better characterize the full range of known OIB sources. All selected samples have radiogenic isotope data and show limited evidence of alteration (e.g. low loss on ignition, freshness on inspection of thin section). The 48 new analyses comprise 32 EM-type (13 'EMI', 19 other EM) and 16 HIMU lavas (Table 3.1). We aim to evaluate, on a global scale, the potential relationships between Tl elemental abundances, Tl stable isotopes, and radiogenic isotopic compositions in OIB to investigate the nature of mantle components and the efficiency of Tl cycling between crust and mantle.

Table 3.2: Key geochemical data for OIB samples analysed in this study.

Sample	MgO* (wt%)	LOI* (wt%)	Ce (µg/g)	Tl (ng/g)	Ce/Tl	ε^{205}Tl	2sd	Dissolutions	Measurements (*n*)
Gough (EMI)									
G6	7.94	2.12	101	26	3915	0.5	2.2	2	3 (1 Nu + 2 Nu II)
G102	5.28	0.62	107	76	1402	−2.5	0.6	2	3
G117	4.52	2.49	113	39	2921	3.8	0.6	1	4
G118	12.97	1.18	73.9	49	1495	−0.6	0.5	1	2
G132	5.04	1.06	87.1	95	919	−4.7	0.5	1	3
G135	5.85	0.88	112	53	2104	−0.6	0.5	1	2
B167	3.39	3.67	107	74	1437	−3.2	0.5	1	1
Tristan da Cunha (EMI)									
T16	4.74	0.25	134	101	1321	−2.3	0.5	1	2
T60	12.2	−0.52	60.9	38	1600	−0.3	0.5	1	2
T64	8.91	−0.30	115	64	1796	−1.1	0.5	1	1
T122	7.28	−0.47	104	55	1888	−1.2	0.5	1	2
T497	7.61	−0.52	136	87	1559	−1.2	0.8	2	9
T557	8.00	−0.37	112	56	2006	−1.2	1.5	1	6
T557 (leached)						*-1.6*	*0.9*	*1*	*1 (Nu II)*
Fatu Hiva, Marquesas (EM†)									
FH01	10.6	0.00	110	7	16 740	0.0	0.5	1	1
FH11	6.8	0.00	99.0	26	3837	−3.6	0.8	2	3
FH18	12.2	0.00	81.5	32	2554	−1.8	0.5	1	1
Hiva Oa, Marquesas (EM†)									
HV64	8.00	1.29	81.1	17	4649	0.7	0.5	1	1
HV76	5.14	0.32	72.7	63	1162	−0.3	0.7	1	2

continued on next page

Table 3.2 continued

Sample	MgO* (wt%)	LOI (wt%)*	Ce (µg/g)	Tl (ng/g)	Ce/Tl	ε^{205}Tl	2sd	Dissolutions	Measurements (*n*)
Montane, Marquesas (EM†)									
MT04	5.63	0.01	71.6	18	3996	−3.9	1.0	3	3 (2 Nu + 1 Nu II)
MT08	5.53	0.00	82.0	25	3224	0.6	0.5	2	2
Tahuata, Marquesas (EM†)									
TH4	6.37	1.01	108	77	1415	−2.9	0.5	1	1
TH5	7.44	1.91	137	66	2064	−0.5	0.5	1	2
TH8	4.67	0.60	96.3	24	4045	1.0	0.5	1	1
TH8 (leached)						*2.2*	*0.8*	*1*	*1 (Nu II)*
TH13	6.09	−0.06	80.7	15	5482	−3.5	0.6	2	4
TH14	8.37	1.10	109	177	614	−6.4	0.5	1	4
TH18	6.40	0.28	87.6	43	2014	0.8	0.5	1	2
TH18 (leached)						*-0.2*	*0.8*	*1*	*1 (Nu II)*
TH31	5.6	3.00	82.1	18	4574	−1.9	1.1	2	2 (1 Nu + 1 Nu II)
TH39	9.2	0.40	81.5	18	4533	4.4	0.8	1	1 (Nu II)
Ua Huka, Marquesas (EM†)									
UH53	0.38	0.76	155	235	663	−1.8	0.5	1	4
UH81	7.75	0.84	90.4	121	748	−1.9	0.5	2	5
UH89	7.2	1.63	89.8	39	2278	−3.5	0.5	1	3
UH93	9.85	0.38	72.8	97	753	−1.2	0.5	2	3
St Helena (HIMU)									
H28	6.64	0.13	101	26	3936	−0.9	0.5	1	5
H38	15.87	2.38	41.3	40	1043	−3.1	0.5	1	2
H64	10.97	0.72	61.7	14	4360	−0.7	0.5	1	2
H69	9.09	2.10	62.8	94	665	−3.3	0.9	2	9
Rurutu, Austral-Cook (HIMU)									
RRT-032	6.02	1.20	47.9	45	1073	−6.4	1.3	2	4
RRT-037	7.4	0.76	59.8	40	1489	6.6	0.5	1	1
RRT-037 (leached)						*4.9*	*0.8*	*1*	*1 (Nu II)*
74-386	7.24	1.58	56.5	14	4024	−2.4	0.5	2	2 (1 Nu + 1 Nu II)
74-390	6.29	1.35	74.9	44	1709	−6.3	0.5	1	1
74-390 (leached)						*-3.7*	*0.8*	*1*	*1 (Nu II)*
74-396	7.89	1.06	73.9	32	2290	−3.4	0.5	1	3
Tubuai, Austral-Cook (HIMU)									
TBA9	17.9	0.25	96.4	18	5371	−2.1	1.2	1	2 (Nu II)
K109	15.5	0.3	117	19	6108	−5.9	0.5	1	1
108B	10.85	0.68	88.4	10	9069	−3.1	0.5	1	1
5433	6.2	1.42	145	31	4691	−0.3	0.5	1	2
5434	11.26	0.74	84.0	25	3393	−3.5	0.5	1	1
5435	4.85	2.58	226	50	4497	−4.8	2.4	2	3 (1 Nu + 2 Nu II)
5436	9.59	1.26	111	12	9279	−2.1	0.5	1	1

* MgO and LOI values per Table 3.1 and references therein (see Appendix B3.i for full details). † Marquesas lavas exhibit variable composition: at a given $^{87}Sr/^{86}Sr$ value, lavas from the 'Ua Huka' group (Ua Huka, young Hiva Oa) have higher Nd isotopic compositions, and lavas from the 'Fatu Hiva' group (Fatu Hiva, old Hiva Oa, Montane, Tahuata) have higher $^{206}Pb/^{204}Pb$ (see Chauvel et al. 2012; Appendix B3.i).
2sd: where less than 3 measurements were possible, we adopt a conservative estimate based on the external reproducibility of reference materials on the instrument used. For measurements on the Nu HR, this is ±0.5 based on BCR-2 measurements. For the Nu Plasma II, this is ±0.8, based on Aldrich Tl solution data, for which there are the most measurements. The average of 2 measurements is quoted if it exceeds the external reproducibility of BCR-2 on either instrument.

3.2 Results

3.2.1 Trace element concentrations

Key major and trace element concentrations for the 48 OIB samples are provided in Table 3.2. Thallium concentrations range from 7 to 235 ng/g. The full dataset of 39 elements is provided in Appendix B3.ii, along with results for the reference materials measured contemporaneously with

the OIB samples. Trace element concentrations obtained for repeated measurement of BCR-2 and JB-2 are in good agreement with accepted values (Appendix B3.ii). For most elements, RSDs are generally <3%; for Tl, RSDs are <7% for 34 samples, and >10% for 5 samples (Fatu Hiva: FH01, FH11, FH18; St Helena: H28; and Tubuai: K109; Appendix B3.ii).

Many samples have existing trace element data published on the same powders (Appendix B3.i), and there is generally good agreement with previous work (Appendix B3.iii). We emphasize that the new data was collected with particular attention to the calibration of Tl concentration measurements, and is therefore used throughout the remainder of this work.

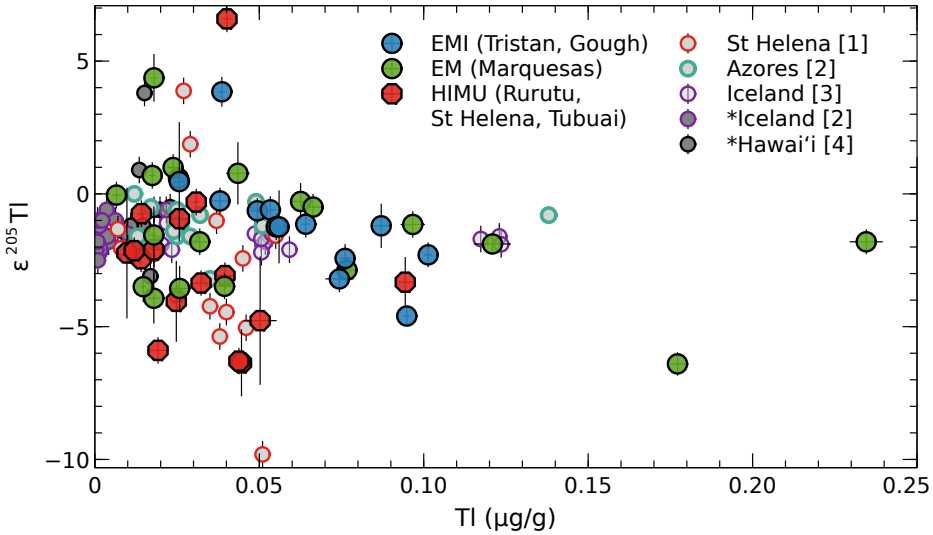


Figure 3.1: Plot of ε^{205}Tl versus Tl concentration. There is no co-variation. Large symbols: this study. Other data sources: [1] Blusztajn et al. (2018); [2] Nielsen et al. (2007); [3] Prytulak et al. (2017); [4] Nielsen et al. (2006b). * picrites.

3.2.2 Thallium isotope ratios

The Tl isotopic compositions of the 48 global OIB measured in this study are presented in Table 3.2, highlighting samples with isotopic compositions determined for both leached and unleached powders. Thallium isotopic compositions range from -6.4 to +6.6 and do not co-vary with Tl concentrations (Fig. 3.1).

The long-term intermediate precision of the Aldrich Tl solution measured on the *Nu HR* contemporaneously with OIB samples was ε^{205}Tl = -0.8 ± 0.4 (2sd; n = 211, 14 sessions, 4 years), calculated using the average ε^{205}Tl values obtained during each measurement session due to the large number of analyses. Unleached digestions of USGS reference materials AGV-2 (one digestion), BCR-2 (10 digestions) and BHVO-2 (2 digestions) yielded ε^{205}Tl values of -2.9 ± 0.5 (2sd; n = 3, 1 session), -2.6 ± 0.5 (2sd; n = 21, 4 sessions), and -1.2 ± 0.8 (2sd; n = 3, 1 session) for measurements with signal intensity >1 V on mass 205. For measurements of BCR-2 (4 digestions) with signal intensity <1 V, ε^{205}Tl = -2.5 ± 1.3 (2sd; n = 21, 3 sessions). For both Aldrich solution and USGS reference materials, many of these determinations were first reported in Brett et al. (2018), and the values obtained are in good agreement with previous compilations (Nielsen et al. 2017b, Prytulak et al. 2017).

The average obtained for the Aldrich Tl solution on the *Nu Plasma II* was ε^{205}Tl = -0.8 ± 0.8 (2sd; n = 28, 2 sessions, 2 months), with the higher uncertainty reflecting both the smaller num-

ber of analyses and the lower concentration of solutions. One unleached dissolution of BCR-2 yielded ε^{205}Tl = -3.1 (n = 1), while one leached dissolution yielded ε^{205}Tl = -2.1 (n = 1). Where only single measurements were possible, we assign the 2sd of Aldrich solution standard measurements (±0.8) as an estimate of minimum uncertainty. Therefore, there may be a small difference between leached and unleached BCR-2. However, it is at the limits of what we can confidently interpret.

Assessing secondary effects on Tl isotope ratios

Melt evolution. Many stable isotope systems display isotope fractionation during fractional crystallisation of melt (e.g. Teng et al. 2017). Thallium behaviour has previously been investigated using two cogenetic suites with invariant radiogenic isotopic compositions from different tectonic settings: Hekla, Iceland, and Anatahan, Mariana arc (Prytulak et al. 2017). Neither suite fractionates hydrous phases, nor do they exhibit resolvable Tl isotope fractionation during differentiation. Rader et al. (2018) showed that hydrous K-rich phases such as micas can exhibit distinct Tl isotopic compositions (ε^{205}Tl from -12.1 to +5.3) coupled with significant Tl enrichments (>5 µg/g). As such, while it is not possible to completely rule out crystallisation-induced fractionation, it is highly unlikely for the OIB studied here. With the caveat that our samples are not genetically related, there is no systematic variation of ε^{205}Tl with inferred or observed phenocryst phases or with MgO content in the current dataset (Fig. 3.2). We thus do not exclude any samples on this basis.

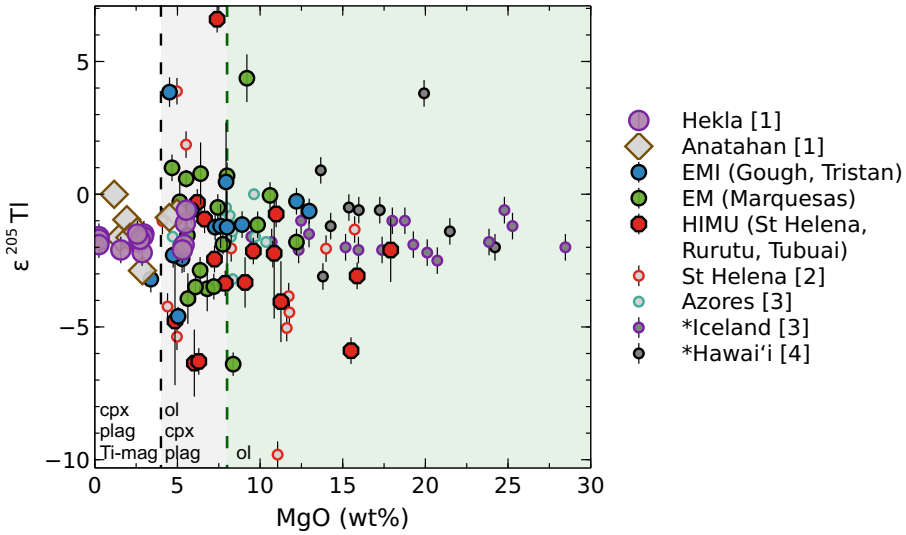


Figure 3.2: Plot of ε^{205}Tl versus MgO content of samples included in this study and from the literature. ε^{205}Tl does not vary systematically with melt evolution. As the majority of samples are not cogenetic, two suites of lavas following common liquid lines of descent (Hekla, Iceland; Anatahan, Mariana arc; Prytulak et al. 2017) are highlighted, showing that even at low MgO there is no correlation with ε^{205}Tl. Approximate fields of fractionating phases are indicated. Large symbols: this study. Other data sources: [1] Prytulak et al. (2017), [2] Blusztajn et al. (2018), [3] Nielsen et al. (2007), [4] Nielsen et al. (2006b). * picrites.

Degassing. Magmatic degassing can induce kinetic Tl isotope fractionation (Baker et al. 2009, Nielsen et al. 2021), theoretically producing residues with heavy Tl isotopic compositions and low Tl concentrations relative to incompatible refractory elements in contrast with condensates with isotopically light Tl, though these have yet to be reliably identified in nature. Various ratios have been employed to assess sample degassing, including Th/Tl (Nielsen et al. 2007), Pb/Tl

(Rehkämper and Nielsen 2004, Baker et al. 2009), Cs/Tl (Prytulak et al. 2013) and Ce/Tl (Nielsen et al. 2017a, 2021). The use of such ratios is challenging: Nielsen et al. (2017a) note that in arc settings, high Ce/Tl ratios potentially indicative of kinetic processes are still lower than the average value for the upper mantle. In the current dataset, there is no co-variation indicative of degassing between ε^{205}Tl and relevant trace element concetrations or ratios for samples from individual volcanoes (not shown). This lack of chemical evidence is coupled with a lack of textural evidence for significant degassing, in that samples are thought to have been emplaced during effusive eruptions and show no significant vesicularity. Therefore, no data are rejected on this basis.

Post-depositional effects. In submarine lavas, both contamination (increasing the Tl contents of the rocks) and alteration (decreasing the Tl contents, via weathering) potentially cause resolvable differences in ε^{205}Tl. As little as 1 µg of FeMn oxyhydroxide coating per gram of sample can cause an analytically resolvable shift to heavier isotopic signatures, while submarine alteration may efficiently strip Tl (at high temperatures) or add isotopically light Tl (at low temperatures; Nielsen et al. 2006b). Samples exhibiting very low Tl concentration and ε^{205}Tl require scrutiny for other evidence of alteration, whereas samples with very high Tl concentration and extreme ε^{205}Tl require scrutiny for contamination. A good example of the effects of alteration on Tl concentrations and isotopic compositions is provided by Blusztajn et al. (2018), in their study of St Helena lavas. In this case, a sample (SH-75) was excluded from interpretation due to its high Tl concentration (339 ng/g) combined with an isotopic composition of ε^{205}Tl = -4.06 and visual evidence of alteration. The authors consider surficial contamination by secondary clay minerals to be the most likely explanation for these features.

All OIB analysed in this study were collected subaerially, although ambiguous records mean that it is unclear if the oldest Rurutu lavas were erupted in a subaerial or submarine environment (Chauvel et al. 1997). One Rurutu lava (RRT-037) shows the highest ε^{205}Tl value (6.6 ± 0.5 2sd) reported for oceanic basalts thus far, warranting further assessment. However, rather than relying solely on chemical variation to identify such effects, five samples with ε^{205}Tl signatures significantly different from the mantle value (including RRT-037) were leached and reanalysed alongside USGS reference material BCR-2. The residues from the cold HCl leach retained 1% to 50% of the original Tl, leaving 0.05 to 1.9 ng/g total Tl available for analysis (∼6 ng/g for BCR-2), thus resulting in larger analytical errors for ε^{205}Tl (typically about ±1 ε unit). Notably, there is no systematic offset in ε^{205}Tl for the leached relative to the unleached sample powders (Table 3.2). This provides strong evidence that the positive and negative ε^{205}Tl end-members in our dataset are not due to surficial contamination. Therefore, we do not exclude any samples on this basis.

Assessment of subaerial post-depositional alteration is more challenging. These processes may remove Tl from the sample without significant Tl isotope fractionation. While large fractionations do arise in low-temperature environments, strong mineralogical control is exerted by secondary sulphides in low-T hydrothermally altered oceanic crust (Coggon et al. 2014) and by birnessite in FeMn sediments (Peacock and Moon 2012, Nielsen et al. 2013). Suspended riverine particulate matter, created through weathering, exhibits ε^{205}Tl very similar to that of loess, with the oxyhydroxide fraction generally containing only minor Tl that is not isotopically distinct (Nielsen et al. 2005). However, loss on ignition (LOI) is a traditional qualitative indicator of such

alteration. All 48 analysed samples have LOI <4%, and 41 have LOI <2%. The 7 samples with LOI >2% were described as showing no identifiable petrological evidence of alteration (see Table 3.1 and references therein). Therefore, no data are excluded on this basis.

3.3 Discussion

We combine our new dataset with published studies to explore Tl behaviour at constructive plate margins and in intraplate settings. We first revisit the relative compatibility of Tl during mantle melting, then present models of Tl behaviour during MORB and OIB melting. Finally, we examine Tl isotope systematics alongside Sr-Nd-Pb radiogenic isotopic compositions in the global OIB dataset to explore implications for cycling of Tl through the solid Earth.

3.3.1 Thallium elemental systematics

Thallium is highly incompatible during magmatic processes. Absolute Tl concentrations in OIB are thus principally determined by the extent of partial melting and fractional crystallisation. To compare the geochemistry of samples representing different degrees of melting, normalised incompatible element diagrams and ratios of trace elements with similar chemical partitioning are often employed. Quantitative assessment of how similarly two elements partition is superficially straightforward: in a log-log plot of element concentrations, pairs of element with similar incompatibility produce a linear trend with a slope of unity (e.g. Sims and DePaolo 1997). Such assessments are improved by taking into account the uncertainties in concentration for *both* elements (e.g. by using York regressions: York et al. 2004, Reed 2010). In reality, however, analytical and statistical errors potentially obscure small deviations from linearity, especially between highly incompatible elements. It is therefore important to keep in mind that such relationships are at best indicative of relative compatibility contrasts. For MORB data, Nielsen et al. (2014) calculated that La, Ce, and Pb had partitioning most similar to Tl, with log[Tl]–log[Ce] yielding a slope of 0.999 ± 0.034 (2sd, n = 594). Results for the expanded dataset incorporating Yang et al. (2018) are very similar (Table 3.3).

Table 3.3: Slopes obtained for York regressions (York et al. 2004) between log[Tl] and log[Element] (see text). For MORB, n = 909 except Cs, for which n = 702. For OIB, n = 48.

	MORB		OIB	
Element	slope	2sd	slope	2sd
Ce	0.994	0.030	0.102	0.122
Cs	2.608	0.036	2.033	0.571
La	1.285	0.047	0.116	0.136
Pb	0.875	0.021	1.131	0.488
Rb	3.114	0.218	1.091	0.504

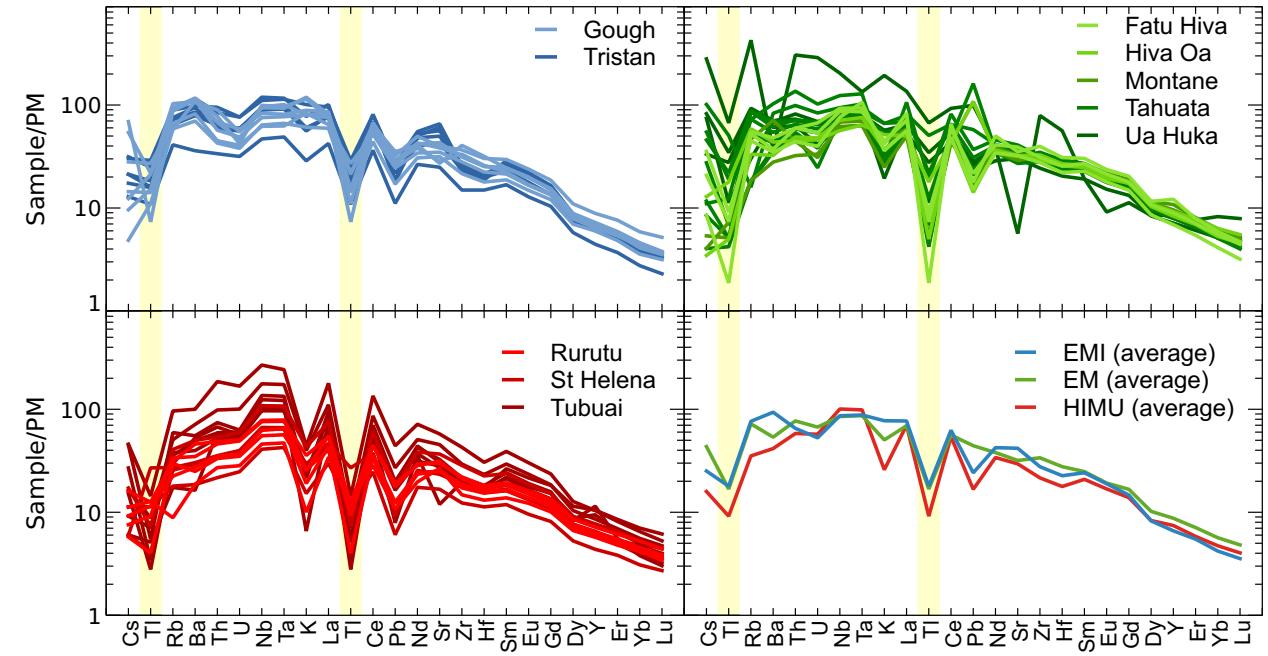


Figure 3.3: Primitive Mantle-normalised trace element plots. Note that Tl appears twice (highlighted), positioned both between Cs and Rb (Prytulak et al. 2017) and between La and Ce (Jenner 2017). For almost all samples there is a clear negative Tl anomaly regardless of position, as emphasised by the averages for each end-member.

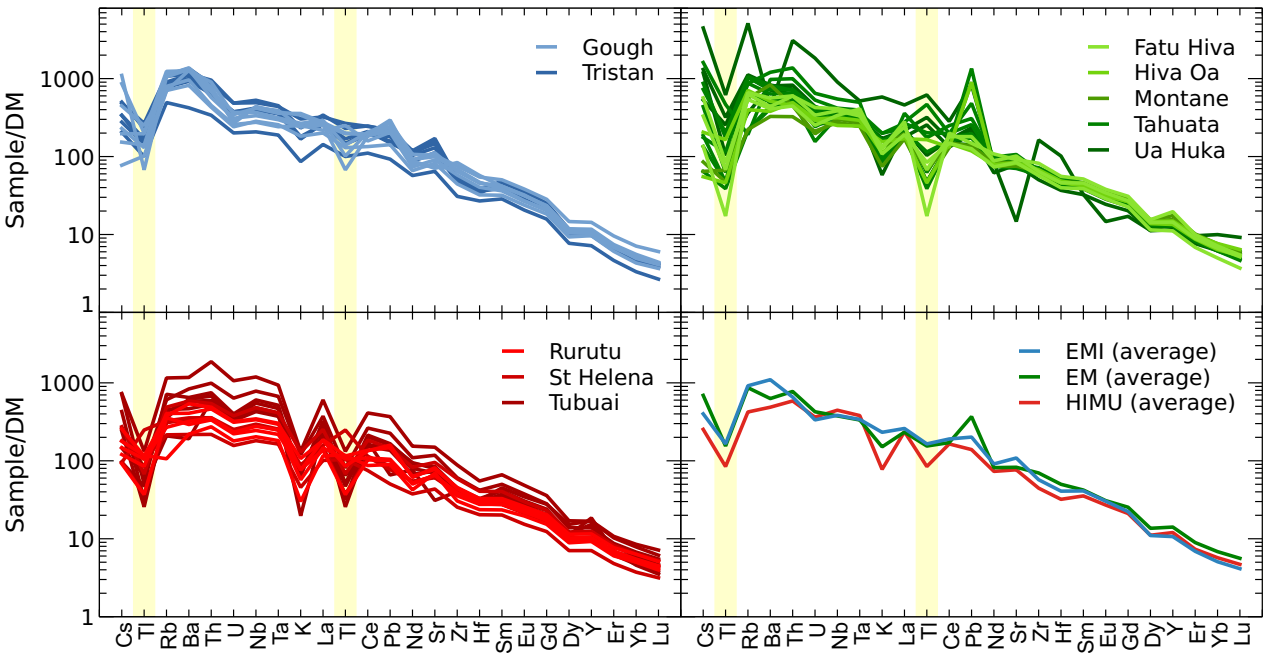


Figure 3.4: Depleted Mantle-normalised trace element plots. Here the negative Tl anomaly, while still present on average, is less pronounced – particularly for EM-type lavas.

OIB clearly derive from heterogeneous sources. As such, there is no expectation that log-log plots would provide anything other than a very approximate indication of relative partitioning. Indeed, even for samples from a single location there is a marked lack of coherence in log-log diagrams of Tl versus any trace element (not shown). Of all analysed elements, the closest approach to a slope of unity with log[Tl] is achieved for log[Rb], as found by Dupuy et al. (1973) for acidic volcanic rocks (Table 3.3). However, the uncertainty is so high that this is not a robust result. While lower uncertainties are achieved for log[Ce] and log[La], the slope does not approximate

unity. Attempting to identify elements with similar bulk partition coefficients to Tl during OIB generation via log-log plots is therefore problematic.

Normalised incompatible element diagrams. Thallium has been placed both between La and Ce, for low-pressure fractionation of MORB (Jenner 2017), and between Cs and Rb (Prytulak et al. 2017, following Dupuy et al. 1973). Given the ambiguity regarding placement and the lack of compelling indications from log-log plots, we consider both compatibility orderings for the presentation of OIB data. Incompatible elements normalised to PM abundances are shown in Figure 3.3, with normalisation to DM shown in Figure 3.4. Notable is the marked negative Tl anomaly compared to other large-ion lithophile elements (47 of 48 samples) and REE (all samples). The La-Tl-Ce ordering produces visually similar Tl depletions to elements that are fluid-mobile during subduction processing, particularly Pb. Interestingly, the magnitude of the negative Tl anomaly co-varies with absolute Tl abundance, regardless of ordering (Fig. 3.5). Such co-variation would be anticipated if the ambient mantle contains negligible Tl, such that increasing Tl abundances from exotic source(s) correlate directly with less negative Tl anomalies. In this scenario, the normalising PM (and DM) Tl concentration would be overestimated.

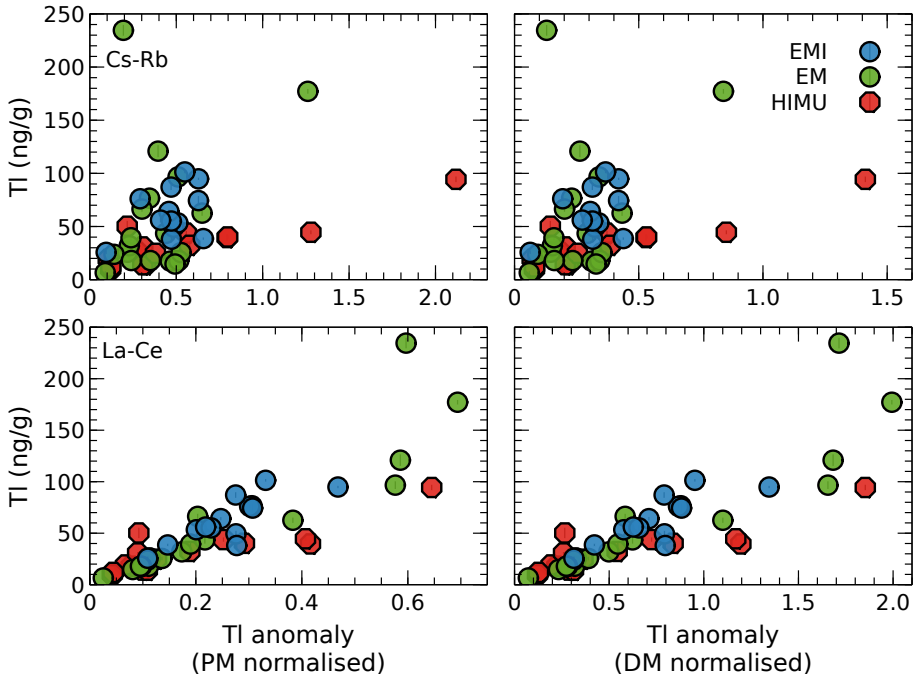


Figure 3.5: Tl anomaly exhibits clearer co-variation with absolute Tl abundance when calculated relative to REE than when calculated relative to LILE (with the possible exception of HIMU).

'Invariant' trace element ratios. Ratios of trace elements with similar partitioning are commonly used to 'see through' the effects of magmatic evolution: where partitioning is identical, ratios should be identical in source and product. However, selecting a suitable ratio for Tl in OIB is challenging. The Cs/Tl ratio has been used, as partitioning of these two elements and their fluid mobility was assumed to be similar (e.g. Nielsen et al. 2006b, Prytulak et al. 2013, 2017). However, Cs/Tl can be affected by both degassing and possible sequestration of Tl in accessory minerals during subduction (e.g. Prytulak et al. 2013), and although Cs concentration determinations are routinely performed during ICP-MS analyses they often have relatively large errors due to the low abundance of Cs in igneous systems. The Ce/Tl ratio has also been used to assess Tl systematics

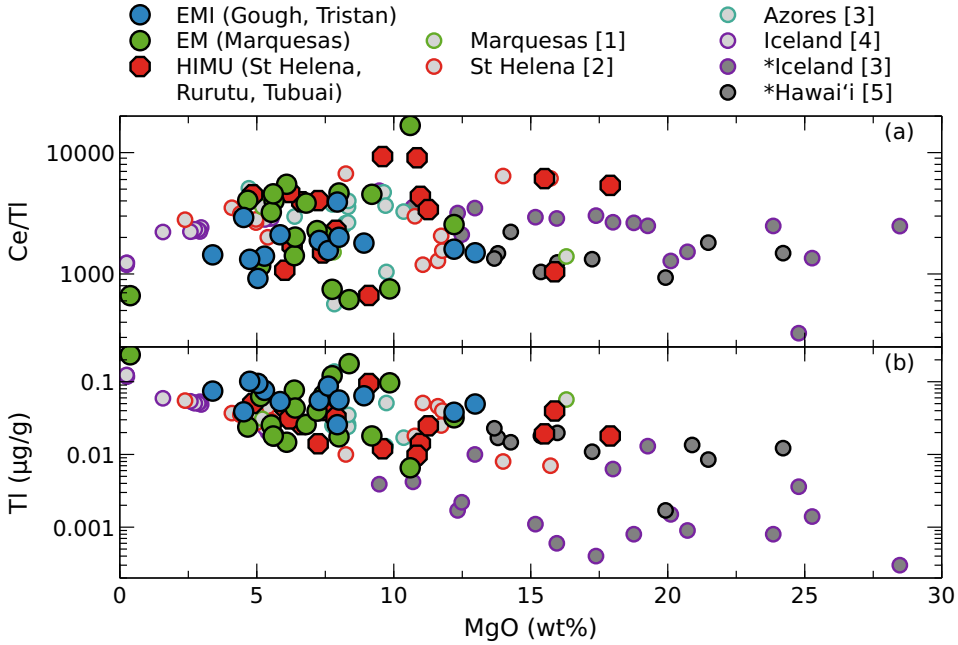


Figure 3.6: (a) Ce/Tl and (b) Tl concentrations plotted against MgO contents. Thallium is a highly incompatible element, and consequently the absolute abundance co-varies with indices of melt differentiation, such as MgO. However, Ce/Tl ratios do not exhibit co-variation with melt evolution for OIB samples, indicating that Ce and Tl exhibit similar incompatibility with respect to magmatic processes in the mantle. Large symbols: this study. Other data sources: [1] Chauvel et al. (2012), [2] Blusztajn et al. (2018), [3] Nielsen et al. (2007), [4] Prytulak et al. (2017), [5] Nielsen et al. (2006b). * picrites.

in igneous settings, and has the advantage of a limited range in MORB (e.g. Nielsen et al. 2014, 2017b). As Tl partitioning is clearly different between MORB and OIB regimes, no single ratio will be invariant for both tectonic settings.

In the new OIB dataset, Ce/Tl varies over an order of magnitude at a similar degree of magmatic differentiation. While absolute Tl concentrations in OIB vary with MgO content, taken as a measure of the extent of differentiation, Ce/Tl ratios do not (Fig. 3.6). Therefore, the range of Ce/Tl in OIB lavas likely arises from some combination of source heterogeneity and melting processes. For example, Shu et al. (2019) observed a wide range of Ce/Tl in subducted eclogites, which are geochemically similar to altered subducted oceanic crust that is thought to be a common component in OIB sources. Some authors have noted generally higher Ce/Tl ratios in OIB compared to MORB (Nielsen et al. 2014, Blusztajn et al. 2018). When examining all available data, a clear tectonic distinction between MORB, arc and OIB lavas is apparent (Fig. 3.7): (i) arc lavas generally exhibit the lowest Ce/Tl and highest Tl concentrations, alongside the most scattered distribution, even when filtered to exclude non-basaltic samples; (ii) MORB Ce/Tl clusters around 1140, as previously discussed in Nielsen et al. (2014); and (iii) global OIB form a remarkably coherent array that is clearly distinct from MORB, with overlap between the different mantle components defined by radiogenic isotopes. Similar patterns are observed for ratios of Tl with Rb, Cs, La and Pb, though with these latter ratios the different tectonic settings are less clearly distinguished (Fig. 3.8), motivating the further focus on Ce/Tl systematics.

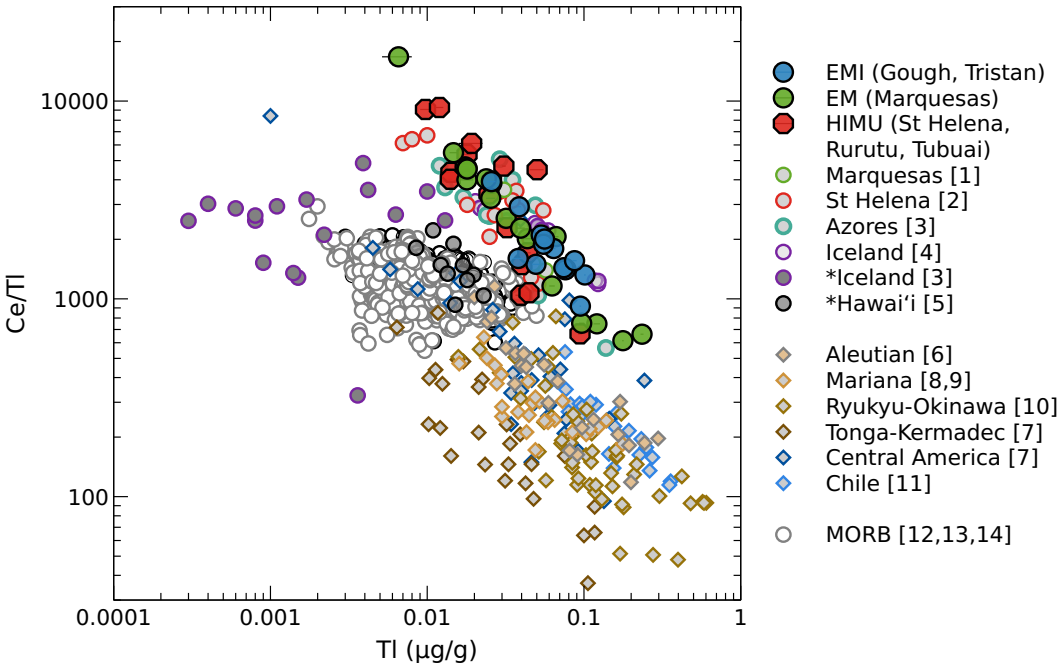


Figure 3.7: Plot of Ce/Tl ratios versus Tl concentrations in oceanic basalts and arc lavas. Ce/Tl trends clearly distinguish between tectonic melting regimes for fresh lavas. Note that Hawai'ikiian and Icelandic picritic lavas (dark grey) lie off the general OIB trend. Large symbols: this study. Other data sources (see Table 3.2, Appendix B3.i): [1] Chauvel et al. (2012); [2] Blusztajn et al. (2018); [3] Nielsen et al. (2007); [4] Prytulak et al. (2017); [5] Nielsen et al. (2006b); [6] Nielsen et al. (2016); [7] Nielsen et al. (2017a); [8] Prytulak et al. (2013); [9] Prytulak et al. (2017); [10] Shu et al. (2017); [11] Cox et al. (2019); [12] Jenner and O'Neill (2012a); [13] Nielsen et al. (2014); [14] Yang et al. (2018). * picrites.

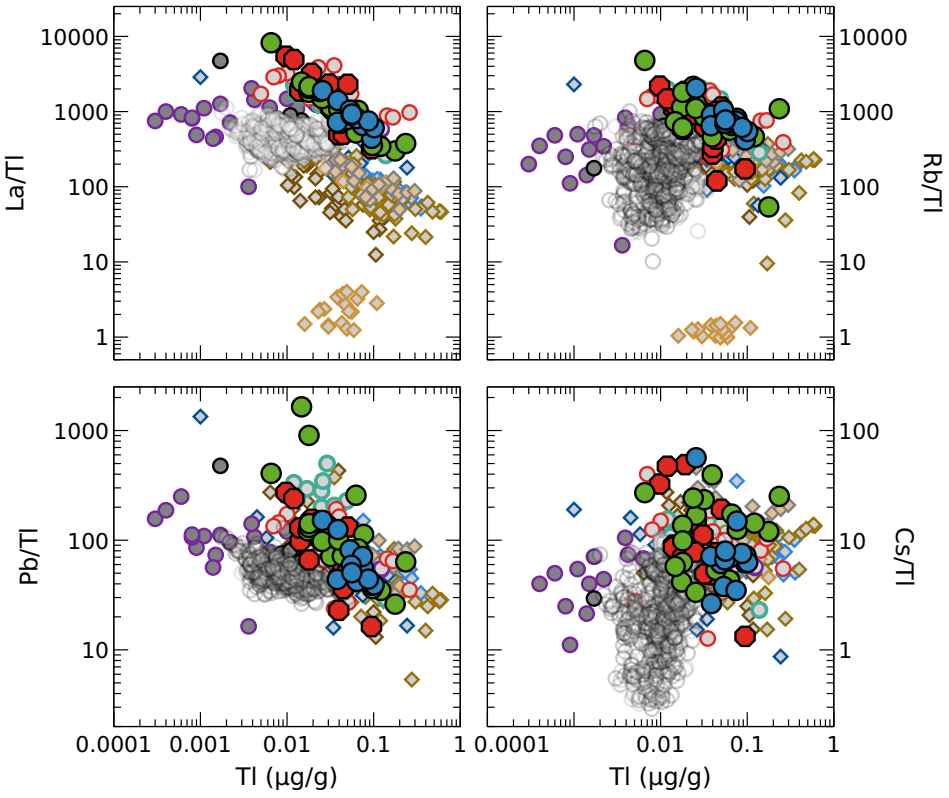


Figure 3.8: Plot of La/Tl, Pb/Tl, Rb/Tl and Cs/Tl ratios against Tl concentration. Only the La/Tl ratios distinguish tectonic settings as clearly as the Ce/Tl ratios. Symbols and data sources as in Figure 3.7.

Table 3.4: Modal mineralogy and melt reaction coefficients used in modelling.

	spinel lherzolite (MORB)		garnet lherzolite (OIB)	
Mineral	vol proportion (%)[1]	melting coefficient[2]	vol proportion (%)[3]	melting coefficient[3]
olivine	0.57	-0.2	0.55	0.08
clinopyroxene	0.13	0.8	0.25	0.81
orthopyroxene	0.28	0.32	0.15	-0.19
spinel	0.02	0.08	-	-
garnet	-	-	0.05	0.3
sulphide	variable	SCSS*	variable	SCSS

* Sulphur concentration at sulphide saturation (see text). [1] Workman and Hart (2005); [2] Baker and Stolper (1994) and Wasylenki et al. (2003), as modified by Nielsen et al. (2014); [3] Elliot et al. (2007).

Table 3.5: Parameters used in models of MORB and OIB melting.

		MORB (Nielsen et al. 2014)		MORB		OIB	
Variable	Symbol	Value range	References	Value range	References	Value range	References
Melting							
melt fraction	F	0-16%	-	0-16%	- 0-18%	-	
melt increment		0.01%	-	0.1%	-	0.1%	-
mean pressure		1.5 GPa	-	1.5GPa	-	3 GPa	-
mean T		1350 °C	-	1350 °C	-	1445 °C	-
FeO in melt		∼10%	*8*	∼10%	*8*	∼10%	*sample data*
SCSS		1200 µg/g	*9-11*	1200 µg/g	*9-11*	1200 µg/g	*9-11*
Partition coefficients							
Thallium	$D^{Tl}_{cpx/melt}$	0.0006	*1*	0.0006	*1*	0.0006	*1*
	$D^{Tl}_{opx/melt}$	0.00045	*1*	0.00045	*1*	0.00045	*1*
	$D^{Tl}_{ol/melt}$	4.5×10^{-5}	*1*	4.5×10^{-5}	*1*	4.5×10^{-5}	*1*
	$D^{Tl}_{sp/melt}$	0	*1*	0	*1*	-	-
	$D^{Tl}_{gt/melt}$	-	-	-	-	0	*assumed (3)*
	$D^{Tl}_{sulph/sil}$	18-100	*model*	1-25	*model*	1-25	*model*
	Bulk D	0.0002-0.11		0.0002-0.028		0.0002-0.0007	
Cerium	$D^{Ce}_{cpx/melt}$	0.14	*2*	0.01-0.8	*4-7*	0.01-0.8	*4-7*
	$D^{Ce}_{opx/melt}$	0.006	*2*	0.006	*2*	0.0026	*7*
	$D^{Ce}_{ol/melt}$	4×10^{-5}	*2*	4×10^{-5}	*2*	4×10^{-5}	*2*
	$D^{Ce}_{sp/melt}$	0	*assumed*	0	*assumed*	-	-
	$D^{Ce}_{gt/melt}$	-	-	-	-	0.003	*3*
	$D^{Ce}_{sulph/sil}$	0	*assumed*	0	*assumed*	0	*assumed*
	Bulk D	0.02		0.003-0.1		0.002-0.16	

[1] Assumed identical to Rb partition coefficients of Donnelly et al. (2004); [2] McDade et al. (2003b); [3] Adam and Green (2006) were unable to determine a partition coefficient for Tl between garnet and silicate melt, but for LILE, values were very low; [4] Frey (1969); [5] Irving and Frey (1984); [6] Nagasawa et al. (1969); [7] Matsui et al. (1977); [8] Gale et al. (2013); [9] Liu et al. (2007); [10] Mavrogenes and O'Neill (1999); [11] O'Neill and Mavrogenes (2002).

Table 3.6: Thallium and cerium concentrations in reservoirs used in modelling.

Reservoirs	Ce (µg/g)	References	Tl (ng/g)	Refs	S (µg/g)*	References
DM	0.55	*1*	0.27-0.48	*9, model*	0-400	*2, model*
PM	1.675	*2*	3.5	*2*	0-400	*2, model*
Peridotites	0.020-0.39	*3*	0.05-3.5	*3*	76-360	*3, 12*
FeMn sediment (hydrogenetic)	700	*8*	90000	*11*	-	-
Subducted eclogites†	20 (1–210)	*13*	60 (2–350)	*11*	-	-
Subduction-processed oceanic crust	∼23–75	*calculated*	∼2–6	*calculated*	-	-

* Sulphide abundance was converted to S concentration using the assumption that on average mantle sulphides are 36 wt% S, i.e. dominantly FeNi sulphides. † mean (ranges). [1] Workman and Hart (2005); [2] McDonough and Sun (1995); [3] Wang et al. (2018); [4] Sparks (1995); [5] Zuleger et al. (1996); [6] Bach et al. (1996); [7] Sun and McDonough (1989); [8] Piper (1974); [9] Nielsen et al. (2014); [10] Nielsen et al. (2006c); [11] Rehkämper et al. (2002); [12] Ding and Dasgupta (2018); [13] Shu et al. (2019).

3.3.2 Modelling Tl variations in MORB and OIB

The systematic variation of Tl versus Ce/Tl in global MORB and OIB can be explored with simple melting and mixing models. Fractional, non-modal melting models help explore the contrasting Ce/Tl patterns of MORB and OIB, though simplifying assumptions must be made for several parameters (Tables 3.4–3.6). Nielsen et al. (2014) identified constraints for the majority of these parameters for MORB generation, and modelled production of the "near-uniform" Ce/Tl ratio for MORB through variation of S concentrations and associated $D^{Tl}_{sulph/sil}$ values. However, subsequent findings warrant some re-evaluation of parameters.

Thallium partitioning. While it is clear that Tl is hosted in sulphides to some extent, recent investigations into the partitioning of Tl indicates that it is less strongly chalcophile than previously assumed (e.g. Kiseeva and Wood 2015, Wood and Kiseeva 2015, Jenner 2017). Nielsen et al. (2014) based their values of $D^{Tl}_{sulph/sil}$ during MORB melting (18–100) on data from Kiseeva and Wood (2013), who reported $D^{Tl}_{sulph/sil}$ = 4–24. However, a growing body of evidence supports the concept that 'mixed affinity' behaviour is exhibited by Tl, i.e. elemental behaviour cannot be described as either predominantly chalcophile or predominantly lithophile.

Kiseeva and Wood (2015) report $D^{Tl}_{sulph/sil}$ of 4–33, and note that "partitioning of most elements is a strong function of the oxygen (or FeO) content of the sulphide", which "increases linearly with the FeO content of the silicate melt and decreases with the Ni content of the sulphide." Wood and Kiseeva (2015) go on to state that Tl partitioning does not obey this simple model, nor one extended through consideration of additional parameters: "Despite simple and predictable partitioning behavior for many elements, several important elements (Ni, Cu, Ag, Mn, Tl) show strongly non-linear dependences of $\log D_i$ on log[FeO] and we were unable to assign them to any one particular category in terms of affinity for sulphide."

Overall, there is a growing consensus that Tl exhibits 'mixed affinity' behaviour, e.g. as reported by Greaney et al. (2017) during magmatic differentiation at Kīlauea Iki. Jenner (2017) calculated that for typical MORB melting $D^{Tl}_{sulph/sil}$ = 7. Wang et al. (2018) suggested that a significant proportion of the Tl contents of peridotites are hosted in interstitial late-crystallising silicate phases, finding that sulphides typically contribute <30% of the bulk rock Tl budget. These observations are consistent with poor correlation of Tl concentrations with chalcophile element concentrations in most igneous contexts (e.g. Prytulak et al. 2017). We therefore explored $D^{Tl}_{sulph/sil}$ values between 1 and 25 and present results for $D^{Tl}_{sulph/sil}$ = 10 (e.g. Kiseeva and Wood 2013, 2015).

Although Tl is known to be highly incompatible, partitioning of Tl between silicate minerals and melt remains poorly constrained. Nielsen et al. (2014) therefore assumed $D^{Tl}_{min/melt}$ identical to $D^{Rb}_{min/melt}$ due to the similarity in ionic charge and radius. Tl^+ is well-known to substitute for K^+ in silicate minerals (e.g. Shaw 1952), as documented by e.g. Rader et al. (2018), and we also assume similar partitioning behaviour of Rb and Tl in silicate contexts.

Cerium partitioning. While variation in mineral-melt partitioning of Ce between clinopyroxene and basaltic melt (herein $D^{Ce}_{cpx/melt}$) is not required to model the MORB Ce/Tl array, it is likely that such variation does exist and does contribute to the observed pattern. Variations in $D^{Ce}_{cpx/melt}$

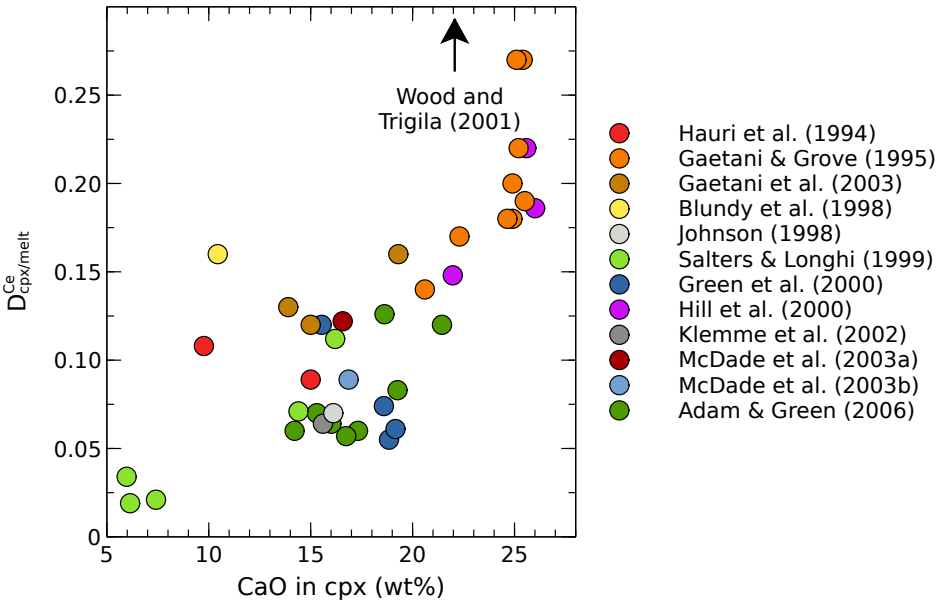


Figure 3.9: $D^{Ce}_{cpx/melt}$ values versus CaO in clinopyroxene. This illustrative plot has not been corrected for pressure and temperature, or for other compositional variables including degree of hydration. With the notable exception of Green et al. (2000) and the two McDade studies, which examine melting under strongly hydrous conditions, there is a general sense of increasing Ce compatibility as CaO in cpx increases both within and between studies.

have been attributed to differences in mineral chemistry, with $D^{Ce}_{cpx/melt}$ generally observed to increase with increasing wollastonite and tetrahedrally-coordinated Al content of clinopyroxene.

As of May 2021, the GERM database documents a range in $D^{Ce}_{cpx/melt}$ from 0.017 (Frey 1969) to 0.82 (Vannucci et al. 1998), excluding the values of Nagasawa (1973), which were determined on natural samples showing signs of significant alteration (Uchimizu 1966). The data compilation of Sun and Liang (2012) features a range of $D^{Ce}_{cpx/melt}$ from 0.019 (Salters and Longhi 1999) to 0.27 (Gaetani and Grove 1995), and is presented graphically in Figure 3.9 (excluding the data of Wood and Trigila 2001, which were determined for highly potassic melts, yielding $D^{Ce}_{cpx/melt}$ from 0.48 to 1.31). Johnston and Schwab (2004) additionally determined a $D^{Ce}_{cpx/melt}$ value of 0.47 during experiments on the partial melting of peridotite (not shown). Further data for partitioning of REE in the presence of high-Ca clinopyroxenes was compiled by Bédard (2014), though the dataset for terrestrial basalts is limited.

While Sun and Liang (2012) provided recommended values for $D^{Ce}_{cpx/melt}$ during MORB melting ($\sim$0.08 for anhydrous melting of spinel lherzolite), they note that these values are based on highly simplified thermodynamic models of clinopyroxene that may represent unrealistically restricted mineral composition ranges. We therefore explore a range of $D^{Ce}_{cpx/melt}$ from 0.01 to 0.8 in our modelling (Table 3.5). We do not consider 0.8 a value that is likely to be achieved in natural rocks, but it is informative as an end-member scenario.

MORB melting models. The MORB dataset in Figure 3.10 combines the studies of Jenner and O'Neill (2012a), Nielsen et al. (2014), and Yang et al. (2018), excluding samples with MgO < 6wt%, sea-mounts, back-arc basins and aseismic ridges. These studies yield a combined mean MORB Ce/Tl of 1220 ± 570 (2sd, n = 909).

Fractional melting models assuming a spinel lherzolite source with variations in $D^{Ce}_{cpx/melt}$ and initial elemental concentration are shown in Figure 3.10, with the fractional melting model of Nielsen et al. (2014) reproduced in Figure 3.10a. For Ce concentration, we use the values of

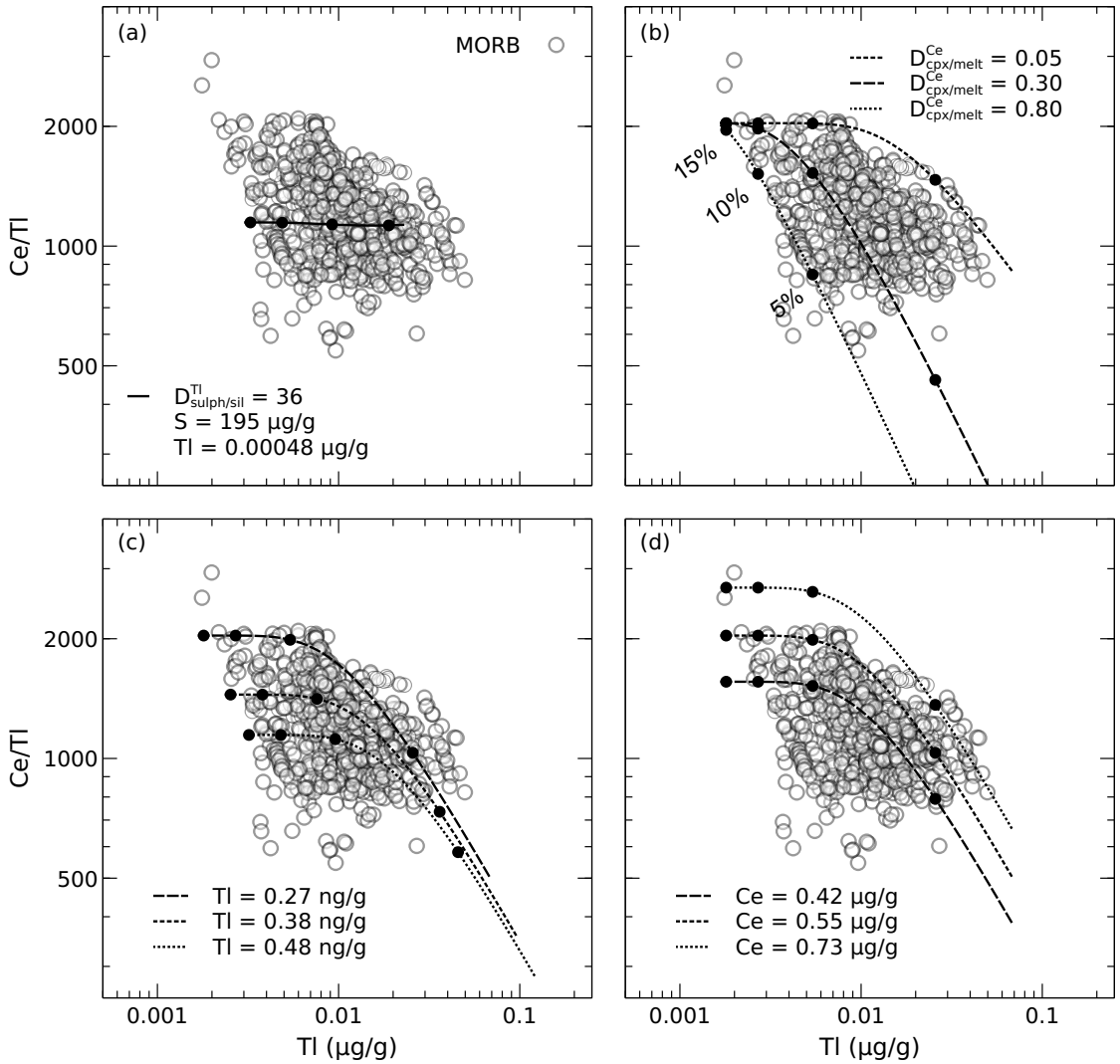


Figure 3.10: (a) MORB melting model of Nielsen et al. (2014), with Tl_{DM} = 0.48 ng/g, S_{DM} = 195 µg/g and $D^{Tl}_{sulph/sil}$ = 36 (for other parameters see Table 3.5). (b) Modified MORB melting model assuming S_{DM} = 100 µg/g and $D^{Tl}_{sulph/sil}$ = 10; lower $D^{Tl}_{sulph/sil}$ increases the melt percentage required to achieve any given Tl-Ce/Tl data pair. In this modified model we permit variation of $D^{Ce}_{cpx/melt}$ (see text, Table 3.5), reproducing both the average MORB Ce/Tl and the sense of variation. Best fit is achieved with a lower Tl_{DM} of 0.27 ng/g, implying a DM Ce/Tl of ∼1800. (c) Modified model with variable Tl (see legend), Ce = 0.55 µg/g, S = 100 µg/g, $D^{Tl}_{sulph/sil}$ = 10, $D^{Ce}_{cpx/melt}$ = 0.1 (d) Modified melting model with Tl = 0.27 ng/g, variable Ce (see legend; Workman and Hart 2005), and other values as for subfigure *(c)*. MORB data is from Jenner and O'Neill (2012b), Nielsen et al. (2014) and Yang et al. (2018) (see text for details); compiled data is provided in Appendix B3.vi.

Workman and Hart (2005) for Depleted MORB Mantle (DMM), Enriched MORB Mantle (EMM), and the average MORB source. For Tl concentration, we consider previous DM estimates along with values that provide the best fit for our model. We explore a range of $D^{Ce}_{cpx/melt}$ in Figure 3.10b, reproducing not only the average Ce/Tl value observed for MORB but also the sense of variation in the data. Compared to the model of Nielsen et al. (2014), the reduced compatibility of Tl in sulphides means that the model is less sensitive to the S concentration of the upper mantle. Considering only variations in the bulk partitioning of Ce, over 80% of MORB samples can be explained with a range of $D^{Ce}_{cpx/melt}$ up to ∼0.35. Furthermore, about 50% of MORB samples are explained by $D^{Ce}_{cpx/melt} \leq 0.2$, while fewer than 2% of MORB samples require $D^{Ce}_{cpx/melt} \geq 0.8$.

We also present the effects of variation in initial Tl and Ce concentration on our melting model (Fig. 3.10c, 3.10d), with $D^{Ce}_{cpx/melt}$ = 0.1 (equivalent to bulk D^{Ce} = 0.015, i.e. the average value for peridotite melting calculated by Stracke and Bourdon 2009). Again, variation in either of these

parameters can account for both the average Ce/Tl ratio in MORB and the sense of the observed variation.

The models thus highlight two main points:

1. As previously noted, MORB Ce/Tl exhibits some variation with Tl concentration that exceeds measurement uncertainties (Nielsen et al. 2014). We suggest that Ce/Tl variations in MORB can be explained through a combination of melting effects, a range of $D^{Ce}_{cpx/melt}$ associated with variations in the mineral composition of clinopyroxene, and variations in source concentrations of Tl and Ce. Notably, this model does not require that bulk partition coefficients for Ce and Tl be approximately equal, and is nonetheless able to satisfy the constraint that a log-log concentration plot should exhibit a slope close to unity given the observed maximum concentration of Tl in MORB.

2. Regardless of the chosen value of $D^{Ce}_{cpx/melt}$, a model incorporating lower compatibility of Tl in sulphides than previously assumed yields a best fit for a Tl_{DM} abundance of 0.27 ng/g. This value is calculated assuming (i) that samples with the lowest Tl concentrations on average represent the highest degree of melting, i.e. the closest approach to the DM Ce/Tl ratio, and (ii) an average Ce_{DM} of 0.55 µg/g (Workman and Hart 2005). Our proposed Tl_{DM} is considerably lower than the estimate of Salters and Stracke (2004) of 0.38 ng/g, and much lower than that of Nielsen et al. (2014) of 0.48 ng/g.

OIB melting models. Fractional melting models assuming either a PM or a DM source (Table 3.4) with up to 15% melting are shown in Figure 3.11a. For PM composition, we used the Tl and Ce concentrations of McDonough and Sun (1995) as our initial values, then varied concentrations as required to fit our model to the data. It is immediately apparent that partial melting alone cannot produce the observed OIB Ce/Tl array from a PM or DM source, even for extreme values of $D^{Ce}_{cpx/melt}$. The systematics in a plot of Tl/Ce versus Tl (Fig. 3.12; Minster and Allègre 1978) emphasise that the observed range exceeds that which can be explained by partial melting and fractional crystallisation alone, consistent with longstanding radiogenic isotopic evidence for the heterogeneous and mixed nature of OIB sources. Notably, variations in S concentration or $D^{Tl}_{sulph/sil}$ have no significant effect on model fit, but do affect the required degree of partial melting.

To explain the variation in the OIB array we first establish constraints on the mixed source compositions. In this context, solid state mixing is assumed, rather than mixing of partial melts of distinct components. Parameters including partition coefficients and initial elemental concentrations were varied until approximate matches between model output and the observed data array for up to 15% melting were achieved (Fig. 3.11b). We then incorporate the assumption that OIB lavas are typically the product of ∼3-5% melting. In this scenario, the required source materials vary over an order of magnitude in terms of Tl concentration even within a single island (Figures 3.11c, 3.11d). A striking feature of the model is that the majority of the array requires a source that is significantly more enriched in Ce than PM estimates, *without* similar enrichment in Tl. Indeed, most lavas require Tl source concentrations lower than PM estimates, and in some instances more depleted than DM. Of all the OIB samples analysed to date (n = 93) only 10 (∼11%) require a source Tl concentration >3.5 ng/g, i.e. more enriched in Tl than PM. These include samples from Faial in the Azores (Nielsen et al. 2007), and Tahuata and Ua Huka in Polynesia (Chauvel

et al. 2012 and this work). Notably, although lavas from individual islands require source heterogeneity in terms of Tl concentration, lavas representing distinct radiogenic isotopic compositions have overlapping Ce/Tl ranges.

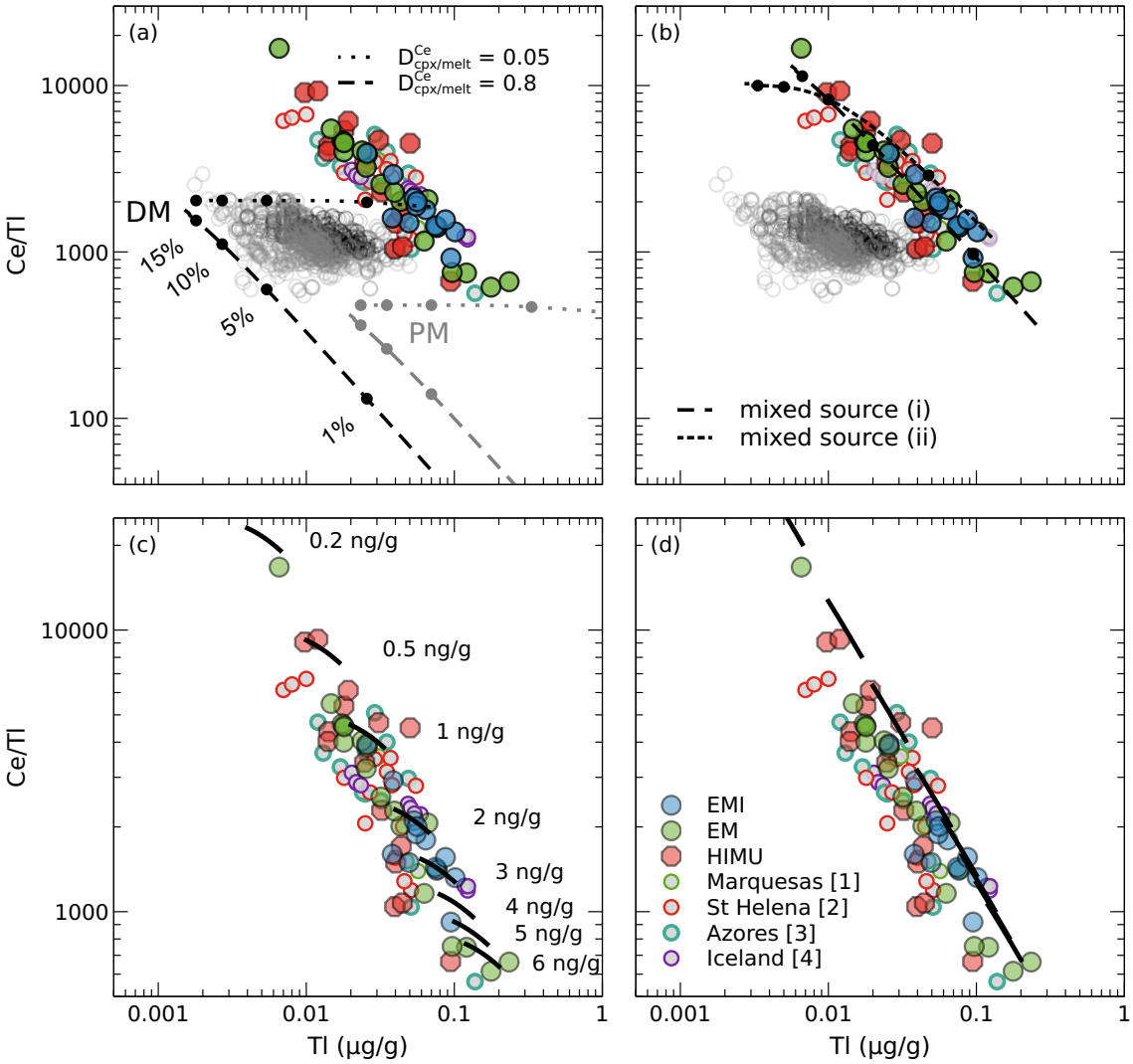


Figure 3.11: (a) Melting of PM (grey) and DM (black) sources (Table 3.6) with varying $D^{Ce}_{cpx/melt}$; (b) melting of (i) a hypothetical mixed source with Tl = 1 ng/g, Ce = 15 µg/g, and $D^{Ce}_{cpx/melt}$ = 0.8; (ii) a hypothetical mixed source with Tl = 0.5 ng/g, Ce = 5 µg/g, and $D^{Ce}_{cpx/melt}$ = 0.15. (c) 3–5% melting of a hypothetical source with Ce = 5 µg/g and $D^{Ce}_{cpx/melt}$ = 0.1. Source Tl concentration varies as indicated on figure. (d) As subfigure *(c)*, but instead Ce = 15 µg/g and $D^{Ce}_{cpx/melt}$ = 0.5. Large symbols: this study. Other data sources: [1] Chauvel et al. (2012), [2] Blusztajn et al. (2018), [3] Nielsen et al. (2007), [4] Prytulak et al. (2017). All displayed models assume 100 µg/g S (Ding and Dasgupta 2018) and $D^{Tl}_{sulph/sil}$ = 10. All melting percentages as marked on subfigure *(a)*.

The mixed source concentrations required by the OIB Ce/Tl array can be interpreted as a mantle 'background' that is extremely depleted in Tl, with addition of a material characterised by high Ce and heterogeneous Tl concentrations, broadly consistent with models of widespread addition of subducted materials to the mixed OIB source. However, prior to subduction surface materials with high Ce concentrations (e.g. FeMn sediments) also exhibit elevated Tl concentrations that greatly exceed values that can be accommodated by the mixing-melting model. If subducted materials are the exotic addition controlling Ce/Tl systematics in OIB, it is necessary that the majority of Tl must be removed or otherwise lost during subduction processing, rather than being recycled into

the deep mantle. A ∼20% addition of such 'subduction-processed oceanic crust' (Table 3.6) to mantle strongly depleted in Tl would produce an appropriate mixed OIB source.

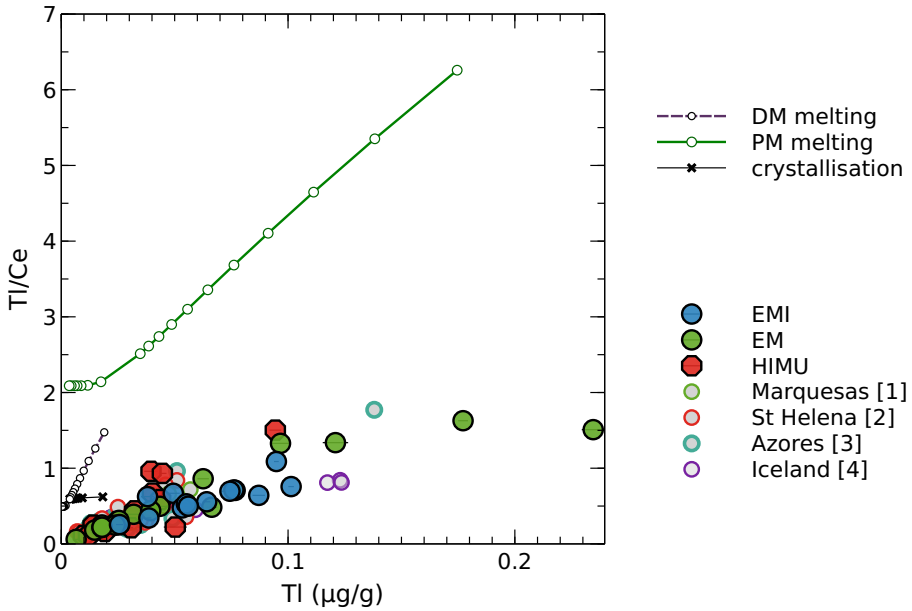


Figure 3.12: Process identification plot (Minster and Allègre 1978) of Tl/Ce against 1/Tl. Also shown are melting patterns (melt fraction F = 0.0001 to 1) for DM (Tl = 0.00038 µg/g, Ce = 0.772 µg/g) and PM (Tl = 0.0035 µg/g, Ce = 1.675 µg/g), in addition to the fractional crystallisation trend (F = 1 to 0.1), assuming bulk D^{Tl} = 0.02 and bulk D^{Ce} = 0.06. While most of the variation in OIB is subparallel to the DM melting trend, with scatter leaving room for some fractional crystallisation, the observed range significantly exceeds that which can be explained simply through a combination of melting and fractional crystallisation. The OIB trend therefore requires mixing melts from different sources, one of which cannot contain more than negligible Tl (note y-intercept of trend). Large symbols: this study. Other data sources: [1] Chauvel et al. (2012), [2] Blusztajn et al. (2018), [3] Nielsen et al. (2007), [4] Prytulak et al. (2017).

Recently, Shu et al. (2019) analysed the trace element and Tl isotopic composition of a number of eclogites subducted to a maximum depth of ∼90 km before being exhumed, which might represent such 'subduction-processed' oceanic crust. This sample suite has an average Ce concentration of 20 µg/g with an average Tl concentration of 55 ng/g (Table 3.6). While the Ce concentration is consistent with the requirements for our proposed subduction-processed oceanic crust, the Tl concentration is an order of magnitude more than the maximum we invoke to satisfy our constraints on OIB source concentrations. However, as the eclogite samples remained within the stability field of Tl-rich phengite, it is likely that further Tl loss would occur during deeper subduction beyond the phengite stability field (e.g. Schmidt et al. 2004, Kessel et al. 2005; see detailed discussion in Chapter 4).

We agree with the findings of Shu et al. (2019) that OIB Ce/Tl systematics indicate widespread incorporation of subduction-processed oceanic crust into the OIB source, which may consist of (ancient, relatively enriched) oceanic crust with variable addition of a continental crust component. The Ce/Tl systematics of OIB thus highlight *similarities*, not differences, between mantle components distinguished by their radiogenic isotopic compositions. The complete overlap between different lavas representing distinct (enriched) mantle end-members strongly implies that a high-Ce, low-Tl material such as subduction-processed oceanic crust is common to OIB sources, and that Tl is near quantitatively removed during subduction.

3.3.3 Thallium isotopic composition of OIB

The Tl isotopic composition of the mantle is strikingly homogeneous, and no resolvable Tl isotope fractionation is observed during partial melting or fractional crystallisation. Therefore, the significant Tl isotopic variability observed in global OIB (ε^{205}Tl from -10.0 to +6.6) requires the addition of isotopically distinct material to the lavas. The addition of such material can happen in the source, *en route* to the surface, and/or via subaerial/submarine alteration. We have already argued that alteration does not play a significant role in the new data, and previous work on OIB samples (see Table 3.1) has similarly screened and discounted altered samples.

Thallium isotopic compositions were predicted to co-vary with the Sr-Nd-Pb radiogenic isotopes used to classify mantle components, depending on whether AOC or recycled sediments were the primary contributor of exotic material. However, the elemental systematics of Tl in OIB appear to require highly efficient removal of Tl during subduction, which potentially weakens the link between deep mantle recycling and OIB sources in terms of Tl isotopes. Indeed, the first order observation for our global dataset is that primary Tl isotopic compositions do not co-vary with radiogenic Pb, Sr, Nd, or Hf isotopes (Fig. 3.13), even within the chemically diverse Marquesas island group. Although the range is large, the average ε^{205}Tl for HIMU and EM-type lavas overlap within error. For HIMU ε^{205}Tl = -2.6 ± 6.6 (2sd, n = 37), and for EM ε^{205}Tl = -1.3 ± 4.4 (2sd, n = 32). The overlap remains even if the comparison is restricted to main-phase St Helena lavas and EMI-type lavas, for which ε^{205}Tl = -3.2 ± 3.1 (2sd, n = 10) and ε^{205}Tl = -1.1 ± 4.0 (2sd, n = 13), respectively. The absence of correlation between Tl isotopic compositions and Sr-Nd-Pb-Hf radiogenic isotope systems is consistent with trace element modelling that requires the mantle sources to be ubiquitously depleted in Tl, likely due to near-quantitative removal of Tl during the subduction process. Elemental parent-daughter pairs for radiogenic isotopes do not show this same level of depletion in OIB sources, and thus Tl and radiogenic Sr-Nd-Pb-Hf isotopic compositions can be easily decoupled, as noted by the first study of Tl isotopic composition in OIB (Nielsen et al. 2006b).

However, our finding that Tl isotope systematics may not be a straightforward 'fingerprint' of recycled AOC or FeMn sediment contributions to OIB source regions is at odds with previous work. While no variation in Tl isotopic composition was found in lavas from the Azores or Iceland (Nielsen et al. 2007), incorporation of deeply subducted FeMn sediment was invoked to explain variations observed in Hawai'ian picrites (Nielsen et al. 2006b), and HIMU-type St Helena basalts have been argued to show evidence for incorporation of subducted AOC (Blusztajn et al. 2018). In the case of Hawai'i, the absence of correlation between Tl stable and Os radiogenic isotopes was noted, despite the potential for FeMn sediment contributions to control both systems, and ascribed to the very high Tl/Os ratio such sediments exhibit.

Our new data provide a basis for re-evaluating the systematics of Tl isotopes in the HIMU mantle endmember. The isotopic criterion most commonly used to distinguish HIMU lavas is their radiogenic Pb isotopic compositions (i.e. ^{206}Pb/^{204}Pb > 19.5), which is commonly interpreted to arise from the subduction of AOC with high ^{238}U/^{204}Pb ratios ('high μ'), that was isolated in the mantle for 1–2 Ga (e.g. Hofmann and White 1982, Zindler and Hart 1986, Chauvel et al. 1992, Stracke et al. 2005). While acknowledging decoupling of Tl and Sr-Nd-Hf-Pb isotopes, Blusztajn

et al. (2018) argue that Tl isotopic compositions that are generally lighter than those found for MORB combined with Ce/Tl variations provide evidence for the presence of a recycled upper AOC component in the St Helena source, from which up to 90% of Tl (relative to Ce) was stripped during subduction processing. Subsequent work investigated eclogites from Cabe Ortegal (Spain) and the Raspas Complex (Ecuador), thought to represent the metamorphic equivalents of altered oceanic crust (Shu et al. 2019). The eclogites have a similar range in Tl isotopic compositions as the main phase St Helena lavas (ε^{205}Tl ≈ -5.5 to -1.0), and thus (Shu et al. 2019) proposed a genetic link between the two.

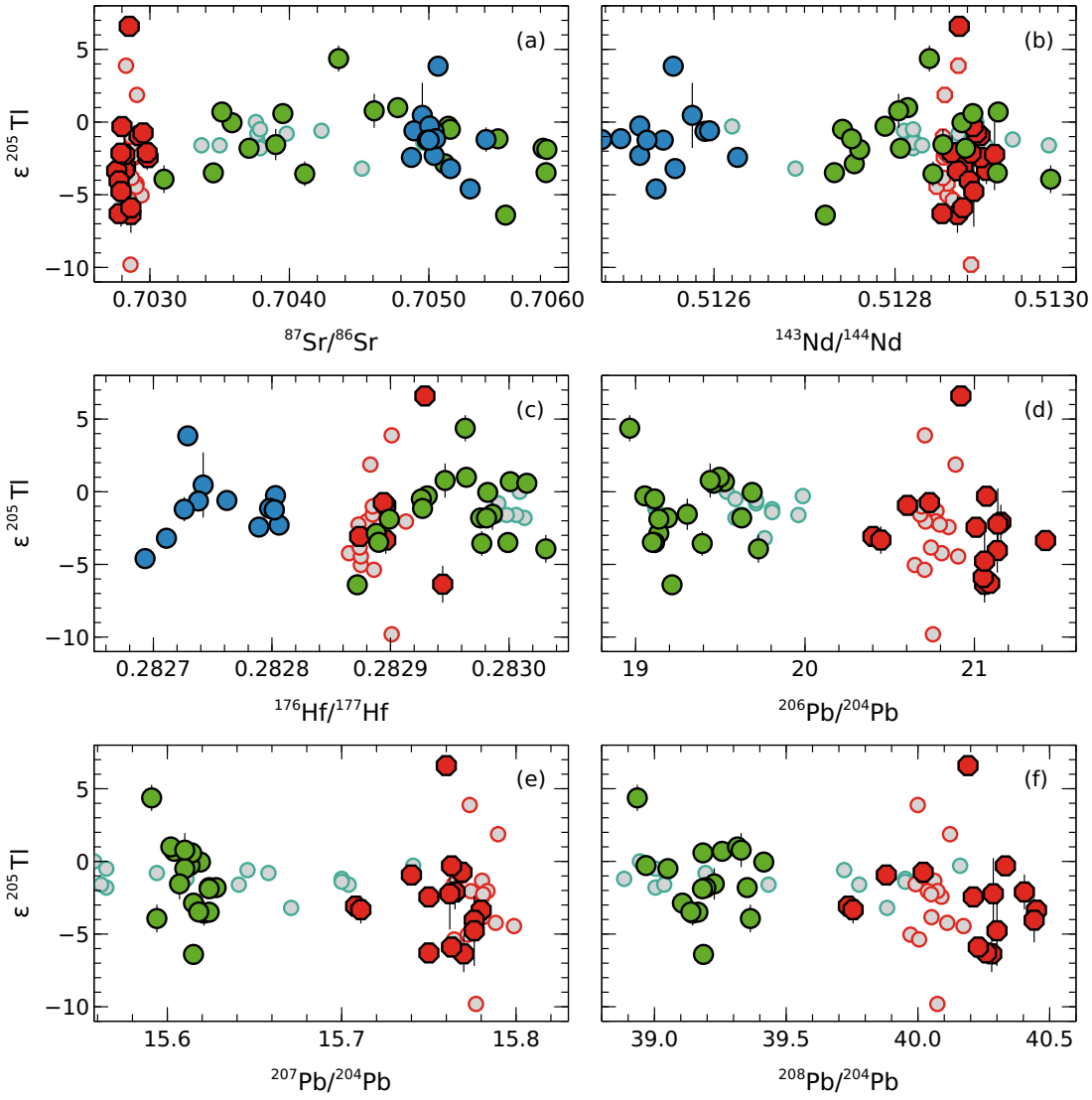


Figure 3.13: Plots of ε^{205}Tl against (a) $^{87}Sr/^{6}Sr$, (b) $^{143}Nd/^{144}Nd$, (c) $^{176}Hf/^{177}Hf$, (d) $^{206}Pb/^{204}Pb$, (e) $^{207}Pb/^{204}Pb$, (f) $^{208}Pb/^{204}Pb$. For OIB samples, there is no co-variation of ε^{205}Tl and the radiogenic isotope systems commonly used to define mantle components, with the possible exception of $^{143}Nd/^{144}Nd$ in Icelandic picrites. Error bars are generally smaller than symbols. Symbols and data sources as in Figure 3.7.

This interpretation is complicated by the observation that, for the full OIB dataset (Fig. 3.14), the majority of HIMU samples have ε^{205}Tl values that overlap with the range of results obtained for EM-type samples (ε^{205}Tl $\geq$ -6.5; Figures 3.14b, 3.14d). In addition, there is no convincing co-variation of ε^{205}Tl with Ce/Tl and Ce/Pb for either St Helena lavas (Figures 3.14a, 3.14c) or the complete OIB dataset, with EM-type samples again overlapping the whole range of HIMU-type

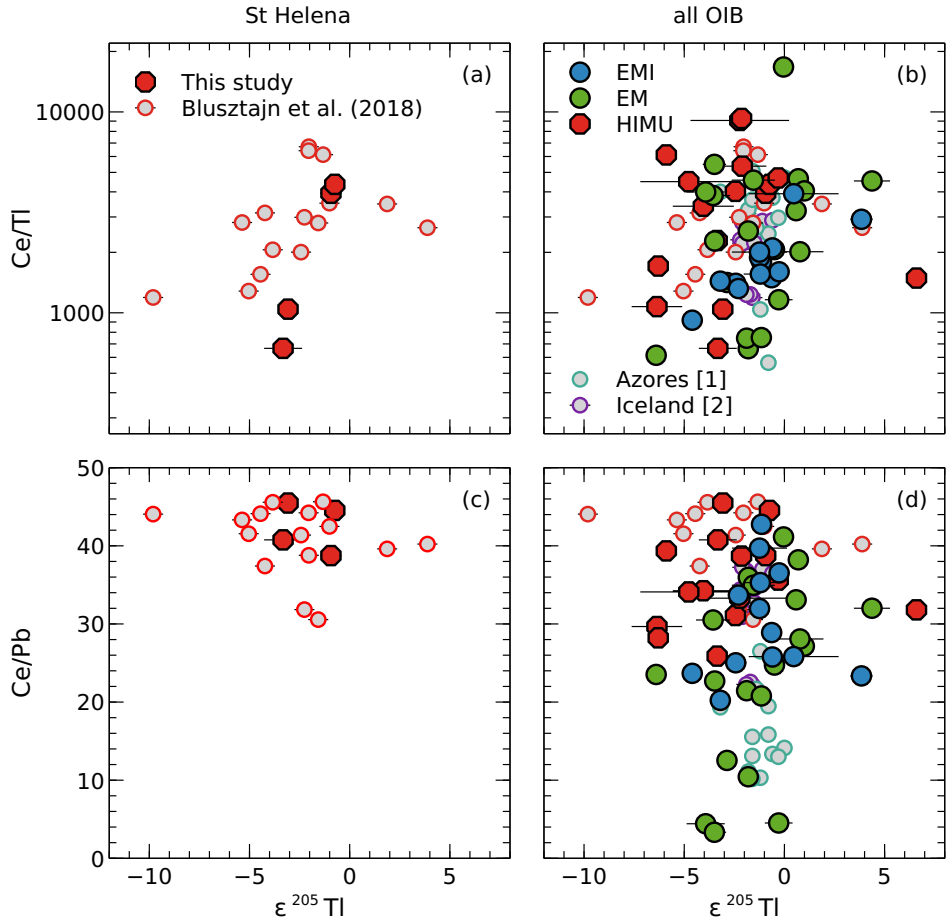


Figure 3.14: Plots of ratios employed to track AOC contributions to OIB source against ε^{205}Tl. (a) Ce/Tl against ε^{205}Tl, showing literature main-phase St Helena lavas and St Helena samples from this study; (b) Ce/Tl against ε^{205}Tl for all OIB samples; (c) Ce/Pb against ε^{205}Tl with the same samples as subfigure *(a)*; (d) Ce/Pb against ε^{205}Tl for all OIB samples. Blusztajn et al. (2018) argued that a sense of correlation for main-phase St Helena lavas indicated a role for subduction-processed AOC in generating the HIMU array. However, this trend is not replicated in HIMU lavas from other localities, and is not unique to HIMU-type lavas. Large symbols: this study. Other data sources: [1] Nielsen et al. (2007), [2] Prytulak et al. (2017).

lavas. While one HIMU-type lava does exhibit the lightest reported Tl isotopic composition of any OIB sampled to date (ε^{205}Tl ≈ -10), the broad overlap in ε^{205}Tl for HIMU- and EM-type OIB does not provide a clear distinction between different mantle end-members based on Tl isotopic compositions alone. It therefore appears that Tl isotopic compositions are decoupled not just from radiogenic isotopes and Tl concentrations, as suggested by Shu et al. (2019), but also – at least on a global scale – from incompatible trace element ratios held to be indicative of AOC contributions.

We concur with the conclusion of Blusztajn et al. (2018) that the Ce/Tl ratios of OIB appear to be broadly complementary to those found in island arc lavas. It is therefore necessary to explain how Tl isotopic systematics become (apparently) decoupled from Tl elemental systematics. Fitting our model to elemental systematics data requires highly efficient (∼99%, relative to Ce) removal of Tl from heterogeneous subducting materials, with only a small proportion of subducted Tl returned to OIB source regions in the deep mantle. Therefore, the low Tl concentrations of the OIB sources produce magmas with Tl signatures that can be readily overprinted by addition of isotopically distinct material.

The notion that Tl isotopic compositions distinct from mantle values are due to the input of Tl-rich, isotopically distinct materials can be further examined via the magnitude of the negative

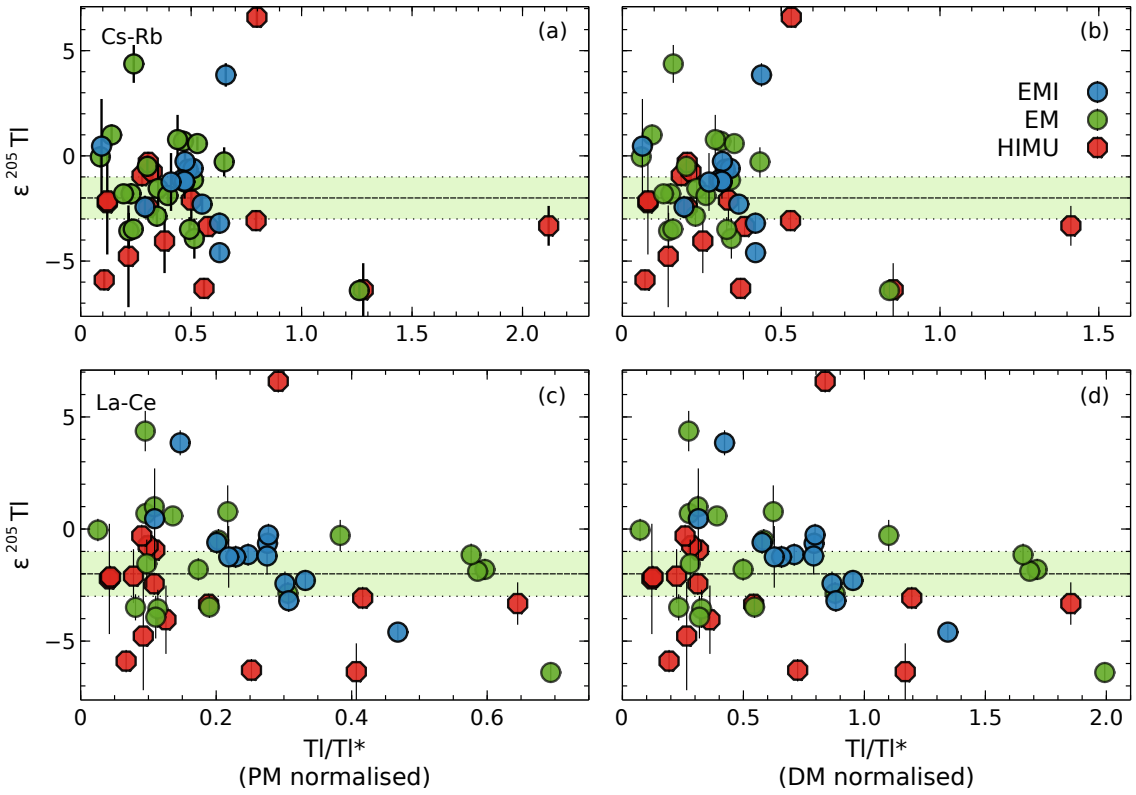


Figure 3.15: Plot of ε^{205}Tl against Tl/Tl* ratios, where Tl* = Tl/$\sqrt{\text{Cs}_\text{N} \times \text{Rb}_\text{N}}$ or Tl/$\sqrt{\text{La}_\text{N} \times \text{Ce}_\text{N}}$, where *N* denotes concentration values normalised to PM (a,c), or DM (b,d). Relative to Cs and Rb, Tl/Tl* values >0.5 (for both PM and DM normalisations) are associated with Tl isotopic compositions that are distinct from the mantle range (green band). Relative to La and Ce, it is less clear whether there is any association.

Tl concentration anomaly observed for OIB relative to geochemically similar elements. When the magnitude of the Tl anomaly Tl/Tl* (see caption to Fig. 3.15) is plotted against Tl isotopic composition, samples with Tl/Tl* $\gtrsim$0.5 (calculated relative to Cs and Rb) generally have Tl isotopic compositions that differ from the mantle (Figures 3.15a, 3.15b). As would be expected given the decoupling of Tl and radiogenic isotopic compositions, this pattern is not restricted to or consistent within any one radiogenic isotope end-member, and some samples with Tl/Tl* $\lesssim$0.5 also display non-mantle values. Ruling out post-depositional isotopic effects, the question that arises is: where does the addition of material with non-mantle Tl isotopic compositions take place? The mantle source or *en route* to eruption?

Addition of isotopically distinct Tl to the OIB source via residual Tl from a subduction-processed slab and/or addition during ascent through the crust via assimilation of country rock, including sediments and previously-erupted and subsequently altered lavas, are both reasonable processes. For example, variation in the extent and type of material assimilated during different stages of magmatism might account for the distinct average Tl isotopic compositions observed by Blusztajn et al. (2018) for St Helena early-, main-, and late-stage lavas. Given the Tl concentration contrast between magma and potential inputs, neither origin for Tl isotope variations – source heterogeneity or assimilation – would necessarily cause resolvable changes to other geochemical markers (e.g. model of Nielsen et al. 2006b; Fig. 3.16). Caution is therefore advisable when interpreting Tl isotopic compositions of OIB as a direct reflection of the mantle source. However, there is the potential that variable crustal assimilation of isotopically distinct Tl might be identifiable in high

resolution studies of lavas from individual volcanic edifices, yielding insight into their magmatic plumbing architecture.

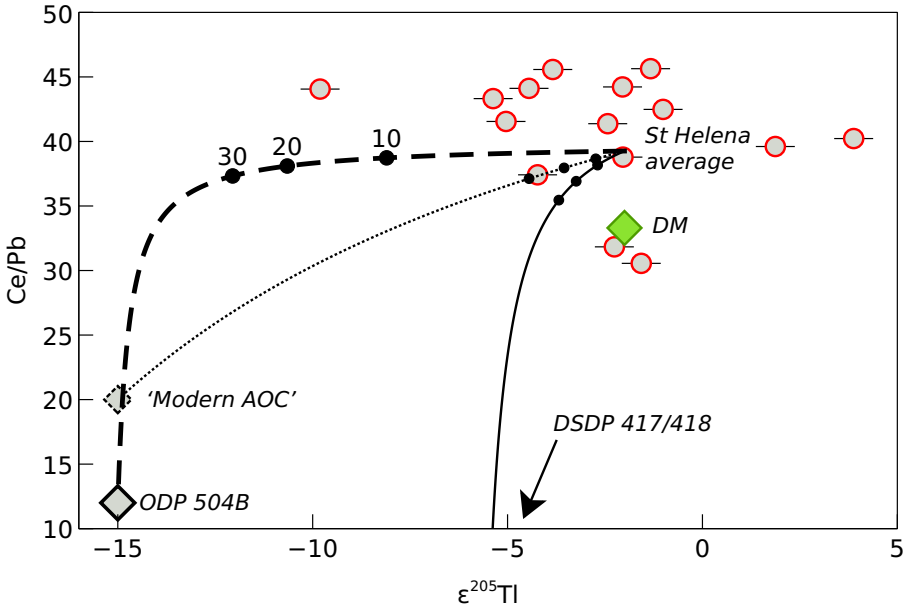


Figure 3.16: Mixing between St Helena HIMU average composition (Blusztajn et al. 2018) and three 'AOC' values (see Table 3.7). Ticks correspond to admixture of 10%, 20% and 30% of AOC as labelled for ODP 504B.

Table 3.7: Mixing parameters for St Helena lavas.

	DM	St Helena average	ODP 504B (∼6.6 Ma)	DSDP 417/418 (∼109 Ma)	"Modern AOC"
Tl (µg/g)	0.00038	0.03	0.25	0.07	$\underline{0.017}$
Ce (µg/g)	0.772	80.83	4.31	6.19	$\underline{12}$
Pb (µg/g)	0.0232	2.06	0.36	0.69	$\underline{0.6}$
Ce/Pb	33	∼40	12	9	$\underline{20}$
ε^{205}Tl	-2	∼-2	-15	-5.4	-15

For DM, values are taken from Salters and Stracke (2004), except ε^{205}Tl (Nielsen et al. 2006b). For DSDP 417/418, supercomposite values are taken from Blusztajn et al. (2018) and Staudigel et al. (1995). ODP 504B values are taken from Nielsen et al. (2006c) and Bach et al. (2003). "Modern AOC" values are taken from Blusztajn et al. (2018) or inferred (underlined). St Helena average values are as reported by Blusztajn et al. (2018).

3.4 Conclusions

Fresh lavas from divergent, convergent and intraplate settings can be distinguished by their distinct systematics in plots of Ce/Tl ratios versus Tl concentrations. The observed patterns can be reproduced by models of fractional, non-modal melting, providing insights into the cycling of Tl through the mantle. The Ce/Tl systematics of MORB can be reproduced by the combined effects of different extents of partial melting, variations in $D^{Ce}_{cpx/melt}$, and variations in initial Tl and Ce concentrations, without a significant role for sulphides. In contrast, the Ce/Tl systematics of OIB cannot be generated from a primitive mantle source, but instead require a source that is markedly depleted in Tl (<1 ng/g) prior to the addition of exotic thallium. The requirement for Tl-depleted OIB source regions is consistent with mounting evidence that the extent of present day mantle depletion may be underestimated (e.g. Stracke 2012, Stracke et al. 2011, 2019, Salters et al.

2011, Salters and Dick 2002, Cipriani et al. 2004, Sanfillippo et al. 2019). The OIB array can be generated from a depleted mantle source with addition of up to 20% subducted material from which >99% of Tl (relative to Ce) has been stripped during subduction processing. This suggests that Tl constitutes an extreme example of the behaviour of fluid-mobile elements in subduction zone settings, such that co-variations of Tl with other elements may further constrain elemental subduction zone cycling.

Thallium and radiogenic isotopic compositions are decoupled, and Tl isotopic compositions cannot be used in isolation to distinguish between continental and oceanic crust contribution to OIB source regions. The observed decoupling of Tl and radiogenic isotopic compositions most likely reflects (i) the sensitivity of Tl to small variations in the isotopic composition of residual Tl, and/or (ii) the extreme Tl concentration contrast between mantle and surface materials. Despite the lack of co-variation with radiogenic isotopes, global OIB display a significant range in primary Tl isotopic compositions which must reflect addition of isotopically distinct material. However, where this Tl addition takes places remains ambiguous. The potential incorporation of Tl-rich materials at crustal levels during magma ascent is a feasible alternative interpretation to the generation of Tl isotopic variability due to incorporation of residual slab-derived Tl at mantle depths following subduction processing.

Chapter 4

Thallium transfer from slab to wedge: elemental evidence from arc lavas

4.1 Introduction

At subduction zones, oceanic plates are recycled into the mantle, bearing chemical signatures modified by surface and near-surface processes. Evidence that recycling takes place is identifiable in mantle-derived lavas, from both arc and oceanic intraplate settings (§ 1.2). The chemistry of ocean island basalts (OIB; Chapter 3, Brett et al. 2021) suggests that there is near-quantitative removal of thallium from the downgoing plate in subduction zones, leaving little residual Tl to be recycled deeper into the mantle. This chapter provides a more detailed examination of the processes that are potentially involved in the release and/or retention of thallium from the downgoing plate. To achieve this, existing trace element data for arc lavas are compiled, evaluated, and integrated with available information relating to thallium abundances and partitioning in relevant phases.

As a guide, Figure 4.1 highlights thallium concentrations in reservoirs of interest. Fresh mid-ocean ridge basalt (MORB) glasses have low Tl contents (∼12 ± 7 ng/g 1sd; Jenner and O'Neill 2012a, Nielsen et al. 2014, Yang et al. 2018, as compiled in Chapter 3 and Appendix B3.vi). High-temperature (>250 °C) hydrothermal circulation of seawater strips Tl from the lower oceanic crust (typically <1 ng/g), while low-temperature (<150 °C) hydrothermal processes deposit Tl in the upper oceanic crust (Nielsen et al. 2006c, Coggon et al. 2014). Thallium concentrations have been determined for drill core from several drilling expeditions (Fig. 4.2). Within the upper altered oceanic crust (AOC), following alteration at low temperatures, Tl concentrations are clearly elevated relative to fresh MORB. Coggon et al. (2014) conclude that Tl is primarily hosted within secondary sulphides, on the basis that Tl and S concentrations are correlated in the upper crustal basalts they analysed. Depth distribution remains ambiguous, however, in part because of the highly variable concentrations reported for a limited number of drill cores.

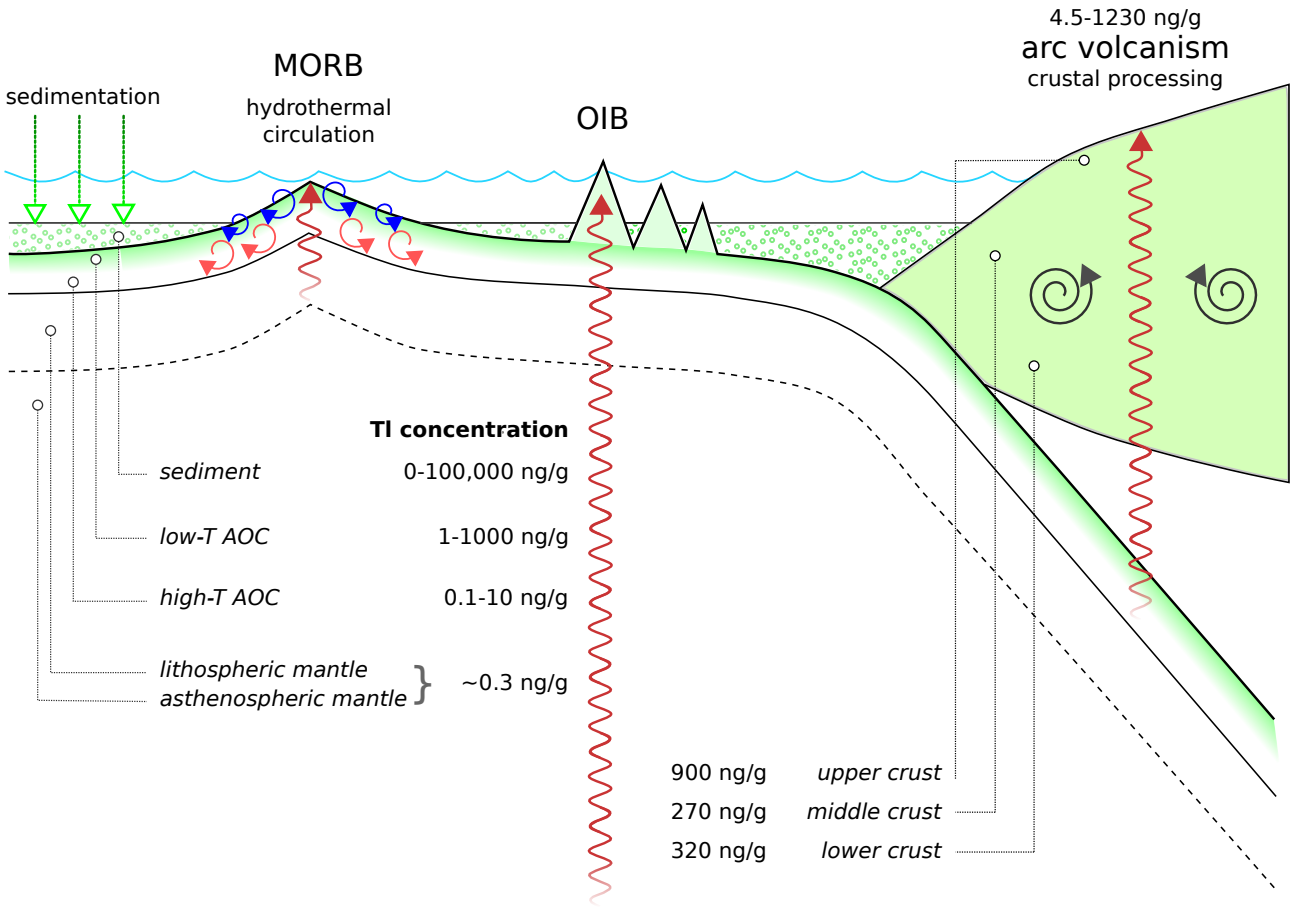


Figure 4.1: Schematic of plate tectonic processes relevant to the Tl cycle (not to scale), with regions of high Tl concentration shown in green. As an incompatible element, Tl is concentrated in magmas during melting (dark red arrows). Low-temperature hydrothermal circulation in the upper part of the plate (blue arrows) is associated with deposition of Tl, whereas high-temperature hydrothermal circulation (red arrows) removes Tl. Further Tl is then added to the subduction package via sediment deposition (green arrows) and intraplate volcanism. Thallium incorporated into arc crust potentially undergoes reprocessing (grey arrows). Data sources as for Figure 1.1.

The sediment layer overlying oceanic crust is also a significant reservoir for thallium. Thallium concentrations in FeMn deposits can reach >100 µg/g (Rehkämper et al. 2002, Peacock and Moon 2012, Nielsen et al. 2013), while pelagic clays exhibit Tl concentrations of up to ~1 µg/g (e.g. Nielsen et al. 2017a). Diagenetic pyrites have also been documented with Tl concentrations of up to ~0.3 µg/g (Nielsen et al. 2011). Comparatively low concentrations of Tl in other sediments are unlikely to significantly affect the Tl budget of the subduction package (e.g. Nielsen et al. 2017a report one carbonate from DSDP 495 with 33 ng/g Tl). Any assessment of thallium cycling in subduction zones based on arc lavas must, therefore, consider the sediment package of the downgoing plate. Figure 4.3 shows Tl concentrations and lithologies for subducting sediments outboard of five subduction zones. These subduction zones have been examined in detail for Tl elemental and isotopic systematics, providing the foundation for this chapter's trace element compilation. The weighted averages of trace element abundances in subducting sediment packages outboard individual trenches calculated by Plank and Langmuir (1998) did not include Tl due to the lack of adequate Tl data then available. More recently, Nielsen et al. (2016) and Shu et al. (2017) obtained concentration data for subducting sediment at the Aleutian and Ryukyu arcs, respectively, and calculated weighted averages for subducting Tl concentrations in these locations (Fig. 4.3). Unfortunately, for the majority of arcs high-resolution analyses of Tl concentrations in sediments have not been performed. However, Tl concentrations in subducting materials exceed

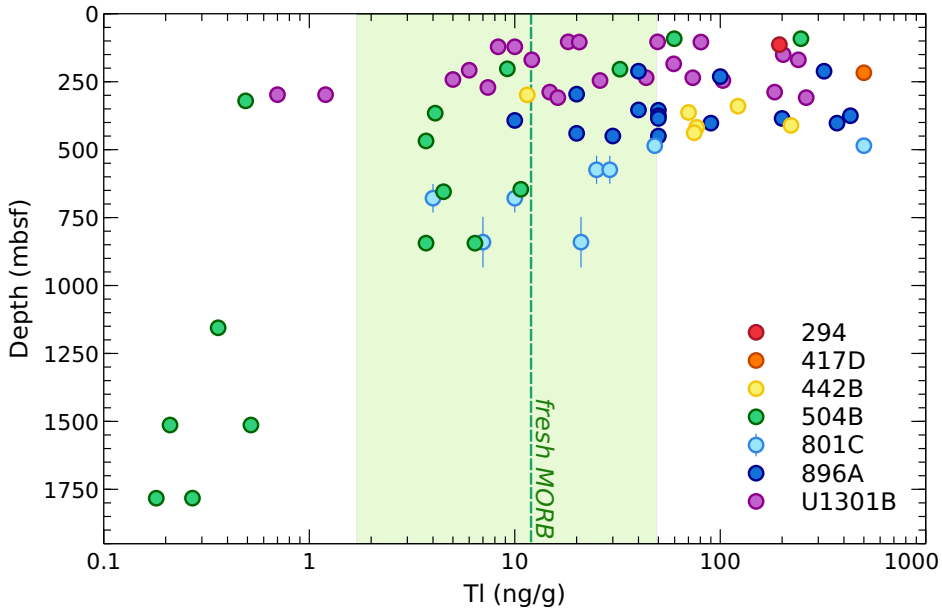


Figure 4.2: Variation of Tl concentration with depth in altered oceanic crust (AOC) as sampled by DSDP/ODP/IODP drilling. Thallium concentrations for Hole 294 are from Shu et al. (2017). 417D: Nielsen et al. (2006c). 442B: Shu et al. (2017). 504B: Nielsen et al. (2006c). 801: Prytulak et al. (2013). 896A: Teagle et al. (1996). U1301B: Coggon et al. (2014). For Hole 801, AOC composites were analysed. Error bars for depth indicate the interval represented by each composite.

those found in the depleted mantle (∼0.27 ng/g, Brett et al. 2021, Chapter 3; 0.48 ng/g, Nielsen et al. 2014; 0.38 ng/g, Salters and Stracke 2004) by many orders of magnitude.

Continental crust, as the cumulative product of subduction-related magmatism (see e.g. discussion in Rudnick and Gao 2003), is enriched in Tl relative to the mantle. The bulk continental crust contains an estimated 500 ng/g Tl (Rudnick and Gao 2003), consistent with loess data reported by Nielsen et al. (2005). By way of comparison, the arc lavas compiled for examination in this chapter have Tl concentrations that range from 4.5 to ∼1300 ng/g.

The Tl concentration data now available for reservoirs relevant to subduction enable a detailed examination of thallium retention and release in the downgoing plate. However, there is ambiguity about which phase(s) are the primary host for Tl in the subducting slab. A growing body of data for Tl concentrations in specific minerals (e.g. Rader et al. 2018) can be explored in combination with arc lava data to investigate evidence regarding which phases are most likely to retain Tl in the downgoing plate. Once identified, the stability of those phases during subduction is critical to understanding the retention versus release of thallium.

Both magmatic and non-magmatic element transfer processes operate in subduction zones. Initial attempts to assess the degree of Tl fluid mobility during slab dehydration were hampered by the lack of substantial datasets including Tl concentrations for MORB and OIB (Noll et al. 1996). High-precision Tl concentration data have now been compiled for both MORB and OIB (Chapter 3, Brett et al. 2021, Appendices B3.v, B3.vi), providing a robust point of comparison with arc data.

Recent studies of Tl behaviour in arc settings have focussed on isotope systematics (e.g. review of Nielsen et al. 2017a). Historically, poorly-constrained Tl abundances in widely-used reference materials have complicated comparison of Tl concentrations determined in different laboratories. However, the collection of robust Tl data for reference materials (e.g. Chapter 2, Brett et al. 2018, Braukmüller et al. 2020) now makes assessment of the quality of reported Tl concentration data feasible.

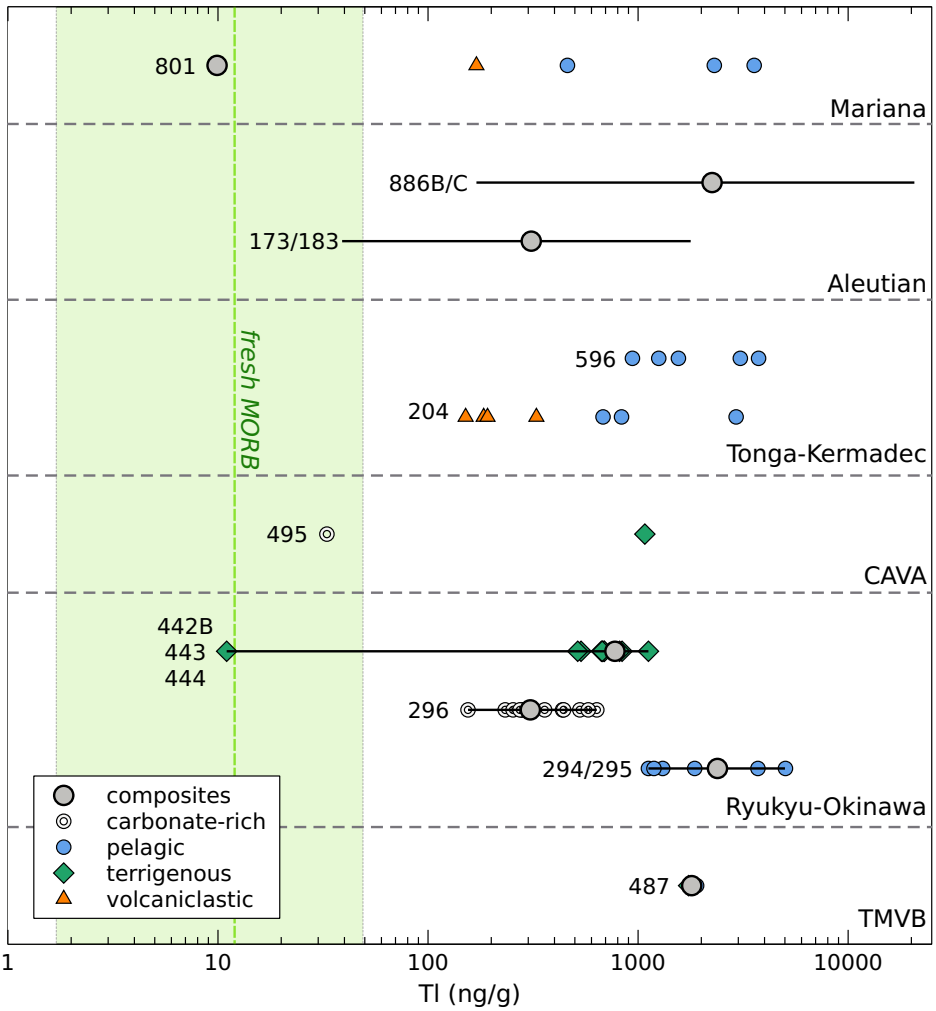


Figure 4.3: Variations in thallium concentration in sediments subducted at arcs considered in this chapter. All sediments are from DSDP/ODP/IODP drill sites. Thallium concentration data for Hole 801 are from Prytulak et al. (2013). 886B/C and 173/183: Nielsen et al. (2016). 204 and 596: Nielsen et al. (2017a). 495: Nielsen et al. (2017a). 442B/443/444, 296, and 294/295: Shu et al. (2017). 487: LaGatta (2003). 'Composites' are weighted averages calculated by the relevant authors, with the exception of Hole 801. Here, the 'SED composite' (see Plank et al. 2000 and Kelley et al. 2003) is plotted. CAVA = Central American Volcanic Arc; TMVB = Trans-Mexican Volcanic Belt.

In this chapter, an approach to compiling and filtering existing Tl concentration data for arc lavas is outlined. The resulting dataset is used to investigate:

(i) whether host phase(s) for Tl in the downgoing slab can be chemically fingerprinted;

(ii) how Tl is transferred from subducting slabs to overlying plates, with implications for the use of Tl to distinguish between 'fluid' and 'sediment' contributions to arc lavas; and

(iii) the accumulation of Tl within continental crust.

Table 4.1: Details of the core arc lava dataset. Numerals in parentheses indicate how many of the included samples are classified as 'OIB-type', as opposed to 'arc-type' (see text for details). CAVA = Central American Volcanic Arc; TMVB = Trans-Mexican Volcanic Belt.

Study	Overlying crust	Arc	Islands/Regions	# samples ('OIB')
Prytulak et al. (2013)	oceanic	Mariana	Anatahan	8
Prytulak et al. (2017)	oceanic	Mariana	Sarigan	1
			Guguan	5
			Alamangan	2
			Pagan	2
			Agrigan	3
			Uracas	4
Nielsen et al. (2016)	oceanic	Eastern Aleutian	Okmok	4
			Westdahl	4
		Central Aleutian	Kanaga	4
			Moffett	4
			Korovin	8
		Western Aleutian	dredged	19 (3)
Nielsen et al. (2017a)	oceanic	Tonga-Kermadec	Tafahi	4
			Niuatoputapu	3
			Fonualei	4
			Late	4
			Kao	2
			Tofua	1
			Hunga Ha'apai	1
			Hunga Tonga	1
			Raoul Group	4
			Macauley	2
			Curtis	2
			L'Esperance	2
	juvenile continental?	CAVA	Costa Rica	8 (4)
			Nicaragua	12
			El Salvador	6
			Guatemala	7
Shu et al. (2017)	oceanic	Ryukyu-Okinawa	South Kyushu	10 (1)
			North Ryukyu	8
			Central Ryukyu arc	4
			Southern Ryukyu arc	1
			South Ryukyu volcanic front	11
			Northern Okinawa Trough	5
			Middle Okinawa Trough	7
			Southern Okinawa Trough	10
Cox et al. (2019)	continental	Andean	Antuco volcano	26
Mangler et al. (2019)	continental	TMVB	Popocatépetl volcano	62

4.2 Methods

To address the aims of this chapter, existing Tl concentration data for volcanic arcs was assembled from the literature. The core of the arc Tl concentration dataset are 186 arc lavas analysed during Tl-focussed studies (Table 4.1, Appendix B4.i). Identical protocols were followed for digestion and analysis, and all but one of these studies (Nielsen et al. 2017a) report analyses of Tl concentration in USGS standards in agreement with recommended values (Chapter 2, Brett et al. 2018, Jochum et al. 2005, Braukmüller et al. 2020). As such, these data are directly comparable. The majority of samples reported in this set of studies are from oceanic arcs. The exceptions are 33 samples from the Central American Volcanic Arc (CAVA), often considered juvenile continental crust (e.g. Vogel et al. 2004, Hayes et al. 2014, Whattam and Stern 2015).

In addition to these 186 samples, two recent studies have reported Tl concentration data for samples from continental arc localities obtained, for the most part, using the same protocols and instrument (ICP-QQQ, Open University, Milton Keynes) as the analyses described in this work for reference materials (Chapter 2, Brett et al. 2018) and OIB samples (Chapter 3, Brett et al. 2021). These data are for samples from Popocatépetl volcano, Mexico (n = 62; Mangler et al. 2019) and

Antuco volcano, Chile (n = 26; Cox et al. 2019). Measurements of USGS reference materials made alongside Popocatépetl and Antuco samples are in good agreement with recommended values.

The compiled arc data are shown in Figure 4.4a, together with compiled MORB and OIB data. Coherent trends in MORB and OIB Ce/Tl data can be explained with simple melting models (Chapter 3, Brett et al. 2021). Arc lavas from both oceanic and continental margins are generally enriched in Tl relative to OIB and MORB, and exhibit coherent variation in Ce/Tl ratios, occupying a field that is visually distinct from both MORB and OIB. This apparently systematic variation is surprising, because subduction inputs have both variable Tl contents and varying Ce anomalies (see e.g. Bellot et al. 2018). Creating even simplified quantitative models of Tl behaviour during subduction zone melting is not straightforward due to the number of unknown parameters, including partitioning data for potentially Tl-rich accessory minerals.

Of 275 arc samples, only 8 fall in the 'OIB field' as opposed to the 'arc field', and five of these outliers have previously been identified as having OIB-like characteristics in other geochemical systems. Specifically, three (CR-IZ-63A, CR-IZ-D6, CR-B2) are associated with Irazú volcano in Costa Rica, which has a Galapagos-influenced source (Gazel et al. 2009, 2011). The fourth Costa Rican sample (CR-PO10) is a geochemically unusual high-Ti basalt previously described by Prosser and Carr (1987), with an OIB-like chondrite-normalised REE pattern. Sample NK01 from South Kyushu (Ryukyu-Okinawa arc) also exhibits anomalous OIB-type characteristics (Shu et al. 2017). Finally, three samples dredged from the Western Aleutian arc also overlap with the OIB field. While they were not identified by Nielsen et al. (2016) as anomalous, these samples have markedly higher concentrations of the light REEs La, Ce, and Pr than all but one other Aleutian sample, in addition to elevated Sm and Nd concentrations. Plots of Ce/Tl versus Tl thus act as an effective MORB-OIB-arc tectonic discriminant.

These observations provide a foundation for filtering existing data and expanding the database of Tl concentrations in arc lavas. As a starting point, the GeoROC database provides precompiled files of geochemical data. Unfortunately, Tl calibration values have only recently begun to be routinely quoted. Studies can therefore be initially sorted according to whether (i) the authors describe how Tl measurements were calibrated, and/or (ii) Tl concentrations are reported for reference materials well-characterised for Tl. If this information is provided, studies can then be classified as: (1) good, if quoted Tl data for the reference materials are in good agreement (<10% deviation) with recommended values and span the full sample range; (2) acceptable, if e.g. quoted values are in reasonable agreement ($\leq$15% deviation) with recommended values but the range of Tl concentrations in samples significantly exceeds the range represented by standards; or (3) unacceptable, if quoted values do not agree with recommended values (>15% deviation).

As an example of the filtering process, the GeoROC precompiled file for the Mexican volcanic belts (accessed March 2020) includes 20 studies (published between 2000 and 2019) reporting Tl concentrations for a total of 478 samples. Of these:

- no studies meet the criteria for grade 1 (i.e. quote calibration or RM values in good agreement with recommended values, that span the entire range of Tl concentrations in samples)
- 9 studies (n = 232; Losantos et al. 2017, Gómez-Tuena et al. 2018a, 2003, Petrone 2010, Gómez-Tuena et al. 2011, Sosa-Ceballos et al. 2018, Pérez-Orozco et al. 2018, Maldonado-

Sánchez and Schaaf 2005, Gómez-Tuena et al. 2007) meet the criteria for grade 2 (i.e. calibration or RM values show $\leq$15% deviation, but sample range exceeds calibration range)

- 3 studies (n = 148; Mori et al. 2007, 2009, Straub et al. 2012) used incorrect calibration values for Tl, or report Tl concentrations in reference materials that are not in agreement with recommended values (grade 3)
- 6 studies (n = 98; Carrasco-Núñez et al. 2012, Straub et al. 2015, Arce et al. 2015, Gómez-Tuena and Carrasco-Núñez 2000, Straub et al. 2008, Petrone et al. 2014) provide no information about calibration or reference materials (ungraded).

A further two studies (n = 31; Gómez-Vasconcelos et al. 2015, Mahar et al. 2019) report Tl concentrations to only the nearest 100 ng/g, which is not precise enough for interpretations in this chapter. These data were, therefore, excluded from the compilation.

In Figures 4.4b,c, and d, graded data are shown overlain on the OIB and core arc datasets. Overall, grade 2 data are in reasonable agreement, with 'OIB-like' lavas overlapping with the OIB field, and 'arc-type' lavas typically plotting toward higher Ce/Tl at a given Tl than lavas from predominantly oceanic-oceanic margins.

The discrimination exhibited by Ce/Tl ratios can therefore be exploited to evaluate published Tl data quality where no calibration information is available. Unclassified data are scattered, but if considered on a per-study basis, three (n = 52) show good congruence with the core dataset, while three (n = 46) do not. This filtering can be repeated for other arcs, though at time of writing only files for the Mexican Volcanic Belts have been processed. The expanded dataset, representing both oceanic and continental margins, is used to address questions relating to Tl processing in arcs. For full details of the filtered data considered throughout the remainder of this chapter, please see Appendix B4.ii.

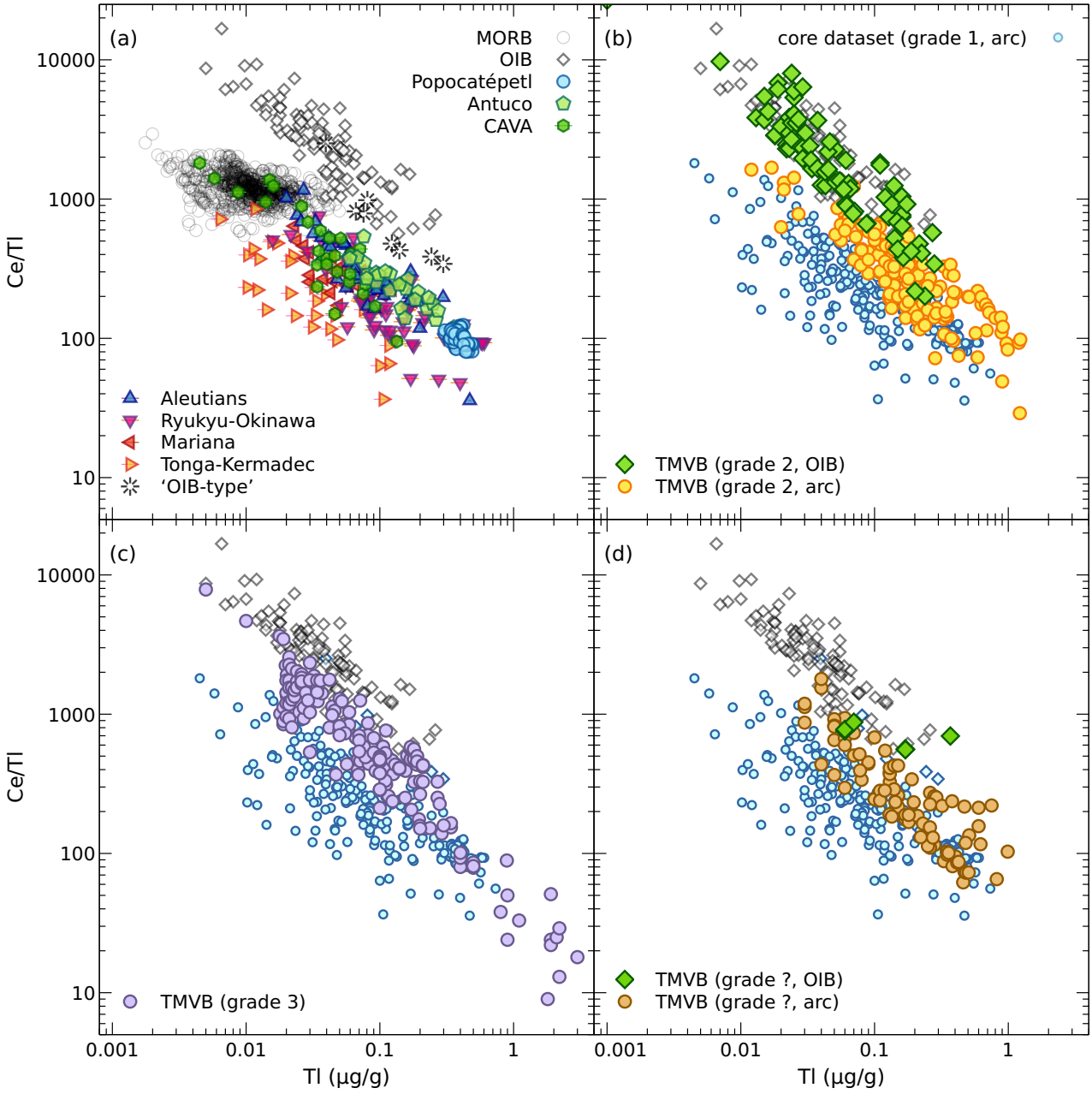


Figure 4.4: Variation of Ce/Tl with Tl for arc lavas and OIB. The arc lava trend is approximately parallel to the OIB trend. (a) The core arc dataset. (b) Comparison of 'OIB-type' and 'arc-type' TMVB lavas with acceptable Tl calibration (grade 2). (c) Unacceptable TMVB lavas (grade 3). (d) Ungraded TMVB lavas. This figure was used to help exclude studies with uncertain Tl calibration. CAVA = Central American Volcanic Arc; TMVB = Trans Mexican Volcanic Belt. In addition to compilations for OIB (Appendix B3.v), MORB (Appendix B3.vi) and the core arc dataset (Appendix B4.i), data from the GeoROC precompiled file for the Mexican volcanic belts are shown for (subfigure *b*) Losantos et al. (2017), Gómez-Tuena et al. (2018a, 2003), Petrone (2010), Gómez-Tuena et al. (2011), Sosa-Ceballos et al. (2018), Pérez-Orozco et al. (2018), Maldonado-Sánchez and Schaaf (2005), Gómez-Tuena et al. (2007); (subfigure *c*) Mori et al. (2007, 2009), Straub et al. (2012); and (subfigure *c*) Carrasco-Núñez et al. (2012), Straub et al. (2015), Arce et al. (2015), Gómez-Tuena and Carrasco-Núñez (2000), Straub et al. (2008), Petrone et al. (2014).

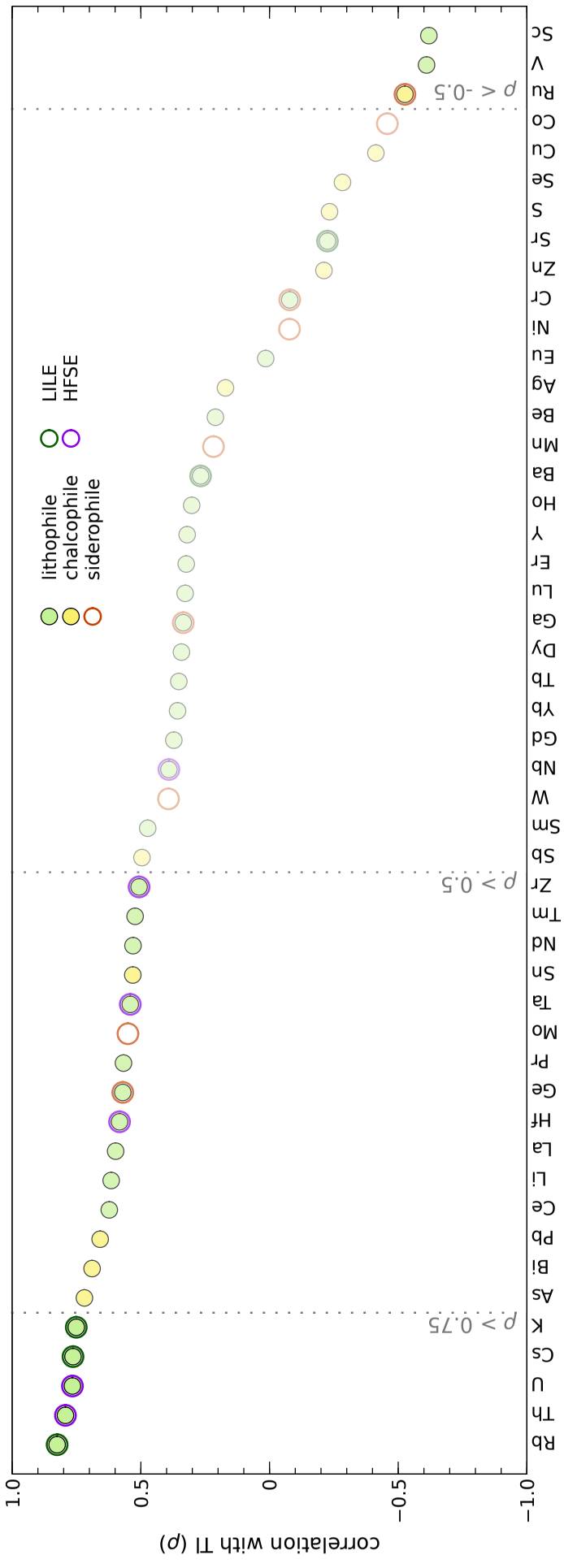


Figure 4.5: Pearson correlation coefficients, ρ, for variation of Tl with other elements, for 'arc-type' lavas of the arc database. Note that different amounts of data are available for each element. Geochemical classifications follow White (2013). For data sources, see Appendices B4.i and B4.ii.

4.3 Results

Examining the database as a whole allows assessment of which elements most closely mirror Tl variations in arc settings. It is helpful to consider similarities to both individual elements and geochemical groupings such as Goldschmidt classification (lithophile, chalcophile and siderophile), and behaviour within the silicate portion of the Earth (e.g. large ion lithophile elements, LILE; high field strength elements, HFSE; and rare earth elements, REE). While recognising that many elements display complex and sometimes ambiguous geochemical behaviour, for the purposes of this comparison the classifications of White (2013) are used.

Correlation matrices offer a good first-order impression of which elements behave most similarly, although the calculated values are strongly affected by outliers. A spreadsheet programme was used to calculate the Pearson correlation coefficient, ρ, for pairs of elements X and Y:

$$\rho_{X,Y} = \frac{cov(X,Y)}{\sigma_X \sigma_Y}$$

where $cov(X, Y)$ is the covariance of X and Y and σ_X and σ_Y are the standard deviation of X and Y, respectively. A value of $\rho = 1$ indicates that X and Y show perfect positive correlation; ρ = -1 indicates a perfect negative correlation; and $\rho = 0$ indicates that the two variables are not correlated. Calculated correlation coefficients are indicative, rather than definitive, but relative values provide the basis for broad inferences about the geochemical behaviour of Tl. Correlation coefficients for 49 elements are presented in Figure 4.5, and the variation of selected elements with Tl concentration is shown in Figures 4.6 and 4.7.

It is important to emphasise that while the calibration of Tl was considered during data compilation, concentration determinations for more commonly-analysed elements have been assumed to be robust. A wide variety of rock types are directly compared, with SiO_2 ranging from 44 to 83 wt%, and extreme compositions might be expected to be associated with unusual geochemical compositions. Unsurprisingly, the set of trace elements for which concentrations are reported is inconsistent across the >20 studies included in the database, such that the size of the dataset varies significantly depending on the element(s) under consideration.

4.3.1 Chalcophile and siderophile elements

Chalcophile elements preferentially partition into sulphide phases relative to silicate or metal phases. In general, these elements have intermediate electronegativities and tend to form covalent or metallic bonds, in contrast to lithophile elements, which tend to form ionic bonds. Siderophile elements preferentially partition into metal phases relative to silicate or sulphide phases.

Assessment of co-variation between Tl and chalcophile and siderophile elements is hindered by the limited availability of concentration data, particularly within the core dataset. However, the majority of these elements (11 of 19, including S) have correlation coefficients in the range -0.5 to 0.5, indicating negligible correlation with Tl. Overall, in the arc lava dataset Tl does not covary with chalcophile elements as a group. Examination of relationships with individual elements

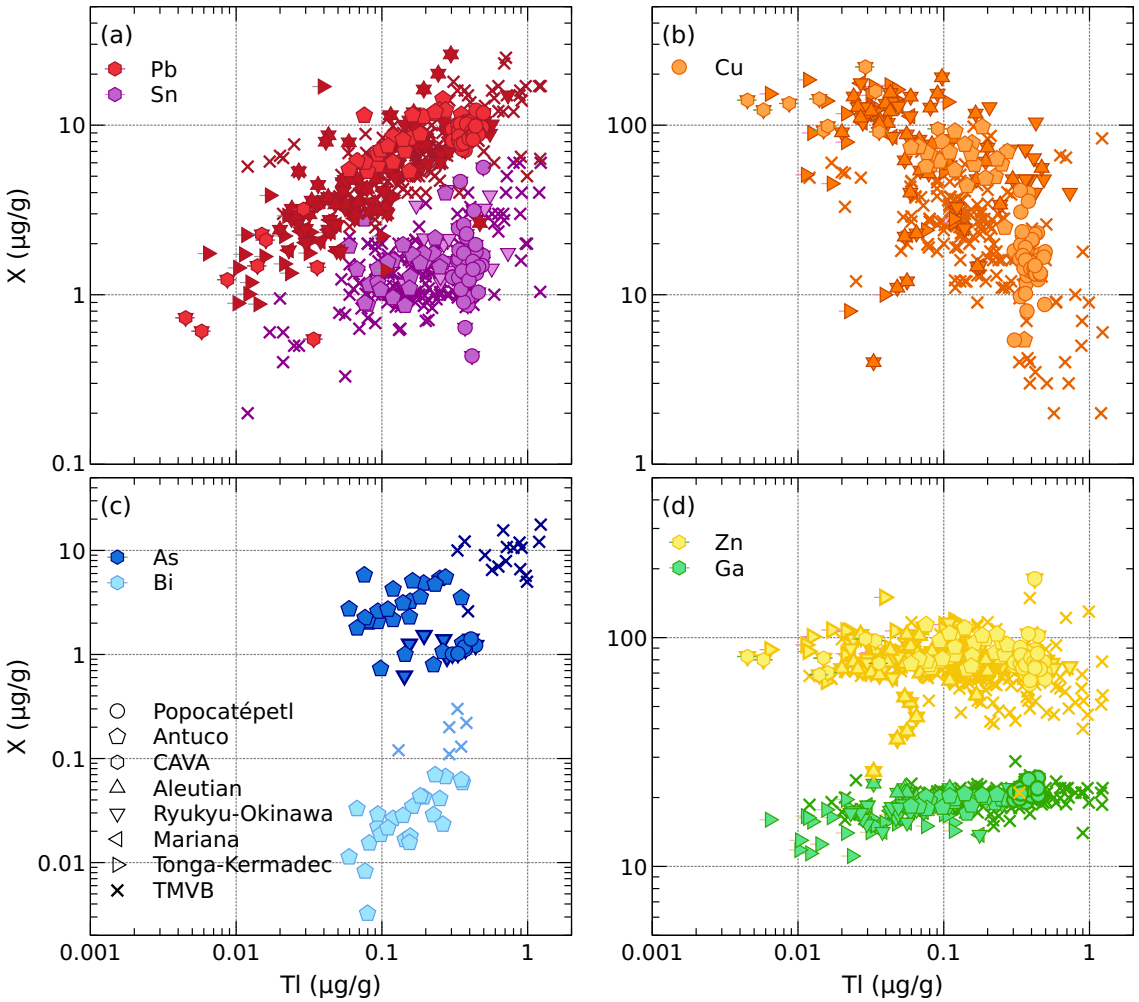


Figure 4.6: Variations of the concentration of chalcophile elements and Tl within the arc database. For data sources, see Appendices B4.i and B4.ii.

is likely more informative. Of the ten chalcophile elements considered, four (As, Bi, Pb, Sn) have correlation coefficients >0.5 (Figures 4.6a,b). However, As and Bi concentration data are only available for a relatively small number of samples (n = 55 and n = 30, respectively), all of which are taken from Antuco (Chile) and the Trans-Mexican Volcanic Belt (TMVB; including Popocatépetl). The dataset for Sn is larger (n = 267), and again data is from the TMVB and Antuco.

Lead is best-constrained, with 495 reported concentrations representing all subduction zones included in the database. The clear positive correlation of Tl with Pb (Fig. 4.6c) is perhaps unsurprising. Chemical similarities between Pb and Tl have been noted since the discovery of Tl (Lamy 1862, Crookes 1862). However, it is worth noting that in sulphur-undersaturated systems, Pb is sometimes classed as a LILE due to the large radius of the Pb^{2+} ion (Table 4.2). In the arc dataset, Pb correlates more strongly with lithophile elements than chalcophile elements (not shown).

The chalcophile elements (other than Pb) for which most data are available are Zn (n = 402), Cu (n = 348), and Ga (n = 342). Thallium arguably shows a weak negative correlation with Cu, and no correlation with Zn or Ga (Figures 4.6b,d).

Table 4.2: Effective ionic radii of LILE. All data from Shannon (1976). Z/r is the ratio of ionic charge to ionic radius.

Ion	Coordination number	Effective ionic radius (Å)	Z/r
Major elements			
Ca^{2+}	VI	1.00	2.0
	VIII	1.12	1.8
Na^{+}	IV	0.99	1.0
	VI	1.02	1.0
	VIII	1.18	0.8
Trace elements			
Ba^{2+}	VI	1.35	1.5
	VII	1.42	1.4
Cs^{+}	VI	1.67	0.6
	VIII	1.74	0.6
K^{+}	IV	1.37	0.7
	VI	1.38	0.7
	VIII	1.51	0.7
	XII	1.64	0.6
Pb^{2+}	VI	1.19	1.7
	VIII	1.29	1.6
Rb^{+}	VI	1.52	0.7
	VIII	1.61	0.6
	XII	1.86	0.5
Sr^{2+}	VI	1.18	1.7
	VIII	1.26	1.6
Tl^{+}	VI	1.50	0.7
	VIII	1.59	0.6
	XII	1.70	0.6

4.3.2 Lithophile elements (LILE, HFSE and REE)

Rudnick (1998) defined large-ion lithophile elements (LILE) as lithophile elements with small ratios of charge to ionic radius, and ionic radii greater than Ca^{2+} and Na^{+} (Table 4.2). The strongest correlations identified for Tl in the dataset are with the lithophile elements Rb, K, Th, U and Cs ($\rho > 0.75$; Fig. 4.7a), of which three (Rb, K, Cs) are LILE.

The similarity in ionic radius for Tl and Rb has been long remarked upon and invoked to explain the similar distribution patterns of these two elements (e.g. Ahrens 1948). Thallium exhibits no correlation with Ba and Sr, which are LILE with markedly smaller radii.

In contrast to LILE, high-field-strength elements (HFSE) have small ionic radii and high charges, with $Z/r > 2.0$ (Salters 1998). Zirconium (which can exist in the +4 state), hafnium (+4), tantalum (+5) and niobium (+5) are shown in Figures 4.7c,d. In arc lavas, Tl concentrations show weak positive correlations with these elements. Uranium and thorium are sometimes also classified as HFSE due to their high charges (+4 and +6, and +4, respectively), though the +4 ions are larger than those of Zr and Hf. Thallium concentrations correlate positively with both U and Th ($\rho >$0.75; Fig. 4.7d), likely reflecting the greater mobility of U and Th.

Finally, of the rare earth elements (REE), Tl correlates most strongly with the light REE Ce and La (Fig. 4.7b). These are also the REE with which Tl correlates most strongly during MORB melting (Chapter 3, Brett et al. 2021, Nielsen et al. 2014). Overall, Tl generally exhibits weak positive (>0.5) correlations with light REE (atomic numbers 57 to 61), and no correlation (0.4 to 0) with heavy REE.

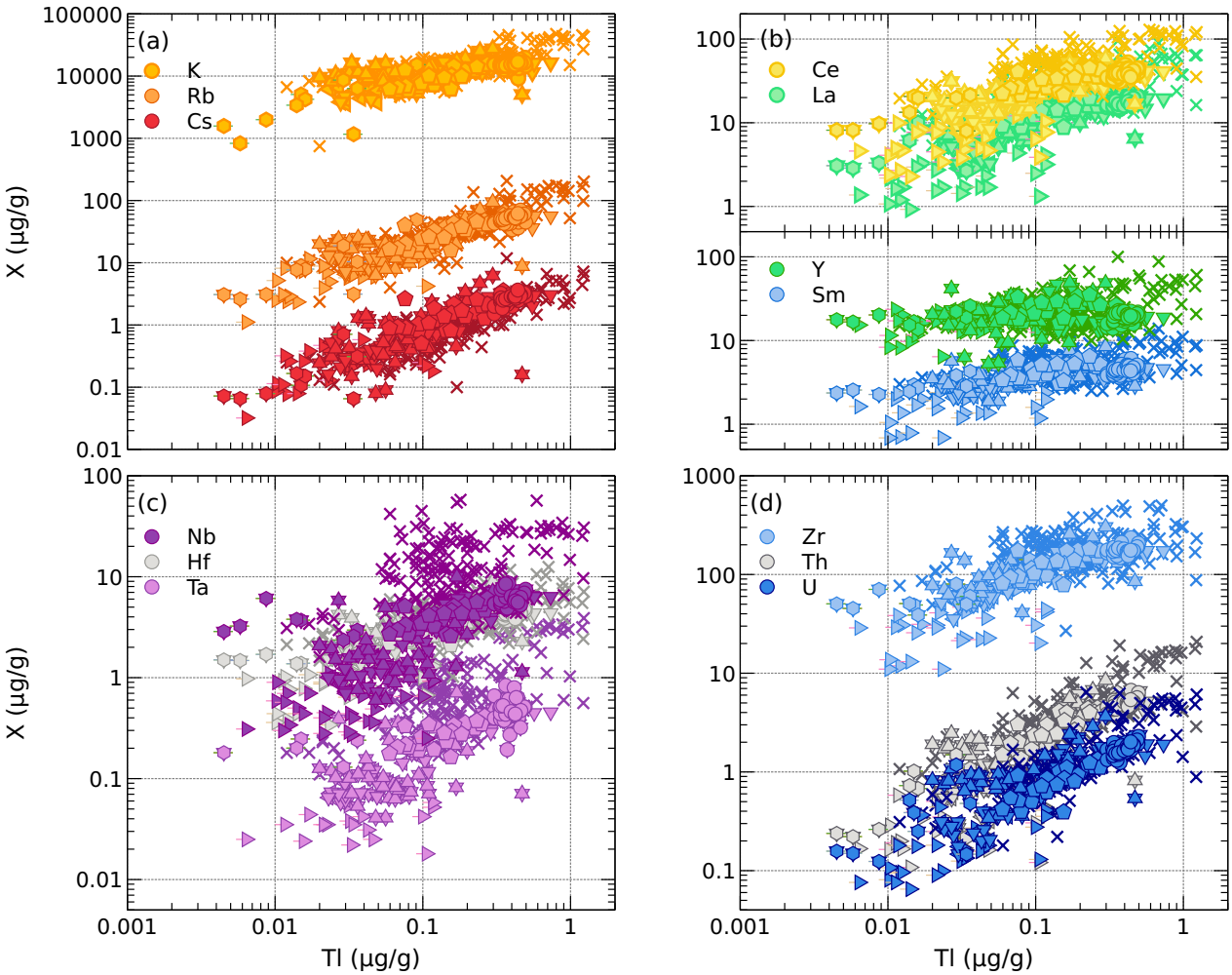


Figure 4.7: Variations of the concentration of lithophile elements and Tl within the arc database. (a) LILE, (b) REE, (c) and (d) HFSE. For data sources, see Appendices B4.i and B4.ii.

4.4 Discussion

4.4.1 Which phase(s) host Tl in the subducting slab?

The thallium budget of the oceanic lithosphere is controlled by the upper altered oceanic crust and, depending on lithology, overlying sediments (Fig. 4.1). Prior to subduction, the principal hosts of Tl in sediments are likely FeMn phases and detrital material, whereas in AOC sulphides – and hydrous alteration minerals – are likely of greatest importance (see Nielsen et al. 2017b and references therein). As the plate descends into the mantle, the (altered) basaltic crust and its sediment package undergo a series of metamorphic phase transitions and dehydration reactions (e.g. Hacker 2008). These changes and reactions are crucial to understanding how Tl is retained in or removed from the subducting slab. In principle, co-variations between Tl and other element abundances might fingerprint the contribution of a specific Tl-rich phase to arc magmas. However, to do so unambiguously, the mineral would have to be the primary host of both thallium and some other element for which concentrations have been determined.

Sulphide minerals

Thallium can be highly concentrated in sulphides, and indeed was first identified in the by-products of pyrite roasting (Lamy 1862, Crookes 1862). Chalcophile behaviour exhibited by Tl has been explained by the tendency for the Tl^{3+} ion to form bonds with covalent character (e.g. Rader et al. 2018, Schauble 2007). Studies of Tl partitioning between sulphide and silicate melts at mantle conditions show that while $D^{Tl}_{sulph/sil}$ is only minimally affected by changing temperature and pressure (Kiseeva and Wood 2015), there is a strong non-linear dependence on the composition of the silicate melt (e.g. Wood et al. 2008, Kiseeva and Wood 2013, Wood and Kiseeva 2015). Kiseeva and Wood (2013) experimentally determined values of $D^{Tl}_{sulph/sil}$ between ~4 and ~24 for a range of silicate and sulphide compositions. During normal MORB melting, $D^{Tl}_{sulph/sil}$ is ~7 (Jenner 2017, using the calculator of Kiseeva and Wood 2015 for 9wt% FeO_{TOT}). However, studies of mantle sulphides are not directly applicable to the lower temperature and pressure hydrothermal sulphides that potentially host Tl in the subducting slab.

In lower-temperature systems, uptake of Tl during sulphide formation has been attributed to crystallisation of a metamorphic sulphide melt (e.g. Hettmann et al. 2014a), precipitation from pore waters trapped in sediment piles (e.g. Nielsen et al. 2011), or precipitation from circulating hydrothermal fluids, with or without a role for microbial sulphate reduction (e.g. Coggon et al. 2014, Hettmann et al. 2014b, Fitzpayne et al. 2018). Thallium and sulphur concentrations co-vary in the portion of the upper oceanic crust that is enriched in Tl relative to fresh MORB glass, which is taken as evidence that Tl taken up during low-temperature hydrothermal alteration is primarily hosted in (secondary) sulphides (Holes U1301B, 405B, 896A; Coggon et al. 2014). Similarly, within the sediment pile, Nielsen et al. (2011) inferred concentrations of up to ~0.3 µg/g Tl for early diagenetic pyrites. While there is no clear evidence for chalcophile behaviour in the arc magma dataset, thallium is likely concentrated in low-temperature hydrothermal sulphides in the subducting slab.

Subsequent thallium retention in or release from hydrothermal sulphides during subduction is determined by the sulphide phases(s) that exist and their stability regimes. Studies of thallium concentrations in, and distribution between, various sulphide minerals have focussed on samples associated with ore deposits. Rader et al. (2018) reported Tl concentrations in 38 sulphides, of various compositions and from a range of tectonic settings, along with over 100 other mineral samples, providing the most comprehensive assessment of Tl occurrence in sulphide minerals to date. While concentrations of Tl in sulphides vary over several orders of magnitude, Tl is generally enriched in Pb^{2+}- and As^{3+}-bearing sulphides, but not in Cu- and Fe-bearing sulphides (Rader et al. 2018). No Tl was measurable in either sphalerite ((Zn,Fe)S, $n = 3$) or pyrrhotite ($Fe_{(1-x)}S$ with x = 0 to 0.2, $n = 3$) samples, and of seven pyrite (FeS_2) samples only one (potentially contaminated by Tl-rich hutchinsonite) contained measurable Tl. These patterns of Tl concentration in sulphides are attributed to crystal chemistry effects. In addition to its large ionic radius (see Table 4.2, Shannon 1976), Tl^+ has an inert lone pair of electrons that contribute to unusually large Tl polyhedra and the irregular coordination of anions around Tl (Kyono and Kimata 2001), with the result that Tl substitutes for Pb or As more readily than Cu or Fe.

Sulphosalts from the Lengenbach Pb-As-Tl-Zn deposit (Switzerland) were analysed by Hettmann et al. (2014a), and the results support a stronger association between Tl and Pb than Tl and Cu. Specifically, jordanite ($Pb_{14}(As,Sb)_6S_{23}$) and sartorite ($PbAs_2S_4$) had Tl concentrations of ∼0.1 wt% and ∼0.3–0.6wt%, respectively. In contrast, tennantite ($Cu_6[Cu_4(Fe,Zn)_2]As_4S_{13}$) had a maximum Tl concentration of 0.07 wt%, with the majority of samples having Tl concentrations below the detection limit (∼200 µg/g). Rocks and sulphides from the peralkaline Ilimaussaq complex (southwest Greenland) were analysed for their Tl isotopic and elemental systematics by Hettmann et al. (2014b). Again, the analysed sphalerite and pyrrhotite samples contained no detectable Tl. Significant Tl was found only in djerfisherite, an unusual K-Fe-Cu sulphide with the general formula $(K,Tl)_6(Cu,Fe,Ni,Zn)_{25}S_{26}Cl$. No K or Tl were detectable in alteration assemblages replacing djerfisherite, implying that K and Tl were mobilised during alteration.

Sulphide stability during subduction has received significant attention because subducting sulphides contain a large proportion of the budget of economically important metals. Whether these potential resources are subducted to the (inaccessible) deep mantle or transferred into arc magma source regions is consequently of interest (e.g. Hutchinson et al. 2020). As a result, sulphide stability fields are well-characterised, with models indicating that at <1.8 GPa and <680 °C, pyrrhotite is the major sulphide in subducting materials (e.g. Walters et al. 2020). Pyrrhotite is then replaced by pyrite, and finally at pressures above ∼2.8–3.3 GPa, anhydrite is the only stable sulphur phase (see e.g. discussion in Walters et al. 2020). Studies of hydrothermal systems suggest that even at low pressure Tl is not readily accommodated in pyrrhotite and pyrite structures, which again is likely due to crystal chemistry effects (see discussion in Rader et al. 2018). There is no data available for Tl contents in anhydrite ($CaSO_4$), but the properties of the crystallographic sites are unlikely to encourage Tl incorporation. It is therefore unlikely that stable sulphide phases retain significant Tl during subduction.

Oxygen fugacity (fO_2) exerts significant control over sulphur stability, with more sulphur released from cold, oxidised slabs (e.g. Canil and Fellows 2017, Walters et al. 2020). The oxidised upper portion of the slab, i.e. the region of the altered oceanic crust in which Tl is enriched, therefore contributes disproportionately to sulphur release compared to other regions of the slab. There is significant transfer of sulphur from the slab through the release of fluids (e.g. Jégo and Dasgupta 2013, 2014, Tomkins and Evans 2015, Walters et al. 2020), and data from ore environments suggest that such fluids carry large quantities of Tl. Therefore, even if Tl is hosted by sulphides within the subducting slab, it is likely that sulphides would not be sufficiently stable to retain Tl during subduction processing.

If Tl behaves as a predominantly chalcophile element (either hosted in residual sulphides in the subducting slab or e.g. partitioning into sulphides that stall at the base of the crust, per Jenner 2017), the extent of sulphide retention/release of Tl is expected to be reflected at least to some extent in positive correlations between Tl and other chalcophile elements. While a growing body of work (e.g. Reekie et al. 2019, Wieser et al. 2020) indicates that magmas can experience multiple sulphide saturation and resorption events, complicating relationships between chalcophile element concentrations, there is a striking absence of any positive correlation between Tl and chalcophile elements in arc lavas for which concentration data are available (Fig. 4.6). Within the compilation of global arc data there is thus no straightforward evidence for significant sulphide

retention of Tl in the downgoing slab, consistent with (i) modelling of sulphide stability, (ii) reports of Tl distribution within exhumed eclogites, assumed to be representative of the subducting slab (Shu et al. 2019), and (iii) the limits from OIB on deep-mantle recycling of Tl. Whilst the overall behaviour of Tl appears to be strongly lithophile in magmatic systems, each volcanic system should be evaluated on a case-by-case basis.

Silicate minerals

The size and charge of thallium are most similar to incompatible large ion lithophile elements such as Rb, Cs, and K (Table 4.2). Within the arc lava database, Tl co-varies most strongly with these elements. It has long been known that Tl is concentrated in micas and K-feldspars, explained by direct substitution of Tl^+ for K^+ (e.g. Ahrens 1948, Shaw 1952). High concentrations in a wide variety of micas and K-feldspars were recently reported by Rader et al. (2018), including 23 co-existing mineral pairs. While the samples are not necessarily in equilibrium, gross textural, chemical, or optical zoning patterns indicative of disequilibrium are not present. As such, Rader et al. (2018) provide some constraints on the distribution of Tl between co-existing potential hosts. They find that Tl concentrations can be greater than 20 µg/g in micas and potassium feldspars, with Tl apparently substituting into micas in preference to feldspars where both minerals are present. The latter observation is supported by a higher average Tl concentration in micas (∼3.3 µg/g) than in potassium feldspars (∼1.2 µg/g), with the majority of feldspars containing <1 µg/g Tl.

Rader et al. (2018) argued that their observed distribution of Tl between silicate minerals arises from crystal chemistry effects. The preferential incorporation of Tl^+ into micas over K-feldspars is explained by (i) the relative sizes of the 12-fold coordinated K^+ site (4.14 Å in micas, versus 3.76 Å in K-feldspars); (ii) the relative ionic radii of Tl^+ and K^+ (see Table 4.2), and (iii) the significant inert pair effect associated with Tl, resulting in unusually large coordination polyhedra (Kyono and Kimata 2001). Similarly, the authors suggest that a weak enrichment of Tl in Mg-rich over Fe-rich micas is due to the relative ionic sizes of $^{VI}Mg^{2+}$ (0.72 Å) and $^{VI}Fe^{2+}$ (0.61 Å) (Shannon 1976).

Of the silicate phases known to host Tl, many are important during subduction, due to, for example, their role in transport of water to the deep mantle. As a result, although mineral-melt and mineral-fluid partition coefficients for Tl are largely unknown, the stability fields of key silicate minerals (micas, K-feldspars) have been mapped in detail (see e.g. reviews of Poli and Schmidt 2002, Harlow and Davies 2004). This phase stability information can be used to make inferences about the recycling of Tl.

Mineral stability is dependent on pressure, temperature, and composition. On average, volcanic arcs are located ∼100 km above the top of the subducting slab (Syracuse and Abers 2006), corresponding to pressures of ∼4 GPa. Temperatures at the slab surface are dependent on factors including the age of the subducting slab, slab dip, and the rate of convergence. In terms of composition, an important factor for mica stability – and therefore Tl retention or release – is the distribution and availability of water (e.g. Hermann and Green 2001).

Under anhydrous conditions, potassium feldspars ($KAlSi_3O_8$) can be stable up to ∼6.5 GPa at ∼1300 °C (e.g. Seki and Kennedy 1964, Yagi et al. 1994, Urakawa et al. 1994), i.e. well above the P-T conditions relevant to arc magmatism. However, models of phase stability under hy-

drous subduction conditions suggest that 'wet' conditions favour a more limited stability field for K-feldspars. For example, of the scenarios considered by Hacker (2008), which include both unmetasomatised and metasomatised oceanic volcanic rocks as well as sediments, K-feldspars are only a stable phase in subducted granitic gneiss. Similarly, in experiments with synthetic materials, formation of K-feldspar as an accessory mineral during melting occurred only if no water was added to the starting materials (∼3.5 GPa and ∼1050 °C; Hermann and Green 2001). Within subducting sediments, K-feldspars appear to be stable up to maximum pressures of 1.6–2.2 GPa (Massonne and Schreyer 1987). As such, potassium feldspars are unlikely to play a major role in retention of thallium in the downgoing plate, either in the (altered, upper) oceanic crust or in sediments.

All micas are hydrous minerals, and phlogopite (the magnesium end-member of the biotite solid solution, $KMg_3AlSi_3O_{10}(F,OH)_2$) is a common phase in metasomatized mantle xenoliths. In particular, 'glimmerite' xenoliths, mostly derived from the sub-continental mantle (e.g. Grégoire et al. 2002), sometimes contain large modal abundances of phlogopite. The stability of phlogopite is strongly dependent on bulk composition. In peridotites, phlogopite is stable to >6 GPa at 1100 °C (e.g. Konzett 1997), whereas in bulk compositions similar to subducted pelites phlogopite breaks down at ∼3 GPa at 1000 °C (e.g. Massonne 1999). Rader et al. (2018) analysed six phlogopites, and found Tl concentrations ranging from 0.23 to 6.45 µg/g. Similarly, Fitzpayne et al. (2020) determined Tl concentrations of 0.25 to 3.48 µg/g in 26 different phlogopite mineral separates derived from glimmerites.

Phengite ($K(AlMg)_2(OH)_2(SiAl)_4O_{10}$) is a potassium-rich mica in the muscovite series. Shu et al. (2019) presented an investigation of Tl concentrations and isotopic compositions in exhumed eclogites, which experienced maximum P-T conditions of <3 GPa and <800 °C. Where present, phengite was identified as the primary host of Tl, based on correlations between Tl and K, Rb, Cs and Ba in whole rock samples. Hermann and Green (2001) concluded that, where present, phengite is the most important host of LILE at pressures >2 GPa. Schmidt and Poli (1998) reported that phengite can be stable in hydrous basalts up to ∼10 GPa across a wide temperature range. Subsequent work (Schmidt et al. 2004) indicates that for pressures >6.5 GPa, phengite breaks down entirely at temperatures of ∼1050 °C in the presence of as little as 1.5 wt% water, via the formation of supercritical liquids. Considering the conditions expected at the slab surface beneath volcanic arcs, phengite is expected to be stable within the subducting slab and thus has the potential to carry Tl to postarc depths.

In order to unambiguously identify the contribution of a specific Tl-rich phase to arc magmas using co-variations between Tl and other element abundances, the mineral would have to be the dominant host of both thallium and that other element. Thallium co-varies most strongly with LILE in a variety of settings, including arcs. However, LILE are more widely distributed than Tl in common mineral phases, and thus may not derive solely from a single mineral phase (e.g. phengite), such that simple co-variations only indicate similar incompatibilities rather than identical sources. It is not clear how contribution of K-feldspar or phlogopite might be identified using Tl systematics. Prytulak et al. (2013) tentatively identified evidence for phengite retention of Tl in the Mariana arc using a Tl/Yb versus Cs/Rb discrimination diagram, after Busigny et al. (2003). Thallium is normalised to Yb because the latter is an immobile element that is incompatible in

the absence of garnet. The Cs/Rb ratio was chosen because it is, in principle, a ratio of LILE that should be sensitive to the dissolution of phengite (Busigny et al. 2003). At conditions relevant to subduction, Rb partitions more strongly into phengite relative to K, whereas Cs partitions more strongly into coexisting aqueous fluid. Therefore, decreasing Tl/Yb ratios with increasing Cs/Rb would suggest that Tl (and Rb) are retained in phengite while Cs is removed (Busigny et al. 2003, Prytulak et al. 2013). Therefore, a negative trend is predicted if phengite retains significant Tl. For the expanded arc dataset, such trends are not obvious (Fig. 4.8). However, the data show significant scatter, which is unsurprising given the likely influence of other silicate phases and heterogeneous mantle source compositions.

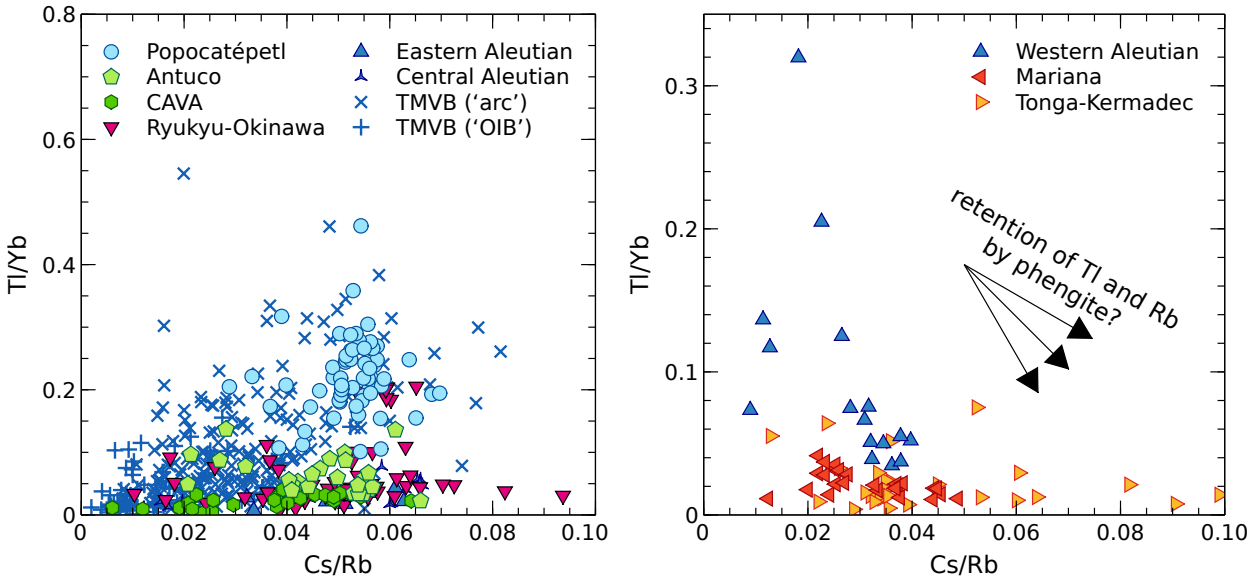


Figure 4.8: Different degrees of phengite retention in lava sources is predicted to result in a negative trend in Tl/Yb versus Cs/Rb (see text for details). A possible negative trend is seen only for the Mariana arc, the Western Aleutian arc, and the Tonga-Kermadec system. For data sources, see Appendices B4.i and B4.ii.

Host phases: synthesis

Limited, ambiguous evidence for retention of Tl in the slab is consistent with evidence that the majority of Tl is never recycled into the deep mantle (Chapter 3, Brett et al. 2021). Notably, constraints imposed by OIB data are consistent with the results of Schmidt et al. (2004) and Kessel et al. (2005), who argue that leaching and melting remove all potassium and associated phengite-hosted trace elements from the slab during subduction to 300 km, except in the case of extremely cold slabs. Although thallium was not explicitly considered in this study, the conclusion most likely also applies to Tl. Fundamentally, because so little Tl is retained it is not possible to identify from arc lava chemistry whether sulphide or silicate minerals are the primary host phase(s) of Tl in the subducting slab.

4.4.2 How is Tl transferred from slab to mantle?

Three main mechanisms are proposed for the transfer of subducting material into the mantle wedge: non-magmatic (fluid) transfer, sediment and/or slab melts, and metamorphic mélanges,

i.e. mixing between mantle and bulk subducted material before any melting takes place (e.g. Marschall and Schumacher 2012).

All three processes have been invoked to explain Tl transport in previous work. For example, Prytulak et al. (2013) used the relative co-variation of Tl abundances with fluid-mobile and sediment-derived highly incompatible elements to argue that, in the Central Island Province of the Mariana arc, the Tl budget is dominated by sediment – rather than fluid – contributions. For Tonga-Kermadec and the Central American Volcanic Arc, Nielsen et al. (2017a) pointed out that phengite stability is affected by the presence of fluids, with phengite breaking down at lower temperatures for a given pressure where excess water is present (∼875 °C at ∼3 GPa with 1.2 wt% excess H_2O, versus ∼925 °C with no excess H_2O; Hermann and Green 2001). They therefore suggest that variations in Cs/Tl ratios of lavas are controlled by residual phengite during melting or, when phengite is exhausted, by fluid transfer of both Tl and alkali metals. For the Ryukyu-Okinawa system, Shu et al. (2017) used isotope mixing relationships between Sr and Nd, and between Tl and Sr-Nd-Pb, to argue for addition to the source of up to 2% sediment via mélange formation (i.e. mixing of mantle with bulk slab material) prior to melting.

Of course, thallium sources and transport processes need not be the same in every arc, nor is it possible to evaluate sources and transport using Tl data alone. The partitioning of Tl between sediment melts and residual minerals under subduction conditions is not well studied, and Tl partition coefficients between phengite and silicate melt or water-rich fluids have yet to be established. Identification of mélange formation via elemental systematics alone is not straightforward. However, the new arc dataset presented here has the potential to provide information about the fluid mobility of Tl.

Melt and mélange transfer

Thallium is a highly incompatible element during mantle, slab, or sediment melting. Therefore, with the possible exception of retention in phengite, thallium should be readily transferred by a melt phase. Mechanical mixing of sediment and altered crust, with the mixture then rising as metamorphic mélanges to the hotter interior of the wedge, should also allow effective transfer of Tl from the subducted material. However, it is still unclear how effectively Tl can be transferred by slab-derived fluids in the absence of a melt phase.

Non-magmatic fluid transfer

In a landmark study, Noll et al. (1996) investigated hydrothermal fluid transfer of siderophile and chalcophile trace elements during subduction processing using the principle of invariant trace element ratios. If, for a large set of samples, two elements are observed to produce an approximately uniform ratio, it is often assumed that they partition similarly between solids and melt during common magmatic processes (see Chapter 3, Brett et al. 2021 for detailed discussion). The observation that the Pb/Ce ratio was approximately uniform for MORB and OIB, but elevated in arc lavas and continental crust, therefore implied that the relative bulk partition coefficients of Pb and Ce differed between these settings (e.g. Hofmann et al. 1986, Newsom et al. 1986). Noll et al. (1996) pointed out that a similar “bimodal” distribution was observed for the ratio B/La, with the

same tectonic discrimination. Like Pb and Ce, B and La exhibit similar partitioning during normal fractional crystallisation (e.g. Leeman et al. 1994). Lanthanum and cerium are incompatible rare earth elements that partition similarly. However, unlike boron and lead, rare earth elements are relatively fluid-immobile (e.g. Michard and Albarède 1986). Noll et al. (1996) therefore inferred that elevated B (and Pb) concentrations in arc lavas resulted from the non-magmatic transfer of these elements by hydrothermal fluids during subduction processing. The authors likewise inferred pronounced fluid-mobile behaviour for As and Sb, whereas other siderophile and chalcophile elements investigated (Sn, W, Mo) appeared to show little evidence for mobilisation by hydrothermal fluids. The lack of mobilisation was inferred because arc lavas overlapped with the X/REE field of MORB and OIB, where X is the element of interest, and REE is the rare earth element with the most similar inferred partition coefficient during magmatic processing.

While Tl was also considered, the paucity of precise and accurate Tl data for MORB and OIB samples at the time made it impossible to reach robust conclusions on enrichments versus depletions of Tl in arc lavas. Nevertheless, a possible "bimodal" distribution (as seen for B/La and Pb/Ce) was tentatively identified for Tl/La, potentially indicating fluid transfer of Tl from subducting materials to arc lavas. Fluid mobility of Tl is well-documented at relatively low temperatures (maximum ∼500 °C) in a variety of settings (e.g. processing at mid-ocean ridges, Nielsen et al. 2006c, Coggon et al. 2014; surface weathering, Rehkämper and Nielsen 2004; ore deposits and their surroundings, e.g. Baker et al. 2010a, Hettmann et al. 2014b, Fitzpayne et al. 2018).

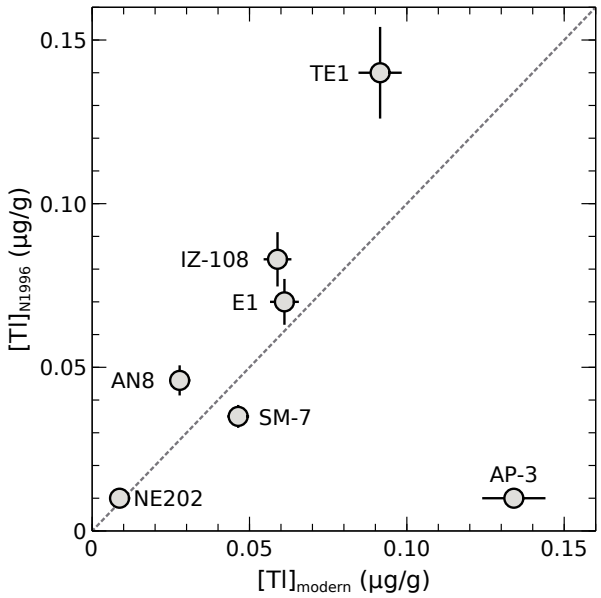


Figure 4.9: Seven samples reported by Noll et al. (1996) have subsequently been reanalysed for Tl concentration by other workers. Points are labelled with sample names. Data sources: Noll et al. (1996), Prytulak et al. (2013), Nielsen et al. (2017a).

While Tl should not be classified as a strictly chalcophile element in magmatic environments, this does not render the approach of Noll et al. (1996) irrelevant. Indeed, if Tl exhibits strictly lithophile behaviour, it is more directly comparable to boron than are unambiguously chalcophile elements. As such, the substantial datasets now available for Tl concentrations in MORB, OIB and arc lavas permit re-evaluation of the fluid mobility of Tl during subduction.

The data reported by Noll et al. (1996) are not included in this assessment. While reasonable values were obtained for determinations of Tl concentrations in BHVO-1 and AGV-1, seven of the

samples for which Noll et al. (1996) determined Tl have subsequently been reanalysed during Tl isotopic studies (Prytulak et al. 2013, Nielsen et al. 2017a). For the most part, new determinations yielded significantly lower Tl concentrations (Fig. 4.9), with correspondingly lower Tl/La ratios. It is also immediately apparent that the estimate of Noll et al. (1996) for Tl/La in MORB and OIB was significantly too high, at ∼0.005 (ranging from ∼0.003 to ∼0.008), compared with Tl/La ratios of 0.0024 ± 0.0007 (1sd, n = 909; range 0.0009–0.006; Appendix B3.vi) and 0.001 ± 0.001 (1sd, n = 127; range 0.0001–0.01; Appendix B3.v) for the modern MORB and OIB databases, respectively. That is, both overestimates of MORB and OIB Tl/La and underestimates of arc Tl/La contributed to the impression that Tl exhibits only limited fluid mobility in subduction contexts.

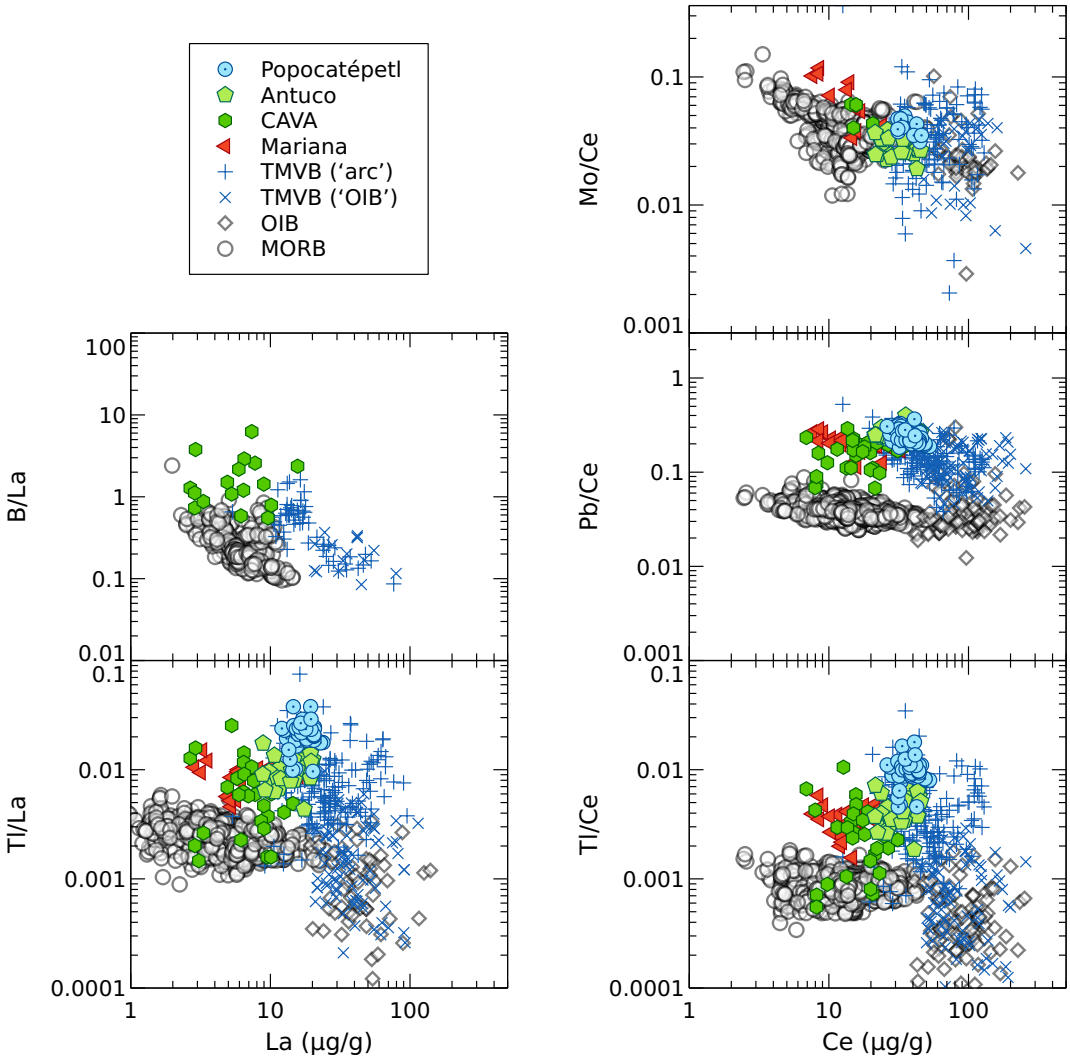


Figure 4.10: Plots of X/REE versus REE (where X is an incompatible element and REE is the rare earth element that is understood to partition most similarly during magmatic processes) were used by Noll et al. (1996) to identify possible non-magmatic transfer of fluid-mobile elements during subduction. Conceptually, if arc lavas plot in a distinct field from MORB and OIB, this indicates a possible role for fluid transfer, as with B/La. Here new MORB, OIB and arc datasets (Chapters 3 and 4) are used to explore the fluid mobility of Tl, in comparison to Mo (largely fluid-immobile) and B and Pb (fluid-mobile). Thallium is shown compared with both La (per Noll et al. 1996) and Ce (per subsequent investigations of Tl partitioning during MORB melting). Unlike Mo, and similar to B and Pb, Tl/REE fields for arcs do not show consistent overlap with the MORB-OIB field.

In Figure 4.10, variation diagrams as used by Noll et al. (1996) are replotted using modern datasets. In addition to the Tl/La ratio used by Noll et al. (1996), Tl/Ce is shown. Subsequent research has demonstrated that during MORB melting Tl and Ce partition more similarly than Tl and La (Nielsen et al. 2014, Brett et al. 2021, Chapter 3). Although there is some overlap between arc

lavas and OIB, particularly in 'OIB-type' TMVB samples, Tl/La and Tl/Ce fields are clearly distinct from MORB. Unfortunately, comparison of distributions is complicated by the limited availability of modern B and Mo data for subduction zones that are well-characterised for Tl. However, where Mo concentrations are available, Mo/Ce ratios overlap entirely with the MORB-OIB field, consistent with the distributions reported by Noll et al. (1996) and their interpretation that Mo is largely fluid-immobile during subduction. While recent work suggests that Mo can exhibit fluid mobility (e.g. Freymuth et al. 2015), this reinforces that the distinguishable distributions of MORB and OIB versus arc lavas seen for Tl/La and Tl/Ce imply significant fluid mobility of Tl during subduction.

This assessment is in agreement with the conclusions of Cox et al. (2019), who performed a detailed study of chalcophile element systematics at Antuco volcano (Chile). These authors report that enrichments in a suite of nominally-chalcophile elements, including Tl, relative to "parental-MORB" (Jenner 2017) indicate their mobilisation by slab-derived fluids. Enrichments in Pb and Tl relative to parental-MORB and co-variation between the two elements are apparent for the entire global arc compilation (Fig. 4.11), following the general pattern of bulk continental crust, as observed by Cox et al. (2019) for Antuco.

It is therefore highly likely that Tl can be transferred from the slab whether or not a melt phase is present, in agreement with the assertion of Brett et al. (2021) (Chapter 3) that near-quantitative removal of thallium during subduction must occur.

4.4.3 Thallium accumulation in the continental crust

The continental crust has been calculated to contain up to 70% of the Earth's incompatible elements (see e.g. Rudnick and Gao 2003), and arc magmatism plays a key role in its formation. Rudnick and Gao (2003) estimated the Tl concentration of the continental crust at 0.50 µg/g, distributed unevenly between the lower (∼0.32 µg/g) and upper (∼0.9 µg/g) crust. Jenner (2017), considering Tl as a chalcophile element, ascribed this distribution to the relatively high incompatibility of Tl during differentiation of sulphide and silicate cumulates in the lower crust. It therefore appears that subducted Tl is eventually reprocessed into continental crust. However, very little is currently known about the mechanisms involved.

A striking feature of normalised trace-element diagrams of arc lavas is the geochemical similarity to bulk continental crust (Fig. 4.12), particularly for arc volcanoes sited on thick continental crust (e.g. Popocatépetl, México, and Antuco, Chile). However, even subduction zones with high Tl inputs, such as Tonga-Kermadec, produce arc lavas with a negative Tl anomaly relative to the bulk continental crust (Fig. 4.12).

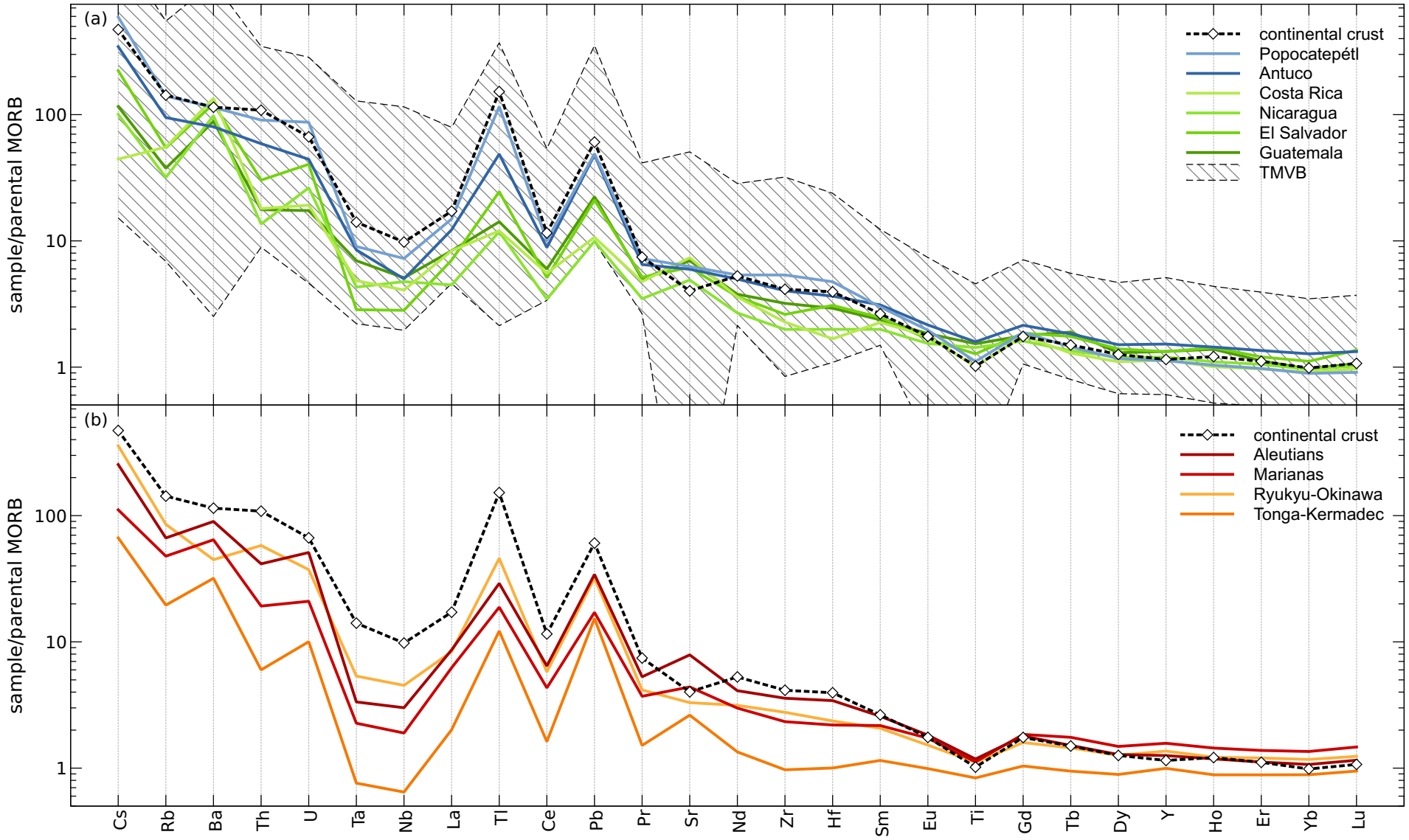


Figure 4.11: Average trace element contents of arc lavas normalised to parental-MORB (Jenner 2017). (a) continental arcs; (b) oceanic arcs. TMVB = Trans-Mexican Volcanic Belt. For data sources, see Appendices B4.i and B4.ii.

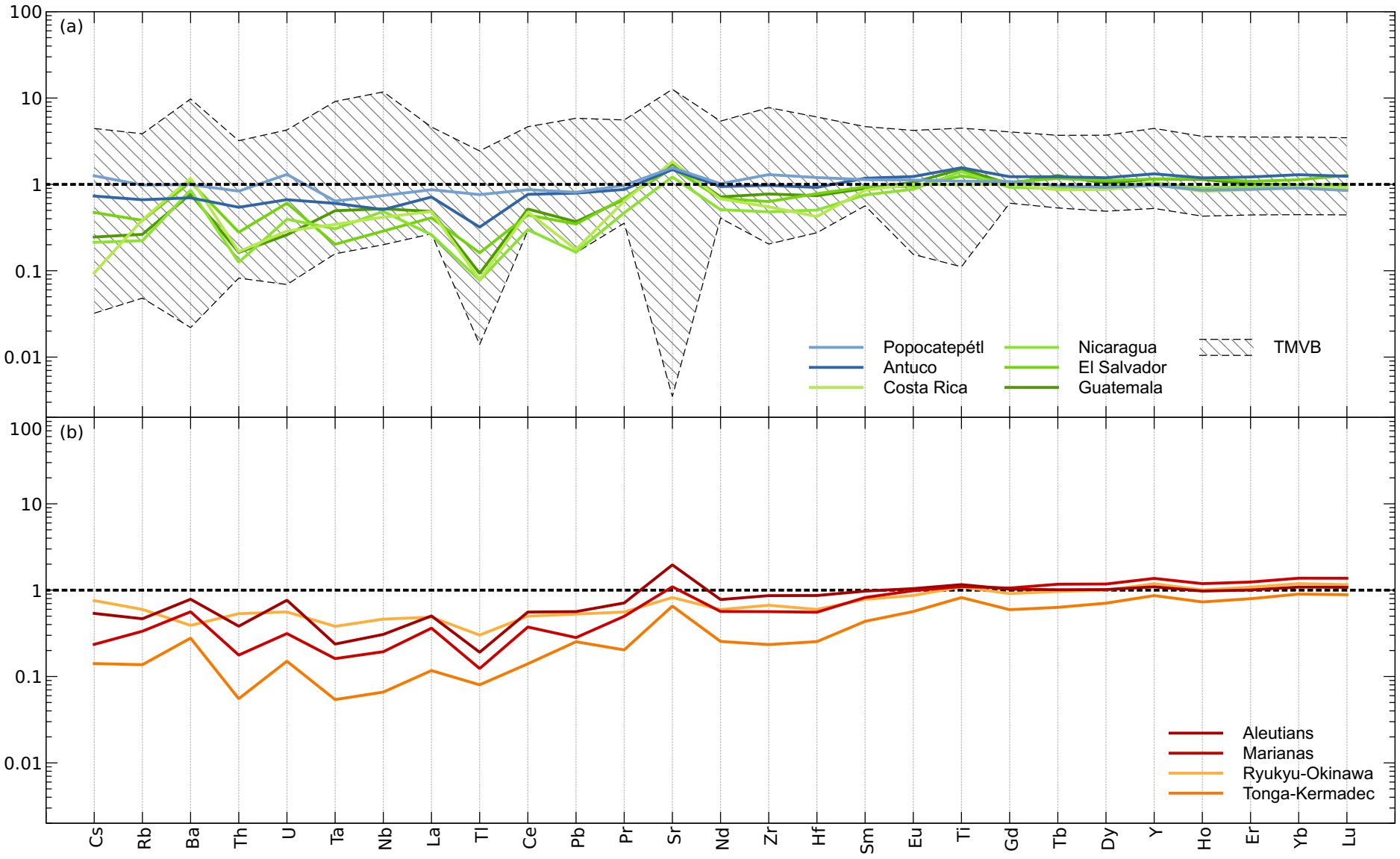


Figure 4.12: Average trace element contents of arc lavas normalised to continental crust (Rudnick and Gao 2003). (a) continental arcs; (b) oceanic arcs. TMVB = Trans-Mexican Volcanic Belt. For data sources, see Appendices B4.i and B4.ii.

In addition to direct inputs of Tl from the subduction of oceanic plates, recycling of upper-crustal material via forearc erosion (e.g. Straub et al. 2020) potentially contributes to the apparent progressive accumulation of Tl in continental arcs. While some efforts have been made to quantify the subduction flux of Tl sourced from sediment of the lower plate, so far these are relatively geographically restricted (e.g. for the Aleutians: Nielsen et al. 2016). However, since almost all subducted Tl is reprocessed through arc volcanism, there is the potential that Tl abundances could be used to help constrain the contribution of forearc-eroded upper-plate materials to the trace element budgets of arc volcanics.

Quantitative assessment of Tl accumulation in the continental crust is – to some extent – possible. Assuming that (within a single arc) variations in crustal thickness are a proxy for crustal maturity, Tl anomalies (relative to La and Ce, and normalised to bulk continental crust, as defined by Brett et al. 2021, Chapter 3) would be expected to become more positive (i.e. approach and/or exceed a value of 1) as crustal thickness increases if Tl does indeed undergo progressive accumulation.

Employing the crustal thickness estimates of Farner and Lee (2017) for lavas from the TMVB, there is perhaps a sense of such a correlation (Fig. 4.13), despite the limited set of data for which crustal thickness estimates are available. There is a notable absence of data at intermediate thicknesses for this area. Further exploration of possible co-variation between these geophysical and geochemical parameters would require either an expanded database of crustal thicknesses and/or targeted measurements of Tl in samples for which such estimates are already available.

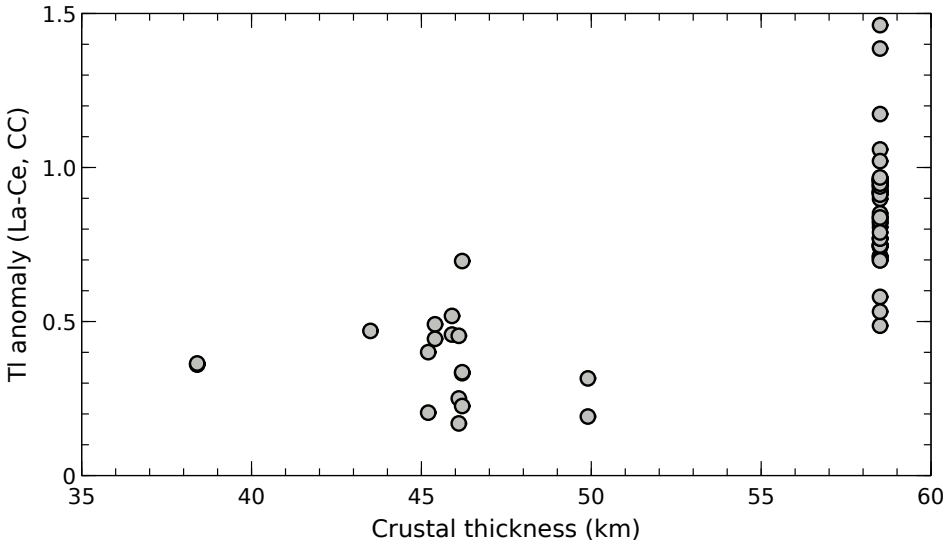


Figure 4.13: Thallium anomaly (see § 3.3.3) versus estimated crustal thickness (Farner and Lee 2017) for samples from the Trans-Mexican Volcanic Belt. For additional data sources, see Appendices B4.i and B4.ii.

4.5 Summary

The ability to use Ce/Tl ratios and their variation with Tl concentration as a tectonic discriminant was demonstrated using well-calibrated Tl data reported in the literature for OIB and arc lavas. An expanded database of arc lavas for which Tl concentrations are available was therefore compiled, based in part on the use of Ce/Tl ratios as a tectonic discriminant.

It was not possible to identify clear geochemical evidence for the primary host phase(s) of Tl within the subducting slab, although Tl does exhibit identifiable co-variation with (highly incompatible) LILE in arc lavas. The near-complete loss of Tl from the subducting slab is consistent with instability of likely Tl host phases during subduction. This conclusion is consistent with both indications from Tl systematics in OIB (Chapter 3, Brett et al. 2021) and existing literature (e.g. Schmidt et al. 2004, Kessel et al. 2005, Jenner 2017)).

Transfer of Tl from the slab appears to be at least in part due to dissolution of Tl in non-magmatic fluids, as well as partitioning into silicate melts. Fluid mobility contributes to efficient removal of Tl from the subducting slab. As a result of both fluid mobility and marked incompatibility during partial melting, thallium progressively accumulates in continental crust.

Chapter 5

Thallium isotope insight into processes operating in thick continental crust

5.1 Introduction

5.1.1 Thallium isotope studies in arcs

Thallium isotopes are a powerful tool for identifying the contribution of subducted material to arc magmatism, due to concentration and isotopic contrasts between the mantle and potential subduction inputs (Fig. 5.1). So far, studies investigating this application of Tl isotopes have examined subduction settings where the overlying plate consists of either oceanic crust (Aleutian arc, Ryukyu-Okinawa arc, Mariana arc, Tonga-Kermadec arc) or oceanic crust transitional to (relatively thin) juvenile continental crust (Central American Volcanic Arc) (Fig. 5.2). Oceanic arcs generally exhibit restricted ranges in ε^{205}Tl, with lavas that are often isotopically heavier than estimated mantle values (i.e. ε^{205}Tl > -2 ± 1; Fig. 5.3). For example, the average Tl isotopic composition of lavas from the Mariana and Tonga-Kermadec arcs (excluding samples identified in previous studies as showing potential evidence of degassing) is statistically significantly heavier than that of MORB at the 95% confidence level (Table 5.1), and many individual lava samples are also resolvably heavy (Fig. 5.3, Appendix B4.i).

Variations in the Tl isotopic composition of arc lavas are interpreted as reflecting the variable but widespread incorporation of isotopically heavy Tl from subducted pelagic sediments into their source regions, which can dominate the elemental Tl budget of the sub-arc mantle when present. This interpretation is supported by along-arc variations in the Tl isotopic composition of lavas, which for most localities can be directly linked with those of sediments sampled by drill cores on the downgoing plate outboard of the respective arcs (Mariana arc, Prytulak et al. 2013; Central and Eastern Aleutian arc, Nielsen et al. 2016; Ryukyu-Okinawa arc, Shu et al. 2017; Tonga-Kermadec arc, Nielsen et al. 2017a; Central American Volcanic Arc north of Costa Rica, Nielsen et al. 2017a; see Fig. 5.4). There are exceptions, namely Costa Rica (Central American Volcanic Arc, Nielsen

et al. 2017a) and the Western Aleutian arc (Nielsen et al. 2016). Both arcs produce lavas that exhibit a possible altered oceanic crust (AOC) signature, i.e. lavas contain isotopically light thallium (ε^{205}Tl < -2 ± 1). For Costa Rican lavas, this has been explained by the subduction of an oceanic ridge with only thin sediment cover consisting predominantly of carbonates with low Tl concentration (Nielsen et al. 2017a). Minimal sediment input, which may prevent the overprinting of a light AOC isotopic signature, has also been invoked in the Western Aleutian arc (Nielsen et al. 2016). The scarcity of identifiable 'AOC' Tl signatures can be explained by the significantly higher Tl concentrations of Tl-bearing sediments (up to ∼100,000 ng/g) than of AOC (up to ∼1000 ng/g; Nielsen et al. 2017b). Where such sediments are present, they are expected to dominate the Tl budgets of the subarc mantle, regardless of whether they are of pelagic (typically ε^{205}Tl > -2) or terrigenous (typically ε^{205}Tl ≈ -2) origin.

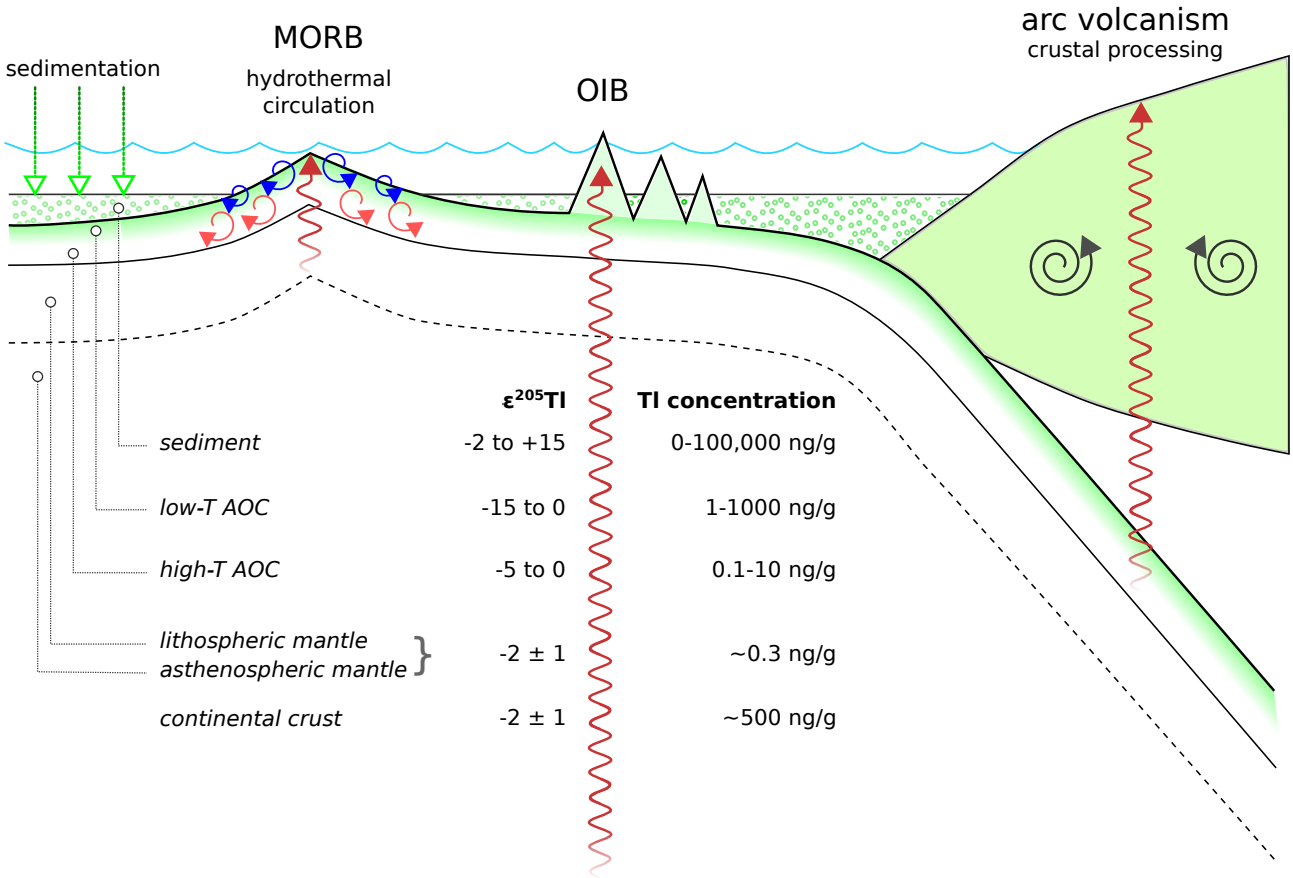


Figure 5.1: Schematic of plate tectonic processes relevant to the Tl cycle (not to scale), with regions of high Tl concentration shown in green. As an incompatible element, Tl is concentrated in magmas during melting (dark red arrows). Low-temperature hydrothermal circulation in the upper part of the plate (blue arrows) is associated with deposition of Tl, whereas high-temperature hydrothermal circulation (red arrows) removes Tl. Further Tl is then added to the subduction package via sediment deposition (green arrows) and intraplate volcanism. During subduction processing, Tl is efficiently removed from the subducting slab. Thallium incorporated into arc crust potentially undergoes reprocessing (grey arrows). Data sources as for Figure 1.1.

The behaviour of Tl isotopes in subduction settings with overlying thick, mature continental crust has not yet been assessed. The continental crust has elevated Tl concentrations (∼0.5 µg/g; Rudnick and Gao 2003) compared to the mantle, and an approximately uniform isotopic composition is inferred from a study of widespread, continentally-derived loess (ε^{205}Tl = -2 ± 1; Nielsen et al. 2005). The indistinguishable values inferred for the Tl isotopic composition of the mantle and continental crust contrast with (i) the marked heterogeneity observed in subduction inputs to

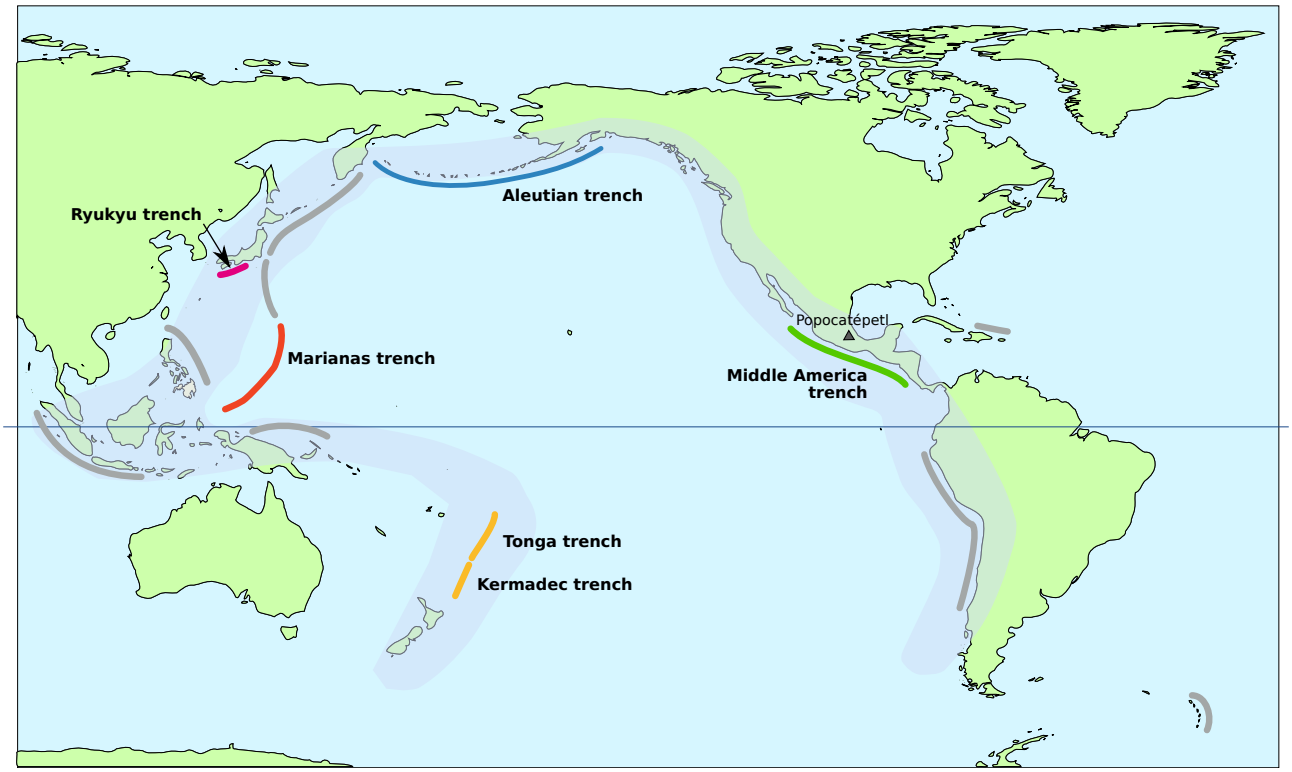


Figure 5.2: Thallium isotope data is currently available for five subduction zones, with associated trenches highlighted in colour. The location of Popocatépetl volcano, for which new data is presented in this chapter, is also shown.

Table 5.1: The difference between the Tl isotopic compositions of arc lavas and MORB can be assessed for statistical significance using unpaired two-tailed Student's *t*-tests. The calculated *p*-value indicates the probability that any two normally-distributed populations of lavas (e.g. "all MORB lavas" and "all Mariana lavas") have the same average Tl isotopic composition, given a set of samples drawn from that population. For $p < 0.05$ (i.e. <5% probability that the average compositions of the two groups are indistinguishable), differences are here considered statistically significant. On average, lavas from the Mariana and Tonga-Kermadec arcs are isotopically heavier than MORB.

Arc	Reference	Samples (*n*)	average ε^{205}Tl	2sd	*p*-value
MORB	Nielsen et al. (2006b)	5	−1.9	1.3	-
Aleutian	Nielsen et al. (2016)	43	−1.5	3.8	0.657
Ryukyu-Okinawa	Shu et al. (2017)	56	−1.0	2.8	0.184
Mariana	Prytulak et al. (2013, 2017)	24	−1.2	1.2	0.025
Tonga-Kermadec	Nielsen et al. (2017a)	30	1.9	5.2	0.003
Central American Volcanic Arc	Nielsen et al. (2017a)	34	−1.2	6.8	0.692

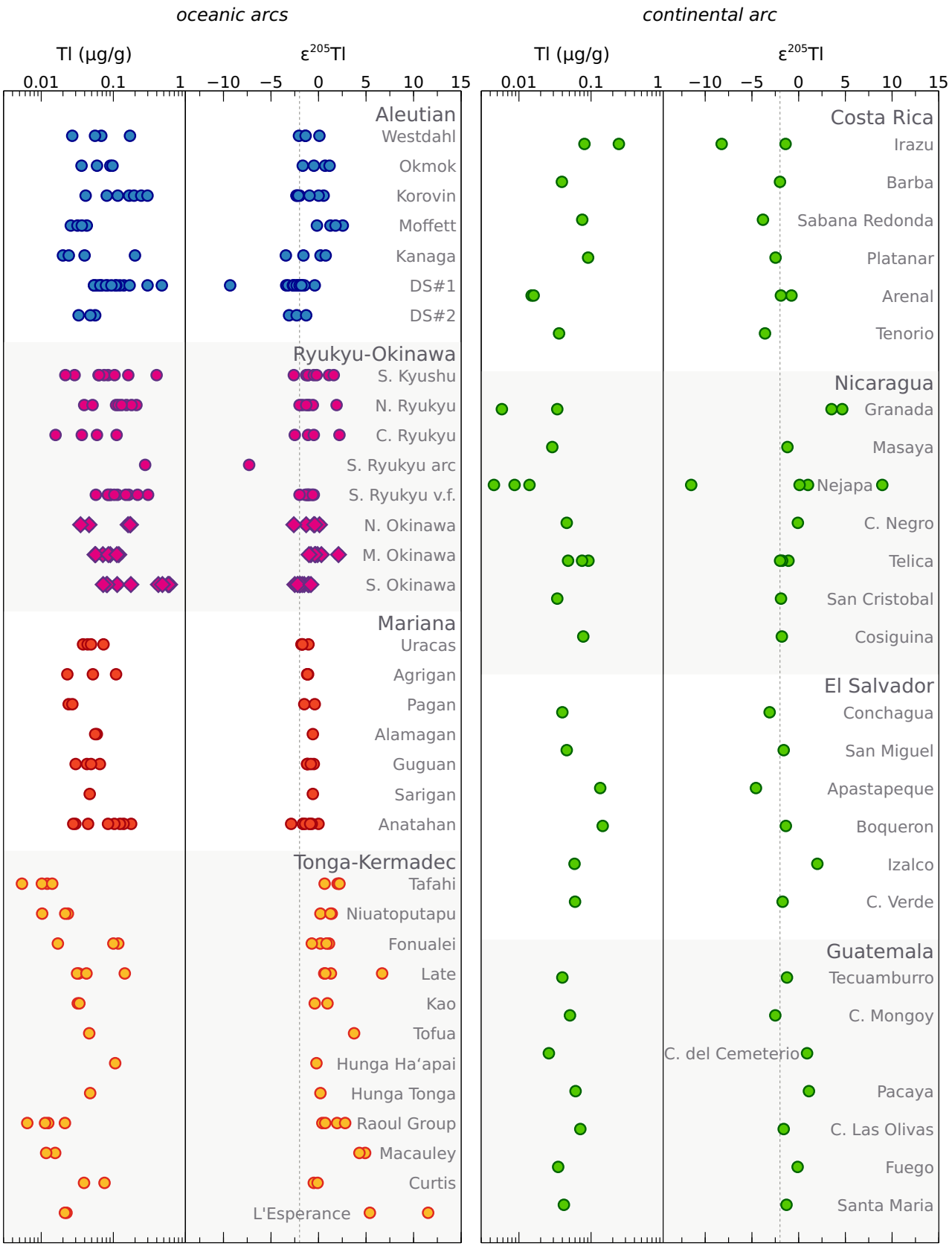


Figure 5.3: Thallium concentration and isotope ratios for lavas from the Aleutian arc (Nielsen et al. 2016), Ryukyu-Okinawa arc [circles] and back-arc basin [diamonds] system (Shu et al. 2017), Mariana arc (Prytulak et al. 2013, 2017), Tonga-Kermadec arc (Nielsen et al. 2017a), and Central American Volcanic Arc (CAVA; Nielsen et al. 2017a). Within each arc, sample locations are listed geographically along strike. For oceanic arcs (left) "C." = "Central"; "M." = "Middle"; "v.f." = "volcanic front". For the CAVA (right), "C." = "Cerro". The dotted line on Tl isotope ratio panels indicates estimated average mantle ε^{205}Tl (= -2 ± 1). Error bars (1sd for concentration, 2sd for isotope ratios) are smaller than symbols.

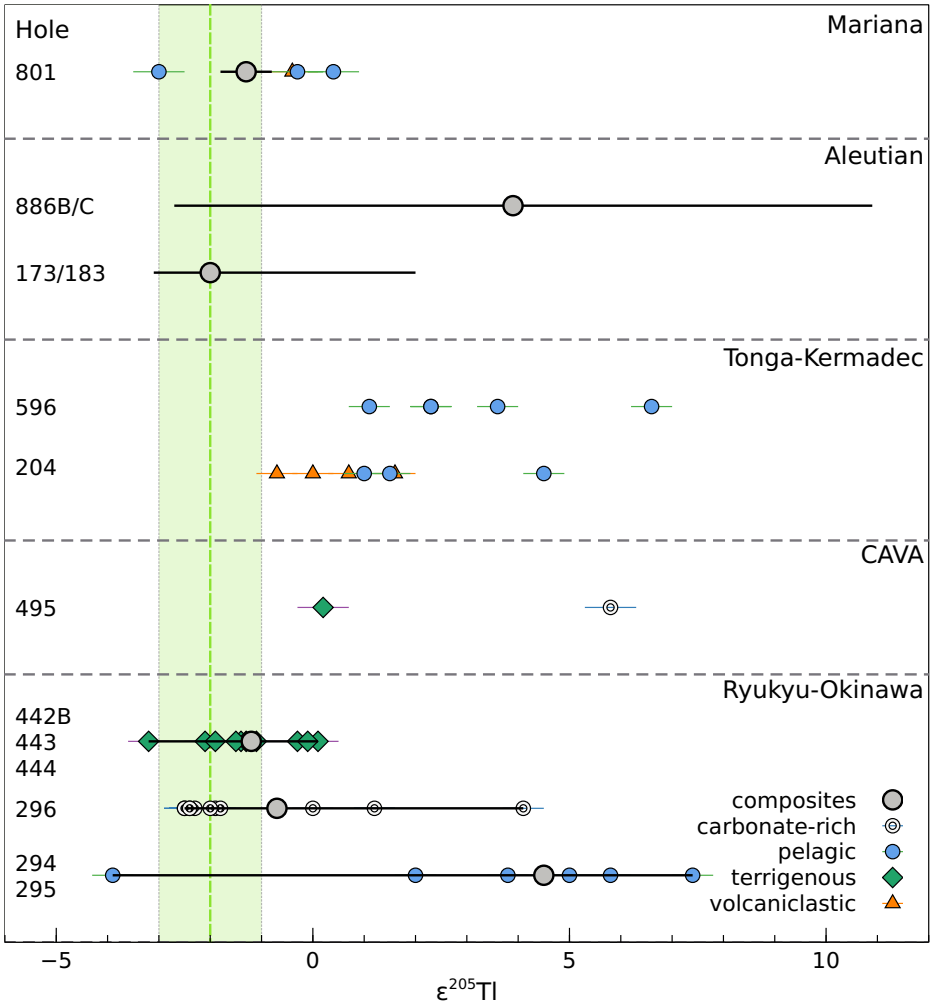


Figure 5.4: Variations in thallium isotopic composition of sediments subducted at arcs considered in this chapter. All sediments are from DSDP/ODP/IODP drill sites. Thallium concentration data for Hole 801 are from Prytulak et al. (2013). 886B/C and 173/183: Nielsen et al. (2016). 204 and 596: Nielsen et al. (2017a). 495: Nielsen et al. (2017a). 442B/443/444, 296, and 294/295: Shu et al. (2017). 'Composites' are weighted averages calculated by the relevant authors, with the exception of Hole 801, for which the 'SED composite' (see Plank et al. 2000 and Kelley et al. 2003) is plotted.

volcanic arcs and (ii) the heterogeneity that is documented in oceanic arc lavas. If the continental crust is built in part via accretion of arc terrains, then the discrepancy between heterogeneous arc building blocks and an apparently homogeneous continental crust requires explanation. We currently have a critical gap in our understanding of the preservation potential of unusual Tl isotopic signatures when magmas are processed through thick crust at continental arcs.

5.1.2 A role for kinetic isotope fractionation?

During processes such as open-system evaporation, isotope fractionations can arise due to kinetic effects. Specifically, less energy is required to cause lighter isotopes to enter the vapour phase than to evaporate heavier isotopes of the same element. If the vapour is then segregated from the melt, and therefore unable to attain equilibrium with same, the distinct isotopic compositions that evolve in melt and vapour phases due to these kinetic effects can be preserved (see § 1.3 for detailed discussion).

Thallium is volatile in volcanic environments, and is enriched in gas plumes produced by arc volcanoes relative to those at ocean islands and mid-ocean ridges (e.g. Edmonds et al. 2018). Baker

et al. (2009) investigated gas condensates and particulates from volcanic gases (from Kīlauea, Hawai'i; Mount Etna and Vulcano, Italy; Mount Merapi, Indonesia; and White Island and Ngāuruhoe, Aotearoa-New Zealand) to investigate possible kinetic Tl isotope fractionation. The range of Tl isotopic compositions they observed was analytically resolvable from mantle values, with both isotopically light and heavy signatures (ε^{205}Tl $\approx$ -6 to +5, n = 33). They interpreted the range in terms of kinetic isotope fractionation during partial evaporation, and some combination of kinetic and equilibrium isotope fractionation during partial condensation. Very recently, Nielsen et al. (2021) reported laboratory degassing experiments using a natural basalt from the Reykjanes Peninsula (Iceland), doped with trace elements including ~400 µg/g Tl. The results of these experiments were used to identify possible degassing trends in new data for lavas from Kamchatka (Russia) and to reassess data reported in the literature for arc lavas. A small number of samples that had previously been flagged as exhibiting signatures of potential degassing were identified as fitting the degassing trends calculated from experimental results. However, overall Nielsen et al. (2021) concluded that most subaerial basaltic lavas exhibit Tl isotope systematics that are affected only minimally, or not at all, by degassing.

Although kinetic isotope fractionations of Tl are observed in igneous contexts in nature (Baker et al. 2009, Nielsen et al. 2021), the origins of stable Tl isotope fractionations observed in arc lavas can for the most part be confidently traced to contamination of the magma sources by Tl derived from sediments and AOC. Previous studies of arcs have, therefore, ruled out a significant or widespread role for kinetic isotope fractionation in generating the Tl isotope variations observed in lava samples. Baker et al. (2009) noted that the average Tl isotopic composition of volcanic gas condensates and particulates is $\varepsilon^{205}\text{Tl} = -1.7 \pm 2.0$, which is indistinguishable from the averages determined for igneous rocks from a variety of settings and inferred for the mantle and the continental crust. The absence of any obvious overall sense of isotope fractionation between igneous rocks and volcanic gases implies that, in general, the Tl isotopic composition of lavas is not significantly affected by degassing. The authors argue that this is due to competing effects whereby the light isotope is concentrated in the vapour phase during evaporation and the condensate during cooling. Such effects would explain the limited evidence for kinetic isotope fractionation of Tl found to date.

However, thus far all investigations have taken place in settings where the crust is at most ~35 km thick. Continental arc settings with thick overlying crust are associated with silicic magmas, highly explosive eruptions, and significant outgassing, which might contribute to larger and therefore more readily detectable kinetic isotope fractionation effects. Underscoring this point, recent elemental work by Paisley et al. (2019) has revealed Tl enrichments in bombs from Cordón Caulle (Chile), argued to reflect the rapid resorption of gas-phase Tl by silicate melt during depressurisation and cooling at the point of ejection from the vent during explosive eruption. Conceptually, this type of process could lead to (some of) the range of ε^{205}Tl reported by Baker et al. (2009) for volcanic gases being preserved in igneous rocks. The lack of Tl isotope data from such settings necessarily limits our understanding of the behaviour of thallium during igneous processing and eruption.

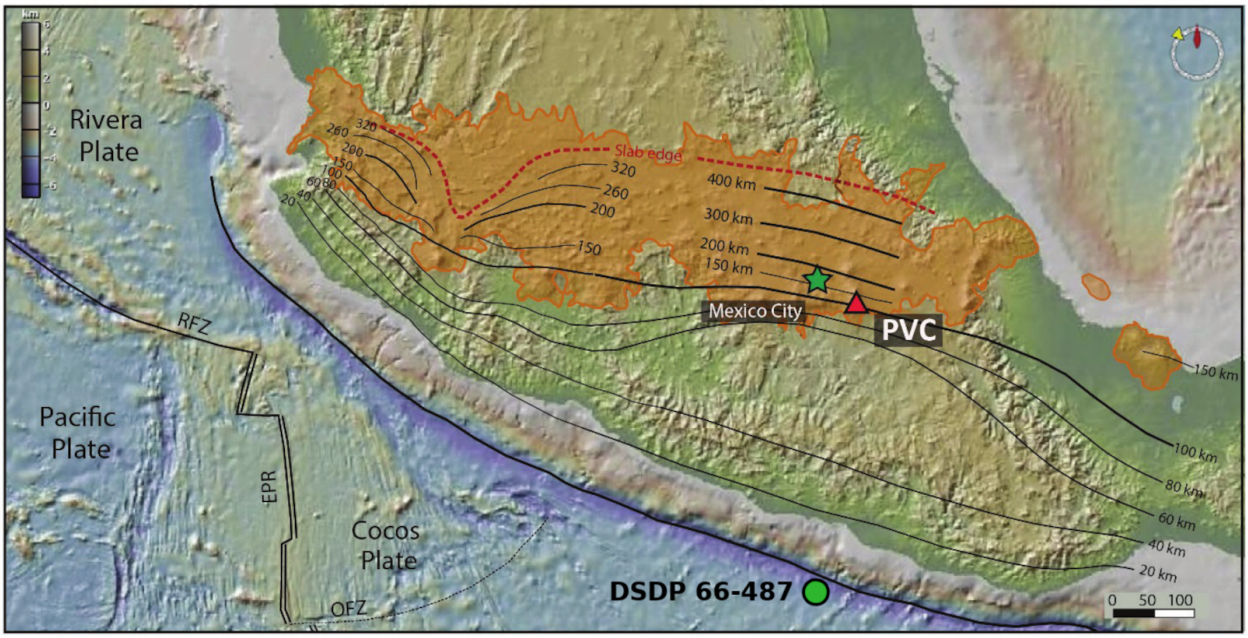


Figure 5.5: A regional map of Mexico, with the Trans-Mexican Volcanic Belt (TMVB) highlighted in orange. Lines running approximately parallel to the trench indicate the depth of the subducting plates. The Popocatépetl Volcanic Complex (PVC; red triangle), Mexico City (green star), and DSDP Leg 66 Site 487 (green circle) are marked. Modified from Ferrari et al. (2012) and Mangler (2018).

5.1.3 Aims and study location

Key questions about the behaviour of Tl in continental arc settings remain unanswered, particularly relating to magmatic processes in thick continental crust and potential kinetic isotope fractionation related to degassing.

Volcanic activity in the Trans-Mexican Volcanic Belt (TMVB) occurs due to subduction of the Cocos and Rivera plates beneath the North American Plate. The TMVB as a whole produces lavas that range in composition from calc-alkaline to unusual "OIB-like" geochemical signatures (as fingerprinted via Ce/Tl systematics in Chapter 4; see e.g. Ferrari et al. 2001, Petrone et al. 2003, Orozco-Esquivel et al. 2007, Straub et al. 2008, 2012). Popocatépetl volcano is an active stratovolcano located in central México (Figures 5.5, 5.6), producing predominantly calc-alkaline andesites and dacites (Fig. 5.7). It is situated on continental crust that reaches a thickness of 50–60 km (e.g. Ferrari et al. 2012, Farner and Lee 2017), ∼350 km from the trench and ∼100 km above the subducting Cocos plate (see review of Gómez-Tuena et al. 2018b). The closest ocean drilling location is Deep Sea Drilling Project Hole 487. The lithologies currently being subducted at this location consist of (silicate) terrigenous sediment and FeMn-rich pelagic sediment (see LaGatta 2003 and references therein).

Popocatépetl was chosen as a natural laboratory for the investigation of Tl behaviour in a continental arc setting due to its well-characterised eruptive products, which include high precision Tl concentration measurements (Mangler et al. 2019). Following Mangler et al. (2019), in this chapter the modern (<23.5 ka) cone will be referred to as Popocatépetl, while the larger volcanic centre will be referred to as the Popocatépetl Volcanic Complex (PVC). Thallium concentration variations at the PVC were examined in a global context in Chapter 4.

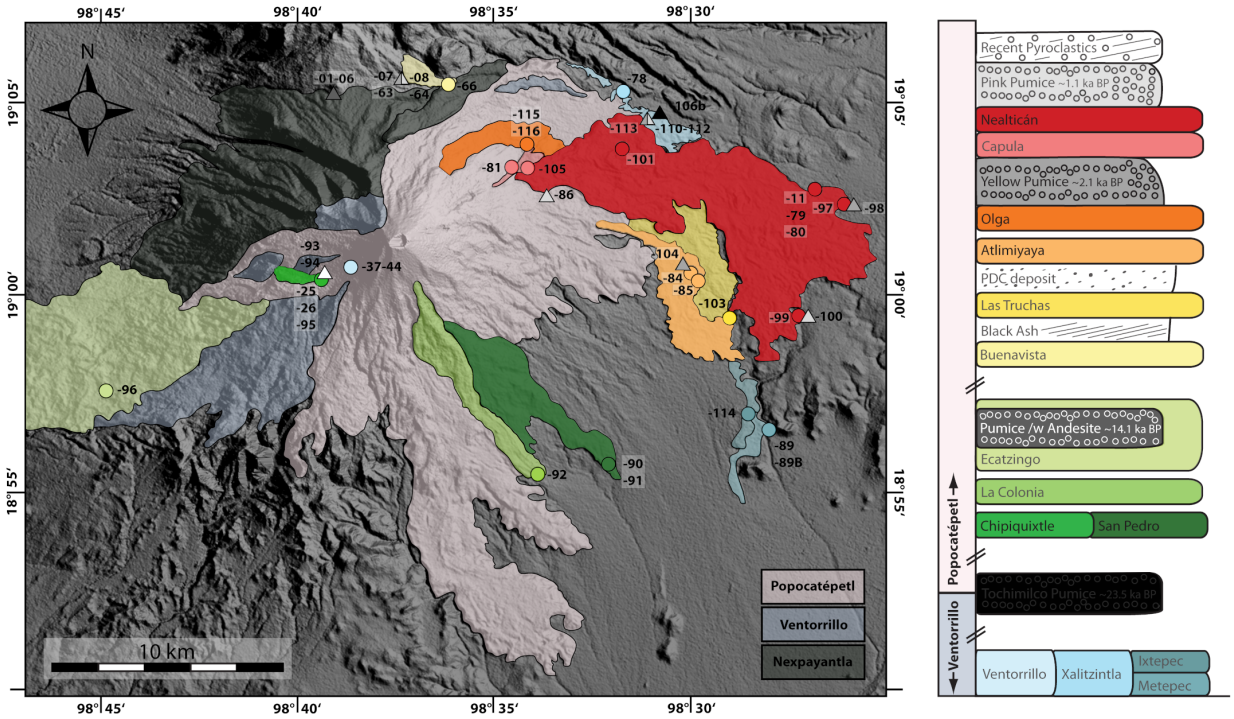


Figure 5.6: Geological map of the Popocatépetl Volcanic Complex, modified from Mangler et al. (2019). Units and samples for which new Tl isotope data are presented in this chapter are highlighted. Explosive units are abbreviated as WP (White Pumice), PwA (Pumice with Andesite), YP (Yellow Pumice) and PP (Pink Pumice) in subsequent text and figure legends.

Recent investigation of effusive and explosive eruptions has helped establish and clarify volcanic stratigraphy over the past ∼23.5 ka, with the aim of improving understanding of the plumbing system and magmatic processes beneath Popocatépetl (Mangler 2018, Mangler et al. 2019, 2020). Mangler et al. (2019) report chemical data for samples taken from 4 deposits of explosive eruptions and 14 lava flows that bracket them. Overall, trace element compositions are very similar to the bulk continental crust of Rudnick and Gao (2003) in terms of both pattern and absolute concentrations (Mangler et al. 2019). Thallium concentrations range between 0.14–0.73 µg/g, with 75% of all samples falling between 0.3 and 0.5 µg/g. In terms of trace element compositions, the “main range” products over the past ∼23.5 ka are remarkably homogeneous (Fig. 5.8). The exceptions are comparatively primitive flank eruptions, which appear to have bypassed the shallow plumbing system (Mangler et al. 2019).

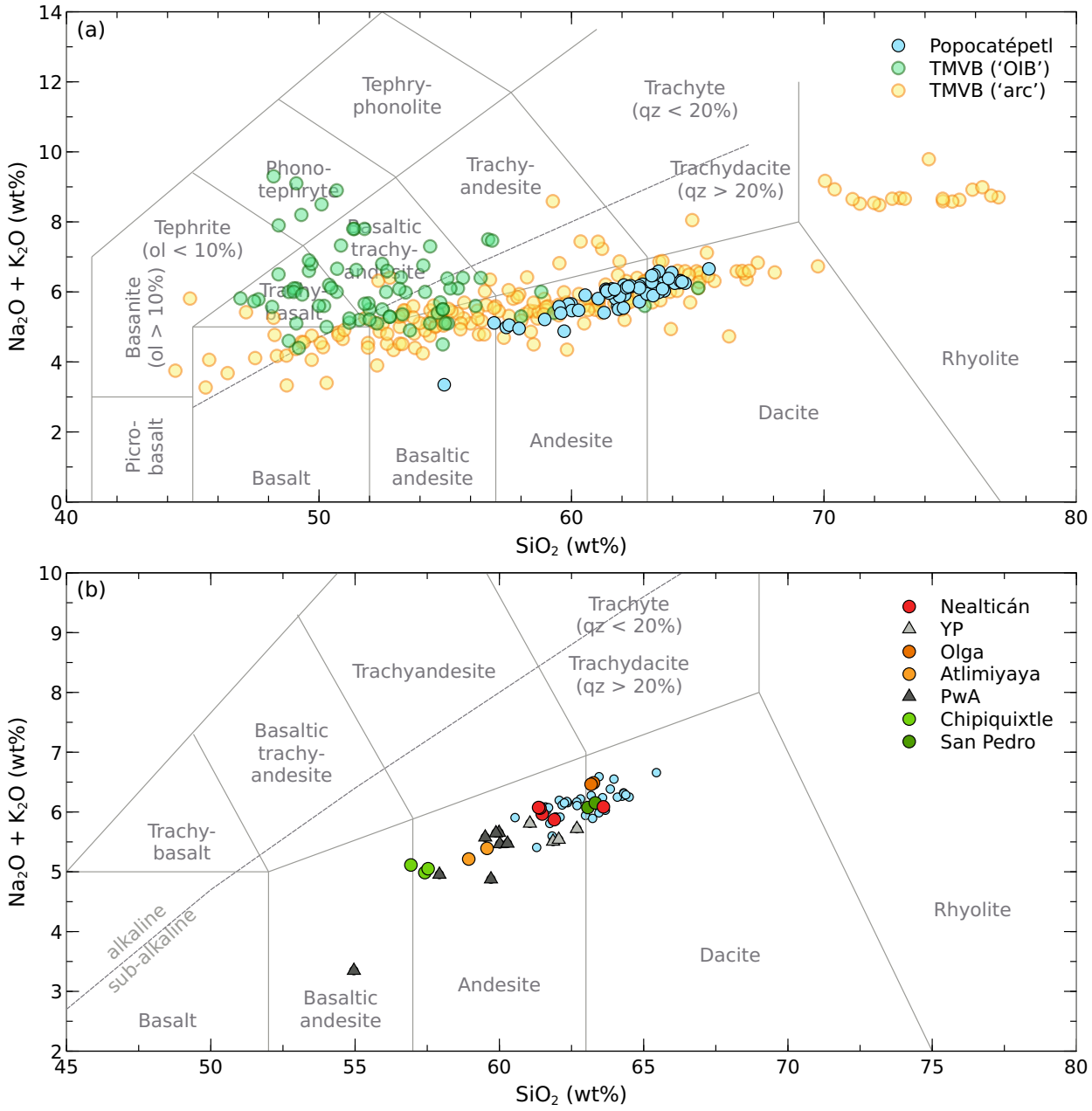


Figure 5.7: Total alkali-silica plots for (a) TMVB lavas and Popocatépetl, and (b) Popocatépetl only, with samples for which Tl isotope ratios were determined shown in large, coloured symbols. Note that Popocatépetl units are listed in stratigraphic order. Fields follow Le Maitre et al. (2002); alkaline-subalkaline dividing line (dashed) from Irvine and Baragar (1971).

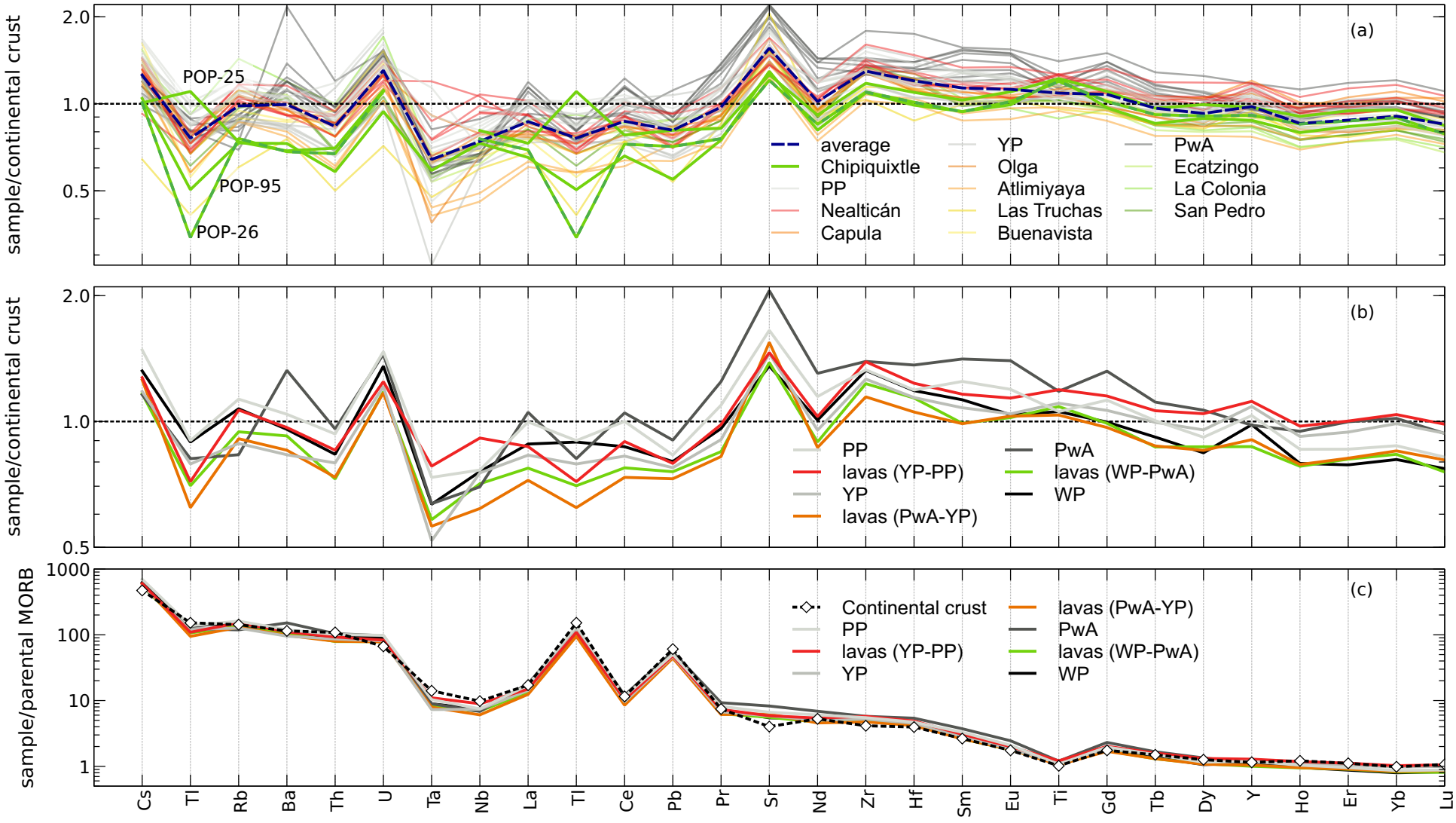


Figure 5.8: Incompatible trace element plots for Popocatépetl samples, normalised to the continental crust composition of Rudnick and Gao (2003) or the parental-MORB composition of Jenner (2017). Concentration data from Mangler et al. (2019). Note that units are listed in stratigraphic order. PwA = Pumice with Andesite, YP = Yellow Pumice, PP = Pink Pumice. (a) Individual samples. Note that the (relatively) primitive Chipiquixtle flank eruption spans the full range of Tl concentrations observed in the modern Popocatépetl edifice. (b) Average concentrations for (i) explosive units and (ii) inter-Plinian effusive units. Note that Tl and, to a lesser extent, Pb are enriched in pumices relative to lavas. (c) Normalisation of unit averages to parental-MORB emphasises the overall similarity of Popocatépetl samples to continental crust.

After almost 70 years of quiescence, the current eruptive episode began in 1994. Study of Popocatépetl has been motivated in part by its human impact, related to its proximity (60 km) to Mexico City. The volcano has a history of explosive (including Plinian) eruptions, with at least six having occurred in the past ∼23.5 ka (e.g. Arana-Salinas et al. 2010, Sosa-Ceballos et al. 2012, Siebe et al. 2017). The degassing behaviour of Popocatépetl has also been explored, due to the role of gas-phase volatiles in driving explosive eruptions and because of sustained release of large quantities (>9 kt/day) of SO_2 during the early phase of the present period of activity (e.g. Delgado-Granados et al. 2001, Roberge et al. 2009).

A focussed study of Tl isotope variations in Popocatépetl samples thus provides the opportunity to explore:

(i) the effects of crustal processing on the preservation of subducted sediment Tl isotopic signatures in continental arc lavas;

(ii) a high-sample-density comparison of explosive and effusive eruptions from the same edifice on the timescale of tens of thousands of years; and

(iii) the effects of explosive eruptions on Tl isotope systematics, in terms of kinetic isotope fractionation.

5.2 Methods

5.2.1 Sample selection

Mangler et al. (2019) report Sr-Nd-(Hf) isotopic composition along with major and trace element concentrations for 62 samples from Popocatépetl, spanning the past ∼23.5 ka of activity. Additional data are available for 5 xenoliths, collected in situ from one effusive flow and one explosive unit. All samples have been petrographically characterised (Mangler 2018, Mangler et al. 2020). Chemical and petrographic characteristics guided the choice of a subset of 23 samples (9 pumices and 14 lavas; locations shown in Fig. 5.6) for detailed study of Tl isotopic systematics. Explosive eruptions bracketed by effusive eruptions were targetted in order to provide a basis of comparison for (i) variations in explosive products and (ii) potential differences between effusive units.

Selection criteria took into account the petrographic characteristics and inter- and intra-unit chemical variations. As Tl systematics are highly sensitive to variations in source composition and assimilation, multiply-sampled units were prioritised to aid interpretation of any inter- and/or intra-unit variations identified.

On this basis, the explosive units Pumice with Andesite ('PwA'; ∼14.1 ka) and Yellow Pumice ('YP'; ∼2.15 ka) were selected for study. The prolonged event that emplaced Pumice with Andesite is interpreted to be the largest explosive eruption from modern Popocatépetl (VEI 6; e.g. Siebe et al. 1999, Espinasa-Pereña and Martin-Del Pozzo 2006, Sosa-Ceballos et al. 2012, Siebe et al. 2017). Stratigraphically, outcrops reach thicknesses of over 2 m, and the total volume of tephra produced is estimated at 5 km^3 (Siebe et al. 2017). The five PwA samples included here were all taken from a single exposure of the entire stratigraphic unit (Mangler et al. 2019). The

eruption that produced the Yellow Pumice is also estimated at VEI 6, but with a smaller total volume (~3.2 km^3) of erupted tephra (Plunket and Uruñela 2008, Panfil et al. 1999, Siebe and Macías 2006). The four samples included here were taken from four different locations (see Mangler et al. 2019).

For effusive lavas, the full geochemical range of sampled lavas derived from the Popocatépetl plumbing system is represented through inclusion of samples from both the Popocatépetl main range (San Pedro B. Juarez, n = 2; Olga, n = 2; Nealticán, n = 3) and the Chipiquixtle-YP trend (Chipiquixtle, n = 3; Atlimiyaya, n = 2; Nealticán; n = 2) as defined in Mangler et al. (2019).

5.2.2 Processing and analysis

All sample preparation and analytical procedures are as described in Chapter 2.

The cold-leaching procedure described in § 2.3.1 was performed on one digestion of the USGS reference material BCR-2, alongside all pumice samples and three effusive lavas. Both leachates and residues were analysed for Tl isotopic compositions.

Pumice samples were leached to provide greater confidence that the Tl isotopic signatures determined for residues were representative of the Tl isotopic composition of the igneous silicate phases. Although field sampling took into account freshness on the scale of hand specimens, the high porosity and permeability of pumices results in a greater surface area for a given mass of sample compared to less vesicular rocks, which in turn increases the risk of surface contamination and alteration.

One sample (POP-26) from the primitive Chipiquixtle flow was selected for leaching because initial results for the unleached powder indicated an unusual Tl isotopic composition. Leaching was performed to rule out surficial contamination as the cause. Two samples from the San Pedro B. Juarez flow (POP-90, POP-91) were processed only as paired residues and leachates. This was primarily due to time constraints such that it would not have been possible to perform additional digestions for leaching had unleached powders yielded unusual Tl isotope results.

5.3 Results

The Aldrich Tl solution in-house secondary standard was measured 21 times alongside Popocatépetl samples, yielding ε^{205}Tl = -0.8 ± 0.5 (2sd; Fig. 5.9), in excellent agreement with the long-term average (see Chapter 2, Brett et al. 2018, Nielsen et al. 2017b; note that this represents a subset of the Aldrich Tl measurements reported in Chapter 2, drawn only from analytical sessions in which Popocatépetl samples were analysed). For the USGS reference material BCR-2, measured repeatedly alongside unknown samples, a result of ε^{205}Tl = -2.5 ± 0.5 (2sd, n = 5) was obtained, which is also in excellent agreement with consensus values (ε^{205}Tl = -2.4 ± 0.2, 2sd; Brett et al. 2018).

Thallium isotope ratio results obtained during this study are given in Table 5.2, along with key analytical and geochemical data. As the majority of determinations were on single dissolutions, the quoted uncertainties are whichever is higher of (i) the long-term uncertainty in measurements of the Aldrich Tl standard, or (ii) multiple measurements of the same digestion.

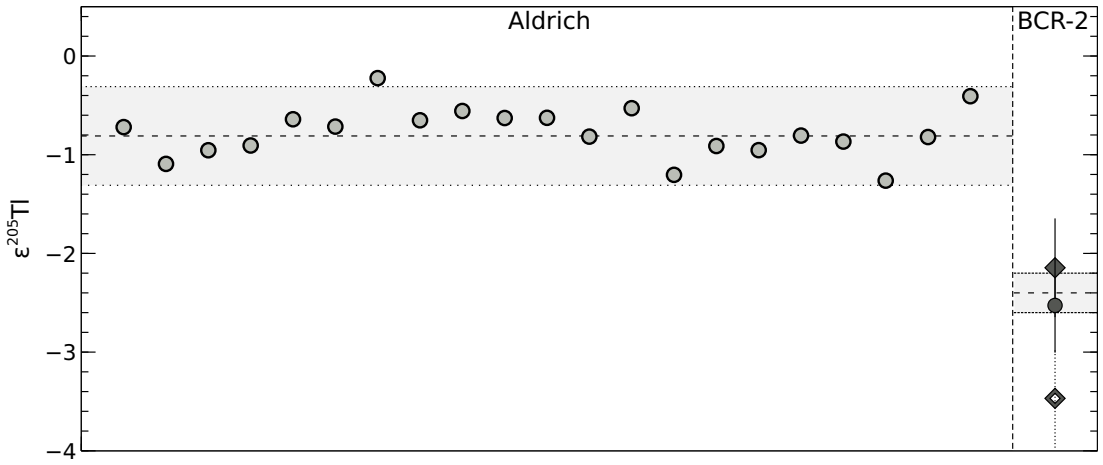


Figure 5.9: Thallium isotope ratios determined for the 'Aldrich' Tl solution standard and BCR-2 (unleached: filled circle; leached residue: filled diamond; leachate: hollow diamond) alongside this study. For the Aldrich Tl solution, the average value with 2sd is shown as a grey bar. For BCR-2, the recommended value is shown as a grey bar. Note that the data in this figure is a subset of that presented in Chapter 2, including only determinations made in the same analytical sessions as samples from Popocatépetl.

Overall, ε^{205}Tl determined for these 23 samples is strikingly homogeneous. Excluding one Chipiquixtle sample, the unleached digestions and leached residues yield ε^{205}Tl = -2.7 ± 1.1 (2sd). This average is similar to the range for both MORB and bulk continental crust of ε^{205}Tl = -2 ± 1 (Nielsen et al. 2017b). Chipiquixtle sample POP-26 has the lowest Tl concentration and is resolvably isotopically heavy, with ε^{205}Tl = +1.5 ± 0.5 (2sd).

The results of leaching tests are also presented in Table 5.2. For effusive San Pedro samples, ε^{205}Tl for leachates is within uncertainty of the values determined for residues. For the Chipiquixtle sample POP-26, the leached residue is isotopically heavy. Similarly, for YP samples, most leachates are slightly isotopically heavy compared to their residues and the Popocatépetl average. For PwA samples, however, leachates are consistently resolvably isotopically lighter than the corresponding residues.

Estimates of Tl concentrations, obtained by MC-ICP-MS during Tl isotope measurements (§ 2.3.5), provide a qualitative sense of the relative amounts of Tl in residue and leachate. The proportion of Tl found in the leachate was generally higher for pumice than lava samples (Table 5.3).

5.4 Discussion

5.4.1 Isotopic composition of Popocatépetl lavas

The Tl isotopic composition of all analysed samples is shown in Figure 5.10. The average isotopic composition of all lavas analysed at Popocetépetl (as unleached rocks or residues) is -2.2 ± 3.0 (2sd, n = 10), or -2.7 ± 1.6 (2sd, n = 9) excluding Chipiquixtle sample POP-26. These values overlap with the compositions inferred for both the mantle and continental crust, and show relatively little variation compared to other arcs (Table 5.1).

Previous work on oceanic arc lavas has demonstrated that the Tl isotopic heterogeneity can be related to variability in slab inputs to the arc system. For example, in the Mariana arc, both the sediment outboard of the trench and the analysed arc lavas exhibit limited variation in ε^{205}Tl, with

Table 5.2: Key geochemical data and results of Tl isotope analyses for Popocatépetl samples. PwA = Pumice with Andesite; YP = Yellow Pumice. * Tl and Ce concentrations were reported for unleached whole rock by Mangler et al. (2019).

Unit	Sample	Type	Tl (µg/g)*	Ce/Tl*	ϵ^{205}Tl	2sd	dissolutions	sessions	analyses
	BCR-2		-	-	−2.5	0.5	1	2	5
	BCR-2	residue	-	-	−2.2	0.5	1	1	1
	BCR-2	leachate	-	-	−3.5	0.5	1	1	1
	BCR-2	recommended (Brett et al. 2018)	-	-	−2.4	0.2	-	-	-
San Pedro	POP-90	residue	0.305	114	−3.0	0.5	1	1	2
		leachate	-	-	−3.3	0.5	1	1	1
	POP-91	residue	0.336	100	−3.1	0.5	1	1	2
		leachate	-	-	−2.7	0.5	1	1	1
Chipiquixtle	POP-25		0.551	61	−3.0	0.6	1	2	4
	POP-26		0.172	181	1.5	0.5	1	1	2
		residue	-	-	0.4	0.5	1	1	2
		leachate	-	-	−0.7	0.5	1	1	1
	POP-95		0.252	113	−0.6	0.5	1	1	2
PwA	POP-01	residue	0.401	124	−2.3	1.2	1	1	3
		leachate	-	-	−3.7	1.0	1	1	2
	POP-02	residue	0.422	125	−3.3	0.5	1	1	2
		leachate	-	-	−4.4	0.5	1	1	2
	POP-03	residue	0.404	120	−3.0	0.5	1	1	2
		leachate	-	-	−5.4	0.5	1	1	3
	POP-05-G	residue	0.368	115	−2.4	0.5	1	1	2
		leachate	-	-	−4.6	0.8	1	1	2
	POP-06-D	residue	0.374	104	−2.5	1.3	1	1	4
		leachate	-	-	−5.5	0.5	1	1	1
Atlimiyaya	POP-84		0.290	95	−2.7	0.5	1	1	2
	POP-85		0.289	90	−3.0	0.6	1	2	3
Olga	POP-115		0.389	93	−2.9	0.5	1	2	2
	POP-116		0.388	93	−2.6	0.6	1	3	4
YP	POP-63 pm	residue	0.391	93	−2.5	0.5	1	1	2
		leachate	-	-	−3.9	0.5	1	1	2
	POP-98	residue	0.363	89	−2.9	0.5	1	1	2
		leachate	-	-	−2.0	0.5	1	1	2
	POP-104	residue	0.372	84	−3.1	0.5	1	2	3
		leachate	-	-	−1.5	0.5	1	1	2
	POP-113	residue	0.355	93	−2.3	0.5	2	2	4
		leachate	-	-	−1.1	0.5	2	2	4
Nealticán	POP-11		0.345	117	−2.6	0.6	1	1	3
	POP-80		0.381	114	−2.9	0.6	1	2	2
	POP-97		0.349	111	−2.9	0.6	1	2	3
	POP-99		0.364	108	−3.0	0.5	1	2	2
	POP-101		0.396	96	−2.7	0.5	1	2	2

Table 5.3: Concentration estimates determined for leachates and residues during Tl isotope analysis by MC-ICP-MS. Note that concentration estimates were only obtained for one of two leachate-residue pairs of POP-113.

Sample name	Source/Unit	Digestion #	Tl in residue (total, ng/g)	Tl in leachate(total, ng/g)	Tl in leachate %
BCR-2	USGS	305/306	16	3	18
POP-90	San Pedro	307/308	21	5	18
POP-91	San Pedro	309/310	26	3	10
POP-26	Chipiquixtle	311/312	11	5	31
POP-63 pm	Yellow Pumice	283/284	40	12	23
POP-98	Yellow Pumice	285/286	34	9	21
POP-104	Yellow Pumice	287/288	30	13	31
POP-113	Yellow Pumice	313/314	19	8	30
POP-01	Pumice with Andesite	293/294	25	14	35
POP-02	Pumice with Andesite	295/296	34	12	26
POP-03	Pumice with Andesite	297/298	24	10	30
POP-05-G	Pumice with Andesite	299/300	27	8	23
POP-06-D	Pumice with Andesite	301/302	25	5	16

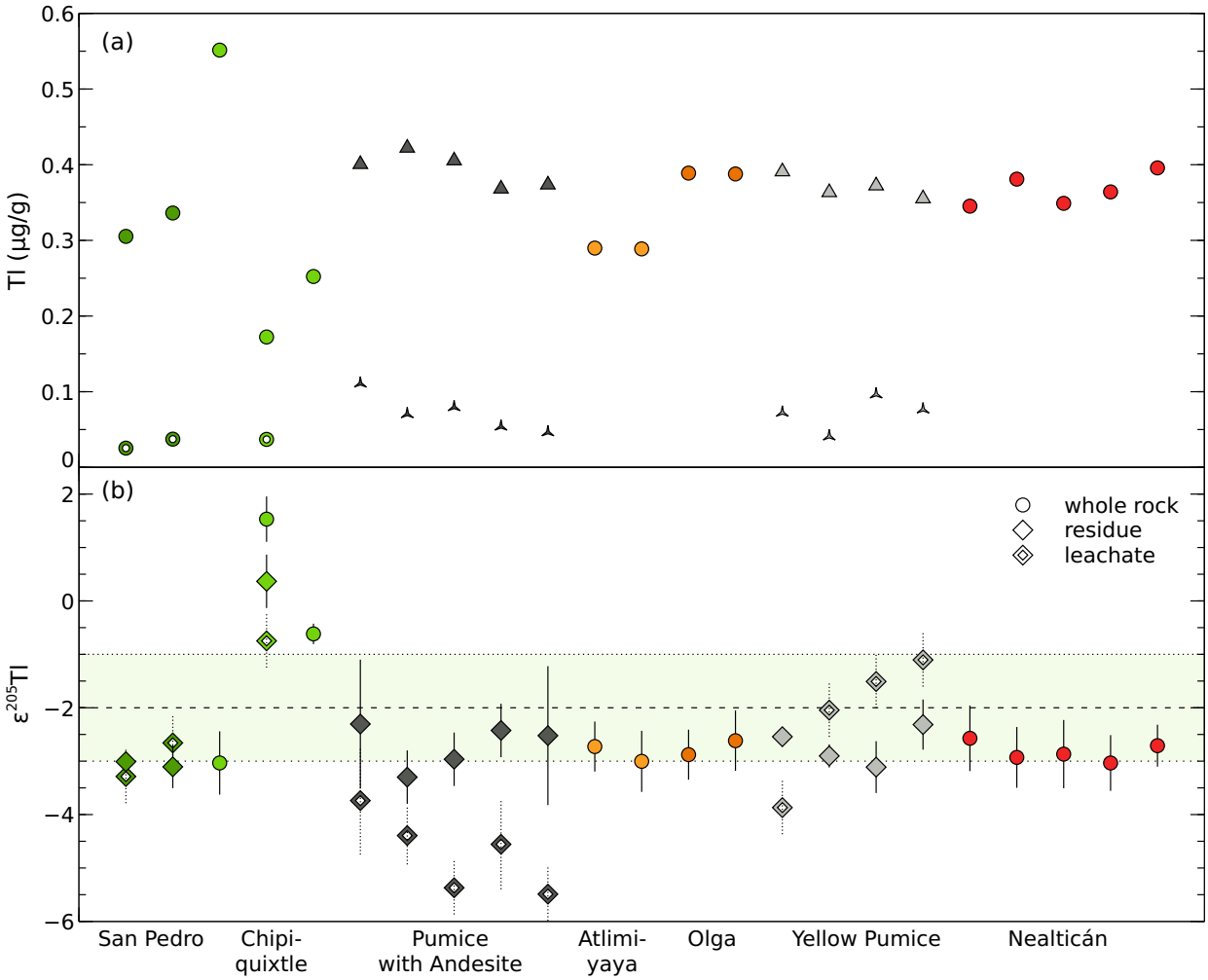


Figure 5.10: (a) Concentration data for selected Popocatépetl samples, from Mangler et al. (2019), except leachates (hollow symbols), for which concentrations were estimated during MC-ICP-MS Tl isotope ratio analysis. For these analyses, errors are uncertain but very large. (b) Thallium isotope ratio determinations for whole rock, residue, and leachate samples, obtained during this study. Units are shown in stratigraphic order. Error bars show 2sd uncertainty.

all values close to the inferred mantle composition (Prytulak et al. 2013). In contrast, changing Tl isotopic composition of sediments along the strike of the Aleutian arc is directly reflected in the erupted lavas (Nielsen et al. 2017a). Therefore, the restricted range in Tl isotopic compositions at Popocatépetl is due to either (i) homogeneous inputs, similar to the Mariana arc, or (ii) homogenisation of heterogeneous isotopic inputs via crustal processes, including assimilation and/or melt mixing between and within crustal reservoirs.

Unfortunately, Tl isotope data for sedimentary inputs to the Middle American Subduction Zone in the vicinity of Popocatépetl are not currently available. However, lithological and concentration data are available for drill cores obtained during DSDP Leg 66, off the coast of Acapulco (Fig. 5.5). Drill core from Site 487 of Leg 66 includes the complete sedimentary column just outboard of the trench, consisting of 100 m of terrigenous (termed “hemipelagic”) sediment above 70 m of pelagic sediment (Leggett 1981, Watkins et al. 1981). The hemipelagic layer is composed mostly of quartz, feldspar and mica crystals; the pelagic layer is red, reddish brown and dark brown clay, reflecting marked enrichments in Fe and Mn (Schumann and Nagel 1981, Leggett 1981).

LaGatta (2003) performed trace element analyses including Tl on 13 splits of DSDP core from Site 487. The Tl results obtained by LaGatta (2003) for USGS reference materials BHVO-1 and

Table 5.4: Reported and recommended Tl concentrations (µg/g) for reference materials used by LaGatta (2003). Uncertainties are quoted as RSD.

RM	LaGatta (2003)	GeoReM (Jochum et al. 2005)	Brett et al. (2018)	Braukmüller et al. (2020)
BHVO-1	0.05 ± 13.2%	0.0461 ± 4.3%	0.045 ± 18%	0.0424 ± 2.7%
BCR-1	0.325 ± 13.2%	0.34 ± 12%	0.28 ± 20%	-
MAR	0.018 ± 13.2%	-	-	-
JB-2	0.04 ± 13.2%	0.034 ± 5.4%	-	0.03523 ± 1.1%
TP10C	0.023 ± 13.2%	-	-	-
IOBC	3.10 ± 13.2%	-	-	-

BCR-1, as well as GSJ JB-2, are in reasonable agreement with recommended values (Table 5.4). As expected, given their lithology, both sediment layers are enriched in Tl, with LaGatta (2003) reporting average Tl concentrations of 1.74 µg/g and 1.90 µg/g for the hemipelagic and pelagic layers, respectively. Following Plank and Langmuir (1998), LaGatta calculated that the average Tl concentration in bulk sediment as sampled at Site 487 is 1.80 µg/g. LaGatta (2003) interpreted trace element and radiogenic lead isotope systematics of lavas from the Mexican Volcanic Belt as evidence for contribution of subducting sediments to their source. Therefore, it is likely that sediments supply significant Tl to the sub-arc mantle wedge beneath Popocatépetl.

It is likely that the hemipelagic layer, of terrigenous origin, has a Tl isotopic composition similar to the continental crust, i.e. ε^{205}Tl = -2 ± 1. In contrast, the pelagic layer, which contains significant FeMn sediment, probably formed in association with (relatively low-T) hydrothermal circulation along the East Pacific Rise (LaGatta 2003). Most sediments of this type carry an isotopically heavy Tl signature that is distinct from the mantle (e.g. results for sediments from DSDP Sites 294 and 295, reported by Shu et al. 2017; pelagic clays, Rehkämper and Nielsen 2004). However, the possibility that the pelagic sediment layer either has a Tl isotopic composition that is indistinguishable from the inferred mantle or has inherited an isotopically light signature (ε^{205}Tl as low as about -5) from seawater cannot be excluded (see Rehkämper et al. 2002).

In the absence of Tl isotope data for subducting sediments at Popocatépetl, it is not possible to either conclusively identify or rule out sediment contributions on the basis of Tl systematics of Popocatépetl lavas. It is, however, possible to speculate. In particular, it is unlikely that sediments being subducted beneath Popocatépetl carry an isotopically homogeneous, mantle-like Tl signature. Even at single drilling locations, isotopic diversity is the norm in sediments from other arcs (Fig. 5.4). At localities investigated so far, heterogeneity in subducting sediments is reflected in heterogeneity of arc lavas (where data is available; Fig. 5.3). The limited isotopic range in Popocatépetl lavas is therefore surprising, in that heterogeneous inputs are expected to result in heterogeneous outputs.

In fact, it is notable that the majority of the ε^{205}Tl variation at Popocatépetl is observed in the comparatively primitive Chipiquixtle flank eruption, which shows significant intra-flow isotopic variability. Chipiquixtle lavas are interpreted to have bypassed the main plumbing system and, as a result, experienced less crustal processing and homogenisation (Mangler et al. 2019).

Three different parts of the same flow were sampled from the same location (POP-25, POP-26 and POP-95; Table 5.5), with resulting Tl isotopic compositions that span the total range observed for Popocatépetl lavas. Sample POP-26, with 172 ng/g Tl, has the lowest Tl concentration of all

Table 5.5: Key geochemical and petrographic data for the three samples taken from the Chipiquixtle flow. All data from Mangler (2018) and Mangler et al. (2019), except ε^{205}Tl (this study).

Parameter	POP-25	POP-26	POP-95	Popocatépetl minimum	Popocatépetl maximum
SiO_2 (wt%)	57.42	57.53	56.93	54.96	65.44
MgO (wt%)	7.09	7.14	7.46	2.66	7.46
Ce (µg/g)	33.5	31.2	28.4	26.1	52.7
Pb (µg/g)	8.9	7.8	6.0		
Tl (µg/g)	0.551	0.172	0.252	0.143	0.733
ε^{205}Tl ± 2sd	-3.0 ± 0.6	1.53 ± 0.5 (residue 0.4 ± 0.5)	-0.6 ± 0.5		
Crystallinity (vol%)	90	98	97		
Vesicularity (vol%)	60	15	5		
Groundmass (vol%)	25	65	60		
Phenocrysts (vol%)	15	20	15		
as glomerocrysts (relative %)	<5	1	1		
Phenocryst assemblage (relative %)	pl (55) cpx (15) ol (15) opx (9) ox (1)	pl (60) ol (17) cpx (15) opx (7) ox (1)	pl (60) cpx (17) ol (12) opx (10) ox (1)		
Groundmass texture	microcrystalline/ cryptocrystalline	microcrystalline	microcrystalline		
Groundmass assemblage (relative %)	pl (85) px (15) ox (<1)	pl (84) px (15) ox (1)	pl (80) px (19) ox (1)		

samples derived from the modern Popocatépetl edifice (i.e. excluding Ventorillo-derived lavas), and heavy ε^{205}Tl = +1.5 ± 0.5 (2sd). Leached residue and leachate yielded ε^{205}Tl of +0.4 ± 0.5 (2sd) and -0.7 ± 0.5 (2sd) respectively, suggesting that the heavy isotopic signature cannot be straightforwardly explained by post-depositional alteration or surface contamination. Sample POP-95 (Tl = 252 ng/g, ε^{205}Tl = -0.6 ± 0.5 2sd) is also isotopically heavy relative to the average composition of Popocatépetl lavas (ε^{205}Tl = -2.7 ± 1.6 2sd). In contrast, POP-25 (Tl = 551 ng/g, ε^{205}Tl = -3.0 ± 0.6 2sd) has the highest Tl concentration observed for all PVC samples (with the exception of two recent pyroclastic pumices), and is isotopically indistinguishable from average Popocatépetl ε^{205}Tl.

Although only three samples are available, the apparently systematic variations of ε^{205}Tl with Tl in the Chipiquixtle lava flow (Fig. 5.11a) invite speculation, particularly because the Chipiquixtle flow samples span the majority of the Tl concentration and isotope ranges observed for the modern Popocatépetl edifice (Fig. 5.12). A similar trend is also apparent in Tl-Ce/Tl space (Fig. 5.11b), extending toward the skarn xenolith POP-97sk.

Interpretation of this apparent trend can be supported with simple mathematical models of geochemical processes. It is, of course, important to consider mixing processes. Thallium's high volatility in volcanic contexts means that the role of degassing must also be assessed, particularly as the Chipiquixtle samples trend toward isotopically heavy Tl at low Tl concentrations, i.e. exhibit the geochemical features expected of a lava that has undergone kinetic isotope fractionation during Tl loss.

Previous modelling of the geochemical characteristics of this Popocatépetl sample set used POP-95 as the most primitive end-member, as this sample has the highest MgO content in the

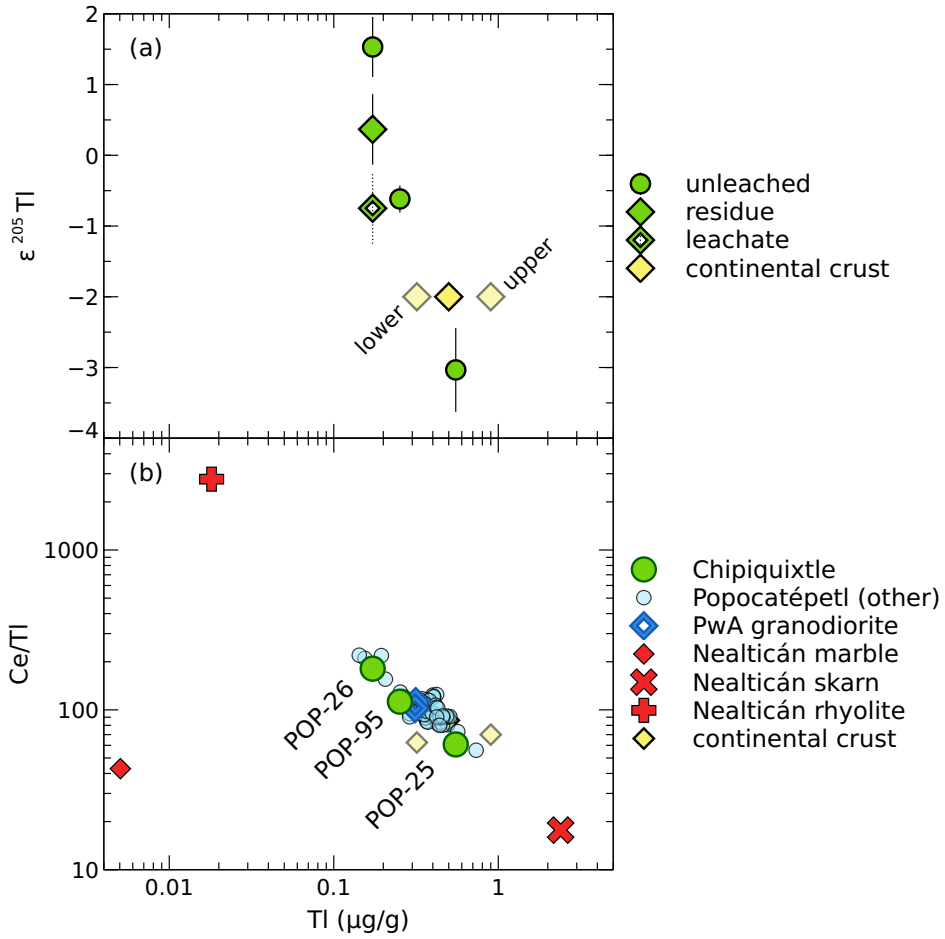


Figure 5.11: The 'Chipiquixtle trend'. (a) Thallium concentration (determined for unleached rock) versus ε^{205}Tl for samples from the relatively primitive Chipiquixtle flank eruption, showing an apparent negative trend. Mixing with estimated continental crustal compositions (Rudnick and Gao 2003, Nielsen et al. 2005) cannot explain the apparent trend. (b) Thallium versus Ce/Tl for Popocatépetl samples, including five xenoliths retrieved from the Pumice with Andesite and Nealticán units. Again, mixing with continental crust (Rudnick and Gao 2003) cannot explain the trend. Sample concentration data: Mangler et al. 2019; thallium isotope data: this work.

sample set. While POP-95 is the middle point of the three-point Chipiquixtle trend, Chipiquixtle lavas show <0.4 wt% variation in MgO content (Table 5.5). Detailed petrographic information and EMPA analyses of phenocrysts in Chipiquixtle lavas (Mangler 2018, Mangler et al. 2020) suggest that the minor variation in MgO content is likely related to minor variations in phenocryst composition and quantity within the sample, rather than reflecting significant intra-flow differentiation. It is therefore appropriate to use any of the three Chipiquixtle samples as a starting composition for the purposes of calculations exploring Tl systematics.

A role for degassing in the Chipiquixtle flow?

The Ce/Tl and Tl isotopic characteristics of Chipiquixtle samples can be used as constraints for degassing models. Assuming that the Ce concentration of a magma is not significantly affected by degassing, the Ce/Tl systematics of POP-26 are consistent with the loss of ∼32% of Tl from a starting composition equivalent to POP-95, or loss of ∼70% Tl from a starting composition equivalent to POP-25 (Fig. 5.13a,b). The potential for extreme Tl loss during degassing has been documented in both laboratory and natural settings. Nielsen et al. (2021) report experimental petrology work showing Tl losses of 60-90% through degassing, while Edmonds et al. (2018) calculated Tl emana-

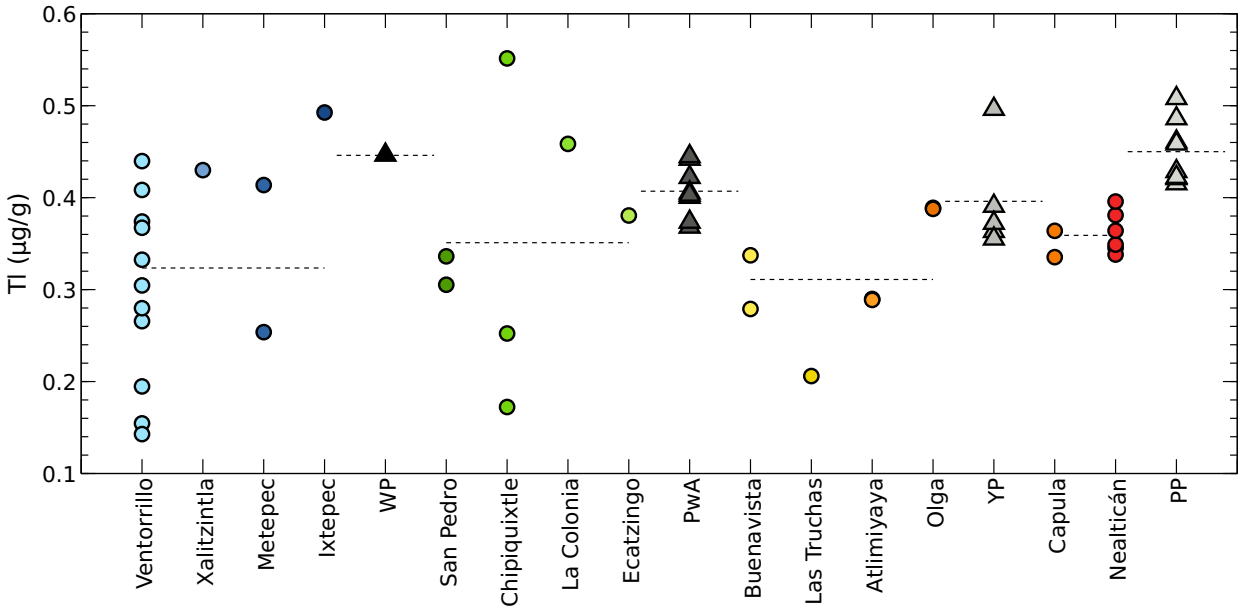


Figure 5.12: Thallium concentrations for all Popocatépetl samples as reported by Mangler et al. (2019). Averages for effusive and explosive units are shown with dotted lines. Note that these are not weighted averages, which are impossible to calculate meaningfully given sampling density and current stratigraphic knowledge. Units are listed in stratigraphic order: WP = White Pumice, PwA = Pumice with Andesite, YP = Yellow Pumice, PP = Pink Pumice.

tion factors (the percentage of the metal that has degassed from the silicate melt) for arc settings ranging from 26% to 98.5%. Therefore, degassing from a starting composition equivalent to either POP-95 or POP-25 is potentially realistic.

The kinetic isotope effects associated with degassing can be predicted using the model of open-system Rayleigh fractionation (after Baker et al. 2009). The key equation for the isotopic composition (as the ratio R = ^{205}Tl/^{203}Tl) of the accumulated vapour phase is

$$R_{vap-acc} = R_0 \frac{(1 - f_{liq}^{\frac{1}{\alpha_{liq-vap}}})}{(1 - f_{liq})}$$

where R_0 is the ^{205}Tl/^{203}Tl ratio of the initial liquid, f_{liq} is the fraction of Tl remaining in the liquid, and $\alpha_{liq-vap}$ is the isotope fractionation factor between liquid and vapour, defined as $\alpha_{liq-vap} = \frac{R_{liq}}{R_{vap}}$. For a given extent of degassing, the isotope ratio of the liquid is thus given by $R_{liq} = \alpha_{liq-vap} \times R_{vap}$. To convert between values of ε^{205}Tl and R, a $(^{205}\text{Tl}/^{203}\text{Tl})_{\text{standard}}$ value is required. Provided it is applied consistently, the value does not affect the outcome of the calculations, so can be chosen arbitrarily. The maximum value of $\alpha_{liq-vap}$ is dependent on the relative difference in atomic or molecular masses ($\alpha = \sqrt{\frac{m_1}{m_2}}$), and for gaseous Tl has a maximum theoretical value of 1.0049. In fact, the main species of Tl during volcanic degassing is likely to be TlCl (e.g. Churakov et al. 2000, Nielsen et al. 2021), for which the maximum theoretical value of α is 1.0042. Effective values of α in natural settings are expected to be lower still due to back-reactions (see discussion in Baker et al. 2009, Nielsen et al. 2021).

The Tl isotopic compositions of POP-26 leached and unleached residues are ε^{205}Tl = 0.4 ± 0.5 (2sd) and 1.5 ± 0.5 (2sd), respectively. Degassing models are shown in Figure 5.13. To reproduce the isotopic compositions observed for POP-26 with 32% Tl loss, from a starting composition

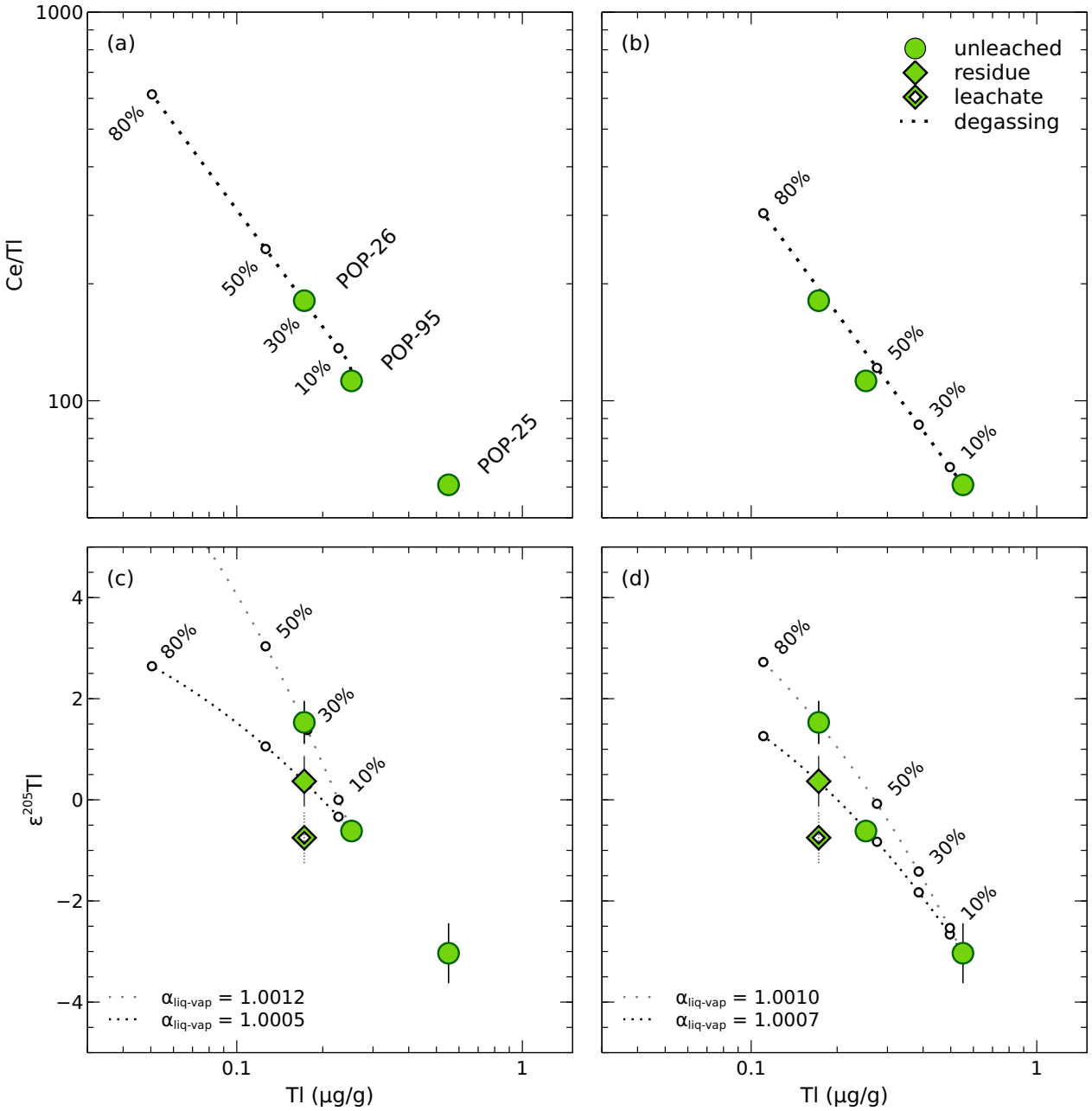


Figure 5.13: Degassing calculations can reproduce the Tl systematics of the Chipiquixtle trend. (a) and (b): thallium concentration versus Ce/Tl ratio, with starting compositions of POP-95 and POP-25, respectively. (c) and (d): thallium concentration versus ε^{205}Tl, again with respective starting compositions of POP-95 and POP-25. With a starting composition of POP-95, loss of ∼32% of Tl is required, whereas for POP-25 ∼70% Tl loss is required. Variations in the isotope fractionation factor between liquid and vapour, $\alpha_{liq-vap}$, can explain the ε^{205}Tl systematics in the Chipiquixtle trend. However, the required degree of Tl loss is not consistent with other trace element systematics (see text for details). Concentration data: Mangler et al. (2019); Tl isotope data: this work.

equivalent to POP-95, requires $\alpha_{liq-vap} \approx 1.0005$ or $\alpha_{liq-vap} \approx 1.0012$, respectively (Fig. 5.13c). To instead reproduce these isotopic compositions with 70% Tl loss, from a starting composition equivalent to POP-25, requires $\alpha_{liq-vap} \approx 1.0007$ and $\alpha_{liq-vap} \approx 1.0010$. In the former case, POP-95 represents ∼42% Tl loss via degassing, and in the latter, ∼54% (Fig. 5.13d). That is, the Tl isotope systematics of the Chipiquixtle trend imply an effective fractionation factor in the range $\alpha_{liq-vap} \approx 1.0005$ to $\alpha_{liq-vap} \approx 1.0012$.

This overlaps with $\alpha_{liq-vap} \approx 1.0008$–$1.0015$, the range inferred by Baker et al. (2009) to explain very isotopically light Tl in a particulate sample from Kīlauea (Hawai'i) and a gas condensate from Ngāuruhoe (Aotearoa-New Zealand). For Kamchatka (Russia) arc lavas, Nielsen et al. (2021) concluded that best fit is achieved with $\alpha_{liq-vap}$ in the range from 1.0003 to 1.0005, and that fractionations of this magnitude can also account for a small number of samples from other subduction zones that had been tentatively identified as affected by degassing. Therefore, the Tl systematics of the Chipiquixtle trend can be explained by Tl loss and isotope fractionation via degassing.

However, lead concentrations are not consistent with this interpretation. For the same set of arc volcanoes, Edmonds et al. (2018) calculated Pb emanation factors between 0.3% and 61%. While lead is generally recognised as less volatile than thallium in volcanic contexts (e.g. Baker et al. 2009, Mather et al. 2012, Gauthier et al. 2016), if degassing were responsible for the observed Tl depletions then Pb depletions would also be expected. Instead, although POP-25 contains 8.9 µg/g Pb, the Pb concentration of POP-26 (7.8 µg/g) is substantially higher than that of POP-95 (6.0 µg/g). Furthermore, there is no obvious reason that Chipiquixtle should be the only Popocatépetl unit to show evidence of degassing.

As such, it is unlikely that the Chipiquixtle Tl trend represents degassing. Instead, POP-26 appears to represent the most 'primitive' Tl signature observed in Popocatépetl samples, implying that the Chipiquixtle parent magma may have carried an isotopically heavy signature, perhaps reflecting contributions of a (likely heterogeneous) FeMn-bearing sediment.

Mixing relationships in the Chipiquixtle flow

In the context of a volcanic plumbing system like Popocatépetl, the obvious candidates for mixing with a magma of interest are (i) earlier volcanic rocks, and (ii) other crustal lithologies in the vicinity. In the case of the Popocatépetl Volcanic Complex, while volcanic material is likely to have relatively high Tl concentrations (the average for PVC samples is ∼0.4 µg/g), the remarkable consistency of Tl isotopic compositions in samples from the modern edifice suggests that such material is unlikely to significantly affect the Tl budgets of ascending magmas.

Table 5.6: Key data for xenoliths sampled from the Pumice with Andesite and Nealticán units. Data from Mangler et al. (2019).

Unit	Pumice with Andesite		Nealticán		
Sample	POP-61gd	POP-69gr	POP-97m2	POP-97sk	POP97sst
Lithology	granodiorite	granodiorite	marble	skarn	rhyolite
Ce (µg/g)	35.3	31.9	0.2	42.4	50.2
Tl (µg/g)	0.31	0.31	0.01	2.39	0.02
Ce/Tl	112	102	43	18	2775

Crustal lithologies in the vicinity of Popocatépetl include volcaniclastic and terrigeneous material (e.g. Espinasa-Pereña and Martin-Del Pozzo 2006) overlying Mesozoic marine sedimentary rocks (limestones, sandstones, shales, and evaporites; Fries 1965, Espinasa-Pereña and Martin-Del Pozzo 2006); and Precambrian and Palaeozoic terranes (Ortega-Gutierrez et al. 1995, Ferrari et al. 2002). Xenoliths representing crustal material, consisting mainly of granodiorite, rhyolite, skarn, and marble, are present in abundance in multiple Popocatépetl units, particularly the explosive Pumice with Andesite (PwA) unit (Sosa-Ceballos et al. 2012). Such xenoliths were sampled by Mangler et al. (2019) from the PwA (granodiorite; $n = 2$) and from the Nealticán lava flow (rhyolite, skarn, and marble; $n = 3$). Thallium concentrations reported by Mangler et al. (2019), along with other geochemical data, are shown in Table 5.6.

While Tl isotope ratios are not available for these xenolith samples, their elemental characteristics allow modelling of possible mixing or assimilation between a Chipiquixtle parent magma and crustal rocks. Two xenoliths, the marble POP-97m2 and the rhyolite POP-97sst, have much lower Tl concentrations than all Popocatépetl lava samples. The low Tl concentration reported for the marble is consistent with low Tl concentrations in carbonate sediments (e.g. Nielsen et al. 2017a). The low Tl concentration of the rhyolite xenolith, however, is surprising, as rhyolites contain K-bearing minerals that have been observed to exhibit very high Tl abundances (e.g. sanidine, with Tl concentrations up to 0.29 µg/g reported, and biotite, with up to 14 µg/g Tl; Rader et al. 2018). The two granodiorites overlap with Popocatépetl lava samples in terms of Tl contents and Ce/Tl, consistent with other documented chemical similarities between such xenoliths and PVC andesites and dacites, which have been interpreted as reflecting comagmatic origins, for example by formation at cool magma chamber margins (Mangler et al. 2019, Schaaf et al. 2005).

In contrast, the skarn POP-97sk has an extremely elevated Tl concentration of 2.39 µg/g, which is well in excess of average continental crust (Tl ≈ 0.5 µg/g; Rudnick and Gao 2003). A general description of skarns found as xenoliths in Popocatépetl products is given by Schaaf et al. (2005), who describe a mineral assemblage dominantly comprising epidote, actinolite, diopside, sphene, magnetite, and sulphate minerals, with occasional minor garnet, wollastonite and idocrase. Mangler (2018) describes the skarn sample POP-97sk as containing garnet, plagioclase and diopside identifiable in hand specimen. Of the minerals identified in skarn samples, only sulphates might host significant Tl (see crystal chemistry arguments discussed in Chapter 4; Rader et al. 2018). Schaaf et al. (2005) also note that skarn xenoliths are porous, with “abundant cavities lined by vapour-phase minerals”. BSE images of POP-97sk appear to show cavities with ingrowth of crystals with acicular habit (Fig. 5.14, Mangler, pers. comm.). High concentrations of Tl (up to several 1000 µg/g) in minerals deposited from fumarolic vapours have been reported from Lascar Volcano, Chile (Sainlot et al. 2020); Vulcano, Italy (Roberts et al. 2006, Campostrini et al. 2008, Demartin et al. 2009); Avacha volcano, Russia (Okrugin et al. 2017); and Tolbachik volcano, Russia (Siidra et al. 2014b,a,c, Pekov et al. 2015). These observations suggest that the unusual high Tl concentration recorded for the skarn could also have developed as a result of mineral deposition from a degassing Tl-enriched vapour phase.

As previously noted, in Tl—Ce/Tl space the Chipiquixtle trend apparently extends toward the skarn xenolith POP-97. Simple bulk mixing calculations indicate that, given a starting composition identical to POP-26, incorporation of ∼3.5% skarn material would result in a Tl—Ce/Tl composition

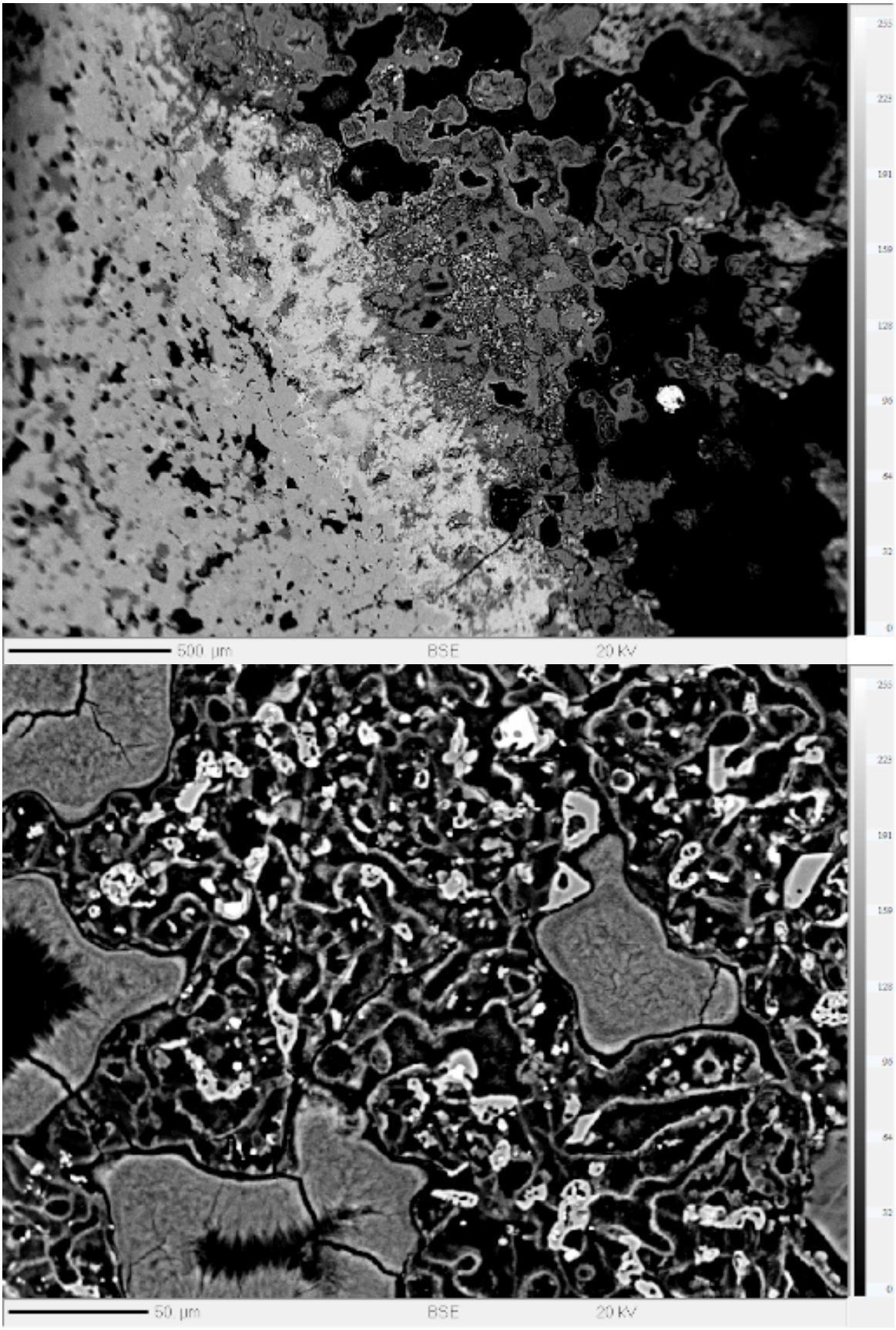


Figure 5.14: BSE images of the skarn xenolith POP-97sk. Top: general view of sample. Bottom: close-up on vugs, with ingrowth of acicular minerals visible. Source: Mangler, pers. comm.

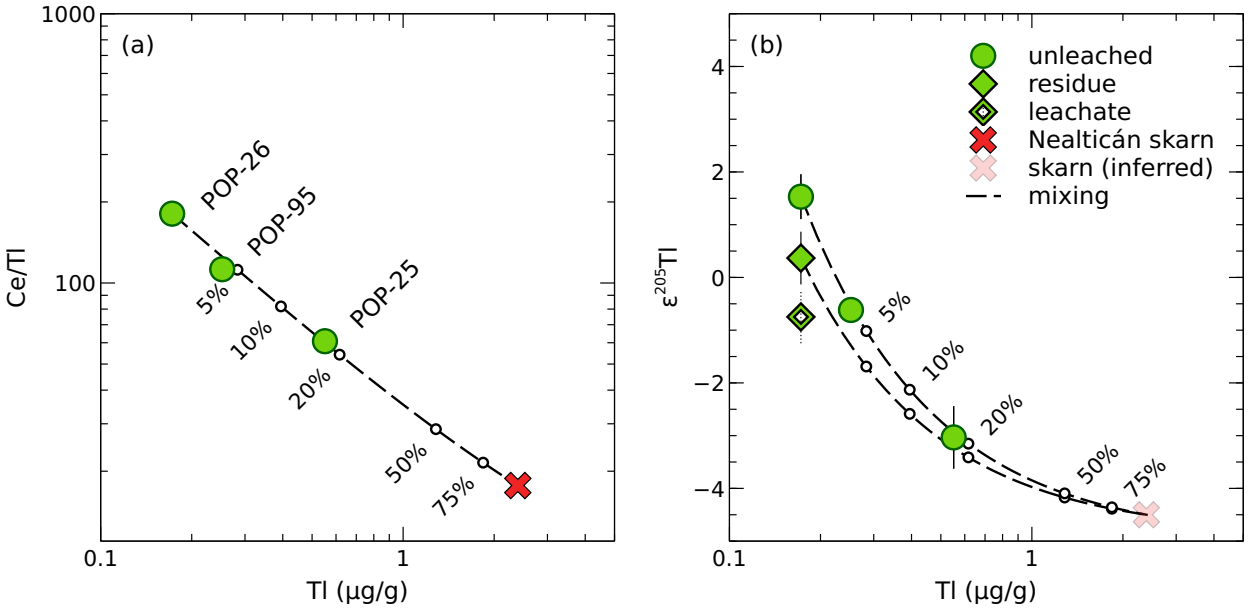


Figure 5.15: Mixing between POP-26 and the skarn POP-97sk can reproduce the Chipiquixtle trend for both (a) Tl elemental and (b) Tl isotope systematics, with the latter requiring ε^{205}Tl ≈ -4.5 for the skarn proposed as an additive. However, addition of 17% of skarn material to a Chipiquixtle parent composition is not consistent with modelling of other trace element and radiogenic isotope systematics. It is likely that the additive instead consists of minerals with a high Tl concentration, and isotopically light Tl composition, remobilised from the skarn (see text for details).

similar to that of POP-95. To reach the composition of POP-25, ∼17% incorporation of skarn would be required (Fig. 5.15). To reproduce the trend in isotope space, given these constraints on the amount of incorporated material, the skarn would be required to have ε^{205}Tl ≈ -4.5.

The ε^{205}Tl value required for the skarn is distinctly lighter than both the inferred average for continental crust (of ε^{205}Tl = -2 ± 0.5) and the average ε^{205}Tl observed for Popocatépetl (ε^{205}Tl = -2.7 ± 1.6 2sd). Conceptually, it is likely that degassed vapours carry an isotopically light Tl signature developed as a result of kinetic isotope fractionation during evaporation, which might then be inherited by Tl-rich minerals deposited from such vapour. Indeed, further isotope fractionation could plausibly occur during vapour condensation, as noted by Baker et al. (2009), which also tends to concentrate the light isotope in the solid phase.

However, the skarn xenolith was used by Mangler et al. (2019), along with the rhyolite xenolith POP-97sst, to represent the local upper crust for the purpose of assimilation and fractional crystallisation (AFC) calculations. Concentration and radiogenic isotope systematics in Popocatépetl samples permit only very limited assimilation (ratio of assimilation to crystal fractionation r = 0.05) of upper crustal material. Although no constraints on the composition of the lower crust beneath Popocatépetl are available, Mangler et al. (2019) used a central Mexican granulite reported by Schaaf et al. (1994), for which no Tl concentration is available, to estimate a likely lower crustal composition. Their calculations show that markedly higher assimilation rates (up to r = 0.30) are permissible for this estimated lower crustal composition. However, in both scenarios chemical systematics (including major elements, trace element ratios, and radiogenic isotope ratios) emphasise that Chipiquixtle samples show minimal variation compared to the whole Popocatépetl range.

It is important to point out the discrepancy between the incorporation of ∼17% 'skarn material' that is required to reproduce Tl systematics, and the extremely limited assimilation of skarn

permitted by AFC modelling focussed on other geochemical systems. On the face of it, the two requirements are mutually incompatible, and this requires explanation. One possibility is that the Chipiquixtle trend represents incorporation not of the skarn itself but instead of the vapour-deposit (and/or sulphate) minerals from the skarn, which are potentially more readily mobilised and reincorporated/assimilated than the skarn itself. Such minerals are not likely to contain significant MgO, REE, and/or important radiogenic isotopes. Furthermore, a material with ε^{205}Tl $\approx$ -4.5 and a Tl concentration of $\sim$100 µg/g (<10% of values documented by Sainlot et al. 2020 and others; see above) could shift the Tl characteristics of POP-26 to those of POP-25 through addition of <0.5%. Another possibility, which is not mutually exclusive, is transfer of Tl from a similar vapour directly to a melt through which it was percolating, perhaps due to variations in solubility due to changing temperature, pressure, and composition regimes.

Importantly, either of these scenarios also provides a potential explanation for the fact that the Popocatépetl average Tl isotope composition is lighter than that of average continental crust, despite Popocatépetl's products' otherwise striking geochemical similarity to average continental crust (Fig. 5.8). Magmas that were resident in the crust for a longer period would have more opportunity to incorporate readily-mobilised vapour-deposited minerals and/or vapour fluxing from magmas stalled at greater depth, which might then result in the uniform, slightly isotopically light Tl signature observed in Popocatepétl samples.

5.4.2 Elemental and isotopic composition of Popocatépetl pumices

Elemental enrichment of Tl in pumices

An extensive geochemical dataset including high precision Tl determinations of both pre-modern interplinian activity and Plinian activity at Popocatépetl was recently made available (Mangler 2018, Mangler et al. 2019). The data set makes it possible to investigate whether Tl isotopic differences can be related to eruptive processes during explosive Plinian activity versus effusive lava production. Notably, explosive products have higher Tl concentrations than lavas (Figures 5.8, 5.12). Despite the marked incompatibility of Tl, which generally results in higher concentrations in more evolved melts, this geochemical feature is independent of melt evolution (Fig. 5.16).

The significance of these differences can be assessed statistically. Using unpaired two-tailed Student's *t*-tests, the difference in Tl concentration between lavas and pumices is statistically significant at a level of $p \ll 0.01$, regardless of whether the analysis considers the whole PVC sample set reported by Mangler et al. (2019), or only those samples from the modern Popocatépetl edifice (i.e. post-White Pumice eruption; Table 5.7). This implies that the higher average Tl concentration of pumices is a robust result that reflects a real feature of rocks at Popocatépetl, rather than arising as an artefact of sampling.

Although pumices are highly susceptible to weathering, alteration causing enrichment in Tl requires formation of secondary clays via surface weathering and breakdown of primary mineralogy and glass (e.g. Wick et al. 2020). Such alteration products are not petrographically observed in any of the chosen samples (Mangler 2018, Mangler et al. 2020). As such, the enrichment of Tl in pumices over effusive lavas cannot be readily explained via weathering processes.

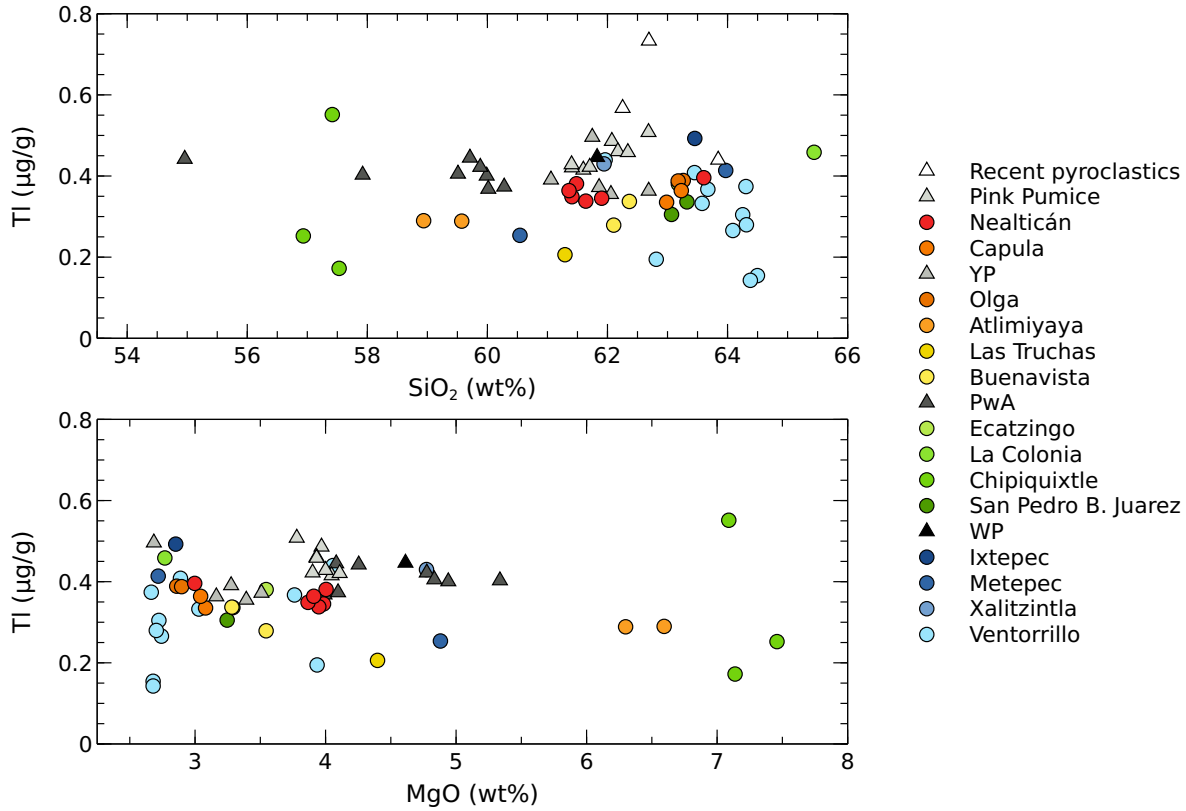


Figure 5.16: Variation of Tl with MgO and SiO_2. In general, thallium concentrations co-vary strongly with indices of differentiation (e.g. Prytulak et al. 2017). However, no such variation is apparent for Popocatépetl samples. Units are listed in stratigraphic order. WP = White Pumice, PwA = Pumice with Andesite, YP = Yellow Pumice, PP = Pink Pumice. Data from Mangler et al. (2019).

Table 5.7: Unpaired two-tailed Student's *t*-tests (see caption to Table 5.1) can be used to evaluate the statistical significance of differences between the average Tl concentration of products of effusive versus explosive eruptions. The low *p*-values indicate that the difference in Tl concentrations between lavas and pumices is a robust result.

		average Tl concentration (µg/g ± 1sd)		
Population #1 (*n*)	Population #2 (*n*)	Population #1	Population #2	*p*-value
all lavas (37)	all pumices (25)	0.33 ± 0.09	0.44 ± 0.08	0.000 01
	less Recent (22)		0.42 ± 0.04	0.000 08
modern lavas (22)	modern pumices (24)	0.34 ± 0.08	0.44 ± 0.08	0.0001
	less Recent (21)		0.42 ± 0.04	0.0002

Direct measurements of the distribution of thallium within the pumices are not available. However, leaching experiments suggest that, in very qualitative terms, leachates from pumices contains a higher proportion of total sample Tl than those from lavas (§ 5.3, Table 5.3). Vitreous glass makes up a significant modal fraction (∼20–30 vol%) of pumice groundmass, whereas the lavas are generally cryptocrystalline (Mangler 2018). Thallium is a highly incompatible element, and so is concentrated in glass where present. Glass is more susceptible to leaching than (Tl-poor) silicate mineral phases. Therefore, the higher proportion of Tl in leachates from pumices compared to lava leachates could simply reflect the larger amount of glass present in pumices.

The volatility of Tl and its comparison with Pb are relevant when contrasting the Tl content of lavas and pumices. Both are volatile elements, and similar – though smaller – Pb enrichments are also seen in Popocatépetl pumices over lavas, in contrast with the concentration patterns of similarly incompatible but less volatile elements such as Ce and La (Fig. 5.8). Indeed, Tl exhibits

greater volatility than Pb across a range of magmatic settings (e.g. Baker et al. 2009, Mather et al. 2012, Gauthier et al. 2016, Edmonds et al. 2018). Both Tl and Pb are known to be enriched in the gaseous emissions of basaltic arcs as compared with hot-spot related emissions (Edmonds et al. 2018), suggesting a possible link between the degassing of volatile elements and the enrichments found in Popocatépetl pumices.

Pumices are highly degassed, with many in the chosen sample set exhibiting vesicularity of >70% (Mangler 2018). The explosive eruptions that produce pumices are commonly associated with large volumes of outgassing, with some of the gas phase sourced from magmas that stall in the deep crust and never reach the surface (for Popocatépetl, see e.g. Delgado-Granados et al. 2001). Paisley et al. (2019) recently presented a study of Cordón Caulle volcano (Chile), which investigated the behaviour of volatile metals, including Tl, during an explosive eruption. They reported Tl enrichments in ash that adhered to the surfaces of volcanic bombs during eruption. In contrast, complementary tuffisites and breccias, representing subsurface environments from the same system, showed depletions in Tl and other volatile metals. The observed depletions of volatile metals along subsurface degassing pathways indicate that these metals were scavenged from ash shards by a fluxing gas phase throughout the subsurface. Further, they imply that the Tl enrichments observed in erupted ash are not (directly) inherited from the mantle source. Paisley et al. (2019) therefore argued that Tl enrichments in ash deposited on bomb surfaces arose as a consequence of Tl scavenging from the gas plume by ash shards at the point of eruption, during abrupt cooling and decompression but prior to quenching. The high diffusivity of Tl relative to other volatile metals (e.g. calculated diffusivity in dacite at 1260 °C of $\log(D_{Tl}) \approx -10.9$, compared with $\log(D_{Pb}) \approx -12.0$, where the diffusivity D_x has units of m^2/sec; Johnson and Canil 2011) was invoked to explain the absence of enrichments of other volatile metals (e.g. Zn and Pb) in these samples. Thallium concentrations of up to 0.6 µg/g in leachates of ash emitted by Popocatépetl have been reported (Armienta et al. 1998), with variations interpreted as indicating a volatile source. Although they did not consider thallium, Larocque et al. (2008) have reported fine-grained mineral assemblages with high concentrations of volatile metals within vesicles of Popocatépetl pumices, apparently deposited from trapped gases. It is therefore possible that Tl enrichments in Popocatépetl pumices might result from deposition, condensation, or resorption of gas-phase Tl by silicate melt upon eruption.

Existing models of degassing at Popocatépetl focus on sulphur output, and require some contribution from outgassing of magmas stalled within the crust (Delgado-Granados et al. 2001), which would also be expected to contribute Tl. However, assessing this hypothesis using trace element data is challenging. Physical separation of pumice samples into ‘surface’ and ‘interior’ materials, which might permit comparative analysis, is not straightforward. Pumice leachates would be expected to reflect the trace element signature of surficial deposits, but full trace element determinations were not performed for leachates in this study. In any case, the findings of Paisley et al. (2019) combined with Tl diffusivity data in silicates (e.g. Johnson and Canil 2011) imply that even if Tl enrichments observed in pumices originate from the gas phase, they might not be accompanied by enrichments in other volatile metals. However, Tl isotope systematics may provide further constraints on the origin of Tl enrichments in pumices.

5.4.3 Thallium isotope variations in pumices

At Popocatépetl, the restricted Tl isotopic range found in effusive lavas provides a useful background for evaluation of explosive products. The leached pumice residues from the two studied explosive eruptions, the PwA and the YP, have ε^{205}Tl = -2.7 ± 0.7 (2sd, n = 9). This range overlaps with that of Popocatépetl lavas excluding the anomalous Chipiquixtle sample (ε^{205}Tl = -2.7 ± 1.6 2sd, n = 9), consistent with the finding that the pumices and lavas are also similar in terms of major and trace element concentrations and radiogenic isotopic compositions (Mangler et al. 2019). In contrast, many pumice leachates have Tl isotopic compositions distinct from their residues, displaced to both heavy and light Tl isotopic values (Fig. 5.10).

The PwA leachates have the lowest ε^{205}Tl values in the dataset ($\sim$ -5), and PwA samples also exhibit the highest Tl and Pb contents (Fig. 5.8). The YP samples exhibit smaller ε^{205}Tl offsets between leachates and residues, and the leachates are generally isotopically heavier than the residues. The YP samples also have less pronounced enrichments in volatile metals (Figures 5.8, 5.12). With one exception, the ε^{205}Tl values of the YP leachates overlap with the range of values for typical mantle and continental crust. As (i) the cold-leaching process does not induce consistent isotope fractionation, and (ii) there is no compelling evidence for post-depositional alteration of the chosen pumices, the isotopic distinction between leachates and residues may be a primary feature. Specifically, the leachate isotopic signature may be derived from gas-phase Tl deposited on the pumices during eruption, potentially recording kinetic isotope fractionations.

A previous attempt to identify evidence for kinetic Tl isotope fractionation focussed on both gas condensates, obtained with a cold-trap system, and particulates from hot volcanic gases collected on filter disks (Baker et al. 2009). These authors found significantly more variable Tl isotope ratios in gases (ε^{205}Tl $\approx$ -6 to +5; n = 33) than observed for igneous rocks, suggesting that evaporation and condensation are capable of causing resolvable isotope fractionations. The best approximation of the average ε^{205}Tl of volcanic gases, however, is quoted by Baker et al. (2009) as -1.7 ± 3.9 (1sd), comparable to that of igneous rocks. Modelling the isotope fractionations due to degassing as open-system Rayleigh fractionation with associated kinetic isotope fractionation can explain the isotopically light signatures, with ε^{205}Tl variably concentrated in the gas phase to produce a range of isotopic compositions depending on the extent of partial re-equilibration and the principal gaseous Tl species. The process of partial condensation can also be modelled in terms of Rayleigh fractionation, which can result in the formation of condensates that are isotopically lighter than the residual gas phase.

Leachates derived from Popocatépetl pumices (n = 9) exhibit ε^{205}Tl from -5.5 ± 0.5 (2sd; POP-06-D, PwA) to -1.1 ± 0.5 (2sd; POP-113, YP). The Tl isotopic compositions of PwA leachates are comparable to light isotopic signatures reported by Baker et al. (2009) for gas particulates and condensates, attributed by those authors to evaporative processes. Although YP leachates are more similar to their residues, the isotopic signatures are still for the most part distinct, in contrast to the residue-leachate pairs of the San Pedro lavas. In combination with elevated Tl concentrations in pumices compared to lavas, the distinct Tl isotopic compositions of pumice leachates versus residues suggest that during these explosive eruptions, gas and silicate phases carried different Tl isotopic signatures. The gas-phase Tl that is subsequently incorporated into

silicate melt is thereby not sourced solely from the coexisting silicate phase. The required "excess" thallium could potentially have the same source as that invoked by Delgado-Granados et al. (2001) for "excess" S in the volcanic gas plume, namely (relatively) primitive magmas that stall deep within the crust. As these magmas cool, volatile species would continue to evaporate and ascend through the volcanic plumbing system, potentially carrying signatures altered by kinetic isotope fractionation.

Deconvolving the various processes that might produce kinetic isotope fractionation of Tl, and quantifying their relative importance, is not at all straightforward. Nevertheless, Popocatépetl pumices do appear to provide evidence for contribution of gaseous Tl that has been affected by stable isotope fractionation to the Tl 'cargo' of solid ejecta.

5.5 Conclusions

Popocatépetl effusive and explosive products are remarkably similar to bulk continental crust in terms of trace element abundances, including Tl concentrations. The majority of the thallium isotopic compositions of lavas and leached pumice residues furthermore overlap with continental crust estimates.

Although no Tl isotope data is available for relevant drill cores, we do know that sediments with high Tl concentrations and likely heterogeneous Tl isotopic signatures are being subducted beneath the relevant portion of the TMVB. Given the results of studies at oceanic arcs, incorporation of such subducted sediment into the arc source would be expected to result in isotopically heterogeneous arc lavas. In this context, the relative homogeneity of Tl isotope ratios in Popocatépetl samples suggests that processing during ascent through and storage within the continental crust plays an important role in homogenising Tl isotopic compositions. The thickness of the crust increases the opportunity for crustal assimilation. Furthermore, the magmatic plumbing system at Popocatépetl has been shown to be effective at homogenising major and trace element compositions, as reflected in the mineral and glass chemistry of the lavas and pumices (Mangler et al. 2019).

The single exception to the restricted isotopic range is the Chipiquixtle flank eruption, which is comparatively primitive and exhibits Tl isotopic compositions that vary systematically with Tl concentration within the same flow. The sample with the lowest Tl concentration has the heaviest isotopic signature, whereas the sample with the highest Tl concentration has an isotopic signature indistinguishable from other Popocatépetl lavas. The observation of a heavy isotopic signature in a primitive flank eruption might reflect the contribution of a Tl-rich, isotopically heavy sediment to the Popocatépetl source region, which is subsequently progressively overprinted by mixing with high-Tl minerals deposited from a vapour phase carrying an isotopically light Tl signature. This underlines the sensitivity of Tl systematics to crustal processes that are not identifiable in other trace element or radiogenic isotope systems.

While leached pumice residues have Tl isotopic signatures that are indistinguishable from lavas, pumices are overall enriched in Tl, and their leachates exhibit Tl isotopic signatures distinct from both pumice residues and lavas. The observation of both Tl enrichments and two distinct isotopic signatures imply that during explosive eruptions, coexisting gas and silicate phases can have dif-

ferent Tl isotopic compositions, and that the composition of the gas phase at the point of eruption can be recorded in solid products as a result of rapid resorption of Tl by silicate melt. These results highlight both the importance of leaching samples associated with explosive eruptions and the significant role that kinetic isotope fractionation associated with evaporation and condensation may play in generating Tl isotopic signatures of rocks.

Chapter 6

Outlook

6.1 Context

The context for this work has changed dramatically over the course of the project. At its beginning, in 2013, thallium isotope ratios of igneous rocks were available for five MORB samples (Nielsen et al. 2006b), a suite of picrites from Hawai'i (Nielsen et al. 2006b), lavas from Iceland and the Azores (Nielsen et al. 2007), altered oceanic crust (AOC; Nielsen et al. 2006c), eclogites from South Africa (Nielsen et al. 2009b), and lavas from the Mariana arc (Prytulak et al. 2013). In addition to work on meteorites and natural waters among others (see reviews in Nielsen and Rehkämper 2011 and Nielsen et al. 2017b), Tl isotope ratios had been reported for continental crustal materials (Nielsen et al. 2005, Baker et al. 2010a), potential subduction inputs (e.g. diagenetic pyrites, Nielsen et al. 2011; ferromanganese sediments, Rehkämper et al. 2002, 2004, Nielsen et al. 2009a), and condensates and particulates from volcanic gases (Baker et al. 2009).

As discussed throughout this work, the mantle contains low Tl concentrations of an apparently approximately uniform Tl isotopic composition (ε^{205}Tl = -2 ± 1). In contrast, FeMn sediments and AOC can exhibit high Tl concentrations, together with distinct Tl isotopic compositions. It also seemed likely that metasomatised mantle might contain both high Tl concentrations and a distinctive Tl isotope fingerprint, potentially permitting discrimination between incorporation of metasomatised and subducted materials in the history and derivation of MORB and OIB lavas. As of 2013, all analysed OIB samples were from predominantly FOZO/PREMA-type localities (Nielsen et al. 2006b, 2007). Nielsen et al. (2006b) had used the contrast between subduction inputs and ambient mantle to argue for incorporation of FeMn sediments in the source of Hawai'ian picrites, on the basis of Cs/Tl and Tl isotope ratios. Unlike Hawai'i, lavas from Iceland and the Azores exhibited Tl isotopic compositions indistinguishable from the average mantle, emphasising the need for investigation of EM- and HIMU-type lavas.

Building on the promising results of the initial Hawai'ian study, the goal of this project – as initially envisaged – was to assess the ability of Tl isotopes to disambiguate between sediment and AOC contribution to OIB sources, with the aim of clarifying the origins of the Enriched Mantle and HIMU 'mantle components'. In particular, EM- and HIMU-type lavas, which have been interpreted as representing incorporation of subducted sediment and oceanic crust respectively, were predicted to be associated with distinct Tl isotopic signatures.

My personal context is also relevant. I am disabled, and the pace of work I can sustain is much slower than is usually expected. As a result, I have had access to a larger body of newly-published work than would ordinarily be expected over the course of completing a PhD, which has been of great help with interpreting my data.

Over the past several years, additional studies in subduction zones have repeatedly observed correlated along-strike variation in Tl isotopic compositions of (i) subducting sediments, and, in their absence, AOC, and (ii) arc lavas (Aleutian arc, Nielsen et al. 2016; Central American Volcanic Arc and Tonga-Kermadec, Nielsen et al. 2017a; Ryukyu-Okinawa, Shu et al. 2017; further results for the Mariana arc, Prytulak et al. 2017), clearly demonstrating that the Tl isotopic signatures associated with these near-surface low-temperature materials could be transferred, via subduction, to the mantle.

Recognising the need for more information about HIMU-type lavas, Blusztajn et al. (2018) reported Tl isotope data for St Helena, a HIMU type locality. The authors interpreted their results as consistent with the incorporation of recycled oceanic crust in the St Helena source.

Work on metasomatised (phlogopite-bearing) glimmerite xenoliths (Fitzpayne et al. 2020) found that, despite high Tl concentrations, the Tl isotopic composition was consistently $\varepsilon^{205}Tl \approx -2$. This strongly suggests that while metasomatic processes can *concentrate* Tl, they are not associated with any Tl isotope fractionation, implying that Tl isotopes cannot be used to trace histories of metasomatism.

Most recently, Nielsen et al. (2021) reported laboratory experiments exploring potential kinetic isotope fractionation effects during degassing of Tl, and combined these results with new analyses of Tl isotope ratios in lavas from the Kamchatka Peninsula, Russia.

These additional datasets, combined with an increasing volume of well-calibrated Tl elemental data in the broader literature, enabled expansion of the scope of the project, from the initial aim of assessing the application of Tl stable isotopes in understanding the origin of 'mantle components', to investigating Tl cycling through the solid Earth via plate tectonics.

6.2 Findings

In Chapter 2, I reviewed published data for Tl igneous reference materials, including compilation and assessment of Tl concentrations for key materials. Of 17 reference materials for which I reported new Tl isotope analyses, literature $\varepsilon^{205}Tl$ values were available for only four (AGV-2, BCR-2, BHVO-2, G-2; Table 2.2). I also reported new determinations of concentrations of 34 trace elements for 16 igneous reference materials. I used these data to assess material heterogeneity in terms of thallium, and provide recommended Tl isotope ratios for this suite of materials. Overall, the reference materials span three orders of magnitude of Tl concentration (10 ng/g to 16 µg/g), six ε units of Tl isotope ratios ($\varepsilon^{205}Tl$ from -4 to +2), and – excluding one massive magmatic sulphide – SiO_2 from 3.47 wt% (USGS carbonatite COQ-1) to 69 wt% (CRPG albite AL-I and USGS granite G-2). These analyses have been published across three papers: Prytulak et al. (2017), Brett et al. (2018), and Brett et al. (2021).

In Chapter 3, I examined Tl elemental and isotope systematics in the contexts of constructive plate margins and intraplate volcanism. I compiled and filtered results from three studies to

yield a MORB dataset containing 909 samples with reported Tl concentrations (Appendix B3.vi). I presented new trace element and Tl isotope analyses of 48 OIB samples, representing both EM and HIMU localities, and integrated these results with literature data (Appendix B3.v). The combined datasets revealed that MORB, OIB and arc lavas form distinct fields in Tl–Ce/Tl space. The ability of simple melting models to reproduce the MORB and OIB trends indicates that:

(i) the MORB Ce/Tl ratio is *not* invariant, and Ce and Tl are not required to partition identically during MORB melting;

(ii) rather than being controlled by the ratio of clinopyroxene and sulphide in the upper mantle, variations in the MORB Ce/Tl ratio are controlled by a combination of melt extent and clinopyroxene composition, affecting the partitioning of Ce between residue and melt;

(iii) both MORB and OIB sources are ubiquitously more depleted in Tl than previously believed; and

(iv) the Tl isotopic compositions of OIB appears to represent some combination of the signature preserved in the small proportion of Tl residual in the slab at post-arc depths, and assimilation during magma ascent. As such, despite promising early indications, Tl stable isotopes cannot be used to unambiguously trace recycling of AOC or subducted sediment to the deep mantle.

This work has been published as Brett et al. (2021).

In Chapter 4, I proposed an approach to assessing the quality of Tl concentration data reported in the literature for which no calibration information is available, based on the Tl–Ce/Tl tectonic discriminant diagram developed in Chapter 3. Using my proposed method, I filtered data downloaded from GeoROC and combined them with literature data collated from arc-focussed Tl isotope studies (Appendices B4.i, B4.ii). Using the expanded arc database, I demonstrated that:

(i) Tl is transferred from slab to wedge so efficiently that it is not possible to identify probable host phases within the subducting slab;

(ii) revisiting the work of Noll et al. (1996) with improved data for Tl abundances in MORB, OIB and arc lavas, elemental systematics imply a significant role for non-magmatic fluids in the transfer of Tl from slab to wedge; and

(iii) within the TMVB, there is a possible sense of increasing Tl concentration with increasing (estimated) crustal thickness, suggesting gradual accumulation of Tl as continental crust matures.

In Chapter 5, I reported new Tl isotope analyses of 23 samples from Popocatépetl (México), including both pumices and effusive lavas. Against a backdrop of remarkable isotopic homogeneity in lavas and leached pumice residues, I found that:

(i) individual pumice samples record two distinct Tl isotopic signatures, inferred to be that of the melt phase and that of the gas phase at the point of eruption; and

(ii) the most primitive unit sampled to date, Chipiquixtle, appears to show a mixing trend with an exotic contribution characterised by very high Tl concentrations with an isotopically light

Tl signature, tentatively identified as skarn present in xenoliths throughout the stratigraphic sequence.

While kinetic isotope fractionation of Tl during evaporation is expected, previous work has generally assumed that this would be detectable either in the form of gas/particulate samples with unusual Tl isotopic compositions, or as rock samples with low Tl concentrations, high Ce/Tl, and isotopically heavy Tl. In that context, the pumice samples – leachates of which carry an isotopically light Tl signature – are surprising. Similarly, I infer that the skarn carries an isotopically light Tl signature inherited via mineral deposition from vapour fluxing through the crust, which can then mix with ascending magmas to produce a uniform, isotopically light Tl signature in lavas with high Tl concentrations.

6.3 Future work

Inevitably, in the course of this project, many potential avenues of future work have become apparent. These include expansion of the arc database following the filtering process described in Chapter 4, exploring the application of Tl isotope systematics to understanding the origins of 'OIB-type' versus 'arc-type' lavas in the TMVB (e.g. Ferrari et al. 2001, Petrone et al. 2003, Orozco-Esquivel et al. 2007), and further investigation of the apparent ability of pumices to record two distinct Tl isotopic signatures. Two projects in particular, however, are potentially of relevance for the wider geochemistry community.

6.3.1 'Invariant' trace element ratios

Invariant trace element ratios are commonly used to infer information about mantle source composition from erupted lavas. A constant, or approximately constant, trace element ratio common to a large sample set implies that the two elements partition similarly during melting and crystallisation processes. A qualitative sense of the relative compatibility of two elements (A and B) can be obtained from plots of log[A] and log[B], which will, if the two elements partition identically, form a line with a slope of unity across the whole range of possible degrees of melting (e.g. Sims and DePaolo 1997, Jochum et al. 1993).

Ce/Tl systematics in MORB provide an illustrative case study of potential complications with this approach. Nielsen et al. (2014) interpreted the Ce/Tl ratio of MORB samples as approximately invariant, and calculated that the line formed by plotting log[Ce] against log[Tl] has a slope of 0.999 ± 0.033 (2sd). They therefore assumed that Ce and Tl partition identically during mantle melting, despite being hosted in different mineral phases, and subsequently used the 'invariant' MORB Ce/Tl ratio to constrain the sulphide concentration of the upper mantle. However, I have demonstrated that it is also possible to reproduce the observed MORB Ce/Tl systematics with very different bulk partition coefficients for Ce and Tl when considering realistic extents of melting (§ 3.3.2, Brett et al. 2021). Importantly, while the resulting relationship between log[Ce] and log[Tl] does not have a slope of unity across the entire range of melting, significant deviations from linearity occur only at relatively low melt fractions (<3%; an example is shown in Fig. 6.1).

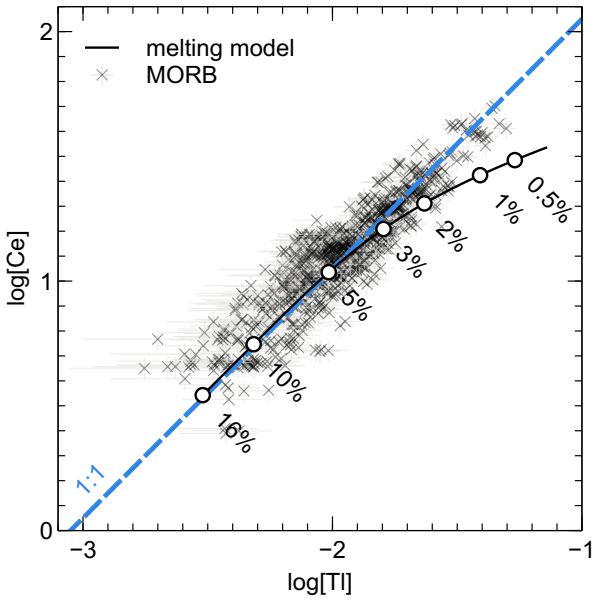


Figure 6.1: Variations in Ce and Tl in MORB (Appendix B3.vi) form a linear array with a slope approximating unity in log[Ce]-log[Tl] space. Melting models that assume different bulk partition coefficients (e.g. D^{Tl} = 0.006 and D^{Ce} = 0.015) can reproduce the observed variation (see Chapter 3 for details). The model shown above assumes melting of a peridotite with a starting composition of Tl = 0.00048 µg/g and Ce = 0.55 µg/g (preferred concentrations of Nielsen et al. 2014). Deviations from linearity only occur at low melt percentages, which are less likely to be sampled. In reality, variations in the starting composition of rocks melting to form MORB are to be expected.

It is therefore probable that MORB, which are estimated to represent ∼10–20% partial melts (e.g. Niu 1997, Kushiro 2001), exhibit Ce/Tl ratios with limited variability not because the partitioning behaviour of Ce and Tl is identical, but instead because both elements are highly incompatible (e.g. D^{Tl} = 0.006 and D^{Ce} = 0.015 for the model displayed in Fig. 6.1; see Chapter 3 for details) such that the melt fraction F is much greater than the bulk partition coefficients of the elements of interest.

While this limitation of log[*A*]–log[*B*] relationships in terms of assessing relative partitioning behaviour is well-understood in principle, it can be easily overlooked. Exploring the theoretical space to generate "information values" for parameter ranges that can replicate the systematics of elements that are believed to partition identically has the potential to facilitate interpretations of geochemical data.

6.3.2 Vapour distillation of heavy metal isotopes within thick crust

Popocatépetl samples have trace element patterns that generally closely resemble those of bulk continental crust. It is, then, surprising that the Tl isotopic signature of Popocatépetl samples is not identical to that inferred for the average continental crust. Excluding Chipiquixtle samples, Popocatépetl lavas and leached residues have ε^{205}Tl = -2.8 ± 0.6 (2sd, n = 20). The continental crust, as sampled only via loess and leached riverine detritus (Nielsen et al. 2005), has ε^{205}Tl = -2.1 ± 0.6 (2sd, n = 15). Performing an unpaired two-tailed Student's t-test indicates that these averages are distinct at a very high confidence level (p = 2.5 × 10^{-6}, i.e. there is a ≪1% chance that these populations have the same average Tl isotopic composition).

The work on Popocatépetl presented in Chapter 5 is the first Tl stable isotope study to have examined the effects of magma processing through thick continental crust. In thicker crust, longer

magma ascent times prior to eruption provide more opportunity for degassing, assimilation, fractional crystallisation, cooling, and stalling than ascent through thinner overlying crust. I propose that the isotopically light Tl signature of erupted Popocatépetl pumices and lavas is evidence that thick continental crust encourages the distillation of heavy metal isotopes through evaporation and subsequent vapour transport (shown schematically in Fig. 6.2). I suggest that magmas stalled in the lower crust are likely to develop an isotopically heavy Tl signature as a result of degassing, with the vapour phase likely to carry a relatively light Tl isotopic signature as a consequence of kinetic isotope fractionation associated with evaporative processes (Baker et al. 2009, Nielsen et al. 2021). This vapour then rises through the crust, both fluxing through (and potentially interacting with) more buoyant (and less degassed) magmas, and likely depositing Tl in cooler rock during its ascent (e.g. Sainlot et al. 2020). Such diffuse degassing at Popocatépetl has been identified in terms of the chemical and isotopic compositions of spring water, which show evidence of interaction with magmatic gases (Inguaggiato et al. 2005).

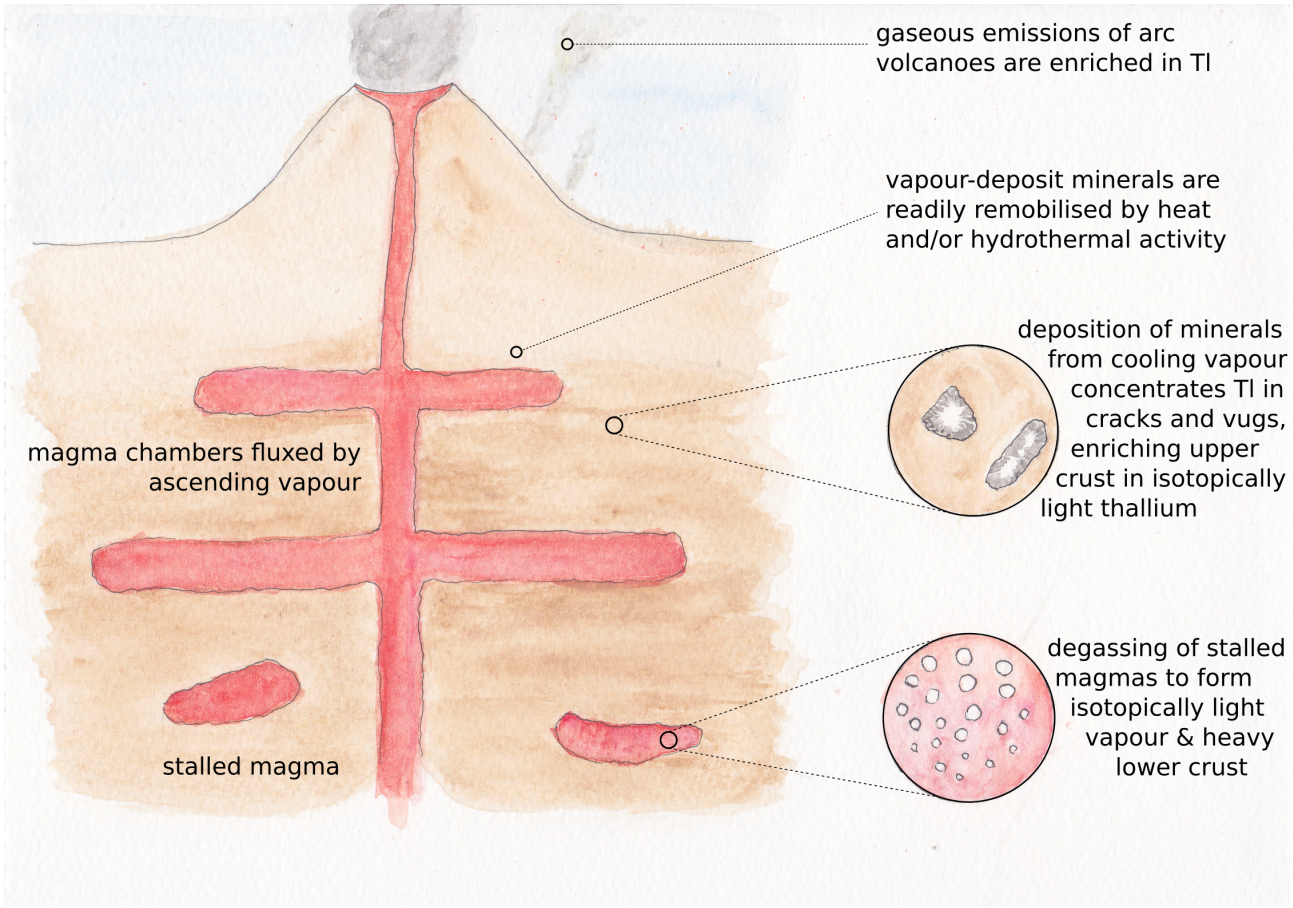


Figure 6.2: Schematic illustration of possible crustal distillation of Tl isotopes. Degassing of stalled magmas in the lower crust leaves such magmas enriched in ^{205}Tl relative to ^{203}Tl, while the escaping gas is enriched in isotopically light ^{203}Tl. The vapour ascends through both magma/mush and crustal degassing pathways (e.g. fractures/cracks). As it rises, it cools, potentially both (i) returning isotopically light Tl to more buoyant magmas that are more likely to erupt and (ii) depositing Tl-rich minerals in cracks/vugs within the crust. Such vapour-deposit minerals are likely to be readily remobilised and incorporated into magmas, dominating their Tl budgets.

Minerals formed during deposition from volcanic vapours can show extreme enrichments in Tl. Scholtysik and Canil (2018) have reported that in benchtop fumarole experiments maximum deposition of Tl on glass occurs in the temperature range 160–295 °C. Sainlot et al. (2020) reported Tl concentrations from 210 to 8800 µg/g in a natural anhydrous alum forming as fumarolic gases

(at ∼330 °C) react with rocks in the near subsurface at Lascar volcano (Chile), which is situated on crust that is an estimated 62 km thick (Farner and Lee 2017). Specific study of modern fumaroles and volcanic outgassing at Popocatépetl have found gas temperatures of ∼200 ± 20 °C (e.g. Love et al. 1998), implying that significant Tl deposition may be occurring in the upper crust as ascending vapours cool. At present the likely isotopic composition of such deposits is poorly constrained, as is any P-T dependence of isotope fractionation factors, although they are likely to inherit a relatively light Tl isotopic signature (i.e. ε^{205}Tl < -2) from their associated vapour phase. The temperature range associated with maximum Tl deposition overlaps with that in which significant (equilibrium) Tl isotope fractionation occurs during hydrothermal circulation through oceanic crust. Further kinetic isotope fractionation could also take place during condensation (e.g. Baker et al. 2009). As thallium hosted in vapour deposits is likely to be extremely readily remobilised, such deposits are likely to dominate the Tl budget of magmas.

To test this hypothesis in the context of Popocatépetl and specifically the potential mixing relationships seen in the Chipiquixtle samples, it will be necessary to re-examine the skarn sample POP-97sk (Mangler et al. 2019, § 5.4.1) to establish whether minerals likely to have been deposited from a vapour phase are present in vugs. If so, Tl isotope ratio analyses of both the whole-rock powder and separate mineral phases should help to clarify the origin of the Chipiquixtle trend.

If skarn-hosted minerals are found to exhibit high concentrations of isotopically light Tl, this would suggest the intriguing possibility that vapour-phase distillation of heavy metal isotopes can take place in nature, resulting in both concentration gradients throughout the crust (as described by e.g. Rudnick and Gao 2003, Jenner 2017) and isotopic gradients.

Such effects might also be seen in other isotope systems. Sainlot et al. (2020) reported that thallium enrichments were associated with high concentrations of tellurium, vanadium and molybdenum. The stable isotope compositions of all three elements have been investigated in geological contexts (e.g. Chen et al. 2020, Huang et al. 2015, Anbar 2004, Kendall et al. 2017). If vapour distillation of thallium can be confirmed, these other systems might reveal similar effects. Stable isotope systematics have the potential to demonstrate and perhaps assist in quantifying the importance of vapour-phase transport in the distribution of volatile heavy elements within the continental crust.

Bibliography

J. Adam and T. Green. (2006) Trace-element partitioning between mica- and amphibole-bearing garnet lherzolite and hydrous basanitic melt: 1. Experimental results and the investigation of controls on partitioning behaviour. *Contributions to Mineralogy and Petrology* **152**:1–17. doi:10.1007/s00410-006-0085-4

L. H. Ahrens. (1948) The unique association of thallium and rubidium in minerals. *The Journal of Geology* **56**:578–590. URL http://www.jstor.org/stable/30080849

R. J. Allenby. (1954) Determination of the isotopic ratios of silicon in rocks. *Geochimica et Cosmochimica Acta* **5**:40–48. doi:10.1016/0016-7037(54)90060-5

C. J. Allègre and D. Turcotte. (1985) Geodynamic mixing in the mesosphere boundary layer and the origin of oceanic islands. *Geophysical Research Letters* **12**:207–210. doi:10.1029/GL012i004p00207

A. D. Anbar. (2004) Iron stable isotopes: beyond biosignatures. *Earth and Planetary Science Letters* **217**:223–236. doi:10.1016/S0012-821X(03)00572-7

E. Anders and C. M. Stevens. (1960) Search for extinct lead 205 in meteorites. *Journal of Geophysical Research* **65**:3043–3047. doi:10.1029/JZ065i010p03043

R. Andreasen, M. Rehkämper, G. K. Benedix, K. J. Theis, M. Schönbächler and C. L. Smith. (2012) Lead-thallium chronology of IIAB and IIIAB iron meteorites and the solar system initial abundance of lead-205. *Lunar and Planetary Science Conference* p. 2902

R. Andreasen, M. Schönbächler and M. Rehkämper. (2009) The ^{205}Pb-^{205}Tl and Cd isotope systematics of ordinary chondrites. *Geochimica et Cosmochimica Acta* **73**:A43

L. Arana-Salinas, C. Siebe and J. L. Macías. (2010) Dynamics of the ca. 4965 yr ^{14}C BP “Ochre Pumice” Plinian eruption of Popocatépetl volcano, México. *Journal of Volcanology and Geothermal Research* **192**:212–231. doi:10.1016/j.jvolgeores.2010.02.022

J. L. Arce, E. Muñoz-Salinas, M. Castillo and I. Salinas. (2015) The ∼2000 yr BP Jumento volcano, one of the youngest edifices of the Chichinautzin Volcanic Field, Central Mexico. *Journal of Volcanology and Geothermal Research* **308**:30–38. doi:10.1016/j.jvolgeores.2015.10.008

J. W. Arden. (1983) Distribution of lead and thallium in the matrix of the Allende meteorite and the extent of terrestrial lead contamination in chondrites. *Earth and Planetary Science Letters* **62**:395–406. doi:10.1016/0012-821X(83)90010-9

M. A. Armienta, A. L. Martin-Del Pozzo, R. Espinasa, O. Cruz, N. Ceniceros, A. Aguayo and M. A. Butron. (1998) Geochemistry of ash leachates during the 1994–1996 activity of Popocatépetl volcano. *Applied Geochemistry* **13**:841–850. doi:10.1016/S0883-2927(98)00012-2

M. G. Babechuk and B. S. Kamber. (2011) An estimate of 1.9 Ga mantle depletion using the high field-strength elements and Nd-Pb isotopes of ocean floor basalts, Flin Flan Belt, Canada. *Precambrian Research* **189**:114–139. doi:10.1016/j.precamres.2011.05.006

M. G. Babechuk, B. S. Kamber, A. Greig, D. Canil and J. Kodolányi. (2010) The behaviour of tungsten during mantle melting revisited with implications for planetary differentiation time scales. *Geochimica et Cosmochimica Acta* **74**:1448–1470. doi:10.1016/j.gca.2009.11.018

W. Bach, J. Erzinger, J. C. Alt and D. A. H. Teagle. (1996) Chemisty of the lower sheeted dike complex, Hole 504B (Leg 148): influence of magmatic differentiation and hydrothermal alteration. *Proceedings of the Ocean Drilling Program, Scientific Results* **148**:39–55. doi:10.2973/odp.proc.sr.148.114.1996

W. Bach, B. Peucker-Ehrenbrink, S. R. Hart and J. S. Blusztajn. (2003) Geochemistry of hydrothermally altered oceanic crust: DSDP/ODP Hole 504B – implications for seawater–crust exchange budgets and Sr- and Pb-isotopic evolution of the mantle. *Geochemistry, Geophysics, Geosystems* **4**:8904. doi:10.1029/2002GC000419

J. Baker, D. Peate, T. Waight and C. Meyzen. (2004) Pb isotopic analysis of standards and samples using a ^{207}Pb–^{204}Pb double spike and thallium to correct for mass bias with a double-focusing MC-ICP-MS. *Chemical Geology* **211**:275–303. doi:10.1016/j.chemgeo.2004.06.030

M. B. Baker and E. M. Stolper. (1994) Determining the composition of high-pressure mantle melts using diamond aggregates. *Geochimica et Cosmochimica Acta* **58**:2811–2827. doi:10.1016/0016-7037(94)90116-3

R. G. A. Baker, M. Rehkämper, T. K. Hinkley, S. G. Nielsen and J. P. Toutain. (2009) Investigation of thallium fluxes from subaerial volcanism—implications for the present and past mass balance of thallium in the oceans. *Geochimica et Cosmochimica Acta* **73**:6340–6359. doi:10.1016/j.gca.2009.07.014

R. G. A. Baker, M. Rehkämper, C. Ihenfeld, C. J. Oates and R. Coggon. (2010a) Thallium isotope variations in an ore-bearing continental igneous setting: Collahusasi Formation, northern Chile. *Geochimica et Cosmochimica Acta* **73**:4405–4416. doi:10.1016/j.gca.2010.04.068

R. G. A. Baker, M. Schönbächler, M. Rehkämper and H. M. Williams. (2010b) The thallium isotope composition of carbonaceous chondrites – new evidence for live ^{205}Pb in the early solar system. *Earth and Planetary Science Letters* **291**:39–47. doi:10.1016/j.epsl.2009.12.044

B. V. Baranov, R. Werner, K. A. Hoernle, I. B. Tsoy, P. van den Bogaard and I. A. Tararin. (2002) Evidence for compressionally induced high subsidence rates in the Kurile Basin (Okhotsk Sea). *Tectonophysics* **350**:63–97. doi:10.1016/S0040-1951(02)00081-1

J. D. Barnes, M. Beltrando, C.-T. A. Lee, M. Cisneros, S. Loewy and E. Chin. (2014) Geochemistry of Alpine serpentinites from rifting to subduction: a view across paleogeographic domains and metamorphic grade. *Chemical Geology* **389**:29–47. doi:10.1016/j.chemgeo.2014.09.012

G. E. Batley and T. M. Florence. (1975) Determination of thallium in natural waters by anodic stripping voltammetry. *Journal of Electroanalytical Chemistry and Interfacial Electrochemistry* **61**:205–211. doi:10.1016/S0022-0728(75)80251-8

N. Bellot, M. Boyet, R. Doucelance, P. Bonnand, I. P. Savov, T. Plank and T. Elliott. (2018) Origin of negative cerium anomalies in subduction-related volcanic samples: constraints from Ce and Nd isotopes. *Chemical Geology* **500**:46–63. doi:10.1016/j.chemgeo.2018.09.006

B. A. Berquist and J. D. Blum. (2009) The odds and evens of mercury isotopes: applications of mass-dependent and mass-independent isotope fractionation. *Elements* **5**:353–357. doi:10.2113/gselements.5.6.353

J. Bigeleisen. (1949) The relative reaction velocities of isotopic molecules. *Journal of Chemical Physics* **17**:675–678. doi:10.1063/1.1747368

J. Bigeleisen. (1996a) Nuclear size and shape effects in chemical reactions. Isotope chemistry of the heavy elements. *Journal of the American Chemical Society* **118**:3676–3680. doi:10.1021/ja954076k

J. Bigeleisen. (1996b) Temperature dependence of the isotope chemistry of the heavy elements. *Proceedings of the National Academy of Science, USA* **93**:9393–9396. doi:10.1073/pnas.93.18.9393

J. Bigeleisen and M. G. Mayer. (1947) Calculation of equilibrium constants for isotopic exchange reactions. *Journal of Chemical Physics* **15**:261–267. doi:10.1063/1.1746492

BIPM, IEC, IFCC, ILAC, IUPAC, IUPAP, ISO and OIML. (2012) The international vocabulary of metrology–basic and general concepts and associated terms (VIM) (3rd edition). *JCGM* **200**. URL https://www.bipm.org/vim

J. D. Blum and B. A. Bergquist. (2007) Reporting of variations in the natural isotopic composition of mercury. *Analytical and Bioanalytical Chemistry* **388**:353–359. doi:10.1007/s00216-007-1236-9

J. D. Blundy, J. A. C. Robinson and B. J. Wood. (1998) Heavy REE are compatible in clinopyroxene on the spinel lherzolite solidus. *Earth and Planetary Science Letters* **160**:493–504. doi:10.1016/S0012-821X(98)00106-X

J. Blusztajn, S. G. Nielsen, H. R. Marschall, Y. Shu, C. M. Ostrander and T. Hanyu. (2018) Thallium isotope systematics in volcanic rocks from St Helena – constraints on the origin of the HIMU reservoir. *Chemical Geology* **476**:292–301. doi:10.1016/j.chemgeo.2017.11.025

L. L. Bolge, M. J. Carr, M. D. Feigenson and G. E. Alvarado. (2006) Geochemical stratigraphy and magmatic evolution at Arenal Volcano, Costa Rica. *Journal of Volcanology and Geothermal Research* **157**:34–48. doi:10.1016/j.jvolgeores.2006.03.036

C. Bouman, T. Elliott and P. Z. Vroon. (2004) Lithium inputs to subduction zones. *Chemical Geology* **212**:59–79. doi:10.1016/j.chemgeo.2004.08.004

P. A. Brandl, C. Beier, M. Regelous, W. Abouchami, K. M. Haase, D. Garbe-Schönberg and S. J. G. Galer. (2012) Volcanism on the flanks of the East Pacific Rise: quantitative constraints on mantle heterogeneity and melting processes. *Chemical Geology* **298–299**:41–56. doi:10.1016/j.chemgeo.2011.12.015

N. Braukmüller, F. Wombacher, A. Bragagni and C. Münker. (2020) Determination of Cu, Zn, Ga, Ag, Cd, In, Sn and Tl in geological reference materials and chondrites by isotope dilution ICP-MS. *Geostandards and Geoanalytical Research* **44**:733–752. doi:doi.org/10.1111/ggr.12352

E. K. A. Brett, J. Prytulak, S. J. Hammond and M. Rehkämper. (2018) Thallium concentration and stable isotope compositions of sixteen international reference materials. *Geostandards and Geoanalytical Research* **42**:339–360. doi:10.1111/ggr.12215

E. K. A. Brett, J. Prytulak, M. Rehkämper, S. J. Hammond, C. Chauvel, A. Stracke and M. Willbold. (2021) Thallium elemental and isotopic systematics in ocean island lavas. *Geochimica et Cosmochimica Acta* **301**:187–210. doi:10.1016/j.gca.2021.02.035

L. Brown, J. Klein, R. Middleton, I. S. Sacks and F. Tera. (1982) ^{10}Be in island-arc volcanoes and implications for subduction. *Nature* **299**:718–720. doi:10.1038/299718a0

R. J. C. Brown and M. J. T. Milton. (2005) Analytical techniques for trace element analysis: an overview. *Trends in Analytical Chemistry* **24**:266–274. doi:10.1016/j.trac.2004.11.010

K. Burke, B. Steinberger, T. H. Torsvik and M. A. Smethurst. (2008) Plume Generation Zones at the margins of Large Low Shear Provinces on the core–mantle boundary. *Earth and Planetary Science Letters* **265**:49–60. doi:10.1016/j.epsl.2007.09.042

V. Busigny, P. Cartigny, P. Philippot, M. Ader and M. Javoy. (2003) Massive recycling of nitrogen and other fluid-mobile elements (K, Rb, Cs, H) in a cold slab environment: evidence from HP to UHP oceanic metasediments of the Schistes Lustrés nappe (western Alps, Europe). *Earth and Planetary Science Letters* **215**:27–42. doi:10.1016/S0012-821X(03)00453-9

J. H. Bédard. (2014) Parameterizations of calcic clinopyroxene—melt trace element partition coefficients. *Geochemistry, Geophysics, Geosystems* **15**:303–336. doi:10.1002/2013GC005112

I. Campostrini, F. Demartin, C. M. Gramaccioli and P. Orlandi. (2008) Hephaistosite, $TlPb_2Cl_5$, a new thallium mineral species from La Fossa Crater, Vulcano, Aeolian Islands, Italy. *The Canadian Mineralogist* **46**:701–708. doi:10.3749/canmin.46.3.701

D. Canil and S. A. Fellows. (2017) Sulphide–sulphate stability and melting in subducted sediment and its role in arc mantle redox and chalcophile cycling in space and time. *Earth and Planetary Science Letters* **470**:73–86. doi:10.1016/j.epsl.2017.04.028

G. Carrasco-Núñez, M. McCurry, M. J. Branney, M. Norry and C. Willcox. (2012) Complex magma mixing, mingling, and withdrawal associated with an intra-Plinian ignimbrite eruption at a large silicic caldera volcano: Los Humeros of central Mexico. *GSA Bulletin* **124**:1793–1809. doi:10.1130/B30501.1

C. Chauvel, S. Bureau and C. Poggi. (2011) Comprehensive chemical and isotopic analyses of basalt and sediment reference materials. *Geostandards and Geoanalytical Research* **35**:125–143. doi:10.1111/j.1751-908X.2010.00086.x

C. Chauvel, A. W. Hofmann and P. Vidal. (1992) HIMU-EM: The French Polynesian connection. *Earth and Planetary Science Letters* **110**:99–119. doi:10.1016/0012-821X(92)90042-T

C. Chauvel, R. C. Maury, S. Blais, E. Lewin, H. Guillou, G. Guille, P. Rossi and M.-A. Gutscher. (2012) The size of plume heterogeneities constrained by Marquesas isotopic stripes. *Geochemistry, Geophysics, Geosystems* **13**:Q07005. doi:10.1029/2012GC004123

C. Chauvel, W. McDonough, G. Guille, R. Maury and R. Duncan. (1997) Contrasting old and young volcanism in Rurutu Island, Austral chain. *Chemical Geology* **139**:125–143. doi:10.1016/S0009-2541(97)00029-6

F. Chayes and Y. Suzuki. (1963) *A replacement for reference sample G-I*, pp. 152–156. Annual report of the Director of the Geophysical laboratory. Carnegie Institute, Washington

J. Chen, C. Leng, D. Xu, D. Wang and K. Li. (2020) Analytical techniques for tellurium stable isotopes and their geological applications: a review. *Acta Geologica Sinica* **94**:1655–1663. doi:10.3724/SP.J.0001-571720200521

J. H. Chen and G. J. Wasserburg. (1987) A search for evidence of extinct lead-205 in iron meteorites. *Lunar and Planetary Science Conference* **XVIII**:165–166

J. H. Chen and G. J. Wasserburg. (1994) The abundance of thallium and primordial lead in selected meteorites – the search for ^{205}Pb. *Lunar and Planetary Science Conference* **XVV**:245

S. V. Churakov, S. I. Tkachenko, M. A. Korzhinskii, R. E. Bocharnikov and K. I. Shmulovich. (2000) Evolution of composition of high-temperature fumarolic gases from Kudryavy volcano, Iturup, Kuril Islands: the thermodynamic modelling. *Geochemistry International* **38**:436–451

A. Cipriani, H. K. Brueckner, E. Bonatti and D. Brunelli. (2004) Oceanic crust generated by elusive parents: Sr and Nd isotopes in basalt-peridotite pairs from the Mid-Atlantic Ridge. *Geology* **32**:657–660. doi:10.1130/G20560.1

R. N. Clayton. (2002) Self-shielding in the solar nebula. *Nature* **415**:860–861. doi:10.1038/415860b

R. N. Clayton, L. Grossman and T. K. Mayeda. (1973) A component of primitive nuclear composition in carbonaceous meteorites. *Science* **182**:485–488. doi:10.1126/science.182.4111.485

R. M. Coggon, M. Rehkämper, C. Atteck, D. A. H. Teagle, J. C. Alt and M. J. Cooper. (2014) Controls on thallium uptake during hydrothermal alteration of the upper ocean crust. *Geochimica et Cosmochimica Acta* **144**:25–42. doi:10.1016/j.gca.2014.09.001

M. Condomines, M. Carpentier and T. Ongendangenda. (2015) Extreme radium deficit in the 1957 AD Mugogo lava (Virunga volcanic field, Africa): its bearing on olivine-melilitite genesis. *Contributions to Mineralogy and Petrology* **169**:29. doi:10.1007/s00410-015-1124-9

D. Cox, S. F. L. Watt, F. E. Jenner, A. R. Hastie and S. J. Hammond. (2019) Chalcophile element processing beneath a continental arc stratovolcano. *Earth and Planetary Science Letters* **522**:1–11. doi:10.1016/j.epsl.2019.06.017

J. A. Crisp. (1984) Rates of magma emplacement and volcanic output. *Journal of Volcanology and Geothermal Research* **20**:177–211. doi:10.1016/0377-0273(84)90039-8

W. Crookes. (1862) Preliminary researches on thallium. *Proceedings of the Royal Society of London* **12**:150–159. doi:10.1098/rspl.1862.0030

I. W. Croudace. (1980) A possible error source in silicate wet-chemistry caused by insoluble fluorides. *Chemical Geology* **31**:153–155. doi:10.1016/0009-2541(80)90074-1

S. B. Dampare, T. Shibata, D. K. Asiedu, S. Osae and B. Banoeng-Yakubo. (2008) Geochemistry of Paleoproterozoic metavolcanic rocks from the southern Ashanti volcanic belt, Ghana: Petrogenetic and tectonic setting implications. *Precambrian Research* **162**:403–423. doi:10.1016/j.precamres.2007.10.001

N. Dauphas, S. G. John and O. Rouxel. (2017) Iron isotope systematics. *Reviews in Mineralogy and Geochemistry* **82**:415–510. doi:10.2138/rmg.2017.82.11

N. Dauphas and E. A. Schauble. (2016) Mass fractionation laws, mass-independent effects, and isotopic anomalies. *Annual Review of Earth and Planetary Sciences* **44**:709–783. doi:10.1146/annurev-earth-060115-012157

D. R. Davies, S. Goes, J. H. Davies, B. S. A. Schuberth, H. Bunge and J. Ritsema. (2012) Reconciling dynamic and seismic models of Earth's lower mantle: The dominant role of thermal heterogeneity. *Earth and Planetary Science Letters* **353–354**:253–269. doi:10.1016/j.epsl.2012.08.016

D. R. Davies, S. Goes and M. Sambridge. (2015) On the relationship between volcanic hotspot locations, the reconstructed eruption sites of large igneous provinces and deep mantle seismic structure. *Earth and Planetary Science Letters* **411**:121–130. doi:10.1016/j.epsl.2014.11.052

F. M. Deegan, V. R. Troll, A. K. Barker, C. Harris, J. P. Chadwick, J. C. Carracedo and A. Delcamp. (2012) Crustal versus source processes recorded in dykes from the Northeast volcanic rift zone of Tenerife, Canary Islands. *Chemical Geology* **344**:324–344. doi:10.1016/j.chemgeo.2012.10.013

H. Delgado-Granados, L. Cárdenas González and N. Piedad Sánchez. (2001) Sulfur dioxide emissions from Popocatépetl volcano (Mexico): case study of a high-emission rate, passively degassing erupting volcano. *Journal of Volcanology and Geothermal Research* **108**:107–120. doi:10.1016/S0377-0273(00)00280-8

F. Demartin, C. M. Gramaccioli and I. Campostrini. (2009) Steropesite, Tl_3BiCl_6, a new thallium bismuth chloride from La Fossa Crater, Vulcano, Aeolian Islands, Italy. *The Canadian Mineralogist* **47**:373–380. doi:10.3749/canmin.47.2.373

H. Deng, T. Kusky, A. Polat, L. Wang, J. Wang and S. Wang. (2013) Geochemistry of Neoarchean mafic volcanic rocks and late mafic dikes in the Zanhuang Complex, Central Orogenic

Belt, North China Craton: implications for geodynamic setting. *Lithos* **175–176**:193–212. doi:10.1016/j.lithos.2013.05.007

S. Ding and R. Dasgupta. (2018) Sulfur inventory of Ocean Island Basalt source regions constrained by modeling the fate of sulfide during decompression melting of a heterogeneous mantle. *Journal of Petrology* **59**:1281–1308. doi:10.1093/petrology/egy061

K. E. Donnelly, S. L. Goldstein, C. H. Langmuir and M. Spiegelman. (2004) Origin of enriched ocean ridge basalts and implications for mantle dynamics. *Earth and Planetary Science Letters* **226**:347–366. doi:10.1016/j.epsl.2004.07.019

R. A. Duncan and M. A. Richards. (1991) Hotspots, mantle plumes, flood basalts, and true polar wander. *Reviews of Geophysics* **29**:31–50. doi:10.1029/90RG02372

C. Dupuy, M. Fratta and D. M. Shaw. (1973) Partition coefficient of thallium compared with rubidium. *Earth and Planetary Science Letters* **19**:209–212. doi:10.1016/0012-821X(73)90116-7

M. Edmonds, T. A. Mather and E. J. Liu. (2018) A distinct metal fingerprint in arc volcanic emissions. *Nature Geoscience* **11**:790–794. doi:10.1038/s41561-018-0214-5

S. M. Eggins, J. D. Woodhead, L. P. J. Kinsley, G. E. Mortimer, P. Sylvester, M. T. McCulloch, J. M. Hergt and M. R. Handler. (1997) A simple method for the precise determination of $\geq$40 trace elements in geological samples by ICPMS using enriched isotope internal standardisation. *Chemical Geology* **134**:311–326. doi:10.1016/S0009-2541(96)00100-3

T. Elliot, J. Blichert-Toft, A. Heumann, G. Koetsier and V. Forjaz. (2007) The origin of enriched mantle beneath São Miguel, Azores. *Geochimica et Cosmochimica Acta* **71**:219–240. doi:10.1016/j.gca.2006.07.043

A. Elmaleh, A. Galy, T. Allard, R. Dairon, J. A. Day, F. Michel, N. Marriner, C. Morhange and F. Couffignal. (2012) Anthropogenic accumulation of metals and metalloids in carbonate-rich sediments: insights from the ancient harbor setting of Tyre (Lebanon). *Geochimica et Cosmochimica Acta* **82**:23–38. doi:10.1016/j.gca.2011.04.032

V. R. Espanon, A. R. Chivas, L. P. J. Kinsley and A. Dosseto. (2014) Geochemical variations in the Quaternary Andean back-arc volcanism, southern Mendoza, Argentina. *Lithos* **208–209**:251–264. doi:10.1016/j.lithos.2014.09.010

R. Espinasa-Pereña and A. L. Martin-Del Pozzo. (2006) Morphostratigraphic evolution of Popocatépetl volcano, México. *Geological Society of America Special Papers* **402**:115–137. doi:10.1130/2006.2402(05)

H. W. Fairbairn, W. G. Schlecht, R. E. Stevens, W. H. Dennen, L. H. Ahrens and F. Chays. (1951) A cooperative investigation of precision and accuracy in chemical, spectrochemical and modal analysis of silicate rocks. *Geological Survey Bulletin* **980**:59

K. A. Farley, J. H. Natland and H. Craig. (1992) Binary mixing of enriched and undegassed (primitive?) mantle components (He, Sr, Nd, Pb) in Samoan lavas. *Earth and Planetary Science Letters* **111**:183–199. doi:10.1016/0012-821X(92)90178-X

M. J. Farner and C.-T. A. Lee. (2017) Effects of crustal thickness on magmatic differentiation in subduction zone volcanism: a global study. *Earth and Planetary Science Letters* **470**:96–107. doi:10.1016/j.epsl.2017.04.025

L. Ferrari, M. López-Martínez and J. Rosas-Elguera. (2002) Ignimbrite flare-up and deformation in the southern Sierra Madre Occidental, western Mexico: Implications for the late subduction history of the Farallon plate. *Tectonics* **21**:17–1–17–24. doi:10.1029/2001TC001302

L. Ferrari, T. Orozco-Esquivel, V. Manea and M. Manea. (2012) The dynamic history of the Trans-Mexican Volcanic Belt and the Mexico subduction zone. *Tectonophysics* **522–523**:122–149. doi:10.1016/j.tecto.2011.09.018

L. Ferrari, C. M. Petrone and L. Francalanci. (2001) Generation of oceanic-island basalt–type volcanism in the western Trans-Mexican volcanic belt by slab rollback, asthenosphere infiltration, and variable flux melting. *Geology* **29**:507–510. doi:10.1130/0091-7613(2001)029<0507:GOOIBT>2.0.CO;2

A. Fitzpayne, J. Prytulak, A. Giuliana and J. Hergt. (2020) Thallium isotopic compositions of phlogopite in kimberlite-hosted MARID and PIC mantle xenoliths. *Chemical Geology* **531**:119347. doi:10.1016/j.chemgeo.2019.119347

A. Fitzpayne, J. Prytulak, J. J. Wilkinson, D. R. Cooke, M. J. Baker and C. C. Wilkinson. (2018) Assessing thallium elemental systematics and isotope ratio variations in porphyry copper systems: a case study of the Bingham Canyon District. *Minerals* **8**:548. doi:10.3390/min8120548

F. J. Flanagan. (1969) U.S. Geological Survey standards – II. First compilation of data for the new U.S.G.S. rocks. *Geochimica et Cosmochimica Acta* **33**:81–120. doi:10.1016/0016-7037(69)90094-5

F. A. Frey. (1969) Rare earth abundances in a high-temperature peridotite intrusion. *Geochimica et Cosmochimica Acta* **33**:1429–1447. doi:10.1016/0016-7037(69)90183-5

H. Freymuth, F. Vils, M. Willbold, R. N. Taylor and T. Elliott. (2015) Molybdenum mobility and isotopic fractionation during subduction at the Mariana arc. *Earth and Planetary Science Letters* **432**:176–186. doi:10.1016/j.epsl.2015.10.006

C. Fries, Jr. (1965) *Geología de la Hoja Cuernavaca, Estados de Morelos, México, Guerrero y Puebla. Carta Geológica de México, scale 1:100,000.* Instituto de Geofísica, Universidad Nacional Autónoma de México

G. A. Gaetani and T. L. Grove. (1995) Partitioning of rare earth elements between clinopyroxene and silicate melt: crystal-chemical controls. *Geochimica et Cosmochimica Acta* **59**:1951–1962. doi:10.1016/0016-7037(95)00119-0

G. A. Gaetani, A. Kent, T. L. Grove, I. Hutchenson and E. M. Stolper. (2003) Mineral/melt partitioning of trace elements during hydrous peridotite partial melting. *Contributions to Mineralogy and Petrology* **145**:391–405. doi:10.1016/0016-7037(95)00119-0

A. Gale, C. A. Dalton, C. H. Langmuir, Y. Su and J.-G. Schilling. (2013) The mean composition of ocean ridge basalts. *Geochemistry, Geophysics, Geosystems* **14**:489–518. doi:10.1029/2012GC004334

A. Gale, S. Escrig, E. J. Gier, C. H. Langmuir and S. J. Goldstein. (2011) Enriched basalts at segment centres: the Lucky Strike (37°17'N) and Menez Gwen (37°50'N) segments of the Mid-Atlantic Ridge. *Geochemistry Geophysics Geosystems* **12**:Q0616. doi:10.1029/2010GC003446

Y. Q. Gao and R. A. Marcus. (2001) Strange and unconventional isotope effects in ozone formation. *Science* **293**:259–263. doi:10.1126/science.1058528

C.-D. Garbe-Schönberg. (1993) Simultaneous determination of thirty-seven trace elements in twenty-eight international rock standards by ICP-MS. *Geostandards Newsletter* **17**:81–97. doi:10.1111/j.1751-908X.1993.tb00122.x

R. M. Gaschnig, R. L. Rudnik and W. F. McDonough. (2014) Determination of Ga, Ge, Mo, Ag, Cd, In, Sn, Sb, W, Tl and Bi in USGS reference materials by standard addition ICP-MS. *Geostandards and Geoanalytical Research* **39**:371–379. doi:10.1111/j.1751-908X.2014.00330.x

P.-J. Gauthier, O. Sigmarsson, M. Gouhier, B. Haddadi and S. Moune. (2016) Elevated gas flux and trace metal degassing from the 2014–2015 fissure eruption at the Bárðarbunga volcanic system, Iceland. *Journal of Geophysical Research: Solid Earth* **121**:1610–1630. doi:10.1002/2015JB012111

E. Gazel, M. J. Carr, K. Hoernle, M. D. Feigenson, F. Szymanski, D. Hauff and P. van den Bogaard. (2009) Galapagos-OIB signature in southern Central America: mantle refertilization by arc–hot spot interaction. *Geochemistry, Geophysics, Geosystems* **10**:Q02S11. doi:10.1029/2008GC002246

E. Gazel, K. Hoernle, M. J. Carr, C. Herzberg, I. Saginor, P. van den Bogaard, F. Hauff, M. Geigenson and C. Swisher III. (2011) Plume–subduction interaction in southern Central America: mantle upwelling and slab melting. *Lithos* **121**:117–134. doi:10.1016/j.lithos.2010.10.008

J. Geldmacher, K. A. Hoernle, P. van den Bogaard, F. Hauff and A. Klügel. (2008) Age and geochemistry of the Central American Forearc Basement (DSDP Leg 67 and 84): insights into Mesozoic arc volcanism and seamount accretion on the fringe of the Caribbean LIP. *Journal of Petrology* **49**:1781–1815. doi:10.1093/petrology/egn046

S. A. Gibson, S. C. McMahon, J. A. Day and J. B. Dawson. (2013) Highly refractory lithospheric mantle beneath the Tanzanian Craton: evidence from Lashaine pre-metasomatic garnet-bearing peridotites. *Journal of Petrology* **54**:1503–1546. doi:10.1093/petrology/egt020

P.-Y. Gillot, Y. Cornette, N. Max and B. Floris. (1992) Two reference materials, trachytes MDO-G and ISH-G, for argon dating (K-Ar and $^{40}Ar/^{39}Ar$) of Pleistocene and Holocene rocks. *Geostandards Newsletter* **16**:55–60. doi:/10.1111/j.1751-908X.1992.tb00487.x

L. González-Álvarez and R. Kerrich. (2011) Trace element mobility in dolomitic argillites of the Mesoproterozoic Belt-Purcell Supergroup, western North America. *Geochimica et Cosmochimica Acta* **75**:1733–1756. doi:10.1016/j.gca.2011.01.006

K. Govindaraju. (1979) Report (1968-1978) on two mica reference samples: Biotite Mica-Fe and Phlogopite Mica-Mg. *Geostandards Newsletter* **3**:3–24. doi:10.1111/j.1751-908X.1979.tb00235.x

K. Govindaraju. (1980) Report (1980) on three GIT-IWG rock reference samples: anorthosite from Greenland, AN-G; Basalte d'Essay-la-Côte, BE-N; Granite de Beauvoir, MA-N. *Geostandards Newsletter* **4**:49–138. doi:10.1111/j.1751-908X.1980.tb00274.x

K. Govindaraju. (1982) Report (1967-1981) on four ANRT rock reference samples: Diorite DR-N, Serpentine UB-N, Bauxite BX-N and Disthene DT-N. *Geostandards Newsletter* **6**:91–159. doi:10.1111/j.1751-908X.1982.tb00347.x

K. Govindaraju. (1984a) 1984 compilation of working values and sample description for 170 international reference samples of mainly silicate rocks and minerals. *Geostandards Newsletter* **8**:1–16. doi:10.1111/j.1751-908X.1984.tb01069.x

K. Govindaraju. (1984b) Report (1984) on two GIT-IWG geochemical reference samples: albite from Italy, AL-I and iron formation sample from Greenland, IF-G. *Geostandards Newsletter* **8**:63–113. doi:10.1111/j.1751-908X.1984.tb00415.x

K. Govindaraju. (1994) 1994 compilation of working values and sample description for 383 geostandards. *Geostandards Newsletter* **18**:1–158. doi:10.1046/j.1365-2494.1998.53202081.x-i1

K. Govindaraju. (1995) 1995 working values with confidence limits for twenty-six CPRG, ANRT and IWG-GIT geostandards. *Geostandards Newsletter* **19**:1–32. doi:10.1111/j.1751-908X.1995.tb00164.x

A. T. Greaney, R. L. Rudnick, R. T. Helz, R. M. Gaschnig, P. M. Piccoli and R. D. Ash. (2017) The behavior of chalcophile elements during magmatic differentiation as observed in Kilauea Iki lava lake, Hawaii. *Geochimica et Cosmochimica Acta* **210**:71–96. doi:10.1016/j.gca.2017.04.033

T. H. Green, J. D. Blundy, J. Adam and G. M. Yaxley. (2000) SIMS determinations of trace element partition coefficients between garnet, clinopyroxene and hydrous basaltic liquids at 2–7.5 GPa and 1080–1200 °C. *Lithos* **53**:165–187. doi:10.1016/S0024-4937(00)00023-2

M. Grégoire, D. Bell and A. Le Roex. (2002) Trace element geochemistry of phlogopite-rich mafic mantle xenoliths: their classification and their relationship to phlogopite-bearing peridotites and kimberlites revisited. *Contributions to Mineralogy and Petrology* **142**:603–625. doi:10.1007/s00410-001-0315-8

A. Gómez-Tuena and G. Carrasco-Núñez. (2000) Cerro Grande volcano: the evolution of a Miocene stratocone in the early Trans-Mexican Volcanic Belt. *Tectonophysics* **318**:249–280. doi:10.1016/S0040-1951(99)00314-5

A. Gómez-Tuena, J. G. Cavazos-Tovar, M. Parolari, S. M. Straub and R. Espinasa-Pereña. (2018a) Geochronological and geochemical evidence of continental crust 'relamination' in the origin of intermediate arc magmas. *Lithos* **322**:52–66. doi:10.1016/j.lithos.2018.10.005

A. Gómez-Tuena, A. B. LaGatta, C. H. Langmuir, S. L. Goldstein, F. Ortega-Gutiérrez and G. Carrasco-Núñez. (2003) Temporal control of subduction magmatism in the eastern Trans-Mexican Volcanic Belt: mantle sources, slab contributions, and crustal contamination. *Geochemistry, Geophysics, Geosystems* **4**:8912. doi:10.1029/2003GC000524

A. Gómez-Tuena, C. H. Langmuir, S. L. Goldstein, S. M. Straub and F. Ortega-Gutiérrez. (2007) Geochemical evidence for slab melting in the Trans-Mexican Volcanic Belt. *Journal of Petrology* **48**:537–562. doi:10.1093/petrology/egl071

A. Gómez-Tuena, L. Mori, S. L. Goldstein and O. Pérez-Arvizu. (2011) Magmatic diversity of western Mexico as a function of metamorphic transformations in the subducted oceanic plate. *Geochimica et Cosmochimica Acta* **75**:213–241. doi:10.1016/j.gca.2010.09.029

A. Gómez-Tuena, L. Mori and S. M. Straub. (2018b) Geochemical and petrological insights into the tectonic origin of the Transmexican Volcanic Belt. *Earth-Science Reviews* **183**:153–181. doi:10.1016/j.earscirev.2016.12.006

M. G. Gómez-Vasconcelos, V. H. Garduño-Monroy, J. L. Macías, P. W. Layer and J. A. Benowitz. (2015) The Sierra de Mil Cumbres, Michoacán, México: transitional volcanism between the Sierra Madre Occidental and the Trans-Mexican Volcanic Belt. *Journal of Volcanology and Geothermal Research* **301**:128–147. doi:10.1016/j.jvolgeores.2015.05.005

B. R. Hacker. (2008) H_2O subduction beyond arcs. *Geochemistry, Geophysics, Geosystems* **9**:Q03001. doi:10.1029/2007GC001707

B. B. Hanan and D. W. Graham. (1996) Lead and helium isotope evidence from oceanic basalts for a common deep source of mantle plumes. *Science* **272**:991–995. doi:10.1126/science.272.5264.991

G. E. Harlow and R. Davies. (2004) Status report on stability of K-rich phases at mantle conditions. *Lithos* **77**:647–653. doi:10.1016/j.lithos.2004.04.010

S. R. Hart, E. H. Hauri, L. A. Oschmann and J. A. Whitehead. (1992) Mantle plumes and entrainment: isotopic evidence. *Science* **256**:517–520. doi:10.1126/science.256.5056.517

E. H. Hauri, T. P. Wagner and T. L. Grove. (1994) Experimental and natural partitioning of Th-U-Pb and other trace elements between garnet, clinopyroxene and basaltic melts. *Chemical Geology* **117**:149–166. doi:10.1016/0009-2541(94)90126-0

J. L. Hayes, W. S. Holbrook, D. Lizarralde, H. J. A. van Avendonk, A. D. Bullock, M. Mora, S. Harder, G. Alvarado and C. Ramírez. (2014) Crustal structure across the Costa Rican Volcanic Arc. *Geochemistry, Geophysics, Geosystems* **14**:1087–1103. doi:10.1002/ggge.20079

Y. He, G. Zhao, M. Sun and Y. Han. (2010) Petrogenesis and tectonic setting of volcanic rocks in the Xiaoshan and Waifangshan areas along the southern margin of the North China Craton: constraints from bulk-rock geochemistry and Sr-Nd isotopic composition. *Lithos* **114**:186–199. doi:10.1016/j.lithos.2009.08.008

E. W. Heinrich. (1960) Kingman feldspar mine. In: *Some rare-earth mineral deposits in Mohave County, Arizona*, pp. 5–11. Arizona Bureau of Mines

H. Heinrichs, B. Schulz-Dobrick and K. H. Wedepohl. (1980) Terrestrial geology of Cd, Bi, Tl, Pb, Zn and Rb. *Geochimica et Cosmochimica Acta* **44**:1519–1533. doi:10.1016/0016-7037(80)90116-7

J. Hermann and D. H. Green. (2001) Experimental constraints on high pressure melting in subducted crust. *Earth and Planetary Science Letters* **188**:149–168. doi:10.1016/S0012-821X(01)00321-1

K. Hettmann, K. Kreissig, M. Rekämper, T. Wenzel, R. Mertz-Kraus and G. Markl. (2014a) Thallium geochemistry in the metamorphic Lengenbach sulfide deposit, Switzerland: thallium-isotope fractionation in a sulfide melt. *American Mineralogist* **99**:793–803. doi:10.2138/am.2014.4591

K. Hettmann, M. A. W. Marks, K. Kreissig, T. Zack, T. Wenzel, M. Rekämper, D. E. Jacob and G. Markl. (2014b) The geochemistry of Tl and its isotopes during magmatic and hydrothermal processes: the peralkaline Ilimaussaq complex, southwest Greenland. *Chemical Geology* **366**:1–13. doi:10.1016/j.chemgeo.2013.12.004

E. Hill, B. J. Wood and J. D. Blundy. (2000) The effect of Ca-Tschermaks component on trace element partitioning between clinopyroxene and silicate melts. *Lithos* **53**:205–217. doi:10.1016/S0024-4937(00)00025-6

A. W. Hofmann. (1997) Mantle geochemistry: the message from oceanic volcanism. *Nature* **385**:219–229. doi:10.1038/385219a0

A. W. Hofmann, K. P. Jochum, M. Seufert and W. M. White. (1986) Nb and Pb in oceanic basalts: new constraints on mantle evolution. *Earth and Planetary Science Letters* **79**:33–45. doi:10.1016/0012-821X(86)90038-5

A. W. Hofmann and W. M. White. (1982) Mantle plumes from ancient oceanic crust. *Earth and Planetary Science Letters* **57**:421–436. doi:10.1016/0012-821X(82)90161-3

S. Homrighausen, K. Hoernle, F. Hauff, J. Geldmacher, J.-A. Wartho and D. Garbe-Schönberg. (2018) Global distribution of the HIMU end member: Formation through Archaean plume-lid tectonics. *Earth-Science Reviews* **182**:85–101. doi:10.1016/j.earscirev.2018.04.009

R. A. Horne. (1958) The ion-exchange resin adsorption of thallium(I) and (III). *Journal of Inorganic and Nuclear Chemistry* **6**:338–343. doi:10.1016/0022-1902(58)80118-9

Z. Hu and S. Gao. (2008) Upper crustal abundances of trace elements: a revision and update. *Chemical Geology* **253**:205–221. doi:10.1016/j.chemgeo.2008.05.010

Z. Hu, W. Zhang, Y. Liu, H. Chen, R. M. Gaschnig, K. Zang, M. Li, S. Gao and S. Hu. (2013) Rapid bulk rock decomposition by ammonium fluoride (NH_4F) in open vessels at an elevated digestion temperature. *Chemical Geology* **355**:144–152. doi:10.1016/j.chemgeo.2013.06.024

J.-H. Huang, F. Huang, L. Evans and S. Glasauer. (2015) Vanadium: global (bio)geochemistry. *Chemical Geology* **417**:68–89. doi:10.1016/j.chemgeo.2015.09.019

J. M. Huey and T. P. Kohman. (1972) Search for extinct natural radioactivity of ^{205}Pb via thallium-isotope anomalies in chondrites and lunar soil. *Earth and Planetary Science Letters* **16**:401–412. doi:10.1016/0012-821X(72)90159-8

M. Hutchinson, R. A. Brooker, J. H. Dilles and J. Blundy. (2020) The stability and composition of sulfate melts in arc magmas. *Contributions to Mineralogy and Petrology* **175**:92. doi:10.1007/s00410-020-01729-6

M. Ikramuddin, Y. Asmeron, P. M. Nordstrom, K. P. Kinart, W. M. Martin, S. J. M. Digby, D. D. Elder, W. F. Nijak and A. A. Afemari. (1983) Thallium: a potential guide to mineral deposits. *Journal of Geochemical Exploration* **19**:465–490. doi:10.1016/0375-6742(83)90038-9

S. Inguaggiato, A. L. Martin-Del Pozzo, A. Aguayo, G. Capasso and R. Favara. (2005) Isotopic, chemical and dissolved gas constraints on spring water from Popocatepetl volcano (Mexico): evidence of gas–water interaction between magmatic component and shallow fluids. *Journal of Volcanology and Geothermal Research* **141**:91–108. doi:10.1016/j.jvolgeores.2004.09.006

T. N. Irvine and W. R. A. Baragar. (1971) A guide to the chemical classification of the common volcanic rocks. *Canadian Journal of Earth Sciences* **8**:523–548. doi:10.1139/e71-055

A. J. Irving and F. A. Frey. (1984) Trace element abundances in megacrysts and their host basalts: constraints on partition coefficients and megacryst genesis. *Geochimica et Cosmochimica Acta* **48**:1201–1221. doi:10.1016/0016-7037(84)90056-5

G. Jacques, K. Hoernle, J. Gill, F. Hauff, H. Wehrmann, D. Garbe-Schönberg, P. van den Bogaard, L. Bindeman and L. E. Lara. (2013) Across-arc geochemical variations in the Southern Volcanic Zone, Chile (34.5–38.0°S): constraints on mantle wedge and slab input compositions. *Geochimica et Cosmochimica Acta* **123**:218–243. doi:10.1016/j.gca.2013.05.016

A. B. Jeffcoate, T. Elliot, S. A. Kasemann, D. Ionov, K. Cooper and R. Brooker. (2007) Li isotope fractionation in peridotites and mafic melts. *Geochimica et Cosmochimica Acta* **71**:202–218. doi:10.1016/j.gca.2006.06.1611

A. M. Jellinek and M. Manga. (2004) Links between long-lived hot spots, mantle plumes, D″, and plate tectonics. *Reviews of Geophysics* **42**:RG3002. doi:10.1029/2003RG000144

F. E. Jenner. (2017) Cumulate causes for the low contents of sulfide-loving elements in the continental crust. *Nature Geoscience* **10**:524–529. doi:10.1038/ngeo2965

F. E. Jenner and H. S. C. O'Neill. (2012a) Analysis of 60 elements in 616 ocean floor basaltic glasses. *Geochemistry, Geophysics, Geosystems* **13**. doi:10.1029/2011GC004009

F. E. Jenner and H. S. C. O'Neill. (2012b) Major and trace analysis of basaltic glasses by laser-ablation ICP-MS. *Geochemistry, Geophysics, Geosystems* **13**. doi:10.1029/2011GC003890

K. P. Jochum, A. W. Hofmann and H. M. Seufert. (1993) Tin in mantle-derived rocks: constraints on Earth evolution. *Geochimica et Cosmochimica Acta* **57**:3585–3595. doi:10.1016/0016-7037(93)90141-I

K. P. Jochum, U. Nohl, K. Herwig, E. Lammel, B. Stoll and A. W. Hofmann. (2005) GeoReM: a new geochemical database for reference materials and isotopic standards. *Geostandards and Geoanalytical Research* **29**:333–338. doi:10.1111/j.1751-908X.2005.tb00904.x

K. P. Jochum, U. Weis, B. Schwager, B. Stoll, S. A. Wilson, G. H. Haug, M. O. Andreae and J. Enzweiler. (2016) Reference values following ISO guidelines for frequently requested rock reference materials. *Geostandards and Geoanalytical Research* **40**:333–350. doi:10.1111/j.1751-908X.2015.00392.x

A. Johnson and D. Canil. (2011) The degassing behavior of Au, Tl, As, Pb, Re, Cd and Bi from silicate liquids: experiments and applications. *Geochimica et Cosmochimica Acta* **75**:1773–1784. doi:10.1016/j.gca.2010.12.023

C. M. Johnson, B. L. Beard and F. Albarède. (eds.) (2004) *Geochemistry of non-traditional stable isotopes*, volume 55 of *Reviews in Mineralogy and Geochemistry*. ISSN 1529-6466

K. T. M. Johnson. (1998) Experimental determination of partition coefficients for rare earth and high-field-strength elements between clinopyroxene, garnet, and basaltic melt at high pressures. *Contributions to Mineralogy and Petrology* **133**:60–68. doi:10.1007/s004100050437

A. D. Johnston and B. E. Schwab. (2004) Constraints on the clinopyroxene/melt partitioning of REE, Rb, Sr, Ti, Cr, Zr, and Nb during mantle melting: first insights from direct peridotite melting experiments at 1.0 GPa. *Geochimica et Cosmochimica Acta* **68**:4949–4962. doi:10.1016/j.gca.2004.06.009

S. Jégo and R. Dasgupta. (2013) Fluid-present melting of sulfide-bearing ocean-crust: experimental constraints on the transport of sulfur from subducting slab to mantle wedge. *Geochimica et Cosmochimica Acta* **110**:106–134. doi:10.1016/j.gca.2013.02.011

S. Jégo and R. Dasgupta. (2014) The fate of sulfur during fluid-present melting of subducting basaltic crust at variable oxygen fugacity. *Journal of Petrology* **55**:1019–1050. doi:10.1093/petrology/egu016

B. S. Kamber, A. Greig and K. D. Collerson. (2005) A new estimate for the composition of weathered young upper continental crust from alluvial sediments, Queensland, Australia. *Geochimica et Cosmochimica Acta* **69**:1041–1058. doi:10.1016/j.gca.2004.08.020

H. Kawabata, T. Hanyu, Q. Chang, J.-I. Kimura, A. R. L. Nichols and Y. Tatsumi. (2011) The petrology and geochemistry of St. Helena alkali basalts: Evaluation of the oceanic crust-recycling model for HIMU OIB. *Journal of Petrology* **52**:791–838. doi:10.1093/petrology/egr003

K. A. Kelley, R. Kingsley and J.-G. Schilling. (2013) Composition of plume-influenced mid-ocean ridge lavas and glasses from the Mid-Atlantic Ridge, East Pacific Rise, Galápagos Spreading Center, and Gulf of Aden. *Geochemistry, Geophysics, Geosystems* **14**:223–242. doi:10.1002/ggge.20049

K. A. Kelley, T. Plank, J. Ludden and H. Staudigel. (2003) Composition of altered oceanic crust at ODP Sites 801 and 1149. *Geochemistry, Geophysics, Geosystems* **4**:8910. doi:10.1029/2002GC000435

B. Kendall, T. W. Dahl and A. D. Anbar. (2017) The stable isotope geochemistry of molybdenum. *Reviews in Mineralogy and Geochemistry* **82**:683–732. doi:10.2138/rmg.2017.82.16

M. Kersten, T. Xiao, K. Kreissig, A. Brett, B. J. Coles and M. Rehkämper. (2014) Tracing anthropogenic thallium in soil using stable isotope compositions. *Environmental Science & Technology* **48**:9030–9036. doi:10.1021/es501968d

R. Kessel, M. W. Schmidt, P. Ulmer and T. Pettke. (2005) Trace element signature of subduction-zone fluids, melts and supercritical liquids at 120–180 km depth. *Nature* **437**:724–727. doi:10.1038/nature03971

M. Kirchenbaur, C. Münster, S. Schuth, D. Garbe-Schönberg and P. Marchev. (2012) Tectonomagmatic constraints on the sources of Eastern Mediterranean K-rich lavas. *Journal of Petrology* **53**:27–65. doi:10.1093/petrology/egr055

E. S. Kiseeva and B. J. Wood. (2013) A simple model for chalcophile element partitioning between sulphide and silicate liquids with geochemical applications. *Earth and Planetary Science Letters* **383**:68–81. doi:10.1016/j.epsl.2013.09.034

E. S. Kiseeva and B. J. Wood. (2015) The effects of composition and temperature on chalcophile and lithophile element partitioning into magmatic sulphides. *Earth and Planetary Science Letters* **242**:280–294. doi:10.1016/j.epsl.2015.05.012

S. Klemme, J. D. Blundy and B. J. Wood. (2002) Experimental constraints on major and trace element partitioning during partial melting of eclogite. *Geochimica et Cosmochimica Acta* **71**:1783–1799. doi:10.1016/j.gca.2007.01.004

J. Kodolányi, T. Pettke, C. Spandler, B. S. Kamber and K. Gméling. (2012) Geochemistry of ocean floor and fore-arc serpentinites: constraints on the ultramafic input to subduction zones. *Journal of Petrology* **53**:235–270. doi:10.1093/petrology/egr058

J. Konzett. (1997) Phase relations and chemistry of Ti-rich K-richterite-bearing mantle assemblages: an experimental study to 8.0 GPa in a Ti-KNCMASH system. *Contributions to Mineralogy and Petrology* **128**:385–404. doi:10.1007/s004100050316

K. A. Kraus, F. Nelson and G. W. Smith. (1954) Anion-exchange studies. IX. Adsorbability of a number of metals in hydrochloric acid solutions. *Journal of Physical Chemistry* **58**:11–17. doi:10.1021/j150511a003

I. Kushiro. (2001) Partial melting experiments on peridotite and origin of mid-ocean ridge basalt. *Annual Review of Earth and Planetary Sciences* **29**:71–107. doi:10.1146/annurev.earth.29.1.71

A. Kyono and M. Kimata. (2001) The crystal structure of synthetic $TlAlSi_3O_8$: influence of the *inert-pair effect* of thallium on the feldspar structure. *European Journal of Mineralogy* **13**:849–856. doi:10.1127/0935-1221/2001/0013-0849

A. B. LaGatta. (2003) *Arc magma genesis in the Eastern Mexican Volcanic Belt*. Ph.D. thesis, Columbia University

C.-A. Lamy. (1862) De l'existence d'un nouveau métal, le thallium. *Comptes rendus* **54**:1255–1258

A. C. L. Larocque, J. A. Stimac, C. Siebe, K. Greengrass, R. Chapman and S. R. Mejia. (2008) Deposition of a high-sulfidation Au assemblage from a magmatic volatile phase, Volcán Popocatépetl, Mexico. *Journal of Volcanology and Geothermal Research* **170**:51–60. doi:10.1016/j.jvolgeores.2007.09.009

R. W. Le Maitre, A. Streckeisen, B. Zanettin, M. J. Le Bas, B. Bonin and P. Bateman. (eds.) (2002) *Igneous rocks: a classifcation and glossary of terms. Recommendations of the International Union of Geological Sciences Subcomission on the systematics of igneous rocks*. Cambridge University Press, Cambridge. ISBN 9780511535581. doi:10.1017/CBO9780511535581

W. P. Leeman, M. J. Carr and J. D. Morris. (1994) Boron geochemistry of the Central American Volcanic Arc: constraints on the genesis of subduction-related magmas. *Geochimica et Cosmochimica Acta* **58**:149–168. doi:10.1016/0016-7037(94)90453-7

J. K. Leggett. (1981) Geochemistry of Cocos Plate pelagic-hemipelagic sediments in Hole 487, Deep Sea Drilling Project Leg 66. *Initial Reports of Deep Sea Drilling Project* **66**:683–686. doi:10.2973/dsdp.proc.66.130.1982

Y. Liu, N.-T. Samaha and D. R. Baker. (2007) Sulfur concentration at sulfur saturation (SCSS) in magmatic silicate melts. *Geochimica et Cosmochimica Acta* **71**:1783–1799. doi:10.1016/j.gca.2007.01.004

E. Losantos, J. M. Cebriá, D. J. Morán-Zenteno, B. M. Martiny, J. López-Ruiz and G. Solís-Pichardo. (2017) Petrogenesis of the alkaline and calcalkaline monogenetic volcanism in the northern sector of the Michoacán-Guanajuato Volcanic Field (Central Mexico). *Lithos* **288–289**:295–310. doi:10.1016/j.lithos.2017.07.013

S. P. Love, F. Goff, D. Counce, C. Siebe and H. Delgado. (1998) Passive infrared spectroscopy of the eruption plume at Popocatépetl volcano, Mexico. *Nature* **396**:563–567. doi:10.1038/25109

J. R. Lyons and E. D. Young. (2005) CO self-shielding as the origin of oxygen isotope anomalies in the early solar nebula. *Nature* **435**:317–320. doi:10.1038/nature03557

M. A. Mahar, P. C. Goodell, A. Ramírez and J. García. (2019) Timing and origin of silicic volcanism in northwestern Mexico: insights from zircon U–Pb geochronology, Hf isotopes and geochemistry of rhyolite ignimbrites from Palmarejo and Guazapares in Southwest Chihuahua. *Lithos* **324–325**:246–264. doi:10.1016/j.lithos.2018.11.010

A. Makishima, H. Kitagawa and E. Nakamura. (2011) Simultaneous determination of Cd, In, Tl and Bi by isotope dilution-internal standardization ICP-QMS with corrections using externally measured MoO^+/Mo^+ ratios. *Geostandards and Geoanalytical Research* **35**:57–67. doi:10.1111/j.1751-908X.2010.00054.x

A. Makishima and E. Nakamura. (2006) Determination of major/minor and trace elements in silicate samples by ICP-QMS and ICP-SFMS applying isotope dilution-internal standardization (ID-IS) and multi-stage internal standardization. *Geostandards and Geoanalytical Research* **30**:245–271. doi:10.1111/j.1751-908X.2006.tb01066.x

G. Maldonado-Sánchez and P. Schaaf. (2005) Geochemical and isotope data from the Acatlán Volcanic Field, western Trans-Mexican Volcanic Belt: origin and evolution. *Lithos* **82**:455–470. doi:10.1016/j.lithos.2004.09.030

M. Mangler, J. Prytulak, G. Gisbert, H. Delgado-Granados and C. Petrone. (2019) Interplinian effusive activity at Popocatépetl volcano, Mexico: New insights into evolution and dynamics of the plumbing system. *Volcanica* **2**:45–72. doi:10.30909/vol.02.01.4572

M. F. Mangler. (2018) *Evolution and dynamics of the plumbing system of Popocatépetl Volcano, Mexico*. Ph.D. thesis, Imperial College London

M. F. Mangler, C. M. Petrone, S. Hill, H. Delgado-Granados and J. Prytulak. (2020) A pyroxenic view on magma hybridization and crystallization at Popocatépetl Volcano, Mexico. *Frontiers in Earth Science* **8**:362. doi:10.3389/feart.2020.00362

H. R. Marschall and J. C. Schumacher. (2012) Arc magmas sourced from mélange diapirs in subduction zones. *Nature Geosciences* **5**:862–867. doi:10.1038/ngeo1634

A. P. Martin, R. C. Price, A. F. Cooper and C. McCammon. (2015) Petrogenesis of the rifted Southern Victoria Land lithospheric mantle, Antarctica, inferred from petrography, geochemistry, thermobarometry and oxybarometry of peridotite and pyroxenite xenoliths from the Mount Morning eruptive centre. *Journal of Petrology* **56**:193–226. doi:10.1093/petrology/egu075

S. K. Marx and B. S. Kamber. (2010) Trace-element systematics of sediments in the Murray-Darling Basin, Australia: sediment provenance and palaeoclimate implications of fine scale chemical heterogeneity. *Applied Geochemistry* **25**:1221–1237. doi:10.1016/j.apgeochem.2010.05.007

S. K. Marx, B. S. Kamber, H. A. McGowan and A. Zawadski. (2010) Atmospheric pollutants in alpine peat bogs record a detailed chronology of industrial and agricultural development on the Australian continent. *Environmental Pollution* **158**:1615–1628. doi:10.1016/j.envpol.2009.12.009

H.-J. Massonne. (1999) Experimental aspects of UHP metamorphism in pelitic systems. *International Geology Review* **41**:623–628. doi:10.1080/00206819909465162

H.-J. Massonne and W. Schreyer. (1987) Phengite geobarometry based on the limiting assemblage with K-feldspar, phlogopite, and quartz. *Contributions to Mineralogy and Petrology* **96**:212–224. doi:10.1007/BF00375235

T. A. Mather, M. L. I. Witt, D. M. Pyle, B. M. Quayle, A. Aiuppa, E. Bagnato, R. S. Martin, K. W. W. Sims, M. Edmonds, A. J. Sutton and E. Ilyinskaya. (2012) Halogens and trace metal emissions from the ongoing 2008 summit eruption of Kīlauea volcano, Hawai'i. *Geochimica et Cosmochimica Acta* **83**:292–323. doi:10.1016/j.gca.2011.11.029

Y. Matsui, N. Onuma, H. Nagasawa, H. Higuchi and S. Banno. (1977) Crystal stucture control in trace element partitioning between crystal and magma. *Tectonics* **100**:315–324. doi:10.3406/bulmi.1977.7155

K. Mauersberger. (1987) Ozone isotope measurements in the stratosphere. *Geophysical Research Letters* **14**:80–83. doi:10.1029/GL014i001p00080

J. A. Mavrogenes and H. S. C. O'Neill. (1999) The relative effects of pressure, temperature and oxygen fugacity on the solubility of sulfide in mafic magmas. *Geochimica et Cosmochimica Acta* **63**:1173–1180. doi:10.1016/S0016-7037(98)00289-0

A. J. McCoy-West, J. A. Baker, K. Faure and R. J. Wysoczanski. (2010) Petrogenesis and origins of mid-Cretaceous continental intraplate volcanism in Marlborough, New Zealand: implications for the long-lived HIMU magmatic mega-province of the SW Pacific. *Journal of Petrology* **51**:2003–2045. doi:10.1093/petrology/egq046

P. McDade, J. D. Blundy and B. J. Wood. (2003a) Trace element partitioning between mantle wedge peridotite and hydrous MgO-rich melt. *American Mineralogist* **88**:1825–1831. doi:10.2138/am-2003-11-1225

P. McDade, J. D. Blundy and B. J. Wood. (2003b) Trace element partitioning on the Tinaquillo lherzolite solidus at 1.5 GPa. *Physics of the Earth and Planetary Interiors* **139**:129–147. doi:10.1016/S0031-9201(03)00149-3

W. F. McDonough and S.-s. Sun. (1995) The composition of the Earth. *Chemical Geology* **120**:223–253. doi:10.1016/0009-2541(94)00140-4

A. Michard and F. Albarède. (1986) The REE content of some hydrothermal fluids. *Chemical Geology* **55**:51–60. doi:10.1016/0009-2541(86)90127-0

J. F. Minster and C. Allègre. (1978) Systematic use of trace elements in igneous processes. *Contributions to Mineralogy and Petrology* **68**:37–52. doi:10.1007/BF00375445

M. R. Mohan, S. J. Piercey, B. S. Kamber and D. S. Sama. (2013) Subduction related tectonic evolution of the Neoarchaean eastern Dharwar Craton, southern India: new geochemical and isotopic constraints. *Precambrian Research* **227**:204–226. doi:10.1016/j.precamres.2012.06.012

R. Montelli, G. Nolet, F. A. Dahlen and G. Masters. (2006) A catalogue of deep mantle plumes: new results from finite-frequency tomography. *Geochemistry, Geophysics, Geosystems* **7**:Q11007. doi:10.1029/2006GC001248

W. J. Morgan. (1971) Convection plumes in the lower mantle. *Nature* **230**:42–43. doi:10.1038/230042a0

L. Mori, A. Gómez-Tuena, Y. Cai and S. L. Goldstein. (2007) Effects of prolonged flat subduction on the Miocene magmatic record of the central Trans-Mexican Volcanic Belt. *Chemical Geology* **244**:452–473. doi:10.1016/j.chemgeo.2007.07.002

L. Mori, A. Gómez-Tuena, P. Schaaf, S. L. Goldstein, O. Pérez-Arvizu and G. Solís-Pichardo. (2009) Lithospheric removal as a trigger for flood basalt magmatism in the Trans-Mexican Volcanic Belt. *Journal of Petrology* **50**:2157–2186. doi:10.1093/petrology/egp072

F. Moynier, T. Fujii, G. A. Brennecka and S. G. Nielsen. (2013) Nuclear field shift in natural environments. *Comptes Rendus Geoscience* **345**:150–159. doi:10.1016/j.crte.2013.01.004

H. Nagasawa. (1973) Rare-earth distribution in alkali rocks from Oki-Dogo Island, Japan. *Contributions to Mineralogy and Petrology* **39**:301–308. doi:10.1007/BF00376470

H. Nagasawa, H. Higuchi and N. Onuma. (1969) Rare earths in peridotite nodules: an explanation of the genetic relationship between basalt and peridotite nodules. *Earth and Planetary Science Letters* **5**:377–381. doi:10.1016/S0012-821X(68)80067-6

O. Nebel and K. Mezger. (2006) Reassessment of the NBS SRM-607 K-feldspar as a high precision Rb/Sr and Sr isotope reference. *Chemical Geology* **233**:337–345. doi:10.1016/j.chemgeo.2006.03.003

H. E. Newsom, W. M. White, K. P. Jochum and A. W. Hofmann. (1986) Siderophile and chalcophile element abundances in oceanic basalts, Pb isotope evolution and growth of the Earth's core. *Earth and Planetary Science Letters* **80**:299–313. doi:10.1016/0012-821X(86)90112-3

S. G. Nielsen, M. Goff, S. P. Hesselbo, H. C. Jenkyns, D. E. LaRowe and C.-T. A. Lee. (2011) Thallium isotopes in early diagenetic pyrite – a palaeoredox proxy? *Geochimica et Cosmochimica Acta* **75**:6690–6704. doi:10.1016/j.gca.2011.07.047

S. G. Nielsen, F. Klein, T. Kading, J. Blusztajn and K. Wickham. (2015) Thallium as a tracer of fluid-rock interaction in the shallow Mariana forearc. *Earth and Planetary Science Letters* **430**:416–426. doi:10.1016/j.epsl.2015.09.001

S. G. Nielsen, S. Mar-Gerrison, A. Gannoun, D. LaRowe, V. Klemm, A. N. Halliday, K. W. Burton and J. R. Hein. (2009a) Thallium isotope evidence for a permanent increase in marine organic carbon export in the early Eocene. *Earth and Planetary Science Letters* **278**:297–307. doi:10.1016/j.epsl.2008.12.010

S. G. Nielsen, J. Prytulak, J. Blusztajn, Y. Shu, M. Auro, M. Regelous and J. Walker. (2017a) Thallium isotopes as tracers of recycled materials in subduction zones: review and new data for lavas from Tonga-Kermadec and Central America. *Journal of Volcanology and Geothermal Research* **339**:23–40. doi:10.1016/j.jvolgeores.2017.04.024

S. G. Nielsen, J. Prytulak and M. Rehkämper. (2017b) Investigation and application of thallium isotope fractionation. *Reviews in Mineralogy and Geochemistry* **82**:799–850. doi:10.2138/rmg.2017.82.18

S. G. Nielsen and M. Rehkämper. (2011) Thallium isotopes and their application to problems in Earth and Environmental Sciences. In: M. Baskaran. (ed.), *Handbook of Environmental Isotope Geochemistry*. Springer-Verlag Berlin, Heidelberg. doi:10.1007/978-3-642-10637-8_13

S. G. Nielsen, M. Rehkämper, J. Baker and A. N. Halliday. (2004) The precise and accurate determination of thallium isotope compositions and concentrations for water samples by MC-ICPMS. *Chemical Geology* **204**:109–124. doi:10.1016/j.chemgeo.2003.11.006

S. G. Nielsen, M. Rehkämper, A. D. Brandon, M. D. Norman, S. Turner and S. Y. O'Reilly. (2007) Thallium isotopes in Iceland and Azores lavas — implications for the role of altered crust and mantle geochemistry. *Earth and Planetary Science Letters* **264**:332–345. doi:10.1016/j.epsl.2007.10.008

S. G. Nielsen, M. Rehkämper and A. N. Halliday. (2006a) Large thallium isotopic variations in iron meteorites and evidence for lead-205 in the early solar system. *Geochimica et Cosmochimica Acta* **70**:2643–2657. doi:10.1016/j.gca.2006.02.012

S. G. Nielsen, M. Rehkämper, M. D. Norman, A. N. Halliday and D. Harrison. (2006b) Thallium isotopic evidence for ferromanganese sediments in the mantle source of Hawaiian basalts. *Nature* **439**:314–317. doi:10.1038/nature04450

S. G. Nielsen, M. Rehkämper, D. Porcelli, P. Andersson, A. N. Halliday, P. W. Swarzenski, C. Latkoczy and D. Günther. (2005) Thallium isotope composition of the upper continental crust and rivers–an investigation of the continental sources of dissolved marine thallium. *Geochimica et Cosmochimica Acta* **19**:2007–2019. doi:10.1016/j.gca.2004.10.025

S. G. Nielsen, M. Rehkämper, D. A. H. Teagle, D. A. Butterfield, J. C. Alt and A. N. Halliday. (2006c) Hydrothermal fluid fluxes calculated from the isotopic mass balance of thallium in the ocean crust. *Earth and Planetary Science Letters* **251**:120–133. doi:10.1016/j.epsl.2006.09.002

S. G. Nielsen, N. Shimizu, C.-T. A. Lee and M. D. Behn. (2014) Chalcophile behaviour of thallium during MORB melting and implications for the sulfur content of the mantle. *Geochemistry, Geophysics, Geosystems* **15**:4905–4919. doi:10.1002/2014GC005536

S. G. Nielsen, Y. Shu, B. J. Wood, J. Blusztajn, C. Auro, C. A. Norris and G. Wörner. (2021) Thallium isotope fractionation during magma degassing: evidence from experiments and Kamchatka arc lavas. *Geochemistry, Geophysics, Geosystems* **22**:e2020GC009608. doi:10.1029/2020GC009608

S. G. Nielsen, L. E. Wasylenki, M. Rehkämper, C. L. Peacock, Z. Xue and E. M. Moon. (2013) Towards an understanding of thallium isotope fractionation during adsorption to manganese oxides. *Geochimica et Cosmochimica Acta* **117**:252–265. doi:10.1016/j.gca.2013.05.004

S. G. Nielsen, H. M. Williams, W. L. Griffin, S. Y. O'Reilly, N. Pearson and F. Viljoen. (2009b) Thallium isotopes as a potential tracer for the origin of cratonic eclogites. *Geochimica et Cosmochimica Acta* **73**:7387–7398. doi:10.1016/j.gca.2009.09.001

S. G. Nielsen, G. Yogodzinski, J. Prytulak, T. Plank, S. M. Kay, R. W. Kay, J. Blusztajn, J. D. Owens, M. Auro and T. Kading. (2016) Tracking along-arc sediment inputs to the Aleutian arc using thallium isotopes. *Geochimica et Cosmochimica Acta* **181**:217–237. doi:10.1016/j.gca.2016.03.010

Y. Niu. (1997) Mantle melting and melt extraction processes beneath ocean ridges: evidence from abyssal peridotites. *Journal of Petrology* **38**:1047–1074. doi:10.1093/petroj/38.8.1047

P. D. Noll, Jr, H. E. Newsom, W. P. Leeman and J. G. Ryan. (1996) The role of hydrothermal fluids in the production of subduction zone magmas: evidence from siderophile and chalcophile trace elements and boron. *Geochimica et Cosmochimica Acta* **60**:587–611. doi:10.1016/0016-7037(95)00405-X

J. O. Nriagu. (ed.) (1998) *Thallium in the environment*. Wiley, New York. ISBN 0471177555

V. Okrugin, M. Favero, A. Liu, B. Etschmann, E. Plutachina, S. Mills, A. G. Tomkins, M. Lukasheva, V. Kozlov, S. Moskaleva, M. Chubarov and J. Brugger. (2017) Smoking gun for thallium geochemistry in volcanic arcs: Nataliyamalikite, TlI, a new thallium mineral from an active fumarole at Avacha Volcano, Kamchatka Peninsula, Russia. *American Mineralogist* **102**:1736–1746. doi:10.2138/am-2017-6057

H. S. C. O'Neill and J. A. Mavrogenes. (2002) The sulfide capacity and the sulfur content at sulfide saturation of silicate melts at 1400 °C and 1 bar. *Journal of Petrology* **43**:1049–1087. doi:10.1093/petrology/43.6.1049

T. Orozco-Esquivel, C. M. Petrone, L. Ferrari and P. Tagami, T. Manetti. (2007) Geochemical and isotopic variability in lavas from the eastern Trans-Mexican Volcanic Belt: slab detachment in a subduction zone with varying dip. *Lithos* **93**:149–174. doi:10.1016/j.lithos.2006.06.006

F. Ortega-Gutierrez, J. Ruiz and E. Centeno-Garcia. (1995) Oaxaquia, a Proterozoic microcontinent accreted to North America during the late Paleozoic. *Geology* **23**:1127–1130. doi:10.1130/0091-7613(1995)023<1127:OAPMAT>2.3.CO;2

R. G. Ostic, H. M. Elbadry and T. P. Kohman. (1969) Isotopic composition of meteoritic thallium. *Earth and Planetary Science Letters* **7**:72–76. doi:10.1016/0012-821X(69)90015-6

J. D. Owens, S. G. Nielsen, T. J. Horner, C. M. Ostrander and L. C. Peterson. (2017) Thallium-isotopic compositions of euxinic sediments as a proxy for global manganese-oxide burial. *Geochimica et Cosmochimica Acta* **213**:291–307. doi:10.1016/j.gca.2017.06.041

R. Paisley, K. Berlo, J. Whattam, C. I. Schipper and H. Tuffen. (2019) Degassing-induced chemical heterogeneity at the 2011–2012 Cordón Caulle eruption. *Volcanica* **2**:211–237. doi:10.30909/vol.02.02.211237

C. S. Palk, M. Rehkämper, R. Andreasen and A. Stunt. (2011) Extreme cadmium and thallium isotope fractionations in enstatite chondrites. *Meteoritics and Planetary Science* **46**:A183

H. Palme and H. S. C. O'Neill. (2014) Cosmochemical estimates of mantle composition. In: D. H. Heinrich and K. T. Karl. (eds.), *Treatise on Geochemistry (Second Edition)*, pp. 1–38. Elsevier, Amsterdam. doi:10.1016/B978-0-08-095975-7.00201-1

M. S. Panfil, T. W. Gardner and K. G. Hirth. (1999) Late Holocene stratigraphy of the Tetimpa archaeological sites, northeast flank of Popocatépetl volcano, central Mexico. *GSA Bulletin* **111**:204–218. doi:10.1130/0016-7606(1999)111<0204:LHSOTT>2.3.CO;2

J.-W. Park, Z. Hu, S. Gao, L. H. Campbell and H. Gong. (2012) Platinum group element abundances in the upper continental crust revisited – new constraints from analyses of Chinese loess. *Geochimica et Cosmochimica Acta* **93**:63–76. doi:10.1016/j.gca.2012.06.026

J. Parks, S. Lin, D. W. Davis, X.-M. Yang, R. A. Creaser and M. T. Corkery. (2014) Meso- and Neoarchean evolution of the Island Lake greenstone belt and the northwestern Superior Province: evidence from lithogeochemistry, Nd isotope data, and U-Pb zircon geochronology. *Precambrian Research* **246**:160–179. doi:10.1016/j.precamres.2014.02.016

C. L. Peacock and E. M. Moon. (2012) Oxidative scavenging of thallium by birnessite: explanation for thallium enrichment and stable isotope fractionation in marine ferromanganese precipitates. *Geochimica et Cosmochimica Acta* **84**:297–313. doi:10.1016/j.gca.2012.01.036

I. V. Pekov, N. V. Zubkova, D. I. Belakovskiy, V. O. Yapaskurt, M. F. Vigasina, I. S. Lykova, E. G. Sidorov and D. Y. Pushcharovsky. (2015) Chrysothallite $K_6Cu_6Tl^{3+}Cl_{17}(OH)_4{\cdot}H_2O$, a new mineral species from the Tolbachik volcano, Kamchatka, Russia. *Mineralogical Magazine* **79**:365–376. doi:10.1180/minmag.2015.079.2.14

A. L. J. Peter and T. Viraraghavan. (2005) Thallium: a review of public health and environmental concerns. *Environment International* **31**:493–501. doi:10.1016/j.envint.2004.09.003

C. M. Petrone. (2010) Relationship between monogenetic magmatism and stratovolcanoes in western Mexico: the role of low-pressure magmatic processes. *Lithos* **119**:585–606. doi:10.1016/j.lithos.2010.08.012

C. M. Petrone, L. Francalanci, L. Carlson, R. W.and Ferrari and S. Conticelli. (2003) Unusual co-existence of subduction-related and intraplate-type magmatism: Sr, Nd and Pb isotope and trace element data from the magmatism of the San Pedro–Ceboruco graben (Nayarit, Mexico). *Chemical Geology* **193**:1–24. doi:10.1016/S0009-2541(02)00229-2

C. M. Petrone, T. Orozco-Esquivel and L. Ferrari. (2014) Petrogenesis and geodynamic significance of silicic volcanism in the western Trans-Mexican Volcanic Belt: role of gabbroic cumulates. *Contributions to Mineralogy and Petrology* **167**:1006. doi:10.1007/s00410-014-1006-6

D. Z. Piper. (1974) Rare earth elements in ferromanganese nodules and other marine phases. *Geochimica et Cosmochimica Acta* **38**:1007–1022. doi:10.1016/0016-7037(74)90002-7

T. Plank and C. H. Langmuir. (1998) The chemical composition of subducting sediment and its consequences for the crust and mantle. *Chemical Geology* **145**:325–394. doi:10.1016/S0009-2541(97)00150-2

T. Plank, J. N. Ludden, C. Escutia, L. J. Abrams, J. C. Alt, R. N. Armstrong, S. R. Barr, A. Bartolini, G. Cairns, M. Fisk, G. Guerin, S. A. Haveman, T. Hirono, J. Honnorez, K. A. Kelley, R. L. Larson, F. M. Lozar, R. W. Murray, T. K. Pletsch, R. A. Pockalny, O. Rouxel, A. Schmidt, D. C. Smith, A. J. Spivack, H. Staudigel, M. B. Steiner and R. B. Valentine. (2000) Izu-Mariana margin. *Proceedings of the Ocean Drilling Program, Initial Reports* **185**. doi:10.2973/odp.proc.ir.185.2000

P. Plunket and G. Uruñela. (2008) Mountain of sustenance, mountain of destruction: the prehispanic experience with Popocatépetl Volcano. *Journal of Volcanology and Geophysical Research* **170**:111–120. doi:10.1016/j.jvolgeores.2007.09.012

S. Poli and M. W. Schmidt. (2002) Petrology of subducted slabs. *Annual Review of Earth and Planetary Sciences* **30**:207–235. doi:10.1146/annurev.earth.30.091201.140550

J. T. Prosser and M. J. Carr. (1987) Poás volcano, Costa Rica: Geology of the summit region and spatial and temporal variations among the most recent lavas. *Journal of Volcanology and Geothermal Research* **33**:131–146. doi:10.1016/0377-0273(87)90057-6

J. Prytulak, E. K. A. Brett, M. Webb, M. Rehkämper, T. Plank, P. S. Savage and J. Woodhead. (2017) Thallium elemental behavior and stable isotope fractionation during magmatic processes. *Chemical Geology* **448**:71–83. doi:10.1016/j.chemgeo.2016.11.007

J. Prytulak, S. G. Nielsen, T. Plank, M. Barker and T. Elliott. (2013) Assessing the utility of thallium and thallium isotopes for tracing subduction zone inputs to the Mariana arc. *Chemical Geology* **345**:129–149. doi:10.1016/j.chemgeo.2013.03.003

J. D. Pérez-Orozco, G. Sosa-Ceballos, V. H. Garduño-Monroy and D. R. Avellán. (2018) Felsic-intermediate magmatism and brittle deformation in Sierra del Tzirate (Michoacán-Guanajuato Volcanic Field). *Journal of South American Earth Sciences* **85**:81–96. doi:10.1016/j.jsames.2018.04.021

S. T. Rader, F. K. Mazdab and M. D. Barton. (2018) Mineralogical thallium geochemistry and isotope variations from igneous, metamorphic, and metasomatic systems. *Geochimica et Cosmochimica Acta* **243**:42–65. doi:10.1016/j.gca.2018.09.019

B. C. Reed. (2010) A spreadsheet for linear least-squares fitting with errors in both coordinates. *Physics Education* **45**:93–96. doi:10.1088/0031-9120/45/1/011

C. D. J. Reekie, F. E. Jenner, D. J. Smythe, E. H. Hauri, E. S. Bullock and H. M. Williams. (2019) Sulfide resorption during crustal ascent and degassing of oceanic plateau basalts. *Nature Communications* **10**:82. doi:10.1038/s41467-018-08001-3

M. Rehkämper, M. Frank, J. R. Hein and A. Halliday. (2004) Cenozoic marine geochemistry of thallium deduced from isotopic studies of ferromanganese crusts and pelagic sediments. *Earth and Planetary Science Letters* **219**:77–91. doi:10.1016/S0012-821X(03)00703-9

M. Rehkämper, M. Frank, J. R. Hein, D. Porcelli, A. N. Halliday, J. Ingri and V. Liebetrau. (2002) Thallium isotope variations in seawater and hydrogenetic, diagenetic, and hydrothermal ferromanganese deposits. *Earth and Planetary Science Letters* **197**:65–81. doi:10.1016/S0012-821X(02)00462-4

M. Rehkämper and A. N. Halliday. (1999) The precise measurement of Tl isotopic compositions by MC-ICPMS: application to the analysis of geological materials and meteorites. *Geochimica et Cosmochimica Acta* **63**:935–944. doi:10.1016/S0016-7037(98)00312-3

M. Rehkämper and S. G. Nielsen. (2004) The mass balance of dissolved thallium in the oceans. *Marine Chemistry* **85**:125–139. doi:10.1016/j.marchem.2003.09.006

M. Rehkämper and K. Mezger. (2000) Investigation of matrix effects for Pb isotope ratio measurements by multiple collector ICP-MS: verification and application of optimized analytical protocols. *Analytical Atomic Spectrometry* **15**:1451–1460. doi:10.1039/B005262K

M. A. Richards, R. A. Duncan and V. E. Courtillot. (1989) Flood basalts and hot-spot tracks: plume heads and tails. *Science* **246**:103–107. doi:10.1126/science.246.4926.103

J. Roberge, H. Delgado-Granados and P. J. Wallace. (2009) Mafic magma recharge supplies high CO2 and SO2 gas fluxes from Popocatépetl volcano, Mexico. *Geology* **37**:107–110. doi:10.1130/G25242A.1

A. C. Roberts, K. E. Venance, T. M. Seward, J. D. Grice and W. H. Paar. (2006) Lafossaite: a new mineral from the La Fossa Crater, Vulcano, Italy. *Mineralogical Record* **37**:165–168

C. C. M. Robin-Popieul, N. T. Arndt, C. Chauvel, G. R. Byerly, A. V. Sobolev and A. Wilson. (2012) A new model for Barberton Komatiites: Deep critical melting with high melt retention. *Journal of Petrology* **53**:2191–2229. doi:10.1093/petrology

R. L. Rudnick. (1998) *Elements: Large-ion lithophile*, pp. 213–214. Springer Netherlands, Dordrecht. ISBN 978-1-4020-4496-0. doi:10.1007/1-4020-4496-8_104

R. L. Rudnick and S. Gao. (2003) Composition of the continental crust. *Treatise on Geochemistry* **3**:1–64. doi:10.1016/B0-08-043751-6/03016-4

N. Sainlot, I. Vlastélic, S. Moune, E. F. Rose-Koga, F. Schiavi, S. Valade and F. Aguilera. (2020) Uptake of gaseous thallium, tellurium, vanadium and molybdenum into anhydrous alum, Lascar volcano fumaroles, Chile. *Geochimica et Cosmochimica Acta* **275**:64–82. doi:10.1016/j.gca.2020.02.009

V. J. M. Salters. (1998) *Elements: High field strength*, pp. 209–210. Springer Netherlands, Dordrecht. ISBN 978-1-4020-4496-0. doi:10.1007/1-4020-4496-8_101

V. J. M. Salters and H. J. B. Dick. (2002) Mineralogy of the mid-ocean-ridge basalt source from neodymium isotopic composition of abyssal peridotites. *Nature* **418**:68–72. doi:10.1038/nature00798

V. J. M. Salters and J. Longhi. (1999) Trace element partitioning during the initial stages of melting beneath mid-ocean ridges. *Earth and Planetary Science Letters* **166**:15–30. doi:10.1016/S0012-821X(98)00271-4

V. J. M. Salters, S. Mallick, S. R. Hart, C. E. Langmuir and A. Stracke. (2011) Domains of depleted mantle: New evidence from hafnium and neodymium isotopes. *Geochemistry, Geophysics, Geosystems* **12**:Q08001. doi:10.1029/2011GC003617

V. J. M. Salters and A. Stracke. (2004) Composition of the depleted mantle. *Geochemistry, Geophysics, Geosystems* **5**:Q05B07. doi:10.1029/2003GC000597

A. Sanfillippo, V. Salters, R. Tribuzio and A. Zanetti. (2019) Role of ancient, ultra-depleted mantle in mid-ocean-ridge magmatism. *Earth and Planetary Science Letters* **511**:89–98. doi:10.1016/j.epsl.2019.01.018

P. Schaaf, W. Heinrich and T. Besch. (1994) Composition and Sm-Nd isotopic data of the lower crust beneath San Luis Potosí, central Mexico: evidence from a granulite-facies xenolith suite. *Chemical Geology* **118**:63–84. doi:10.1016/0009-2541(94)90170-8

P. Schaaf, J. Stimac, C. Siebe and J. L. Macías. (2005) Geochemical evidence for mantle origin and crustal processes in volcanic rocks from Popocatépetl and surrounding monogenetic volcanoes, central Mexico. *Journal of Petrology* **46**:1243–1282. doi:10.1093/petrology/egi015

E. A. Schauble. (2004) Applying stable isotope fractionation theory to new systems. *Reviews in Mineralogy and Geochemistry* **55**:65–111. doi:10.2138/gsrmg.55.1.65

E. A. Schauble. (2007) Role of nuclear volume in driving equilibrium stable isotope fractionation of mercury, thallium, and other very heavy elements. *Geochimica et Cosmochimica Acta* **71**:2170–2189. doi:10.1016/j.gca.2007.02.004

M. W. Schmidt and S. Poli. (1998) Experimentally based water budgets for dehydrating slabs and consequences for arc magma generation. *Earth and Planetary Science Letters* **163**:361–379. doi:10.1016/S0012-821X(98)00142-3

M. W. Schmidt, D. Vielzeuf and E. Auzanneau. (2004) Melting and dissolution of subducting crust at high pressures: the key role of white mica. *Earth and Planetary Science Letters* **228**:65–84. doi:10.1016/j.epsl.2004.09.020

R. Scholtysik and D. Canil. (2018) Condensation behaviour of volatile trace metals in laboratory benchtop fumarole experiments. *Chemical Geology* **492**:49–58. doi:10.1016/j.chemgeo.2018.05.006

D. Schumann and U. Nagel. (1981) Appendix I. X-ray mineralogical analysis. *Initial Reports of Deep Sea Drilling Project* **66**:853–857. doi:10.2973/dsdp.proc.66.app1.1982

Y. Seki and G. C. Kennedy. (1964) The breakdown of potassium feldspar, $KAlSi_3O_8$ at high temperatures and high pressures. *American Mineralogist* **49**:1688–1706

R. D. Shannon. (1976) Revised effective ionic radii and systematic studies of interatomic distances in halides and chalcogenides. *Acta Crystallographica* **A32**:751–767. doi:10.1107/S0567739476001551

R. D. Shannon and C. T. Prewitt. (1969) Effective ionic radii in oxides and fluorides. *Acta Crystallographica* **B25**:925–946. doi:10.1107/S0567740869003220

D. M. Shaw. (1952) The geochemistry of thallium. *Geochimica et Cosmochimica Acta* **2**:118–154. doi:10.1016/0016-7037(52)90003-3

Y. Shu, S. G. Nielsen, H. R. Marschall, T. John, J. Blusztajn and M. Auro. (2019) Closing the loop: subducted eclogites match thallium isotope compositions of ocean island basalts. *Geochimica et Cosmochimica Acta* **250**:130–148. doi:10.1016/j.gca.2019.02.004

Y. Shu, S. G. Nielsen, Z. Zeng, R. Shinjo, J. Blusztajn, X. Wang and S. Chen. (2017) Tracing subducted sediment inputs to the Ryuku arc-Okinawa Trough system: evidence from thallium isotopes. *Geochimica et Cosmochimica Acta* **217**:462–491. doi:10.1016/j.gca.2017.08.035

C. Siebe and J. Macías. (2006) Volcanic hazards in the Mexico City metropolitan area from eruptions at Popocatépetl, Nevado de Toluca, and Jocotitlán stratovolcanoes and monogenetic scoria cones in the Sierra Chichinuatzin Volcanic Field. *Geological Society of America Special Papers* **402**:253. doi:10.1130/2004.VHITMC.SP402

C. Siebe, S. Salinas, L. Arana-Salinas, J. L. Macías, J. Gardner and R. Bonasia. (2017) The ∼23,500 y ^{14}C BP White Pumice Plinian eruption and associated debris avalanche and Tochimilco lava flow of Popocatépetl volcano, México. *Journal of Volcanology and Geothermal Research* **333–334**:66–95. doi:10.1016/j.jvolgeores.2017.01.011

C. Siebe, P. Schaaf and J. Urrutia-Fucugauchi. (1999) Mammoth bones embedded in a late Pleistocene lahar from Popocatépetl volcano, near Tocuila, central Mexico. *GSA Bulletin* **111**:1550–1562. doi:10.1130/0016-7606(1999)111<1550:MBEIAL>2.3.CO;2

O. I. Siidra, L. P. Vergasova, Y. L. Kretser, Y. S. Polekhovsky, S. K. Filatov and S. V. Krivovichev. (2014a) Unique thallium mineralization in the fumaroles of the Tolbachik volcano, Kamchatka Peninsula, Russia. II. Karpovite, $Tl_2VO(SO_4)_2(H_2O)$. *Mineralogical Magazine* **78**:1699–1709. doi:10.1180/minmag.2014.078.7.13

O. I. Siidra, L. P. Vergasova, S. V. Krivovichev, Y. L. Kretser, A. N. Zaitsev and S. K. Filatov. (2014b) Unique thallium mineralization in the fumaroles of Tolbachik volcano, Kamchatka Peninsula, Russia. I. Markhininite, $TlBi(SO_4)_2$. *Mineralogical Magazine* **78**:1687–1698. doi:10.1180/minmag.2014.078.7.12

O. L. Siidra, L. P. Vergasova, Y. L. Kretser, Y. S. Polekhovsky, S. K. Filatov and S. V. Krivovichev. (2014c) Unique thallium mineralization in the fumaroles of Tolbachik volcano, Kamchatka Peninsula, Russia. III. Evdokimovite, $Tl_4(VO)_3(SO_4)_5(H_2O)_5$. *Mineralogical Magazine* **78**:1711–1724. doi:10.1180/minmag.2014.078.7.14

K. W. W. Sims and D. J. DePaolo. (1997) Inferences about mantle magma sources from incompatible element concentration ratios in oceanic basalts. *Geochimica et Cosmochimica Acta* **61**:765–784. doi:10.1016/S0016-7037(96)00372-9

P. D. Snavely, Jr, N. S. MacLeod, F. J. Flanagan, S. Berman, H. G. Neiman and H. Bastron. (1976) Nepheline syenite, STM-1, from Table Mountain, Oregon. In: F. Flanagan. (ed.), *Descriptions and analyses of eight new USGS rock standards*, volume 840 of *United States Geological Survey Professional Paper*, pp. 7–10. United States Geological Survey

G. Sosa-Ceballos, J. E. Gardner, C. Siebe and J. L. Macías. (2012) A caldera-forming eruption $\sim$ 14,100 ^{14}C yr BP at Popocatépetl volcano, México: insights from eruption dynamics and magma mixing. *Journal of Volcanology and Geothermal Research* **213–214**:27–40. doi:10.1016/j.jvolgeores.2011.11.001

G. Sosa-Ceballos, J. L. Macías, D. R. Avellán, N. Salazar-Hermenegildo, M. E. Boijseauneau-López and J. D. Pérez-Orozco. (2018) The Acoculco Caldera Complex magmas: genesis, evolution and relation with the Acoculco geothermal system. *Journal of Volcanology and Geothermal Research* **358**:288–306. doi:10.1016/j.jvolgeores.2018.06.002

J. W. Sparks. (1995) Geochemistry of the lower sheeted dyke complex, Hole 504B, Leg 140. *Proceedings of the Ocean Drilling Program Scientific Results* **137**:81–97. ISSN 0884-5891

H. Staudigel, G. Davies, S. R. Hart, K. M. Marchant and B. M. Smith. (1995) Large scale Sr, Nd, and O isotopic anatomy of altered oceanic crust at DSDP/ODP sites 417/418. *Earth and Planetary Science Letters* **130**:169–185. doi:10.1016/0012-821X(94)00263-X

A. Stracke. (2012) Earth's heterogeneous mantle: A product of convection-driven interaction between crust and mantle. *Chemical Geology* **330–331**:274–299. doi:10.1016/j.chemgeo.2012.08.007

A. Stracke, M. Bizimis and V. J. M. Salters. (2003) Recycling oceanic crust: quantitative constraints. *Geochemistry, Geophysics, Geosystems* **4**:8003. doi:10.1029/2001GC000223

A. Stracke and B. Bourdon. (2009) The importance of melt extraction for tracing mantle heterogeneity. *Geochimica et Cosmochimica Acta* **73**:218–238. doi:10.1016/j.gca.2008.10.015

A. Stracke, F. Genske, J. Berndt and J. M. Koornneef. (2019) Ubiquitous ultra-depleted domains in Earth's mantle. *Nature Geosciences* **12**:851–855. doi:10.1038/s41561-019-0446-z

A. Stracke, A. W. Hofmann and S. R. Hart. (2005) FOZO, HIMU, and the rest of the mantle zoo. *Geochemistry, Geophysics, Geosystems* **6**:Q05007. doi:10.1029/2004GC000824

A. Stracke, J. E. Snow, E. Hellebrand, A. von der Handt, B. Bourdon, K. Birbaun and D. Günther. (2011) Abyssal peridotite Hf isotopes identify extreme mantle depletion. *Earth and Planetary Science Letters* **308**:359–368. doi:10.1016/j.epsl.2011.06.012

S. M. Straub, A. Gómez-Tuena, I. N. Bindeman, L. L. Bolge, P. A. Brandl, R. Espinasa-Perena, L. Solari, F. M. Stuart, P. Vannucchi and G. F. Zellmer. (2015) Crustal recycling by subduction erosion in the central Mexican Volcanic Belt. *Geochimica et Cosmochimica Acta* **166**:29–52. doi:10.1016/j.gca.2015.06.001

S. M. Straub, A. Gómez-Tuena and P. Vannucchi. (2020) Subduction erosion and volcanism. *Nature Reviews Earth & Environment* **1**:574–589. doi:10.1038/s43017-020-0095-1

S. M. Straub, A. Gómez-Tuena, G. F. Zellner, R. Espinasa-Perena, F. M. Stuart, Y. Cai, C. H. Langmuir, A. L. Martin-Del Pozzo and G. T. Mesko. (2012) The processes of melt differentiation in arc volcanic rocks: insights from OIB-type arc magmas in the central Mexican Volcanic Belt. *Journal of Petrology* **54**:665–701. doi:10.1093/petrology/egs081

S. M. Straub, A. B. LaGatta, A. L. Martin-Del Pozzo and C. H. Langmuir. (2008) Evidence from high-Ni olivines for a hybridized peridotite/pyroxenite source for orogenic andesites from the central Mexican Volcanic Belt. *Geochemistry, Geophysics, Geosystems* **9**:Q03007. doi:10.1029/2007GC001583

N. Stromsoe, J. N. Callow, H. A. McGowan and S. K. Marx. (2013) Attribution of sources to metal accumulation in an alpine tarn, the Snowy Mountains, Australia. *Environmental Pollution* **181**:133–143. doi:10.1016/j.envpol.2013.05.051

C. Sun and Y. Liang. (2012) Distribution of REE between clinopyroxene and basaltic melt along a mantle adiabat: effects of major element composition, water, and temperature. *Contributions to Mineralogy and Petrology* **163**:807–823. doi:10.1007/s00410-011-0700-x

S.-s. Sun. (1980) Lead isotopic study of young volcanic rocks from mid-ocean ridges, ocean islands and island arcs. *Philosophical Transactions of the Royal Society of London. Series A, Mathematical and Physical Sciences* **297**:409–445. doi:10.1098/rsta.1980.0224

S.-s. Sun and W. F. McDonough. (1989) Chemical and isotopic systematics of oceanic basalts: implications for mantle composition and processes. *Geological Society, London, Special Publications* **42**:313–345. doi:10.1144/GSL.SP.1989.042.01.19

E. M. Syracuse and G. A. Abers. (2006) Global compilation of variations in slab depth beneath arc volcanoes and implications. *Geochemistry, Geophysics, Geosystems* **7**:Q05017. doi:10.1029/2005GC001045

N. Søager, M. Portnyagin, K. Hoernle, P. M. Holm, F. Hauff and D. Garbe-Schönberg. (2015) Olivine major and trace element compositions in southern Payenia basalts, Argentina: evidence for pyroxenite–peridotite melt mixing in a back-arc setting. *Journal of Petrology* **56**:1495–1518. doi:10.1093/petrology/egv043

D. A. H. Teagle, J. C. Alt, W. Bach, A. N. Halliday and J. Erzinger. (1996) Alteration of upper ocean crust in a ridge-flank hydrothermal upflow zone: mineral, chemical and isotopic constraints from Hole 896A. *Proceedings of the Ocean Drilling Program, Scientific Results* **148**:39–55. doi:10.2973/odp.proc.sr.148.113.1996

F.-G. Teng, J. Watkins and N. Dauphas. (eds.) (2017) *Non-traditional stable isotopes*, volume 82 of *Reviews in Mineralogy and Geochemistry*. ISSN 1529-6466

F.-Z. Teng. (2017) Magnesium isotope geochemistry. *Reviews in Mineralogy and Geochemistry* **82**:165–217. doi:10.2138/rmg.2017.82.6

F. Tera, L. Brown, J. Morris, I. S. Sacks, J. Klein and R. Middleton. (1986) Sediment incorporation in island-arc magmas: inferences from ^{10}Be. *Geochimica et Cosmochimica Acta* **50**:535–550. doi:10.1016/0016-7037(86)90103-1

M. H. Thiemens and J. E. Heidenreich III. (1983) The mass-independent fractionation of oxygen: a novel isotope effect and its possible cosmochemical implications. *Science* **219**:1073–1075. doi:10.1126/science.219.4588.1073

C. Timm, K. A. Hoernle, P. van den Bogaard, I. N. Bindeman and S. D. Weaver. (2009) Geochemical evolution of intraplate volcanism at Banks Peninsula, New Zealand: interaction between asthenospheric and lithospheric melts. *Journal of Petrology* **50**:989–1023. doi:10.1093/petrology/egp029

A. G. Tomkins and K. A. Evans. (2015) Separate zones of sulfate and sulfide release from subducted mafic oceanic crust. *Earth and Planetary Science Letters* **428**:73–83. doi:10.1016/j.epsl.2015.07.028

M. Uchimizu. (1966) Geology and petrology of alkali rocks from Dogo, Oki Islands. *Journal of the Faculty of Science, University of Tokyo, Section 2* **16**:85–159

S. Urakawa, T. Kondo, N. Igawa, O. Shimomura and H. Ohno. (1994) Synchrotron radiation study on the high-pressure and high-temperature phase relations of $KAlSi_3O_8$. *Physics and Chemistry of Minerals* **21**:387–391. doi:10.1007/BF00203296

H. C. Urey. (1947) The thermodynamic properties of isotopic substances. *Journal of the Chemical Society* **5**:562–581. doi:10.1039/JR9470000562

I. T. Uysal, M. Gasparon, R. Bolhar, J.-X. Zhao, Y.-X. Feng and G. Jones. (2011) Trace element composition of near-surface silica deposits—a powerful tool for detecting hydrothermal mineral and energy resources. *Chemical Geology* **280**:154–169. doi:10.1016/j.chemgeo.2010.11.005

F. van der Straaten, V. Schenk, T. John and J. Gao. (2008) Blueschist-facies rehydration of eclogites (Tian Shan, NW-China): implications for fluid-rock interaction in the subduction channel. *Chemical Geology* **255**:195–219. doi:10.1016/j.chemgeo.2008.06.037

R. Vannucci, B. Bottazzi, E. Wulff-Pedersen and E.-R. Neumann. (1998) Partitioning of REE, Y, Sr, Zr and Ti between clinopyroxene and silicate melts in the mantle under La Palma (Canary Islands): implications for the nature of the metasomatic agents. *Earth and Planetary Science Letters* **158**:39–51. doi:10.1016/S0012-821X(98)00040-5

A. Vaněk, Z. Grösslová, M. Mihaljevič, V. Ettler, J. Trubač, V. Chrastný, V. Penížek, L. Teper, J. Cabala, A. Voegelin, T. Zádorová, V. Oborná, O. Drábek, O. Holubík, J. Houška, L. Pavlů and C. Ash. (2018) Thallium isotopes in metallurgical wastes/contaminated soils: a novel tool to trace metal source and behavior. *Journal of Hazardous Materials* **343**:78–85. doi:10.1016/j.jhazmat.2017.09.020

B. W. Vink. (1993) The behaviour of thallium in the (sub)surface environment in terms of Eh and pH. *Chemical Geology* **109**:119–123. doi:10.1016/0009-2541(93)90065-Q

T. A. Vogel, L. C. Patino, G. E. Alvarade and P. B. Gans. (2004) Silicic ignimbrites within the Costa Rican volcanic front: evidence for the formation of continental crust. *Earth and Planetary Science Letters* **226**:149–159. doi:10.1016/j.epsl.2004.07.013

J. B. Walters, A. M. Cruz-Uribe and H. R. Marschall. (2020) Sulfur loss from subducted altered oceanic crust and implications for mantle oxidation. *Geochemical Perspectives Letters* **13**:36–41. doi:10.7185/geochemlet.2011

Z. Wang, H. Becker and F. Wombacher. (2015) Mass fractions of S, Cu, Se, Mo, Ag, Cd, In, Te, Ba, Sm, W, Tl and Bi in geological reference materials and selected carbonaceous chondrites determined by isotope dilution ICP-MS. *Geostandards and Geoanalytical Research* **39**:185–208. doi:10.1111/j.1751-908X.2014.00312.x

Z. Wang, M. Lazarov, L. K. Steinmann, H. Becker, Z. Zou and X. Geng. (2018) The distribution of lead and thallium in mantle rocks: Insights from the Balmuccia peridotite massif (Italian Alps). *American Mineralogist* **103**:1185–1199. doi:10.2138/am-2018-6423

L. E. Wasylenki, M. B. Baker, A. J. R. Kent and E. M. Stolper. (2003) Near-solidus melting of the shallow upper mantle: partial melting experiments on depleted peridotite. *Journal of Petrology* **44**:1163–1191. doi:10.1093/petrology/44.7.1163

J. S. Watkins, K. J. McMillen, S. B. Bachman, T. H. Shipley, J. C. Moore and C. Angevine. (1981) Tectonic synthesis, Leg 66: transect and vicinity. *Initial Reports of Deep Sea Drilling Project* **66**:837–849. doi:10.2973/dsdp.proc.66.143.1982

B. L. Weaver. (1991) The origin of ocean island basalt end-member compositions: trace element and isotopic constraints. *Earth and Planetary Science Letters* **104**:381–397. doi:10.1016/0012-821X(91)90217-6

H. Wehrmann, K. Hoernle, D. Garbe-Schönberg, G. Jacques, J. Mahlke and K. Schumann. (2014) Insights from trace element geochemistry as to the roles of subduction zone geometry and

subduction input on the chemistry of arc magmas. *International Journal of Earth Sciences* **103**:1929–1944. doi:10.1007/s00531-013-0917-1

D. Weis and F. A. Frey. (1991) Isotope geochemistry of Ninetyeast Ridge basement basalts: Sr, Nd, and Pb evidence for involvement of the Kerguelen hot spot. *Proceedings of the Ocean Drilling Program, Scientific Results* **121**:591–610. doi:10.2973/odp.proc.sr.121.170.1991

D. Weis, B. Kieffer, C. Maerschalk, J. Barling, J. de Jong, G. A. Williams, D. Hanano, W. Pretorious, N. Mattielli, J. S. Scoates, A. Goolaerts, R. M. Friedman and J. B. Mahoney. (2006) High-precision isotopic characterization of USGS reference materials by TIMS and MC-ICP-MS. *Geochemistry Geophysics Geosystems* **7**:Q08006. doi:10.1029/2006GC001283

S. A. Whattam and R. J. Stern. (2015) Arc magmatic evolution and the construction of continental crust at the Central American Volcanic Arc system. *International Geology Review* **58**:653–686. doi:10.1080/00206814.2015.1103668

W. B. White. (2015) Probing the Earth's deep interior through geochemistry. *Geochemical Perspectives* **4**:95–251

W. M. White. (1985) Sources of ocean island basalts: Radiogenic isotope evidence. *Geology* **13**:115–118. doi:10.1130/0091-7613(1985)13<115:SOOBRI>2.0.CO;2

W. M. White. (2013) *Geochemistry*. Wiley, New Jersey, USA

W. M. White, F. Albarède and P. Télouk. (2000) High-precision analysis of Pb isotope ratios by multi-collector ICP-MS. *Chemical Geology* **167**:257–270. doi:10.1016/S0009-2541(99)00182-5

W. M. White and A. W. Hofmann. (1982) Sr and Nd isotope geochemistry of oceanic basalts and mantle evolution. *Nature* **296**:821–825. doi:10.1038/296821a0

S. Wick, B. Baeyens, M. Marques Fernandes, J. Göttlicher, M. Fischer, N. Pfenniger, M. Plötze and A. Voegelin. (2020) Thallium sorption and speciation in soils: role of micaceous clay minerals and manganese oxides. *Geochimica et Cosmochimica Acta* **288**:83–100. doi:10.1016/j.gca.2020.07.037

P. E. Wieser, F. Jenner, M. Edmonds, J. Maclennan and B. E. Kunz. (2020) Chalcophile elements track the fate of sulfur at Kīlauea Volcano, Hawai'i. *Geochimica et Cosmochimica Acta* **282**:245–275. doi:10.1016/j.gca.2020.05.018

M. Willbold and A. Stracke. (2006) Trace element composition of mantle end-members: Implications for recycling of oceanic and upper and lower continental crust. *Geochemistry, Geophysics, Geosystems* **7**. doi:10.1029/2005GC001005

M. Willbold and A. Stracke. (2010) Formation of enriched mantle components by recycling of upper and lower continental crust. *Chemical Geology* **276**:188–197. doi:10.1016/j.chemgeo.2010.06.005

S. A. Wilson. (1997a) The collection, preparation, and testing of USGS reference material BCR-2, Columbia River, Basalt. *USGS Open-File Report (in progress)*

S. A. Wilson. (1997b) Data compilation for reference material BHVO-2, Hawaiian Basalt. *USGS Open-File Report (in progress)*

S. A. Wilson. (1998) Data compilation for reference material GSP-2, Granodiorite, Silver Plume, Colorado. *USGS Open-File Report (in progress)*

B. J. Wood and E. S. Kiseeva. (2015) Trace element partitioning into sulfide: how lithophile elements become chalcophile and vice versa. *American Mineralogist* **100**:2371–2379. doi:10.2138/am-2015-5358CCBYNCND

B. J. Wood, S. G. Nielsen, M. Rehkämper and A. N. Halliday. (2008) The effects of core formation on the Pb- and Tl-isotopic composition of the silicate Earth. *Earth and Planetary Science Letters* **269**:326–336. doi:10.1016/j.epsl.2008.01.027

B. J. Wood and R. Trigila. (2001) Experimental determination of aluminous clinopyroxene-melt partition coefficients for potassic liquids, with application to the evolution of the Roman province potassic magmas. *Chemical Geology* **172**:213–223. doi:10.1016/S0009-2541(00)00259-X

J. Woodhead, J. Hergt, A. Greig and L. Edwards. (2011) Subduction zone Hf-anomalies: mantle messenger, melting artefact or crustal process? *Earth and Planetary Science Letters* **304**:231–239. doi:10.1016/j.epsl.2011.01.036

R. K. Workman and S. R. Hart. (2005) Major and trace element composition of the depleted MORB mantle (DMM). *Earth and Planetary Science Letters* **231**:53–72. doi:10.1016/j.epsl.2004.12.005

T. J. Worthington, R. Hekinian, P. Stoffers, T. Kuhn and F. Hauff. (2006) Osbourn Trough: structure, geochemistry and implications of a mid-Cretaceous paleospreading ridge in the South Pacific. *Earth and Planetary Science Letters* **245**:685–701. doi:10.1016/j.epsl.2006.03.018

T. Xiao, J. Guha, D. Boyle, C.-Q. Liu, B. Zheng, G. C. Wilson, A. Rouleau and J. Chen. (2004) Naturally occurring thallium: a hidden geoenvironmental health hazard? *Environment International* **30**:501–507. doi:10.1016/j.envint.2003.10.004

T. F. Xiao, D. Boyle, J. Guha, A. Rouleau, Y. Y. Hong and B. S. Zheng. (2003) Groundwater-related thallium transfer processes and their impacts on the ecosystem: southwest Guizhou Province, China. *Applied Geochemistry* **18**:675–691. doi:10.1016/S0883-2927(02)00154-3

A. Yagi, T. Suzuki and M. Akoagi. (1994) High pressure transitions in the system $KAlSi_3O_8$–$NaAlSi_3O_8$. *Physics and Chemistry of Minerals* **21**:12–17. doi:10.1007/BF00205210

S. Yang, M. Humayun and V. J. M. Salters. (2018) Elemental systematics in MORB glasses from the Mid-Atlantic Ridge. *Geochemistry, Geophysics, Geosystems* **19**:4236–4259. doi:10.1029/2018GC007593

S. Yang and Y. Liu. (2015) Nuclear volume effects in equilibrium stable isotope fractionations of mercury, thallium and lead. *Scientific Reports* **5**:12626. doi:10.1038/srep12626

T. Yokoyama, A. Makishima and E. Nakamura. (1999) Evaluation of the coprecipitation of incompatible trace elements with fluoride during silicate rock dissolution by acid digestion. *Chemical Geology* **157**:175–187. doi:10.1016/S0009-2541(98)00206-X

D. York, N. M. Evensen, M. L. Martinez and J. D. B. Delgado. (2004) Unified equations for the slope, intercept, and standard errors of the best straight line. *American Journal of Physics* **72**:367–375. doi:10.1119/1.1632486

Z. Yu, P. Robinson and P. McGoldrick. (2001) An evaluation of methods for the chemical decomposition of geological materials for trace element determinations using ICP-MS. *Geostandards Newsletter: The Journal of Geostandards and Geoanalysis* **25**:199–217. doi:10.1111/j.1751-908X.2001.tb00596.x

Z. Yu, P. Robinson, A. T. Townsend, C. Münker and A. J. Crawford. (2000) Determination of high field strength elements, Rb, Sr, Mo, Sb, Cs, Tl and Bi at ng g^{-1} levels in geological reference materials by magnetic sector ICP-MS after HF/$HClO_4$ high pressure digestion. *Geostandards Newsletter* **24**:39–50. doi:10.1111/j.1751-908X.2000.tb00585.x

W. Zhang, Z. Hu, Y. Liu, L. Chen, H. Chen, M. Li, L. Zhao, S. Hu and S. Gao. (2012) Reassessment of HF/HNO_3 decomposition capability in the high-pressure digestion of felsic rocks for multi-element determination by ICP-MS. *Geostandards and Geoanalytical Research* **36**:271–289. doi:10.1111/j.1751-908X.2012.00156.x

A. Zindler and S. R. Hart. (1986) Chemical geodynamics. *Annual Reviews of Earth and Planetary Science* **14**:493–571. doi:10.1146/annurev.ea.14.050186.002425

E. Zuleger, J. C. Alt and J. Erzinger. (1996) Data report: trace-element geochemistry of the lower sheeted dike complex, Hole 504B, Leg 140. *Proceedings of the Ocean Drilling Program, Scientific Results* **148**:455–466. doi:10.2973/odp.proc.sr.148.112.1996

Appendix A

List of publications

1. *M. Edmonds, **A. Brett**, R. A. Herd, M. C. S. Humphreys, and A. Woods.* (2014) Magnetite-bubble aggregates at mixing interfaces in andesite magma bodies. *Geological Society*, London, Special Publications, **410**:SP410-7. doi:10.1144/SP410.7

   Contributions:

   - identification and measurement of magnetite and vesicles in pre-existing SEM images
   - statistical analysis of spatial relationships between bubbles and mineral phases, including comparison with synthetic datasets

2. *M. Kersten, T. Xiao, K. Kressig, **A. Brett**, B. J. Coles, and M. Rehkämper.* (2014) Tracing anthropogenic thallium in soil using stable isotope compositions. *Environmental Science & Technology*, **48**:9030-9036. doi:10.1021/es501968d

   Contributions:

   - digestion, chromatographic separation and Tl isotope analysis of Meggen pyrite

3. *M. E. Newcombe, **A. Brett**, J. R. Beckett, M. B. Baker, S. Newman, Y. Guan, J. M. Eiler, E. M. Stolper.* (2017) Solubility of water in lunar basalt at low pH_2O. *Geochimica et Cosmochimica Acta*, **200**:330-352. doi:10.1016/j.gca.2016.12.026

   Contributions:

   - 18 samples (AD1-AD13, LG1-LG7) processed through experimental protocol
   - preparation of samples for analysis, and FTIR analysis of dissolved water content

4. *J. Prytulak, **A. Brett**, M. Webb, T. Plank, M. Rehkämper, P. S. Savage, J. D. Woodhead.* (2017) Thallium elemental behavior and stable isotope fractionation during magmatic processes. *Chemical Geology*, **448**:71-83. doi:10.1016/j.chemgeo.2016.11.007

   Contributions:

   - digestion, chromatographic separation and Tl isotope analysis of USGS reference material BCR-2 and 8 samples from Anatahan, Mariana arc
   - preparation of Figure 1 (location maps)

5. ***A. Brett**, J. Prytulak, S. J. Hammond, M. Rehkämper.* (2018) Thallium mass fraction and stable isotope ratios of sixteen geological reference materials. *Geostandards and Geoanalytical Research*, **42**:339-360. doi:10.1111/ggr.12215

   Contributions: *see preamble to Chapter 2.*

6. ***E. K. A. Brett**, J. Prytulak, M. Rehkämper, S. J. Hammond, C. Chauvel, A. Stracke, M. Willbold.* (2021) Thallium elemental and isotopic systematics in ocean island lavas. *Geochimica et Cosmochimica Acta*, **301**:187–210. doi:10.1016/j.gca.2021.02.035

   Contributions: *see preamble to Chapter 3.*

Appendix B

Supporting data

Data obtained or compiled over the course of this project are included as an electronic spreadsheet. A summary is given below, with each name corresponding to one sheet in the workbook.

For new analyses reported in this work, for individual measurements the naming convention used for samples is SAMPLE-#, where SAMPLE is the sample name and # identifies the digestion that was analysed. For example, “BCR2-5” is digestion #5, containing USGS BCR-2.

B2.i Compilation of literature reports of Tl concentration for reference materials.

B2.ii Concentration data for reference materials, obtained using ICP-QQQ.

B2.iii Individual thallium isotope analysis data of the “Aldrich solution standard”, including unique results file numbers.

B2.iv Individual thallium isotope analysis data for reference materials, including unique results file numbers.

B3.i Compilation of literature reports of geochemical characteristics of OIB samples for which Tl concentration data are available.
(a) geochemical data;
(b) source for each data point;
(c) bibliography.

B3.ii Concentration data for OIB samples, obtained using ICP-QQQ.

B3.iii Comparison between trace element concentations reported in the literature and obtained during this study for OIB samples.

B3.iv Individual thallium isotope analysis data for OIB samples, including unique results file numbers.

B3.v Combination of B3.i, B3.ii and new Tl isotope data, provided for convenience.

B3.vi Compilation of filtered MORB data (see Chapter 3 for details).

B4.i Compilation of arc lava data for which Tl concentrations are confidently known.
(a) geochemical data;
(b) source for each data point;
(c) bibliography and notes.

B4.ii Compilation of filtered data for arc lavas from the Mexican Volcanic Belts, subdivided into ‘arc-type’ and ‘OIB-type’ (see Chapter 4 for details).

B5.i Individual thallium isotope analysis data for Popocatépetl samples, including unique results file numbers.

B5.ii Table 5.2, provided in spreadsheet format for convenience.